

# MicroRNA-184: A Multifaceted Regulator of Epidermal Keratinocyte Biology

Adam Richardson

A thesis submitted in partial fulfilment of the requirements of  
**Liverpool John Moores University**

for the degree of  
**Doctor of Philosophy**

This research programme was carried out in collaboration with  
**Newcastle University**

November 2018

## List of Work

**Richardson, A.,** Owens, D.J. and Ross, K. (2018). MiRNA-184 and its lncRNA sponge UCA1 are induced in wounded keratinocytes in a store-operated calcium entry-dependent manner. *The British Journal of Dermatology*. Epub ahead of print. doi: doi:10.1111/bjd.17576.

**Richardson A.,** Powell, A., Sexton D.W., Parsons, J.L., Reynolds, N.J. and Ross, K. (2018). MicroRNA-184 is induced by store-operated calcium entry and regulates early keratinocyte differentiation. *Manuscript Under Review*. \*Pre-print available: doi: doi.org/10.1101/319541.

**Richardson A.,** Tyng, T.H., Yesudian, P.D., West, E.A., Al-Sharqi, A., Parslew, R. and Ross, K. (2019). Argonaute Expression in Psoriatic Epidermis and Differentiation Keratinocytes. *Manuscript Under Review*.

\* Manuscripts published on the pre-print server BioRxiv are not peer-reviewed and may represent early versions of manuscripts currently undergoing peer-review processes.

## Abstract

The epidermis is vitally important in protecting the organism from environmental insults. Consisting of dynamic outer strata of keratinocytes that terminally differentiate from basal keratinocytes stem cells (KSC), the epidermis is maintained by constant spatial and temporal control. In psoriasis, a dysregulated and intensifying crosstalk between keratinocytes and immune cells disturbs epidermal homeostasis resulting in hyperproliferation and loss of differentiation. Recently, short (~22 nt) genetic molecules called microRNAs (miRNA) that regulate gene expression by repressing messenger RNA (mRNA) have gained attention as robust regulators of keratinocyte biology and key players in psoriasis. A specific miRNA elevated in psoriasis, miR-184, modulates the expression of Argonaute 2 (AGO2), an established effector of miRNA function. However, there is a paucity of research investigating miR-184 and the miR-184:AGO2 axis in epidermal keratinocyte biology. As such, the aim of this thesis was to delineate miR-184 expression and function during keratinocyte proliferation, differentiation and migration.

Firstly, it was revealed that miR-184 was induced during keratinocyte differentiation in a process that relies exclusively on  $\text{Ca}^{2+}$  and the major keratinocyte  $\text{Ca}^{2+}$  entry pathway called store-operated calcium entry (SOCE). Furthermore, miR-184 was upregulated in a cohort of eight psoriasis patient samples. By modulating miR-184 expression it was elucidated that miR-184 promotes early keratinocyte differentiation through concomitant induction of factors related to DNA damage, growth arrest and terminal differentiation.

In addition, this thesis reports the discovery of SOCE-dependent induction of miR-184 during keratinocyte migration as well as a long non-coding RNA, UCA1 that has been implicated in the regulation of miR-184. Importantly, ectopic miR-184 stimulated keratinocyte migration in scratched monolayers while inhibition of miR-184 reduced migration.

Studies on *AGO1-4* transcripts identified that *AGO4* mRNA was the most abundant AGO in human epidermal keratinocytes and revealed no reduction of *AGO2* expression in response to enhanced miR-184 levels during differentiation. Furthermore, both *AGO1* and *AGO4* were downregulated in psoriatic patients. Finally, it was established that AGO2 localises to the nucleus of terminally differentiated keratinocytes in a Ca<sup>2+</sup>-dependent mechanism, pointing to an apparent nuclear role for AGO2 during keratinocyte differentiation.

In summary, the results reported in this thesis highlight an important role for miR-184 in the regulation of epidermal keratinocyte biology, reveal SOCE as a regulator of miRNA pathways in keratinocytes and show for the first time a role for miR-184 in epidermal keratinocyte migration. Together, these studies may facilitate the development of miRNA-based dermaticals for cutaneous diseases.

## Acknowledgements

Firstly, I would like to express my sincere gratitude to my advisor, Dr. Kehinde Ross for his many years of constructive mentorship and training during both my undergraduate and doctoral career. To my co-supervisors, Dr. Andrew Powell and Dr. Darren Sexton. Thank you for all your guidance, expertise and valuable discussion. I would also like to thank the British Skin Foundation for their support and funding of this work.

I would like to express my appreciation to Prof. Nick Reynolds of Newcastle University, Institute of Cellular Medicine, for his valuable advice on primary keratinocyte culture and manuscript critique; Dr. Dan Owens of Sport and Exercise Science, LJMU, for training and advice on all things live cell imaging related; Dr. Adam Sharples previously of LJMU, for his help with PCR related issues and Dr. Jason Parsons, Dr. Katie Nickson and Dr. Carlos Rubbi of Molecular and Clinical Cancer Medicine, University of Liverpool, for making the DNA damage work possible.

Many thanks to all those working and studying at LJMU who have been extremely helpful over the course of this project. In particular, my fellow lab mates Kan, Adrien and especially Ashley for their support and friendship - the Ship and Mitre sessions will be missed!

Huge thanks are due to my family and friends, especially my mother, grandparents and brother, who have been my biggest supporters throughout this PhD. Finally, I would like to save my biggest thank you for my partner, Caoileann, whose unyielding encouragement and support has kept me going through my most difficult times - I could not have done this without you.

## Dedication

I dedicate this thesis to the bright memory of my grandfather

**William “Bill” Richardson**

# Table of Contents

List of Work.....	1
Abstract.....	2
Acknowledgements.....	4
Dedication.....	5
List of Figures.....	9
List of Tables.....	9
Abbreviations.....	12
1. Introduction.....	18
1.1. MicroRNAs.....	19
1.1.1. Biogenesis.....	20
1.1.1.1. Transcription.....	20
1.1.1.2. Nuclear Processing.....	22
1.1.1.3. Nuclear Export.....	24
1.1.1.4. Cytoplasmic Processing.....	25
1.1.2. miRNA Mechanism of Action.....	26
1.2. Argonaute.....	29
1.2.1. Argonaute Structure.....	31
1.2.2. Argonaute Function.....	33
1.2.2.1. Nuclear Activity.....	34
1.2.2.2. Post-Translational Regulation.....	35
1.3. The Skin.....	37
1.3.1. Epidermal Microenvironment.....	37
1.3.1.1. Stratum Basale.....	38
1.3.1.2. Stratum Spinosum.....	39
1.3.1.3. Stratum Granulosum.....	39
1.3.1.4. Stratum Corneum.....	40
1.3.2. Psoriasis.....	41
1.3.2.1. Pathophysiology of Psoriasis.....	42
1.3.2.2. miRNAs & Psoriasis.....	44
1.4. Keratinocytes.....	47
1.4.1. Differentiation.....	47
1.4.1.1. Gene Expression.....	48
1.4.1.2. p21.....	49
1.4.1.3. Cyclin E.....	50
1.4.1.4. Calcium and Store Operated Calcium Entry.....	52
1.4.1.1. miRNAs & Differentiation.....	56
1.4.2. Migration.....	58
1.4.2.1. miRNAs & Migration.....	58
1.5. miR-184.....	60
1.6. Research Aims.....	61

2.	Materials and Methods.....	62
2.1.	Materials .....	63
2.2.	Cell Culture.....	63
	2.2.1. Isolation.....	63
	2.2.2. General Cultivation.....	65
	2.2.3. Differentiation Assay .....	67
	2.2.4. Scratch Assay.....	67
	2.2.5. Treatment with SOCE Inhibitors .....	67
2.3.	Nucleofection.....	69
2.4.	Real-Time Quantitative Polymerase Chain Reaction (RT-qPCR).....	71
	2.4.1. RNA Isolation and Quantification .....	71
	2.4.2. cDNA Synthesis.....	73
	2.4.3. RT-qPCR.....	74
2.5.	Western Blotting .....	78
	2.5.1. Protein Isolation and Quantification .....	78
	2.5.2. Fractional Protein Isolation.....	79
	2.5.3. Western Blotting .....	79
2.6.	Proliferation .....	82
	2.6.1. Flow Cytometric Analysis of Cell Cycle .....	82
	2.6.2. MTT .....	84
2.7.	Microscopy .....	84
	2.7.1. Immunofluorescence (IF) Microscopy .....	84
	2.7.2. Live Cell-Imaging.....	86
2.8.	Statistical Analysis.....	86
3.	Investigation of miR-184 Expression in HPEK and Psoriasis.....	87
3.1.	Introduction.....	88
3.2.	Aims.....	90
3.3.	Results.....	90
	3.3.1. Optimisation of HPEK Differentiation .....	90
	3.3.2. Effect of HPEK Differentiation on Expression of miR-184.....	95
	3.3.3. Effect of SOCE Inhibition on Ca <sup>2+</sup> -dependent miR-184 Induction.....	99
	3.3.4. Expression of miR-184 in Psoriatic Lesions.....	108
3.4.	Discussion .....	110
	3.4.1. Differentiation of HPEK .....	110
	3.4.2. Induction of miR-184 During HPEK Differentiation .....	111
	3.4.3. SOCE Facilitates Induction of miR-184.....	112
	3.4.4. miR-184 is Elevated in Psoriatic Lesions .....	114
4.	Function of miR-184 During HPEK Differentiation .....	115
4.1.	Introduction.....	116
4.2.	Aims.....	117

4.3.	Results.....	117
4.3.1.	Optimisation of Nucleofection.....	117
4.3.2.	The Effects of miR-184 on Keratinocyte Growth.....	121
4.3.3.	The Effects of miR-184 on Keratinocyte Differentiation .....	123
4.3.3.1.	Impact of miR-184 on Involucrin .....	123
4.3.3.2.	Impact of Ectopic miR-184 on Cyclin E.....	125
4.3.3.3.	The Effects of ectopic miR-184 on p21 .....	128
4.3.3.4.	Impact of miR-184 Inhibition on HPEK Differentiation.....	130
4.3.3.5.	The Effects of miR-184 on DNA damage .....	134
4.4.	Discussion.....	139
4.4.1.	Nucleofection Optimisation .....	139
4.4.2.	miR-184 Modulates Keratinocyte Proliferation.....	141
4.4.3.	miR-184 Promotes Early Differentiation.....	143
5.	The Effect of miR-184 on HPEK Migration.....	148
5.1.	Introduction.....	149
5.2.	Aims.....	151
5.3.	Results.....	151
5.3.1.	The Effect of Scratching on miR-184 Expression .....	151
5.3.2.	The Effect of Scratch Assay on Expression of UCA1 .....	153
5.3.3.	Impact of Perturbed miR-184 Levels on Wound Healing .....	155
5.4.	Discussion.....	162
5.4.1.	SOCE-Dependent miR-184 Induction During HPEK Migration .....	162
5.4.2.	Migration Induces UCA1 Expression in a SOCE-Dependent Manner.....	163
5.4.3.	miR-184 Promotes Keratinocyte Migration.....	164
6.	Epidermal Argonaute Dynamics.....	165
6.1.	Introduction.....	166
6.2.	Aims.....	167
6.3.	Results.....	168
6.3.1.	Investigation of Argonaute Expression in HPEK .....	168
6.3.2.	Argonaute Expression in Psoriasis.....	171
6.3.3.	The Effects of AGO2 Perturbation on HPEK Differentiation.....	177
6.3.4.	Subcellular Location of AGO2 .....	182
6.4.	Discussion .....	189
6.4.1.	Effect of HPEK Differentiation on Argonaute Expression.....	189
6.4.2.	Argonauates in the Psoriatic Epidermis.....	191
6.4.3.	siAGO2 Impacts Expression of Differentiation-associated Genes.....	192
6.4.4.	siAGO2 Effects Expression of miR-205, miR-184 and miR-21 .....	194
6.4.5.	AGO2 Accumulates in the Nucleus During Differentiation with Ca <sup>2+</sup> .....	194
7.	Conclusion .....	197
	References.....	201

## List of Figures

Figure 1.1	Genomic Location of miRNA	21
Figure 1.2	miRNA Biogenesis	23
Figure 1.3	Canonical miRNA Seed Types	27
Figure 1.4	AGO:miRNA complex	32
Figure 1.5	The dynamic stratum of the epidermis	38
Figure 1.6	Molecular Mechanism of HPEK Differentiation	51
Figure 1.7	Store-operated Calcium Entry (SOCE)	54
Figure 2.1	Isolation of HPEK	64
Figure 2.2	Differentiation of HPEK Schematic	68
Figure 2.3	Gating strategies used for flow cytometry data analysis	83
Figure 3.1	Effect of stimulation with 1.2 mM Ca <sup>2+</sup> for 3 days on HPEK	91
Figure 3.2	Effect of stimulation with 1.5 mM Ca <sup>2+</sup> for 5 days on HPEK	92
Figure 3.3	Impact of differentiation on cyclin E1, E2 and B transcript expression	93
Figure 3.4	Effect of differentiation on involucrin and cyclin E protein expression	94
Figure 3.5	Effect of 1.2 mM Ca <sup>2+</sup> treatment on miR-184 expression	95
Figure 3.6	Effect of 5 days 1.5 mM Ca <sup>2+</sup> treatment on miR-184 expression	96
Figure 3.7	Impact of PMA treatment on miR-184 expression	97
Figure 3.8	Effect of 1,25(OH)D <sub>3</sub> on miR-184 expression	98
Figure 3.9	Effect of Gd <sup>3+</sup> on miR-184 expression during calcium induced differentiation	100
Figure 3.10	Effect of BTP2 on miR-184 expression during calcium induced differentiation	101
Figure 3.11	Impact of ORAI1 knockdown on miR-184 expression during calcium induced differentiation	102
Figure 3.12	Effect of NFAT1 inhibition on miR-184 expression during calcium induced differentiation	103
Figure 3.13	Effect of Gd <sup>3+</sup> treatment on ORAI1 transcript expression	105
Figure 3.14	Effect of BTP2 treatment on ORAI1 expression	106
Figure 3.15	Impact of siORAI1 nucleofection on ORAI1 transcript expression	107

Figure 3.16	Mean expression of miR-184 in psoriatic lesions	108
Figure 3.17	Patient variation of miR-184 expression in psoriatic lesions	109
Figure 4.1	Effect of time on GFP expressing HPEK	118
Figure 4.2	Effect of miR-184 mimic on basal miR-184 expression	119
Figure 4.3	Impact of miR-184 mimic on miR-184 expression over 5 days	120
Figure 4.4	Effect of miR-184 on cellular health	121
Figure 4.5	The effect of miR-184 on cell cycle dynamics	122
Figure 4.6	Effect of miR-184 on involucrin transcript expression in HPEK	123
Figure 4.7	Impact of miR-184 overexpression on Involucrin in HPEK	124
Figure 4.8	Effect of miR-184 on cyclin E1 transcript expression in HPEK	125
Figure 4.9	Effect of miR-184 on cyclin E2 transcript expression in HPEK	126
Figure 4.10	Effect of miR-184 on Cyclin E protein in HPEK	127
Figure 4.11	Impact of miR-184 on p21 transcript in HPEK	128
Figure 4.12	Impact of miR-184 on p21 protein in HPEK	129
Figure 4.13	Impact of miR-184 inhibition on involucrin in HPEK	131
Figure 4.14	Effect of miR-184 inhibition on Cyclin E in HPEK	132
Figure 4.15	Effect of miR-184 inhibition on p21 in HPEK	133
Figure 4.16	Effect of miR-184 mimic on $\gamma$ H2AX levels in HPEK	135
Figure 4.17	Effect of miR-184 Inhibitor on $\gamma$ H2AX levels in HPEK	136
Figure 4.18	Impact of miR-184 overexpression upon $\gamma$ H2AX foci	137
Figure 4.19	Quantification of fluorescent $\gamma$ H2AX foci	138
Figure 4.20	Schematic Representation of Prospective miR-184: Differentiation Pathway	147
Figure 5.1	Impact of HPEK wounding on expression of miR-184	152
Figure 5.2	Impact of HPEK wounding on expression of UCA1	153
Figure 5.3	Effect of SOCE inhibitors on UCA1 expression during wounding	154
Figure 5.4	Example analysis of live cell images of scratched HPEK	156
Figure 5.5	Impact of control oligonucleotide upon wounded keratinocytes	157
Figure 5.6	Effect of miR-184 mimic on wounded HPEK	158
Figure 5.7	Effect of control inhibitor on wounded HPEK	159
Figure 5.8	Effect of miR-184 inhibitor on wounded HPEK	160
Figure 5.9	Effect of miR-184 perturbation on wound closure	161
Figure 6.1	Effect of differentiation on AGO2 expression	168

Figure 6.2	Impact of differentiation on AGO1, AGO3 and AGO4 expression	169
Figure 6.3	Effect of Differentiation on AGO Expression	170
Figure 6.4	Expression of AGO1 in Psoriatic Lesions	172
Figure 6.5	Expression of AGO2 in Psoriatic Lesions	173
Figure 6.6	Expression of AGO3 in Psoriatic Lesions	175
Figure 6.7	Expression of AGO4 in Psoriatic Lesions	176
Figure 6.8	Effect of siAGO2 on Expression of AGO2 and AGO4 During Differentiation	178
Figure 6.9	Effect of siAGO2 on Cyclin E Expression During Differentiation	179
Figure 6.10	Impact of siAGO2 on Expression of Involucrin During Differentiation	180
Figure 6.11	Effect of siAGO2 on Expression of miRNAs	181
Figure 6.12	Impact of Ca <sup>2+</sup> Induced Differentiation on AGO2 Subcellular Location	183
Figure 6.13	Effect of PMA Induced Differentiation on AGO2 Subcellular Location	184
Figure 6.14	Impact of 1,25(OH)D <sub>3</sub> Induced Differentiation on AGO2 Subcellular Location	185
Figure 6.15	Manders Colocalisation Coefficient Analysis	186
Figure 6.16	Impact of Ca <sup>2+</sup> Induced Differentiation on YFP-AGO2 Subcellular Location	187
Figure 6.17	Fractional Western Blotting for AGO2 Following Differentiation	188

## List of Tables

Table 2.1	Differentiation Medium	68
Table 2.2	Reverse Transcription Mastermix	74
Table 2.3	Pre-designed Qiagen Primers	77
Table 2.4	Thermo Fisher Primers	77
Table 2.5.	Western Blotting Antibodies	81
Table 2.6.	Immunofluorescent Antibodies	85

## Abbreviations

[Ca <sup>2+</sup> ]	Cytosolic Calcium
μg	Microgram
1,25(OH) <sub>2</sub> D <sub>3</sub>	1,25-dihydroxyvitamin D <sub>3</sub>
3'UTR	3' Untranslated Region
AGO	Argonaute
AMP	Antimicrobial Peptide
Amp B	Amphotericin B
ANKRD52	Ankyrin repeat domain-containing protein 52
ANOVA	Analysis of Variance
AP-1	Activator Protein 1
AP-2	Activator Protein 2
ATP	Adenosine Triphosphate
BCA	Bicinchoninic Acid
BP	Band Pass
BSA	Bovine Serum Albumin
<i>C. elegans</i>	<i>Caenorhabditis elegans</i>
Ca <sup>2+</sup>	Calcium
CaM	Calmodulin
CaN	Calcineurin
CARD10	Caspase Recruitment Domain-Containing Protein 10
CARE	Calcium-Response Element
CCL	C-C Motif Ligand
CCNB	Cyclin B
CCNE	Cyclin E
CD	Cluster of Differentiation
cDC	Conventional Dendritic Cell
Cdk	Cyclin Dependent Kinase
CDKI	Cyclin Dependent Kinase Inhibitor
cDNA	Complementary DNA
CE	Cornified Envelope
CnT-Pri	CnT-Prime Medium
CO <sub>2</sub>	Carbon Dioxide

CRAC	Ca <sup>2+</sup> Release-Activated Channel
CREB	cAMP Response Element-Binding Protein
CsA	Cyclosporin A
CSNK1A1	Casein Kinase 1, Alpha 1
Ct	Cycle Threshold
CXCL	C-X-C Motif Ligand
DAG	Diacylglycerol
DAPI	4', 6-diamidino-2-phenylindole
DCC	Dermal Dendritic Cell
DCP	Decapping Protein
DDR	DNA Damage Response
DDX	DEAD Box RNA Helicase
DGCR8	DiGeorge Critical Region 8
DJF	Dean-Jett-Fox
DMEM	Dulbeccos Modified Eagle Medium
DMSO	Dimethyl Sulfoxide
DNA	Deoxyribose Nucleic Acid
DSB	Double-Strand Breaks
dsRNA	Double Stranded RNA
DTT	Dithiothreitol
ECL	Enhance Chemiluminescent
ECM	Extracellular Matrix
EGFR	Epidermal Growth Factor Receptor
eIF	Eukaryotic Initiation Factor
EMP-1	Epithelial Membrane Protein 1
ER	Endoplasmic Reticulum
EYFP	Enhanced Yellow Fluorescent Protein
FBS	Fetal Bovine Serum
FGFR2	Fibroblast Growth Factor Receptor 2
FIH	Factor Inhibiting HIF
FOXP3	Forkhead Box P3
FSC	Forward Scatter
FSC-A	FSC-Absorbance
FSC-H	FSC-Height

GAPDH	Glyceraldehyde Phosphate Dehydrogenase
Gd3+	Gadolinium
gDNA	Genomic DNA
GDP	Guanosine Diphosphate
GFP	Green Fluorescent Protein
GM-CSF	Granulocyte-Macrophage-Colony Stimulating Factor
GOI	Gene of Interest
GTP	Guanosine triphosphate
GWAS	Genome Wide Associated Studies
H2AX	H2A Histone Family Member X
H3K4me3	Histone H3 Lysine 3 Trimethylation
H3K9	Histone H3 Lysine 9
HIF-1 $\alpha$	Hypoxia-Inducible Factor-1 Alpha
HLA	Human Leukocyte Antigen
HPEK	Human Primary Epidermal Keratinocytes
HRP	Horse Radish Peroxidase
Hsc70	Heat Shock Cognate 70
Hsp90	Heat Shock Protein 90
HUVEC	Human Umbilical Cord Vein Endothelial Cell
IFN $\gamma$	Interferon-Gamma
IL-	Interleukin-
IP3	Inositol Trisphosphate
IP3R	IP3 Receptor
IRAK1	IL-1 Receptor-Associated Kinase 1
IVL	Involucrin
kDa	Kilodalton
KSC	Keratinocyte Stem Cell
La3+	Lanthanum
LL37	Cathelicidin
LNA	Locked Nucleic Acid
lncRNA	Long Non-Coding RNA
LOR	Loricrin
MAPK	Mitogen-Activated Protein Kinase
mg	Milligram

MHC	Major Histocompatibility Complex
MID	Middle
Min	Minute
miRNA	MicroRNA
ml	Millilitre
mM	Millimolar
MMP	Matrix Metalloproteinase
mRNA	Messenger RNA
NADPH	Nicotinamide Adenine Dinucleotide Phosphate
NF	Nuclear Factor
NFAT	Nuclear Factor of Activated T Cells
NF- $\kappa$ B	Nuclear factor kappa B
nM	Nanomolar
OD	Optical Density
Oligo	Oligonucleotide
OSM	Oncostatin M
PABP	Poly(A)-Binding Protein
PACT	Protein Activator of the Interferon-induced Protein Kinase
PAZ	PIWI/AGO/Zwilli
PBMC	Peripheral Blood Mononuclear Cells
P-bodies	Processing-Bodies
PBS	Phosphate Buffered Saline
PBST	Phosphate Buffered Saline + Tween 20
PCNA	Proliferating Cell Nuclear Antigen
pDC	Plasmacytoid Dendritic Cell
PFA	Paraformaldehyde
PI	Propidium Iodide
PI3K	Phosphoinositide 3-Kinase
PIC	Protease Inhibitor Cocktail
PIP2	Phosphatidylinositol 4,5-Bisphosphate
piRNA	PIWI Interacting RNA
PKC	Protein Kinase C
PLC	Phospholipase C
PMA	Phorbol-12-myristate-13-acetate

pol II	RNA Polymerase II
pol III	RNA Polymerase III
PP	Lesional Psoriasis
PPP6C	Putative regulatory subunit of protein phosphatase 6
PN	Non-Lesional Psoriasis
pre-miRNA	Precursor miRNA
pri-miRNA	Primary miRNA
PTGS	Post-Transcriptional Gene Silencing
PVDF	Polyvinylidene Difluoride
RHE	Reconstituted Human Epidermis
RIPA	Radio Immunoprecipitation Assay Buffer
RISC	RNA Induced Silencing Complex
RNA	Ribose Nucleic Acid
RNase	Ribonuclease
RCF	Relative Centrifugal Force
RT-qPCR	Real-Time Quantitative Polymerase Chain Reaction
SA-TGS	Senescence Associated-TGS
SDS	Sodium Dodecyl Sulphate
SHIP2	SH2-domain containing inositol 5-phosphatase 2
siRNA	Short Interfering RNA
SNORD	Small Nucleolar RNA
SNP	Single Nucleotide Polymorphism
SOCE	Store-Operated Calcium Entry
SOCS3	Suppressor of Cytokine Signalling 3
SOX7	SRY-Box 7
Sp1	Specificity Protein 1
SSC	Side Scatter
ssRNA	Single Stranded RNA
STAT	Signal Transducer and Activation of Transcription
STIM	Stromal Interaction Molecule
STK40	Serine/Threonine Kinase 40
TA	Transit Amplifying Cells
TACE	TNF- $\alpha$ -Converting Enzyme
TBS	Tris Buffered Saline

TBST	Tris Buffered Saline + Tween 20
TE	Tris-EDTA
TGA	Transcriptional Gene Activation
TGF- $\beta$	Transforming Growth Factor Beta
TGS	Transcriptional Gene Silencing
Th1	T Helper 1
TIMP3	Metalloproteinase Inhibitor 3
Tm	Melting Temperature
TNF- $\alpha$	Tumour Necrosis Factor Alpha
TNRC6	Trinucleotide Repeat-Containing Gene 6
TRAF6	TNF Receptor-Associated Factor 6
TRBP	Transactivating Response RNA-Binding Protein
Treg	Regulatory T Cell
U	Uracil
UCA1	Urothelial Cancer Associated 1
USP2	Ubiquitin-Specific Peptidase 2
UV	Ultraviolet
UV-Vis	Ultraviolet-Visible
v/v	Volume to Volume
VDR	Vitamin D Receptor
VDRE	Vitamin D Response Element
w/v	Weight to Volume
XRN1	5'-3' exoribonuclease 1
$\gamma$ H2AX	Gamma H2A Histone Family Member X

# 1. Introduction

## 1.1. MicroRNAs

In 1993, whilst studying the temporal control of development in *Caenorhabditis elegans* (*C. elegans*) two groups came across a non-protein coding gene called *lin-4*, which produced a single stranded, 22-nucleotide (nt) ribonucleic acid (RNA) molecule. Their work demonstrated that *lin-4* directly suppressed translation of *lin-14* messenger RNA (mRNA) by partially binding to the 3' untranslated region (3'UTR) in an antisense manner, which ultimately led to a reduction in protein level (Lee, Feinbaum and Ambros, 1993; Wightman, Ha and Ruvkun, 1993). Seven years later, further work identified another regulatory non-protein coding gene called *let-7*, which they showed directly regulated a cascade of developmental genes including *lin-14*, confirming these short RNAs as a distinct class of biological regulators (Reinhart et al., 2000). At the time, these non-coding regulatory genes were thought to be specific to *C.elegans* however, shortly after its identification *let-7* was proven to be conserved across most of the bilateral phylogeny including humans (Pasquinelli et al., 2000).

More than two decades since the initial work on *lin-4*, a plethora of regulatory RNAs with similar mechanisms of biogenesis and action have been discovered. In order to distinguish these RNAs from the other classes of regulatory RNAs like short interfering RNA (siRNA) and P-element Induced Wimpy testes (PIWI) interacting RNA (piRNA) they were termed microRNAs (miRNAs) (Lagos-Quintana et al., 2001; Lau et al., 2001; Lee and Ambros, 2001). MiRNAs are short, typically 18-25 nucleotides, non-coding RNA molecules found to be evolutionarily conserved across animals, insects and plants. These single stranded RNA molecules function to disrupt the translation of target mRNAs in a process known as post-transcriptional gene silencing (PTGS) and are thought to significantly influence almost every aspect of cellular biology (Bartel, 2004). In humans, over 1000 miRNA species have been identified making up ~1% of the genome with over 60% of protein coding genes conserved targets of miRNAs (Friedman et al., 2009; Friedlander et al., 2014). Interestingly, translational

disruption of mRNA can occur in a competitive and synergistic nature whereby individual miRNAs can have multiple target mRNAs in one cell type often repressing the same biological pathway at various points. Equally, several miRNAs can target and bind to the same mRNA dependent on the length and specificity of its 3' UTR (Baek et al., 2008; Selbach et al., 2008; Friedman et al., 2009).

### **1.1.1. Biogenesis**

#### **1.1.1.1. Transcription**

A large majority of all known miRNAs are found within introns of protein coding genes or noncoding transcription units. However, dependent on alternative splice site variations, around 10% of miRNAs can also be derived from exonic transcripts (Rodriguez et al., 2004). Intronic miRNAs in the same orientation of protein-coding genes are usually transcribed under the same promoter as part of the pre-mRNA transcript (Fig. 1.1) (Baskerville and Bartel, 2005). It has also been revealed that some miRNAs are under control of their own distinct promoter. For instance, miR-21 is transcribed largely through binding of the transcription factor activator protein 1 (AP-1) to either the protein coding gene where it is located or to its own putative promoter (Cai, Hagedorn and Cullen, 2004; Fujita et al., 2008; Ribas et al., 2012). Many more miRNAs are located far from protein coding genes in intergenic regions but have the same transcription response elements and are most commonly generated as part of a cluster. Clustered miRNAs are usually under control of an individual promoter and often possess highly conserved sequences typically regulating the same transcripts or biological pathway (Fig. 1.1) (Bartel, 2004; Loffler et al., 2007; Friedman et al., 2009).

RNA polymerase III (pol III) transcribes most small RNAs with miRNAs originally thought to follow the same process. However, newly transcribed primary miRNAs (pri-miRNAs) are in some cases several kilobases in length and contain several stretches of uracil

(U) tandem repeats that would most likely terminate pol III transcription. It is now known, in part due to the presence of a 5' 7-methylguanosine cap and a 3' polyadenylated tail, that RNA polymerase II (pol II) transcribes most miRNAs (Fig. 1.2) (Cai, Hagedorn and Cullen, 2004; Lee et al., 2004).

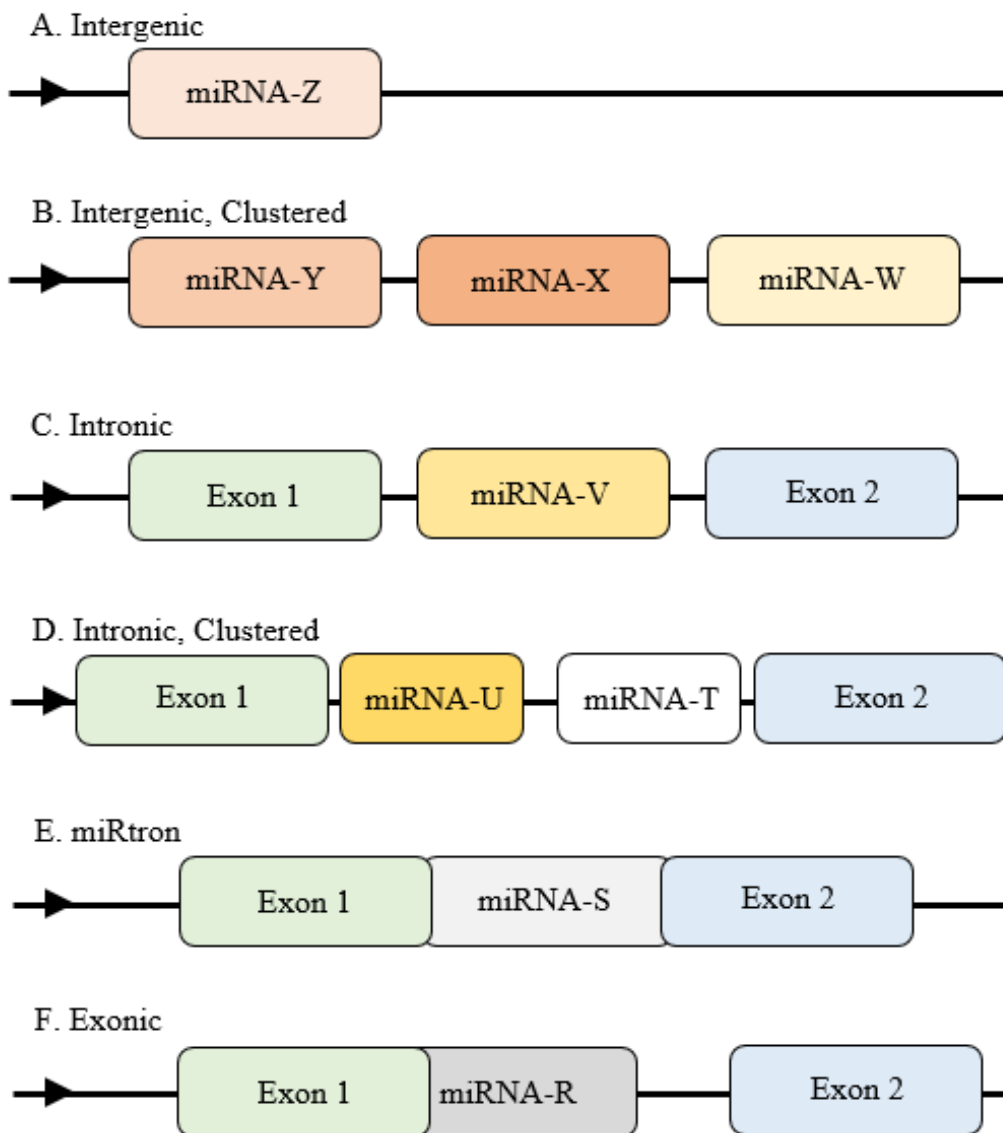


**Figure 1.1. Genomic Location of miRNA.** Intergenic miRNAs are found in regions distinct from transcription units. They can be transcribed by their own promoter (A; monocistronic) or as part of a cluster where multiple miRNAs are concomitantly transcribed (B; polycistronic). Intronic miRNAs are found in the introns of both protein-coding and non-coding genes and can be individual or clustered (C, D). miRtrons are miRNAs that skip nuclear processing and arise through very short introns (E). Exonic miRNAs overlap between exons and introns, resulting in less common miRNA transcripts.

### **1.1.1.2. Nuclear Processing**

Following transcription, initial processing of the pri-miRNAs containing important stem loop hairpins is performed in the nucleus (Fig. 1.2) (Auyeung et al., 2013). Processing is catalysed by the RNase III endonuclease Drosha as part of the larger microprocessor complex with the double stranded RNA binding protein DiGeorge Critical Region 8 (DGCR8), in addition to accessory proteins such as the DEAD box RNA helicases such as p68 (DDX5), p72 (DDX17) or the transcription factors nuclear factor (NF) 45 and NF90 (Lee et al., 2003). DGCR8 acts as a molecular anchor, binding to the stem loop hairpins of pri-miRNA around 11 bp away from the dsRNA-ssRNA junction. It acts to orientate the pri-miRNA and stabilise Drosha allowing for cleavage and releasing precursor miRNA (pre-miRNA). These pre-miRNA molecules are 60-100 nucleotides in length bearing a 5' phosphate and a 2-nt 3' overhang (Han et al., 2006; Nguyen et al., 2015). Some unique pre-miRNA molecules, termed mirtrons, derived from short introns with hairpin potential undergo splicing and debranching, evading Drosha processing before export into the cytoplasm (Berezikov et al., 2007). The output of pre-miRNA can be controlled post-transcriptionally with interactions between Drosha/DGCR8 and pri-miRNA stabilised by p68 and p72, increasing processing efficiency (Gregory et al., 2004; Davis et al., 2008). Conversely, the NF45/NF90 complex associated with the microprocessor has been shown to act as a negative regulator, impairing access of the pri-miRNA to the catalytic core of the microprocessor and dampening pre-miRNA conversion (Sakamoto et al., 2009).

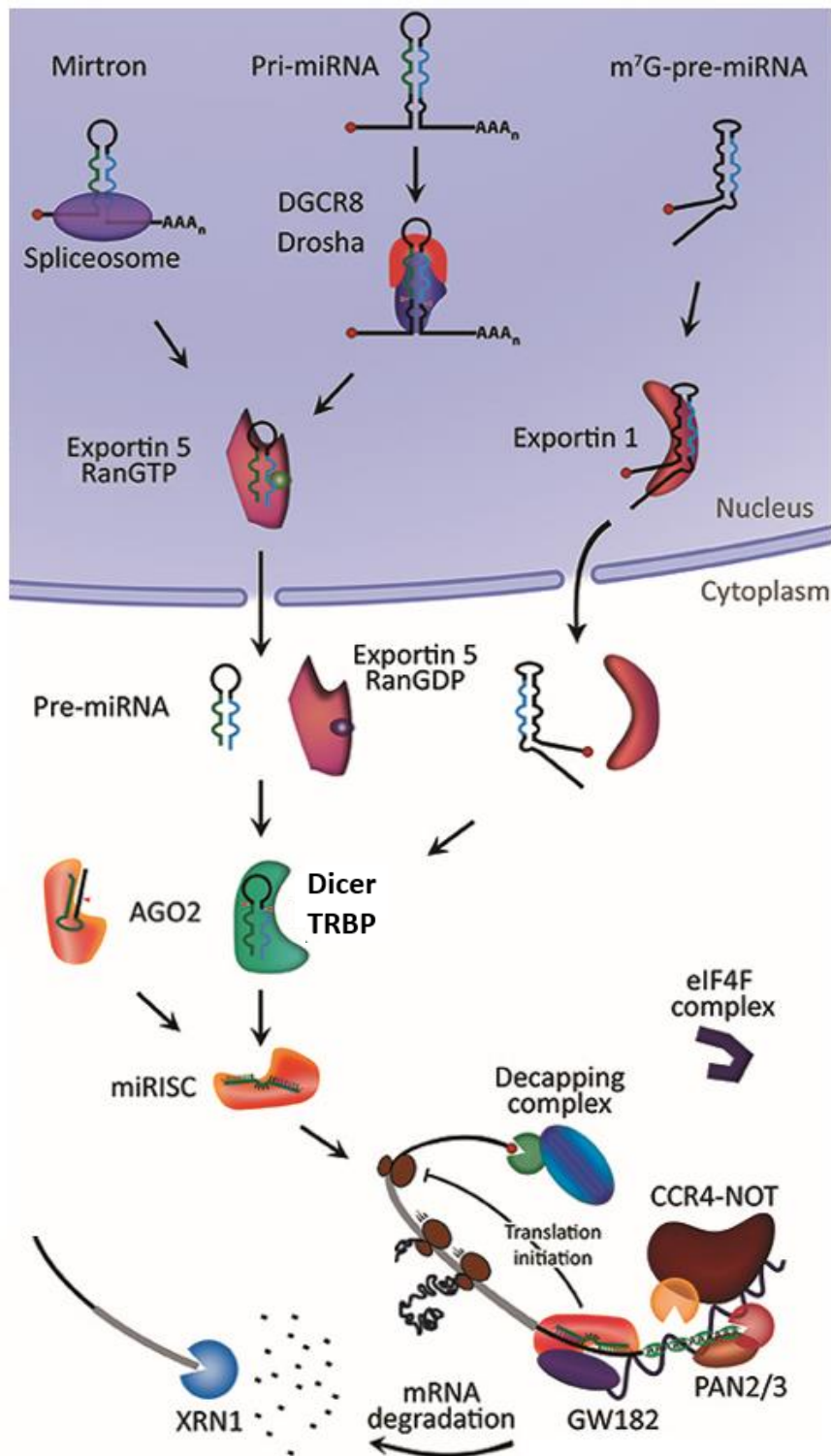


**Figure 1.2. miRNA Biogenesis.** Primary transcripts of miRNA (pri-miRNA) are transcribed by RNA polymerase II (PolII). The microprocessor complex consisting of Drosha along with its cofactor DGCR8 cleaves pri-miRNA forming precursor miRNA (pre-miRNA). Pre-miRNAs are exported from the nucleus by Exportin 5 under the influence of RanGTP. In the cytoplasm, Dicer in complex with TRBP cleaves pre-miRNA leaving a miRNA duplex. Mature miRNA, either 5p or 3p, is loaded into an AGO protein to form the miRISC. Mirtrons and m<sup>7</sup>G-pre-miRNA differ in nuclear processing or nucleocytoplasmic export but ultimately form a functional miRISC complex. Typically, the miRISC binds mRNA targets and represses translation but mRNA degradation can occur through recruitment of poly(A)-deadenylases such as CCR4-NOT by the GW182 (TNRC6) family of scaffold proteins. Adapted from O'Brien et al., 2018.

### **1.1.1.3. Nuclear Export**

Further processing of the imperfect pre-miRNA is required within the cytoplasm. To facilitate this the small hairpin needs to be exported from the nucleus to the cytoplasm. Transportation across the nuclear membrane is mediated in large by the nucleocytoplasmic transporter Exportin-5. Although, recent evidence has suggested a role for Exportin-1 in transport of quiescent related miRNAs with abnormal trimethylguanosine 5' caps (Yi et al., 2003; Xie et al., 2013; Martinez et al., 2017). The binding of pre-miRNA to Exportin not only enables nuclear export but also protects it from exonucleolytic digestion (Zeng and Cullen, 2004). Pre-miRNAs bind to Exportin-5 by recognition of the 2-nt 3' overhang, which via a conformational flip widens the minor groove of the miRNA stem allowing for additional interactions to occur between Exportin-5 residues and pre-miRNA nucleotides (Wang et al., 2011). Exportin-5 can bind to pre-miRNA, but only in the presence of the guanosine triphosphate (GTP)-binding nuclear protein Ran-GTP, which when together are known as the nuclear transport receptor. Nuclear pore complexes such as nucleoporin recognise nuclear transport receptors and allow translocation into the cytoplasm where hydrolysis of Ran-GTP to Ran-GDP by RanGAP induces a disassociation of the pre-miRNA cargo (Fig. 1.2) (Yi et al., 2003; Kim, 2004; Lund et al., 2004).

#### 1.1.1.4. Cytoplasmic Processing

The cytosolic portion of miRNA biogenesis relies on another RNase III endonuclease called Dicer (Hutvagner et al., 2001). Dicer is a multi-domain protein with PAZ (PIWI/Argonaute/Zwilli) domain, two RNaseIII nuclease domains and a dsRNA binding domain, major domains involved in processing of both miRNA and siRNA (Lau et al., 2012). During miRNA maturation, Dicer forms a processing complex with the human immunodeficiency virus transactivating response RNA-binding protein (TRBP) and protein activator of the interferon-induced protein kinase (PACT), which cleaves pre-miRNA close to the terminal loop, creating an additional 2-nt 3' overhang and releasing a small RNA duplex (Fig. 1.2) (Chendrimada et al., 2005; Lee et al., 2006; MacRae, Zhou and Doudna, 2007). The cleavage process is initiated when Dicer recognizes the terminal 5' phosphate and 2-nt 3' overhang of the pre-miRNA, with the distance between Dicers PAZ binding domain and the two RNase III domains determining the site of cleavage upon the pre-miRNA (Macrae et al., 2006; MacRae, Zhou and Doudna, 2007; Park et al., 2011; Fukunaga et al., 2014). Both PACT and TRBP act to stabilise Dicer, with depletion of either co-factors impacting pre-miRNA processing (Lee et al., 2013). The imperfect RNA duplex with adjacent 3' overhangs is 19-25-nt long and was initially termed miRNA:miRNA\* consisting of the functional guide strand involved in mRNA disruption and the passenger strand once thought to be degraded. However, recent evidence suggests that both strands can be biologically active (Chang et al., 2013; Bang et al., 2014) and therefore a newer nomenclature was presented using the suffixes 5p and 3p to term each strand direction, e.g. 5p is forward (5'-3') (Ambros et al., 2003; Fromm et al., 2015). The miRNA duplex is unwound following Dicer cleavage and subsequently loaded onto an Argonaute (AGO) protein with the guide strand selected dependent on the thermodynamic stability of 5' end base pairs and the passenger strand ejected to be either loaded onto another AGO or degraded (Fig. 1.2) (Khvorova, Reynolds and Jayasena, 2003; Carthew and

Sontheimer, 2009). AGO proteins are central catalytic components of the RNA induced silencing complex (RISC) with other co-factors, including both TRBP and PACT, as well as the heat shock cognate 70/heat shock protein 90 (Hsc70/Hsp90) chaperone machinery (Miyoshi et al., 2005; Iwasaki et al., 2010). TRBP and PACT facilitate protein-protein interactions between Dicer and AGO and are thought to sense the thermodynamic asymmetry of the miRNA duplex, thus acting as key factors for efficient loading (Chendrimada et al., 2005; Lee et al., 2006; Noland, Ma and Doudna, 2011). Hsc70/Hsp90 are believed to trigger conformational opening of AGO proteins in an adenosine triphosphate (ATP)-dependent manner which in turn allows them to receive large miRNA duplexes (Iwasaki et al., 2010).

### **1.1.2. miRNA Mechanism of Action**

The region in miRNA responsible for its function is called the ‘seed’ region. The seed region is a conserved sequence within nucleotide residues 1-8 at the 5’ end of the miRNA and is essential for the binding of the guide strand to the target mRNAs 3’ UTR (Fig. 1.3) (Bartel, 2009). The large majority of miRNA/mRNA interactions occur between the 5’ miRNA seed and the mRNA 3’ UTR, although exceptions have been uncovered. Several miRNAs such as miR-314, miR-296 and miR-470 target naturally occurring miRNA seed sites outside of the 3’ UTR within the amino acid coding region to modulate expression of key regulatory genes of stem cell differentiation (Tay et al., 2008). In addition, multiple miRNAs have been demonstrated to function through 5’ UTR target sites, such as miR-10a which alleviates translational repression of ribosomal proteins during amino acid starvation (Lytle, Yario and Steitz, 2007; Orom, Nielsen and Lund, 2008).

Watson-Crick pairing mediates interactions between miRNA seed regions and mRNA seed sites. Four canonical types of seed region/site interactions have been described; 6mer (a perfect match of nucleotide residues 2-7 on the seed site), 7mer-A1 (6mer plus an adenosine



In humans, perfect binding of miRNA to mRNA in the presence of AGO2 can induce cleavage and degradation of target mRNA, hence preventing translation (Fig. 1.2) (Hammond, 2005). However, imperfect seed region complementarity is more prevalent in mammals leading to translational repression by disrupting ribosome binding usually by blockade of initiation factors, such as eukaryotic initiation factor (eIF) 4E (Fig. 1.2) (Humphreys et al., 2005). Interestingly, despite the uncommon endonuclease activity of AGO2 in human cells, when ectopic levels of miRNA are introduced a reduction in target mRNA levels frequently follows (Guo et al., 2010). Reduction of mRNA levels by miRNA occurs through well described mRNA degradation pathways where target mRNA is deadenylated commonly by the CCR4-NOT deadenylase complex, uncapped usually by decapping protein 1 and 2 (DCP1/DCP2) decapping enzymes and degraded typically by 5'-3' exoribonuclease 1 (XRN1) (Decker and Parker, 2012). The process of miRNA silencing was thought to occur in cytoplasmic multiprotein complexes known as processing bodies (P-bodies). Although, through perturbation of P-body formation, it is now known that miRNA silencing is diffused throughout the cytoplasm with the formation of P-bodies a consequence of miRNA silencing (Eulalio et al., 2007).

## 1.2. Argonaute

In 1998, when studying leaf development in a plant species called *Arabidopsis thaliana*, Bohert et al., 1998 likened the phenotype of AGO1 mutants to the tentacles of a pelagic small squid named *Argonauta argo* (Bohmert et al., 1998). AGO proteins are highly conserved between species with many organisms expressing multiple AGO genes (Carmell et al., 2002). They can be phylogenetically divided into two main subtypes: the PIWI subfamily that interact with piRNA that are largely involved in spermatogenic transposon silencing, or the AGO subfamily that interacts with siRNA and miRNA (Hock and Meister, 2008; Ender and Meister, 2010). In humans, there are four members of the ubiquitously expressed AGO, subfamily named AGO1, AGO2, AGO3 and AGO4, that contribute to the regulation of many cellular processes (Hutvagner and Simard, 2008). Interestingly, AGO1, AGO3 and AGO4 are grouped on chromosome 1, whereas the AGO2 gene is located on chromosome 8. It is unclear whether this clustering pattern indicates any differences in biological function (Carmell et al., 2002). The expression patterns of AGO isoforms across differing tissue and cell types remains unclear. In mice, it has been demonstrated that Ago2 is the most abundant epidermal Ago, with little Ago3 or Ago4 detected. However, a level of functional redundancy exists, with overexpression of Ago3 recovering keratinocyte growth defects in Ago1/Ago2 double knockout mice (Wang et al., 2012). In human skin, although protein comparisons have not been made, *AGO1* and *AGO2* transcript expression is comparable, whilst *AGO3* and *AGO4* are detected at low levels (Sand et al., 2012; Völler et al., 2016). Levels of AGO proteins have been shown to be dysregulated in several cutaneous diseases. Changes in AGO levels or activity can lead to regulatory miRNA imbalances, with newly synthesised miRNAs becoming destabilised or a limited pool of AGO molecules preferring abundant miRNAs over sporadic ones (Wang et al., 2012). A large study on multiple skin cancers, including squamous and basal cell carcinoma, determined that expression of *AGO1* and *AGO2* mRNA was significantly increased when

compared with healthy tissues (Sand et al., 2012). Contrastingly, work comparing melanoma and non-melanoma cell lines found that overall expression of AGO transcripts was severely reduced and that *AGO2* was most affected (Völler et al., 2016). *AGO2* has been implicated in the inflammatory disease psoriasis, with transcript levels severely reduced in psoriatic lesions. Recent work has supported this claim, showing that *AGO1* and *AGO2* mRNA levels in psoriasis lesions were significantly decreased when compared with non-lesional controls, although, the sample size for both studies was limited (n=5-10) (Roberts et al., 2013; Hessam et al., 2017). In contrast, recent RNA-sequencing (RNA-seq) derived gene expression data has suggested that *AGO2* expression shows a moderate increase in lesional psoriasis samples when compared with non-lesional and healthy controls (Zhou et al., 2016). Finally, a very recent report has presented a role for *AGO1* and *AGO2* in hidradenitis suppurativa, which is a chronic inflammatory skin disorder where levels of both *AGO1* and *AGO2* transcripts are significantly diminished (Hessam et al., 2017).

### 1.2.1. Argonaute Structure

AGO proteins generally have a molecular weight of around 100 kDa and have a bilobal structure that consists of four main domains including N-terminal, PAZ, Middle (MID) and PIWI domains (Fig. 1.4) (Kuhn and Joshua-Tor, 2013). The N-terminal, linked to the PAZ domain by a linker region, is thought to drive duplex unwinding by acting effectively as a wedge (Nilsen and Paulsen, 1990). The PAZ domain recognises and binds to protruding 3'-nucleotides of pre-miRNA using a basic hydrophobic binding cavity within a Sm-like fold (Yuan et al., 2005). The PIWI domain shares extensive homology with the non-sequence specific bacterial RNase H domain, which is known to cleave RNA in an RNA/DNA mix. A subset of AGO proteins (AGO2 in humans) contribute to the target-cleavage ability of the RISC complex in most species. With the PIWI domain responsible for this “Slicer” activity, partly through a catalytic triad DDH motif (Asp<sup>597</sup>, Asp<sup>669</sup> and His<sup>807</sup>) (Yuan et al., 2005; Hock and Meister, 2008; Boland et al., 2011). The MID domain forms a binding groove anchoring the 5'-phosphate end of miRNA with a rigid loop, providing selective bias for uracil/adenosine (Jinek and Doudna, 2009). A key component to the RISC and therefore AGO function in humans is a scaffold protein known as trinucleotide repeat-containing gene 6 (TNRC6). The PIWI domain of AGO2 provides three tryptophan binding pockets for glycine/tryptophan (GW) rich argonaute binding domains present on the TNRC6 protein family (TNRC6A, B and C). TRNC6 proteins hold intrinsically disordered regions that influence interactions between AGOs and important effectors such as poly(A)-binding protein (PABP), an important factor that identifies and binds to poly(A) tails of mRNA, as well as the multiprotein deadenylase CCR4-NOT complex which removes mRNA poly(A) tails therefore repressing translation and marking mRNAs for degradation (Behm-Ansmant et al., 2006; Fabian et al., 2009; Sheu-Gruttadauria and MacRae, 2018).

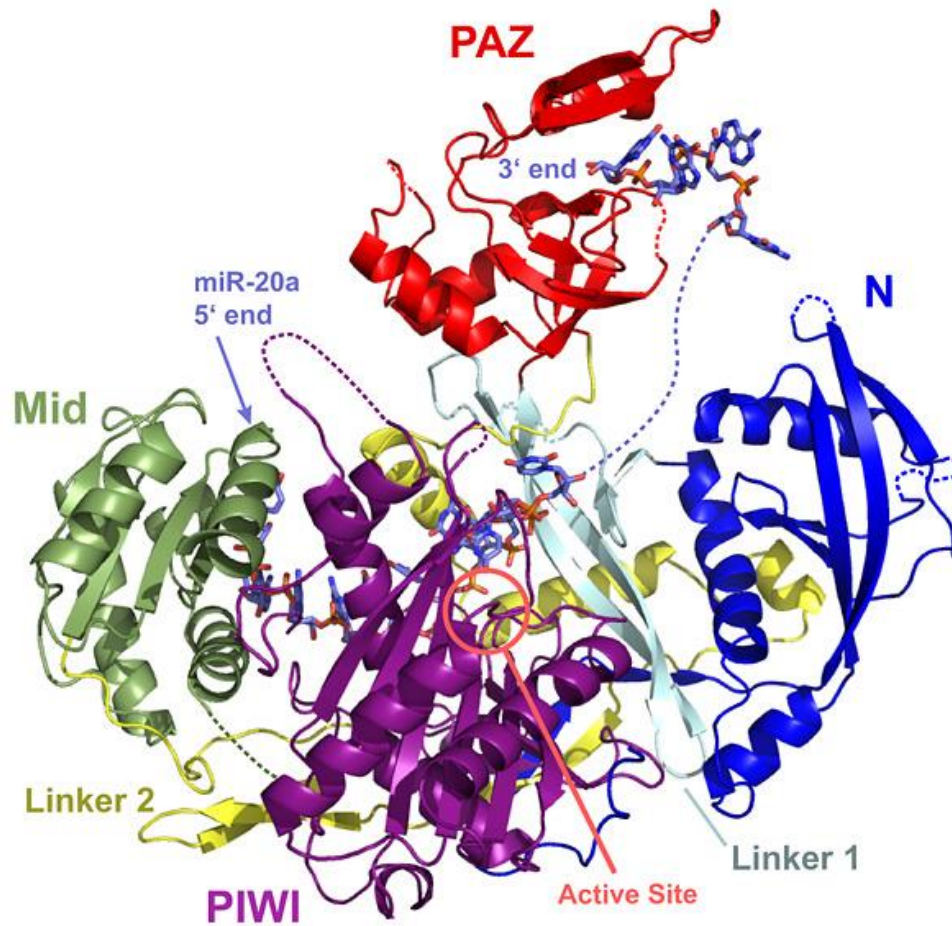


**Figure 1.4. AGO:miRNA complex.** AGO2 complexed with miR-20a indicating the N-terminal domain (blue), the PAZ domain (red), the Mid domain (green), and the PIWI domain (purple). miR-20a is located in the centre in a representation of miRNA binding (Elkayam et al., 2012).

### 1.2.2. Argonaute Function

AGO proteins are core components of the RISC and therefore indispensable to numerous cellular processes. The most defined role of AGO family members is the involvement in small RNA-mediated PTGS where they direct miRNAs to their target mRNA, ultimately leading to degradation (see 1.1.2). Loss of normal AGO function can have detrimental effects, with mutation of AGO orthologs in *C. elegans* resulting in a reduced amount of viable progeny, in addition to heterochrony in surviving cells (Grishok et al., 2001). Furthermore, *Drosophila* AGO1 loss-of-function mutants sustain late embryonic lethality, with those surviving presenting defects in both central and peripheral nervous systems (Kataoka, Takeichi and Uemura, 2001). In mice, total deletion of Ago2 results in loss of embryonic development, whereas single deletion of Ago1, 3 or 4 appears to be dispensable as shown by the maintenance of normalised growth (Cheloufi et al., 2010). Likewise, Ago2 deletion in murine embryonic stem cells results in delayed self-renewal and differentiation that lead to development defects (Shekar et al., 2011). Cutaneous ablation of murine Ago2 led to a striking reduction in global miRNA levels, a response exaggerated further by simultaneous knockdown of Ago1 and Ago2 (Wang et al., 2012).

RISC mediated silencing of mRNAs occurs through a combination of translational repression, deadenylation, decapping and 5'-3' exonuclease degradation. In addition to the basic AGO core, the GW182 family of proteins, termed TNRC6 in humans, play a vital role in RISC complex function and are amongst the most well defined AGO partners. TNRC6 proteins function as scaffolds, overseeing interactions between AGOs and key downstream effectors such as the CCR4-NOT deadenylase complex and when silenced causes severe impairment of RISC function and target mRNA degradation (Liu et al., 2005; Sheu-Gruttadauria and MacRae, 2018). The TNRC6 family have an increased affinity for RNA-loaded AGOs and can utilise three GW binding motifs to recruit multiple AGO/miRNA complexes thereby enhancing the

cooperative silencing of individual mRNA targets from multiple miRNA species (Elkayam et al., 2017).

#### **1.2.2.1. Nuclear Activity**

In addition to PTGS, AGO proteins are frequently found within the nucleus where they are reported to have numerous roles, including transcriptional gene activation (TGA) and transcriptional gene silencing (TGS). The discovery of small RNA-dependent TGA came from efforts to silence gene expression, with Li and colleagues noticing that a set of small RNAs targeted promoters leading to a loss of histone H3 lysine 9 (H3K9) methylation and specific transcription of target genes (Li et al., 2006). Furthermore, studies have shown that AGO2 is an essential component of TGA with knockdown resulting in a loss of target gene transcription compared with the minimal impact observed following loss of AGO1, 3 or 4 (Li et al., 2006; Chu et al., 2010). Additionally, recruitment of AGO2 at gene promoters leads to an enrichment of polIII binding sites and an increase in histone H3 lysine 4 trimethylation (H3K4me3) chromatin modifications which is strongly correlated with transcriptional activity (Huang et al., 2012).

TGS mediated by small RNAs has been studied extensively and was first described in plants, whereby transgene and viral RNAs were shown to guide the methylation of homologous DNA sequences. Later studies indicated that this DNA methylation is reliant on interfaces between AGO, dicer and H3K9 methylation (Wassenegger et al., 1994; Zilberman, Cao and Jacobsen, 2003; Henderson et al., 2006). Similarly, deletion of RNAi components equivalent to AGO and dicer in *Saccharomyces pombe* (*S. pombe*) resulted in a noticeable reduction of H3K9 methylation and a loss in silencing of heterochromatic repeats, leading to accumulation of nascent non-coding centromeric RNAs and subsequent heterochromatin disruption (Reinhart and Bartel, 2002; Volpe et al., 2002). In humans, both AGO1 and AGO2

are responsible for siRNA targeting of gene promoters where they induce histone methylation and inhibit gene expression (Janowski et al., 2006). More recently, a role for AGO2 in miRNA dependent TGS has been established resulting in accumulation of methyl transferase components at gene promoters and chromatin remodelling (Kim et al., 2008; Zardo et al., 2012). Furthermore, in aging fibroblasts, AGO2 has been shown to translocate to the nucleus during senescence where it associates with transcriptionally repressed heterochromatin and acts to functionally silence Rb/E2F target genes, such as cyclin E, in a process known as senescence-associated TGS (SA-TGS) (Benhamed et al., 2012). Finally, although the nuclear function is unknown, AGO2 has been detected in the nucleus of primary human keratinocytes (monolayer and organotypic cultures) as well as in human epithelial tissue. Interestingly, in the continuous keratinocyte cell line HaCaT, presence of nuclear AGO2 was minimal (Sharma et al., 2016).

#### **1.2.2.2. Post-Translational Regulation**

The functional activity and stability of AGOs can be regulated post-translationally. Silencing activity of AGO proteins, particularly AGO2, can be significantly augmented through prolyl-hydroxylation (Qi et al., 2008). In humans, hypoxia potently induces expression of prolyl-4-hydroxylases resulting in hydroxylation of AGO2 at proline-700 (P700) and elevation of silencing capacity (Wu et al., 2011). In addition, several phosphorylation patterns have been shown to affect AGO activity. The 5' phosphates of guide RNA strands are anchored to the RISC at the AGO MID domain, however, phosphorylation within the MID domain specifically at tyrosine-529 (Y529) prevents loading of small RNAs and ultimately RISC deactivation (Rudel et al., 2011). Phosphorylation of AGO2 serine 387 (S387), mediated by Akt3, suppresses AGO2 endonuclease activity, whilst enhancing translational repression through promoting assembly of distinct RISC complexes (Zeng et al., 2008; Horman et al., 2013).

Another phosphorylation event at tyrosine-393 (Y393), mediated by epidermal growth factor receptor (EGFR), prevents the interactions between AGO, Dicer and TRBP resulting in hindered miRNA maturation and accumulation of pre-miRNA (Shen et al., 2013). Multi-site phosphorylation of a highly conserved serine/threonine cluster (S824-S834) in the C-terminal region of AGO2 plays an important role in the functional recycling of the active AGO2 pool. Several phosphorylation events in this serine/threonine cluster by the serine/threonine kinase called Casein Kinase 1, Alpha 1 (CSNK1A1) negatively regulates association of AGO2 with target mRNAs. Conversely, dephosphorylation of this cluster by the serine/threonine phosphatase Ankyrin repeat domain-containing protein 52-Putative regulatory subunit of protein phosphatase 6 (ANKRD52-PPP6C) restores AGO2 target engagement effectively replenishing the pool of active AGO2 molecules (Golden et al., 2017; Quévillon Huberdeau et al., 2017). Finally, AGO activity can be modulated through ubiquitination leading to proteosomal degradation and a rapid decrease in global miRNA levels, a process utilised by T-cells to quickly alter their miRNA expression patterns, resulting in enhanced clonal expansion during activation (Bronevetsky et al., 2013).

## **1.3. The Skin**

The skin is the largest organ covering the entire external surface of the human body. It plays a vital role in preventing loss of water and other bodily components as well as forming a barrier protecting the body from a range of environmental insults such as microorganisms, heat, chemical, mechanical and radiation damage (Eckert, Crish and Robinson, 1997). It is able to adapt to both long and short term environmental changes. For example, individuals in areas of high ultraviolet (UV) radiation indexes have darker skin, better protecting them from potential damage. Thickening at sites of repetitive trauma or friction provides enhanced protection and sweating in hot climates to better regulate body temperature (Menon, 2002). The skin consists of three major structural layers: the insulative fatty deposits of the subcutaneous layer, the deep connective tissues of the dermis and the outermost dynamic stratum of the epidermis (Eckert, 1989).

### **1.3.1. Epidermal Microenvironment**

The epidermis is composed of continually self-renewing, stratified squamous epithelium that consists predominantly of keratinocytes although, other resident cells include melanocytes (pigment), merkel cells (mechanoreceptors) and langerhans cells (immunity) (Menon, 2002). These keratinocytes are organised into layers where they exist at varied stages of differentiation. These layers include; the stratum basale (basal layer), stratum spinosum (spinous layer), stratum granulosum (granular layer) and the stratum corneum (horny layer), as well as a layer specific to thicker skin, such as that present on the palms of hands and feet, called the stratum lucidum (clear layer) (Tobin, 2006). Keratinocytes undergo a continuous process of terminal differentiation through these transitional strata, ultimately forming non-living, flattened, enucleated, terminally differentiated keratinocytes known as corneocytes. This differentiation process is kept under tight temporal and spatial control involving the

formation of a specialised keratin network, development of a cornified envelope (CE) and the creation of lipid lamellae (Fig. 1.5) (Eckhart et al., 2013).

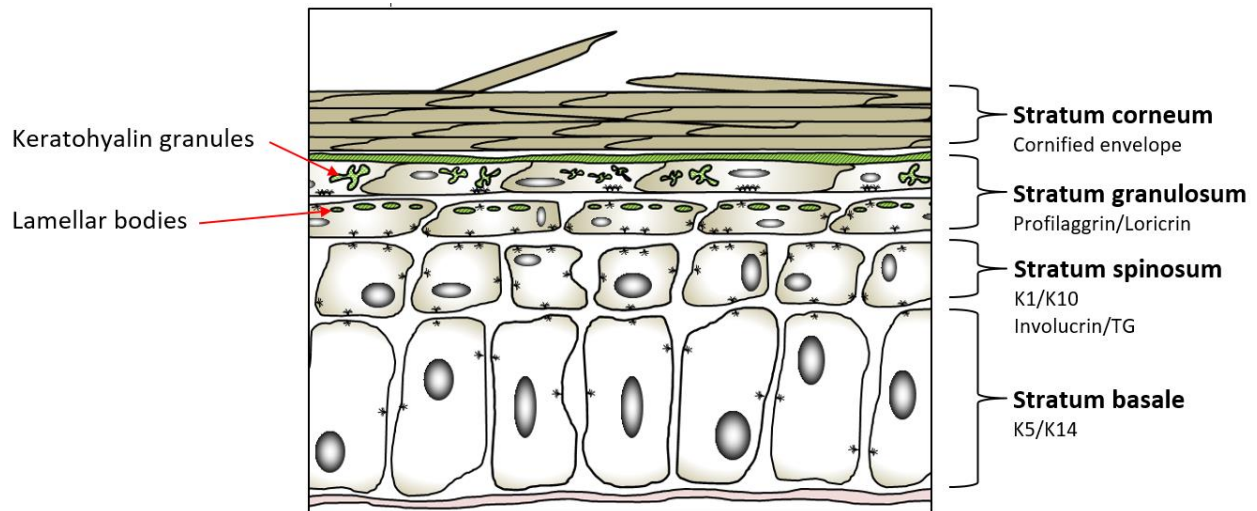


**Figure 1.5. The dynamic stratum of the epidermis.** The epidermis is a self-renewing tissue composed mainly of keratinocytes in various stages of terminal differentiation. TA cells are produced in the stratum basale (basal layer) by KSCs, and move outward through the epidermis, undergoing a programmed series of differentiation events involving production of specialised CE proteins, keratin network and lipid lamellae.

### 1.3.1.1. Stratum Basale

The basal layer is located at the base of the epidermis, attached to the basal lamina (basement membrane) via specialised integrin-mediated attachment assemblies called hemidesmosomes. Continuously dividing keratinocyte stem cells (KSC) or basal keratinocytes reside within the basal layer connected by desmosomes [114]. As they divide, KSCs provide daughter cells for the outer differentiating layers with limited proliferative potential referred to as transit amplifying (TA) cells. TA cells can only divide a finite number of times and when this limit is reached, they delaminate from the basement membrane and are displaced centrifugally into the stratum spinosum, initiating the process of terminal differentiation (Fig 1.5) (Koster and Roop, 2007; Arwert, Hoste and Watt, 2012).

### **1.3.1.1. Stratum Spinosum**

Cells in the stratum spinosum, named from the visual appearance resulting from increased desmosomal interactions between adjacent cells, begin to express distinct markers of differentiation including transglutaminases and involucrin. Transglutaminases catalyse acyl transfer reactions between  $\gamma$ -carboxamide and  $\epsilon$ -amino groups of glutamines and lysines of proteins, in a process known as  $\epsilon(\gamma$ -glutamyl)lysine crosslinking. Involucrin is one of several substrates for transglutaminase, consisting of 45 lysine and 150 glutamine residues, and is the earliest cornfield envelope (CE) protein to be deposited and cross-linked at the cell periphery of the outer layers where it contributes to mechanical resistance and CE insolubility (Candi, Schmidt and Melino, 2005; Eckert et al., 2005). The eponymous product of keratinocytes, keratin, is a fibrous protein that contributes largely to the structural properties of skin. Expression of keratin subsets change dependent on the cellular status of keratinocytes, with K5 and K14 the dominant keratins in the basal layer. As cells progress into the stratum spinosum this subset changes to K1 and K10, representing reorganisation of cytoskeletal intermediate filaments to increase tensile strength and a loss of hemidesmosome attachment sites (Fig 1.5) (Loschke et al., 2015).

### **1.3.1.2. Stratum Granulosum**

The stratum granulosum is the outermost nucleated layer and is identified by the presence of cytoplasmic granules called keratohyalin granules. These granules contain a major intermediate filament associated protein called profilaggrin, which upon modification and release into the cytoplasm as monomeric filaggrin plays a role in the aggregation and compaction of keratin filament bundles during terminal differentiation (Sandilands et al., 2009). Another major differentiation marker produced in the stratum granulosum is loricrin, which migrates to cell peripheries of the outermost layers where it undergoes cross-linking

with several cornification proteins but mainly involucrin (Simpson, Patel and Green, 2011). Loricrin makes up most CE proteins, contributing to mechanical resistance and providing a scaffold for the deposition of extracellular lipid lamellae. The lipid lamellae, consisting of cholesterol, free fatty acids, sphingolipids, ceramides and various hydrolytic enzymes is produced in the upper layers of the stratum spinosum, as well as throughout the stratum granulosum. Following production, the lipid lamellae undergoes compartmentalisation into secretory organelles called lamellar bodies to prevent premature reactions with substrates (Fig 1.5) (Menon, Lee and Lee; Kalinin, Kajava and Steinert, 2002).

### **1.3.1.3. Stratum Corneum**

The stratum corneum requires a major transformation whereby living keratinocytes cease transcriptional and metabolic activity becoming flattened corneocytes in a crucially quick process involving the accumulated pools of differentiation related proteins, enzymes and lipids (Candi, Schmidt and Melino, 2005). Cells in the stratum corneum undergo a unique form of controlled cell death called cornification whereby their nucleus is fragmented and their organelles are degraded all whilst transglutaminases attach the pre-existing cross-linked protein structures together to create a large yet compact proteinaceous scaffold in the place of a living cell. Moreover, by using the protein scaffold as a base the extracellular lipid lamella seals the space between cells forming a protective cutaneous layer (Eckhart et al., 2013; Feingold and Elias, 2014). To maintain structural integrity corneocytes are shed constantly in a process called desquamation with the functional stratum corneum constantly regenerated from pools of suprabasal keratinocytes (Fig 1.5) (Elias, 1983).

### **1.3.2. Psoriasis**

Psoriasis is a chronic inflammatory skin disorder that affects approximately 2% of the population. In the UK, its prevalence rose over the past 15 years from 2.3% to 2.8% with all-cause mortality ~20% higher than people without psoriasis (Springate et al., 2017). Multiple forms of psoriasis exist and differ in morphological and localisation traits, which include: guttate, pustular, inverse and erythrodermic psoriasis. However, the most frequent manifestation is psoriasis vulgaris characterised by scaly, demarcated, erythematous (redness) and squamous plaques with histopathological features containing hyperkeratosis (thickening of stratum corneum), parakeratosis (retention of nuclei), acanthosis (hyperplasia), blood vessel dilation and accumulation of neutrophils (Nestle, Kaplan and Barker, 2009; Di Meglio, Villanova and Nestle, 2014).

Originally, it was thought that psoriasis was solely associated with the skin, however, now there is evidence suggesting that it is a systematic disorder (Davidovici et al., 2010). Psoriasis has a huge impact on life quality, with psoriatic arthritis and other joint complaints present in around one fifth of patients (Gladman et al., 2005). Furthermore, cardiovascular comorbidities frequently feature in psoriasis patients with metabolic syndrome and diabetes particularly common (Yim and Armstrong, 2017). Additionally, autoimmune disorders such as inflammatory bowel disease and multiple sclerosis have been associated with psoriasis (Furue and Kadono, 2017). As well as physical comorbidities, psoriasis has been strongly linked to psychosomatic illnesses with depression affecting ~30% patients (Connor, Liu and Fiedorowicz, 2015).

### 1.3.2.1. Pathophysiology of Psoriasis

Psoriasis is mediated through a dysregulated and intensifying crosstalk between immune cells and keratinocytes, however the initial cause is not fully understood. Studies from twins demonstrate the importance of genetic susceptibility with monozygotic twins exhibiting a 3 to 5-fold higher risk of psoriasis when compared with dizygotic twins (Nestle, Kaplan and Barker, 2009). Genome wide association studies (GWAS) have shown that heritability is linked in large to mutations in the *PSORI* loci, which encodes genes for major histocompatibility complexes (MHCs) including human leukocyte antigens (HLAs). Mutations within HLA alleles are linked with greater risk for severe psoriasis (Nestle, Kaplan and Barker, 2009; Roberson and Bowcock, 2010; Ray-Jones et al., 2016). On the other hand, other genetic susceptibility factors have been defined including mutations within *CARD14* and *IL36RN* genes, most commonly present in pustular psoriasis (Tsoi et al., 2012). In addition to genetic predispositions, physical environmental stresses, including mechanical trauma, infection, medication and UV-exposure, have also been implicated in development of psoriasis in a process called Köbners phenomenon (Nestle, Kaplan and Barker, 2009; Di Meglio, Villanova and Nestle, 2014).

A plethora of dysregulated pathways contributes to the cellular makeup of psoriasis with multiple layers of molecular complexity derived from involvement of both innate and adaptive immune systems. Coupled with copious cytokine interactions and reciprocal activities of keratinocytes, which is progressively amplified by positive and negative feedback loops (Di Meglio, Villanova and Nestle, 2014). Cytokines are the major intermediary in development of psoriasis and exert their effect by activating the expression of more than 1300 genes that are found to be dysregulated within psoriasis through triggering of molecular pathways including signal transducer and activation of transcription 1 and 3 (STAT1; STAT3) and NF- $\kappa$ B (Krueger and Bowcock, 2005).

Originally, psoriasis was thought of as a T helper 1 (Th1) and interferon-gamma (IFN $\gamma$ ) dominant disorder. Despite this characteristic remaining true for disease onset, it is now believed that in the chronic inflammatory phase the interleukin axis (IL-23/IL-17/IL-22) and tumour necrosis factor alpha (TNF- $\alpha$ ) play a critical role (Greb et al., 2016). During initial pathogenic steps, it is thought that stressed keratinocytes produce and release complexes of self RNA/DNA as well as antimicrobial peptides (AMPs) such as S100 proteins,  $\beta$ -defensins and cathelicidin (LL37) which attract and activate plasmacytoid dendritic cells (pDCs) (Morizane and Gallo, 2012). Activation of pDCs results in release of type I interferons, which along with keratinocyte-derived IL-1 $\beta$ , IL-6 and TNF $\alpha$  attract and mediate activation of dermal dendritic cells (DCCs), conventional dendritic cells (cDCs) and specialised epidermal dendritic cells called Langerhans cells (Lowe, Bowcock and Krueger, 2007; Morizane and Gallo, 2012). Stimulated DCCs, cDCs and Langerhans cells produce a range of key cytokines including IL-12 and IL-23 that are responsible for linking innate and adaptive immune responses. IL-12 stimulates differentiation of naïve CD4<sup>+</sup> T-cells into Th1 subset cells leading to production of IFN $\gamma$  and TNF $\alpha$  whereas IL-23 stimulates differentiation into Th17 and Th22 T cell lineages (Aggarwal et al., 2003; Lowe, Bowcock and Krueger, 2007; Teng et al., 2015). Th17 cells produce IL-17, which promotes production and release of factors that stimulate migration of T cells (chemokine C-C motif ligand 20; CCL20), and neutrophils (chemokine C-X-C motif ligand 1; CXCL1, CXCL2, CXCL5, CXCL8 and granulocyte-macrophage colony stimulating factor; GM-CSF) into the epidermal compartment (Aggarwal et al., 2003; Wilson et al., 2007; Di Meglio, Villanova and Nestle, 2014; Ha et al., 2014). Th22 cells produce IL-22 which promotes hyperproliferation of keratinocytes, normally to dispatch internal pathogens by increasing cell turnover. Enhanced levels of IL-22 causes epidermal hyperplasia in psoriasis where psoriatic keratinocytes reach the skin surface in as little as 6 days, as opposed to the 40 days observed in normal cells (Zheng et al., 2007; Wolk et al., 2009). The altered cytokine

profile seems to not only cause the epidermal changes observed in psoriasis but also a self-reliant feedback loop leading to the development and, ultimately, worsening of the disease.

### **1.3.2.2. miRNAs & Psoriasis**

The role of miRNAs in epidermal homeostasis has received a lot of interest over the past decade with a link between miRNAs and psoriasis first suggested by Andor Pivarcsis laboratory in 2007 with hundreds of miRNAs now described as abnormally expressed psoriatic lesions (Sonkoly et al., 2007).

#### **miR-203**

The first miRNA to be identified as skin specific, miR-203 is made solely by keratinocytes where it regulates terminal differentiation, with several studies describing miR-203 dysregulation in patients with psoriasis (Sonkoly et al., 2007; Sonkoly et al., 2010; Zibert et al., 2010; Joyce et al., 2011). In addition to regulating keratinocyte differentiation by p63 inhibition, miR-203 also targets suppressor of cytokine signaling 3 (SOCS3), which regulates STAT3, a transcription factor known to play a role within the development of psoriatic lesions. Increased miR-203 is associated with reduced SOCS3 and elevated STAT3 signalling within psoriasis (Sonkoly et al., 2010). However, studies have since challenged the ability of miR-203 to successfully target SOCS3, presenting pro-inflammatory cytokines such as TNF- $\alpha$  and IL-24 as main targets for elevated miR-203 in psoriasis (Primo et al., 2012).

#### **miR-21**

miR-21, an important oncogenic miRNA responsible for inhibiting apoptosis and promoting inflammation with studies describing elevated levels in psoriatic lesions (Sonkoly et al., 2007; Joyce et al., 2011). Recently, miR-21 has been shown to target Metalloproteinase inhibitor 3 (TIMP3) which in turn elevates TNF- $\alpha$  by activation of the metalloproteinase, TNF- $\alpha$ -converting enzyme (TACE), contributing to the increased levels of TNF- $\alpha$  observed in

psoriasis (Guinea-Viniegra et al., 2014). Furthermore, inhibition of miR-21 increased rates of apoptosis in activated human CD4<sup>+</sup> T cells suggesting that overexpression of miR-21 in psoriasis may contribute T cell infiltration (Meisgen et al., 2012). Additionally, key components that adenylate and degrade miR-21 have been shown to be disrupted in psoriasis leading to enhanced miR-21 levels (Boele et al., 2014).

### **miR-31**

MiR-31, an miRNA with a dramatic 40-fold upregulation in psoriatic lesions has been shown to modulate the production of cytokines and chemokines in keratinocytes by targeting serine/threonine kinase 40 (STK40). STK40 is a negative regulator of NF- $\kappa$ B in keratinocytes. By targeting STK40 miR-31 regulates NF- $\kappa$ B signaling and therefore production of keratinocyte-derived cytokines and chemokines (Joyce et al., 2011; Xu et al., 2013). Interestingly, miR-31 seems to self-regulate its own expression, with NF- $\kappa$ B activity resulting in elevated proliferation and further upregulation of miR-31 expression (Yan et al., 2015).

### **miR-146a**

One of the most highly upregulated miRNAs in psoriasis, miR-146a plays a key role in regulating immune responses, by directly targeting TNF receptor-associated factor 6 (TRAF6), IL-1 receptor-associated kinase 1 (IRAK1) and caspase recruitment domain-containing protein 10 (CARD10) leading to diminished NF- $\kappa$ B activity and reduced production of pro-inflammatory cytokines such as IL-6 and TNF- $\alpha$  (Taganov et al., 2006; O'Connell, Rao and Baltimore, 2012; Rebane et al., 2014). Furthermore, transgenic miR-146a knockout mice exhibit an elevated Th1 type response that subsequently leads to autoimmunity (Lu et al., 2010). Dysregulated miR-146a has been shown to have a strong positive correlation with IL-17 expression in both psoriatic epidermal and dermal compartments as well as peripheral blood mononuclear cells (PBMCs) (Xia et al., 2012; Srivastava et al., 2017). Additionally, a single

nucleotide polymorphism (SNP) of precursor miR-146a has been associated with earlier onset of psoriasis (Srivastava et al., 2017).

### **miR-125b**

miR-125b is an example of a downregulated miRNA associated with psoriasis, with levels significantly decreased in psoriatic skin and serum (Sonkoly et al., 2007; Xu et al., 2011; Koga et al., 2014). In primary human keratinocytes, reductions in endogenous miR-125b resulted in elevated proliferation and decreased differentiation, whereas overexpression suppressed proliferation and promoted expression of several differentiation markers, with these responses mediated by fibroblast growth factor receptor 2 (FGFR2) (Xu et al., 2011). In addition, a very recent study identified ubiquitin-specific peptidase 2 (USP2) as a target for miR-125b in psoriasis, showing that USP2 was upregulated in psoriatic lesions and that knockdown through miR-125b overexpression or targeted siRNA resulted in reduced proliferation and enhanced differentiation (Wei et al., 2017). Furthermore, TNF- $\alpha$  is a direct target of miR-125b, therefore, decreases in miR-125b in psoriatic lesions may contribute to elevated TNF- $\alpha$  observed in lesions (Tili et al., 2007).

### **miR-210**

Increased levels of miR-210, a hypoxia related miRNA, have been observed in psoriasis where it contributes to pathogenesis by disrupting regulatory T (Treg) cell activity (Zhao et al., 2014). miR-210 is significantly upregulated in PBMCs and CD4<sup>+</sup> T cells of psoriasis patients and is associated with increased levels of pro-inflammatory cytokines, such as IL-17, by direct targeting of forkhead box P3 (FOXP3) a master regulator of Treg cell function (Zhao et al., 2014). In addition, a very recent study has demonstrated that elevated miR-210 results in enhanced Th1 and Th17 cells in peripheral blood and skin lesions of psoriasis patients as well as psoriatic mouse models, with miR-210 silencing preventing development of psoriasis-like inflammatory responses (Wu et al., 2018).

## **miR-184**

miR-184, a unique miRNA that can regulate expression of other miRNAs by direct targeting of AGO2, has been shown to be upregulated in psoriatic lesions. The same study also demonstrated that expression of miR-184 can be induced by psoriasis-linked pro-inflammatory cytokines such as IL-22 and oncostatin M in primary human keratinocytes and reconstituted human epidermis. However, prior miRNA profiling studies failed to find a significant dysregulation of miR-184 in psoriatic skin and therefore its involvement remains unclear (Joyce et al., 2011; Roberts et al., 2013).

## **1.4. Keratinocytes**

Keratinocytes are kept under strict homeostasis to maintain normal biological functions with errors in this regulation leading to severe cutaneous disorders such as eczema (Proksch, Folster-Holst and Jensen, 2006), psoriasis (Bowcock and Krueger, 2005), harlequin ichthyosis (Dale et al., 1990) and various cancers (Miller, 1991; Alam and Ratner, 2001). There are several established methods to culture keratinocytes and mimic their differentiation *in vitro* using monolayer or organotypic 3D cultures and addition of a differentiation agent such as calcium (Sun and Green, 1976).

### **1.4.1. Differentiation**

A fine balance between proliferation and differentiation underpins keratinocyte biology. The maintenance of this homeostasis requires precise coordination of molecular events. Differentiation is initiated when basal cells hit their proliferative capacity and exit the basal compartment. Traditionally, it is thought that keratinocytes leave the cell cycle, undergo growth arrest and commit to terminal differentiation. The cell cycle plays a key role in basal cell maintenance and is commonly deregulated upon the onset of differentiation with suprabasal

keratinocytes expressing cell cycle proteins such as cyclin E to support their enlargement (Zanet et al., 2010). Cell cycle progression is controlled largely by cyclins and cyclin dependent kinases (Cdks) with a group of molecules called cyclin dependent kinase inhibitors (CDKI) responsible for the control of the cell cycle at various stages (Sherr and Roberts, 2004).

#### **1.4.1.1. Gene Expression**

Nuclear transcription factors play a huge role in keratinocyte proliferation and differentiation by integrating signals from the cell surface using signal transduction pathways, these transcription factors include: AP-1 (Activator protein-1), AP-2 (Activator protein-2), Sp1 (Specificity protein), NF- $\kappa$ B (Nuclear factor kappa B), CREB (cAMP response element-binding protein) and NFAT (Nuclear factor of activated T cells). AP-1 and AP-2 are homo- or heterodimers that have been shown to be important for activating transcription of K1, K5, loricrin, involucrin, profilaggrin and transglutaminase (Eckert, Crish and Robinson, 1997). Sp1 has been shown to regulate expression of transglutaminase, involucrin and K5 (Eckert, Crish and Robinson, 1997). Moreover, Sp1 is known to interact with the NFAT family of transcription factors which act as coactivators to positively regulate expression of p21 (Santini et al., 2001). NF- $\kappa$ B is essential during keratinocyte differentiation and is thought to protect keratinocytes from apoptosis as they undergo cornification with anti-apoptotic NF- $\kappa$ B gene targets such as those in the Bcl-2 family significantly upregulated during *in vivo* and murine epidermal differentiation (Lippens et al., 2011). NFAT family consists of five Ca<sup>2+</sup>-regulated members (NFAT1-5) closely related to the NF- $\kappa$ B family. NFAT regulates differentiation in several cell types by activating expression of a large array of genes. In human keratinocytes, NFAT1 localises to the nucleus during differentiation where it is believed to activate expression of a cohort of differentiation-linked genes (Santini et al., 2001; Al-Daraji et al., 2002). NFAT is important to the regulation of the cell cycle. In primary epidermal mouse keratinocytes,

NFAT1 and NFAT2 bind directly to a calcium-response element (CARE) in the p21 promoter during  $\text{Ca}^{2+}$ -dependent differentiation leading to induction of p21 and initiation of differentiation through growth arrest (Santini et al., 2001).

#### **1.4.1.2. p21**

p21 was originally identified as an intermediary of p53-induced growth arrest particularly in cellular senescence and is now strongly associated with growth arrest during keratinocyte differentiation. In murine epidermal keratinocytes, when p21 is knocked down, proliferative potential is significantly elevated coupled with a drastic reduction in differentiation marker expression when these cells are differentiated (Missero et al., 1996). In addition, a later study demonstrated keratinocytes from transgenic mice lacking p21 exhibit enhanced proliferative potential with p21 knockout cultures presenting higher clonogenic properties than normal cells (Topley et al., 1999). Furthermore, it has been demonstrated that p21 downregulates proliferation-linked Wnt signalling by binding to its promoter and inhibiting expression (Devgan et al., 2005). In human skin, expression of p21 has been shown to accumulate in early differentiating layers and to promote growth arrest. However, when expression is maintained throughout later stages then differentiation is suppressed, suggesting that p21 is tightly regulated and must be inactivated before late stage differentiation can proceed (Topley et al., 1999; Devgan et al., 2006). Additionally, *in vitro* keratinocyte growth led to induction of p21 and accumulation of G1-stage cells in a cell density-dependent manner (Cho et al., 2008). Furthermore, by removal of the differentiation stimulus, early stages of *in vitro* keratinocyte differentiation have been reversed, a process in which p21 appears to be critical, with a significantly elevated number of p21 knockout keratinocytes returning to a proliferating phenotype following differentiation agent removal when compared to normal cells (Topley et al., 1999).

### **1.4.1.3. Cyclin E**

An emerging body of work challenges traditional keratinocyte differentiation mechanisms and highlights the importance of cyclin E during keratinocyte differentiation (Fig. 1.6). Cyclin E, essential for G1-S phase transition, has been shown to accumulate in differentiating human epidermal keratinocyte and in outer layers of the human epidermis (Zanet et al., 2010; Freije et al., 2012). Moreover, overexpression of cyclin E in basal keratinocytes promoted expression of involucrin, reduced clonogenic potential and ultimately led to terminal differentiation (Murray, 2004; Freije et al., 2012). Furthermore, cyclin E overexpression has been shown to cause genetic instability in several cell types with the subsequent DNA damage response (DDR) programs responsible for the regulation of cellular differentiation (Hwang and Clurman, 2005; Sherman, Bassing and Teitell, 2011). Genotoxic agents such as doxorubicin lead to DNA damage-induced terminal differentiation in human epidermal keratinocytes (Freije et al., 2012). A sensitive marker for DNA double-strand breaks (DSBs) and therefore a key component of DNA repair is the histone protein, H2AX (H2A histone family member X). A histone H2A family member that organises DNA into chromatin, H2AX in humans becomes rapidly phosphorylated on serine139 within the carboxyl terminus, at the sites of DSBs, becoming gammaH2AX ( $\gamma$ H2AX) (Bonner et al., 2008). When cyclin E is abnormally elevated, levels of  $\gamma$ H2AX are significantly elevated. Leading to increases in DDR elements such as p53 and p21, mitosis failure and ultimately terminal differentiation (Freije et al., 2012).

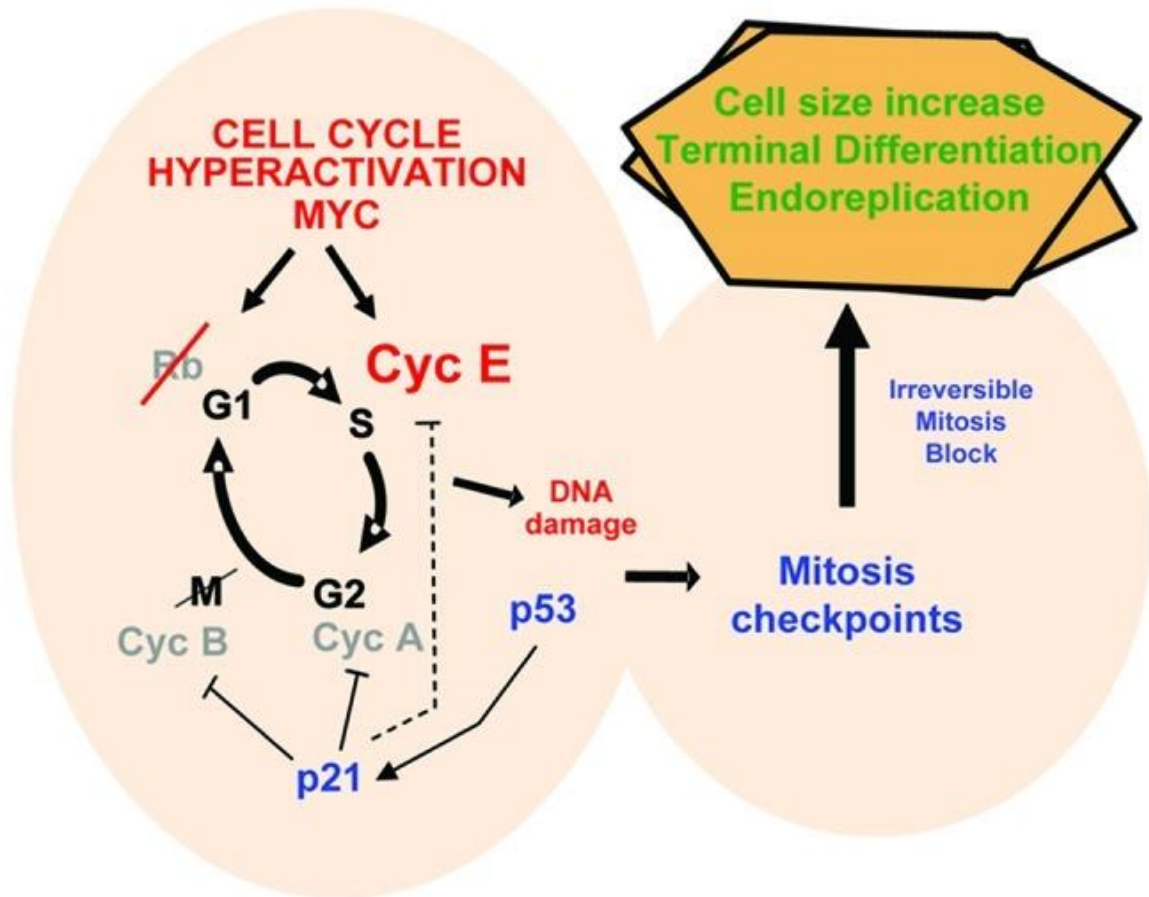


**Figure 1.6. Molecular Mechanism of HPEK Differentiation.** Cell cycle dysregulation resulting from cyclin E accumulation causes replication stress and DNA damage. DDR effectors such as p21 are recruited and inhibit mitotic factors such as cyclin A triggering mitosis checkpoints that prevents cell division. Consequently, cell size increases with DNA re-replication and terminal differentiation is triggered. Taken from Gandarillas, 2012 (Gandarillas, 2012).

#### 1.4.1.4. Calcium and Store Operated Calcium Entry

The most commonly used technique to control keratinocyte differentiation *in vitro* is a calcium switch, whereby the levels of extracellular calcium in the growth medium are elevated. Early work on mouse epidermal keratinocytes by Hennings and colleagues documented that levels of calcium ( $\text{Ca}^{2+}$ )  $<0.1$  mM suppress differentiation and allow keratinocytes to proliferate rapidly whereas high concentrations ( $>1.0$  mM) induce terminal differentiation at varying rates (Hennings et al., 1980). Physiologically,  $\text{Ca}^{2+}$  forms a sharp gradient throughout the epidermis peaking within the stratum granulosum. Although,  $\text{Ca}^{2+}$  levels within the stratum basale are expected to be the lowest, keratinocytes in fact have variable amounts when compared to the stratum spinosum, with a number of keratinocytes holding large amounts of free cytosolic calcium [ $\text{Ca}^{2+}$ ] which is thought to promote differentiation and migration from the basal layer. It is the sustained and steady increase of [ $\text{Ca}^{2+}$ ] that contributes to keratinocyte differentiation, with transient increase in [ $\text{Ca}^{2+}$ ] proving ineffective in reaching the required threshold (Bikle, Xie and Tu, 2012). Elevated [ $\text{Ca}^{2+}$ ] initiates differentiation by promoting expression of a large cluster of differentiation related genes, formation of desmosomes and activation of transglutaminases, as well as  $\text{Ca}^{2+}$ -dependent proteases (Eckert, Crish and Robinson, 1997). In keratinocytes, interactions of various agonists with receptors can stimulate phospholipase C (PLC). Stimulation of PLC leads to hydrolysis of phosphatidylinositol 4,5-bisphosphate ( $\text{PIP}_2$ ) which in turn forms the secondary messengers inositol trisphosphate ( $\text{IP}_3$ ) and diacylglycerol (DAG), with  $\text{IP}_3$  inducing  $\text{Ca}^{2+}$  release from the endoplasmic reticulum (ER) and DAG activating other pathways including protein kinase C (PKC) and mitogen-activated protein kinase (MAPK) (Bootman, 2012). Phorbol-12-myristate-13-acetate (PMA) and vitamin D ( $1,25(\text{OH})_2\text{D}_3$ ), are thought to have overlapping signalling responses with  $\text{Ca}^{2+}$ . PMA is known to promote keratinocyte differentiation through direct and potent activation of PKC, independent of extracellular  $\text{Ca}^{2+}$  levels. PKC, in turn, activates transcription factors such as

AP-1, Sp1, NF- $\kappa$ B and CREB, resulting in expression of key differentiation linked proteins such as K1 and p21 (Matsui et al., 1993; Bikle, 2011). Vitamin D, produced and processed solely in the epidermis, promotes differentiation through activation of genes containing the Vitamin D response element (VDRE) such as involucrin, by means of vitamin D receptor (VDR) transcriptional activity (Bikle, 2011).

Store-operated calcium entry (SOCE), a primary source of  $\text{Ca}^{2+}$  signalling in nonexcitable cells, responds to the  $\text{IP}_3$ -induced ER  $\text{Ca}^{2+}$  depletion utilising  $\text{Ca}^{2+}$  release-activated channel (CRAC) channels. Activation of  $\text{IP}_3$  receptor ( $\text{IP}_3\text{R}$ ) by  $\text{IP}_3$  leads to release of  $\text{Ca}^{2+}$  and a reduction in ER  $\text{Ca}^{2+}$  concentration. This decrease is recognised by stromal interaction molecule (STIM), specifically by  $\text{Ca}^{2+}$  binding EF-hand motifs, which undergo a conformational change promoting oligomerisation and relocalisation within the ER membrane towards ER-plasma membrane junctions, accumulating in puncta. STIM then swiftly recruits a CRAC known as ORAI which becomes reversibly trapped by physical interactions with STIM, causing conformational opening of ORAI and allowing entry of  $\text{Ca}^{2+}$  (Fig. 1.7) (Prakriya and Lewis, 2015). SOCE is a vital pathway for normal keratinocyte biology with knockdown of either STIM or ORAI leading to attenuated growth in basal keratinocytes and a lack of growth arrest during terminal differentiation (Numaga-Tomita and Putney, 2013). The NFAT signalling pathway is key downstream effector of SOCE. Sustained elevated  $[\text{Ca}^{2+}]$  leads to activation of the bilobial  $\text{Ca}^{2+}$ -effector protein, calmodulin (CaM), which contains four  $\text{Ca}^{2+}$  binding EF hands. Following activation, CaM interacts with the serine/threonine protein phosphatase, calcineurin (CaN) and releases the autoinhibitory domain from CaNs active site, which in turn dephosphorylates inactive NFAT, initiating nuclear translocation by exposing a nuclear localisation signal region. Following nuclear translocation, NFAT regulates the expression of responsive genes by binding to their target promoter regions individually or

together with other nuclear transcription factors (Fig. 1.7) (Rumi-Masante et al., 2012; Mognol et al., 2016).

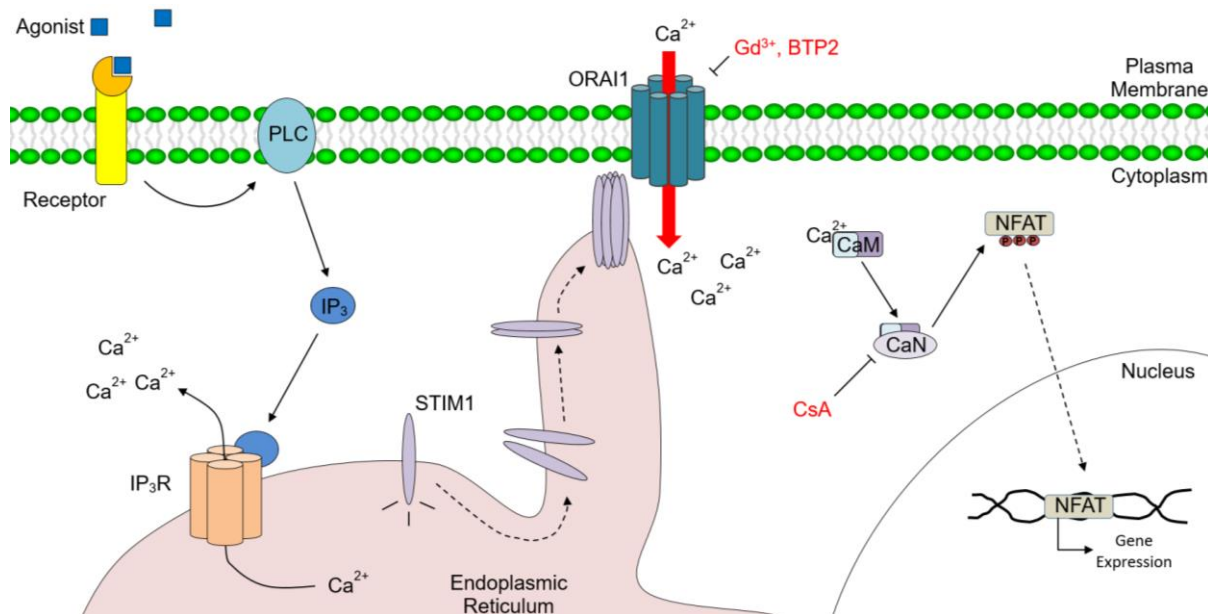


**Figure 1.7. Store-operated Calcium Entry (SOCE).** A graphical depiction of SOCE whereby agonist stimulation of membrane receptors leads to activation of phospholipase C (PLC) that in turn produces inositol trisphosphate (IP<sub>3</sub>). IP<sub>3</sub> stimulates the IP<sub>3</sub> receptor (IP<sub>3</sub>R) and consequently causes depletion of endoplasmic reticulum calcium (Ca<sup>2+</sup>) stores. Stromal interaction molecule (STIM) senses reduced endoplasmic reticulum Ca<sup>2+</sup> pools and translocates to puncta at ER-plasma membrane junctions where it activates the store-operated channel (SOC), ORAI, allowing influx of extracellular Ca<sup>2+</sup>. Sustained increases in cytoplasmic [Ca<sup>2+</sup>] results in activation of calmodulin (CaM) which in turn stimulates calcineurin (CaN). Activated CaN dephosphorylates nuclear factor of activated T-cells (NFAT) family members triggering nuclear translocation and expression of target genes.

The activity of SOCE, and therefore processes dependent on SOCE, can be perturbed using inhibitors. The most commonly used SOCE modulators are the trivalent lanthanides including La<sup>3+</sup> (lanthanum) and Gd<sup>3+</sup> (gadolinium). Submicromolar concentrations are required for complete blockade of SOCE although they show inhibitory activity against other cationic ion channels, which therefore limits their reliability in SOCE specific experiments (Putney, 2010). Another widely used group of SOCE inhibitors are derivatives of pyrazole compounds with BTP2 (*N*-[4-[3,5-Bis(trifluoromethyl)-1*H*-pyrazol-1-yl]phenyl]-4-methyl-1,2,3-thiadiazole-5-carboxamide) the most common. Although the mechanism of action has not been fully clarified, it is thought that BTP2 inhibits NFAT activity without effecting CaN, therefore suggesting likely effects on upstream Ca<sup>2+</sup> signals such as inhibition of ORAI1. Like the

lanthanides, BTP2 is capable of inhibiting SOCE at submicromolar concentrations, but it has considerably more selectivity over other cationic ion channels (Vandenberghe et al., 2013). Cyclosporin A (CsA) is a commonly used downstream inhibitor for SOCE as it modulates NFAT activity. Once in the cell, CsA forms a complex with cyclophilin A which binds to CaN and inhibits its phosphatase activity, consequently preventing nuclear translocation of NFAT (Fig. 1.7) (Matsuda and Koyasu, 2000).

### **1.4.1.1. miRNAs & Differentiation**

Increasing evidence suggests that miRNAs play a significant role within differentiation of epidermal stem cells (Hildebrand et al., 2011; Zhang et al., 2011). Depletion of proteins vital to miRNA function leads to the disruption of skin homeostasis leading to improper barrier formation and hyperproliferation (Ghatak et al., 2015).

miR-203, is a well-known skin-preferred miRNA known to promote differentiation by limiting proliferative capacity and inducing cell-cycle exit within basal keratinocyte progenitors. miR-203 exerts its function through regulation of p63 (Lena et al., 2008; Yi et al., 2008a). miR-205 has been shown to regulate clonal expansion of epidermal stem cells by targeting phosphoinositide 3-kinase/Akt pathway (PI3K/Akt), with downregulated miR-205 promoting differentiation (Wang et al., 2013). MiR-24 has recently been identified as a key keratinocyte differentiation regulator expressed within suprabasal layers, with ectopic basal expression causing accelerated differentiation and premature cell-cycle exit. MiR-24 is thought to regulate actin cytoskeletal rearrangement promoting a shift from basal to suprabasal F-actin structures by targeting important cytoskeletal modulators (Amelio et al., 2012). Recently, miR-214 has been shown to control epidermal stem cell activity, contributing to the regulation of skin morphogenesis by targeting  $\beta$ -catenin, a key component within the Wnt signalling pathway, with miR-214 overexpression inhibiting keratinocyte differentiation (Ahmed et al., 2014). A very recent study demonstrates regulation of keratinocyte differentiation using miR-23b which directly targets TGIF and consequently activates transforming growth factor beta (TGF- $\beta$ ) signalling, leading to keratinocyte differentiation (Barbollat-Boutrand et al., 2017). Comprehensive analysis of miRNA expression within keratinocyte differentiation has revealed a plethora of upregulated miRNAs, suggesting that many miRNAs work in situ contributing to gene regulation during keratinocyte differentiation, yet still our present understanding of global

miRNA expression and its role within keratinocyte biology remains restricted (Hildebrand et al., 2011).

Robert Lavkers laboratory first proposed a role for miR-184 in the regulation of keratinocyte biology when they detected high levels of miR-184 in mouse corneal epithelium but not in foot-pad epithelium. Based on this discovery they later found miR-184 promotes proliferation of corneal epithelium by antagonising miR-205 and indirectly modulating SH2-domain containing inositol 5-phosphatase 2 (SHIP2) (Ryan, Oliveira-Fernandes and Lavker, 2006; Yu et al., 2008). In contrast, a recent study in retinal pigment epithelium has shown that miR-184 targets Akt2 to suppress proliferation and support differentiation (Jiang et al., 2016). Although miR-184 was not listed as a miRNA differentially expressed during epidermal differentiation a very recent study, published following the conception of this project, has shown miR-184 to be significantly elevated in the suprabasal layers of mouse epidermis (Hildebrand et al., 2011; Nagosa et al., 2017). Through use of loss- and gain-of-function mouse models, it was demonstrated that miR-184 maintains the equilibrium between proliferation and differentiation by direct regulation of factor inhibiting HIF (FIH) and K15. Loss of miR-184 led to decreased expression of notch and its downstream targets as well as enhanced p63 activity resulting in hyperplasia of the stratum spinosum. Over expression of miR-184 led to epidermal hypoplasia through heightened Notch signalling and reduced p63 expression (Nagosa et al., 2017). Although the ability of miR-184 to regulate proliferation and differentiation has been demonstrated in ocular keratinocytes, and despite recent work by Nagosa et al., miR-184's role in the regulation of the proliferation: differentiation switch in epidermal keratinocytes has remained relatively unexplored.

## **1.4.2. Migration**

Cell migration plays a fundamental role in the development and maintenance of multicellular organisms. The migration of keratinocytes is a crucial step for processes such as wound healing, where keratinocytes migrate from the wound edge, and differentiation, where keratinocytes migrate upwards through stratified layers. Keratinocyte migration requires complex coordination of cytoskeletal dynamics and cellular adhesions whereby cellular polarisation and formation of protrusions, adhesion of newly formed protrusions to surrounding extracellular matrix (ECM) and adhesion deassembly to aid rear retraction, lead to cellular movement. Despite the emerging role for miR-184 in migration, in the context of epidermal keratinocyte migration the role of miR-184 is unknown.

### **1.4.2.1. miRNAs & Migration**

In recent years, the role of miRNAs in keratinocyte migration and wound healing have begun to surface. The initial phases of wound healing are dominated by inflammatory responses. A recent study has suggested that miR-132 supports transition from inflammatory to proliferative phases. Levels of miR-132 are downregulated in chronic wounds with replenishment ameliorating inflammation and promoting wound closure (Li et al., 2017). Upwards migration of keratinocytes through stratified layers is vital for normal differentiation and is facilitated through regulation of cell-cell connections called desmosomes. A recent study has shown that miR-29 disrupts formation of desmosomes by direct targeting of desmocollin-2 leading to perturbed barrier function (Kurinna et al., 2014). During wound healing, migration of keratinocytes is stimulated by changes in the local environment, including altered ECM (Eming, Martin and Tomic-Canic, 2014). Work on HaCaTs has implicated miR-21 in TGF- $\beta$  induced keratinocyte migration (Yang et al., 2011). MiR-21 was shown to be upregulated by TGF- $\beta$ , where it supported migration by directly targeting TIMP3, an inhibitor of a group of molecules

called matrix metalloproteinases (MMPs) that are responsible for ECM turnover, causing adhesive or non-adhesive phenotypic changes during migration (Yang et al., 2011). Another key factor in keratinocyte migration and wound healing is enhanced cellular proliferation behind the migration front/wound edge. A recent study has demonstrated that miR-31 is highly upregulated during re-epithelization and that the expression of epithelial membrane protein 1 (EMP-1) is negatively correlated with miR-31 levels. It was shown that miR-31 directly targets EMP-1 and derepresses keratinocyte proliferation and migration, with silencing of EMP-1 mimicking miR-31 overexpression (Li et al., 2015). Complex coordination of the actin skeleton is vital to cellular movement whereby actin polymerisation in the direction of migration allows for extension of the cells leading edge and attachment to new ECM, a process completed by quick depolymerisation in the trailing compartment (Petrie and Yamada, 2012). Work by Amelio and colleagues demonstrates that miR-24 causes actin remodelling through suppression of cytoskeletal modulators resulting in inhibition of keratinocyte migration (Amelio et al., 2012). The final stages of migration rely on the arrest of migration and proliferation in order to regain homeostasis and prevent keratinocyte proliferation beyond closure of the wound. A study on mouse keratinocytes has shown that overexpression of miR-483-3p inhibits keratinocyte migration through modulation of proliferation-associated proteins such as Ki67 (Bertero et al., 2011).

There is a growing body of evidence suggesting that miR-184 can regulate migration with an early study in corneal epithelium demonstrating that suppression of miR-184 allows miR-205 to promote keratinocyte migration through repression of SHIP2 (Yu et al., 2010). Recent work backs up the tumour suppressive role of miR-184, showing that miR-184 reduced migration rates over 72 hours in retinal pigment epithelium by directly targeting Akt2 signalling (Jiang et al., 2016). Conversely, a pro-invasive role for miR-184 has been demonstrated in cataracts of mice where suppression of the highly expressed miR-184 results

in attenuated expansion and migration of ocular epithelial tissue (Hoffmann et al., 2012). A recent study backs up the oncogenic role for miR-184 where migration and invasiveness is elevated in human glioma cell lines overexpressing miR-184 by the positive regulation of hypoxia-inducible factor-1 alpha (HIF-1 $\alpha$ ), through suppression of its inhibitor, FIH-1 (Yuan et al., 2014).

## **1.5. miR-184**

In humans, miR-184 is located within region 25.1 on the q-arm of chromosome 15. Producing an 84 bp transcript, miR-184, is an example of an individually transcribed miRNA, whereby it is not clustered with or close to other miRNAs (Weitzel et al., 2011). Over the past decade the ability of miR-184 to regulate cellular growth and differentiation across numerous cells types has been documented. Initial miRNA profiling experiments showed miR-184 to be heavily downregulated in neuroblastoma and that overexpression of miR-184 in neuroblastoma cell lines led to disrupted cell cycle dynamics (Chen and Stallings, 2007). Similarly, in hepatocellular carcinoma cell lines, miR-184 has been shown to promote proliferation by significantly altering cell cycle dynamics (Wu et al., 2014). Furthermore, miR-184 has been shown to regulate the balance between proliferation and differentiation in adult neural stem cells by promoting notch signalling, with cells introduced to elevated levels miR-184 differentiating into ~30% less astrocytes and neurons (Liu et al., 2010). Previous work in our group showed that miR-184 directly represses the central RISC protein known as AGO2 in both HaCaTs and HPEK (Roberts et al., 2013). A recent mice study confirms this finding, demonstrating that miR-184 directly targets Ago2 in pancreatic  $\beta$  cells, resulting in reduced  $\beta$  cell islet mass and subsequent decreases in circulating insulin levels (Tattikota et al., 2014).

## 1.6. Research Aims

The epidermis exists in a homeostasis between proliferating and differentiating keratinocytes and when this homeostasis is upset, it can lead to a plethora of cutaneous disorders. There remains an unmet need in dermatology for innovative topical agents that achieve better long-term outcomes with fewer side effects. Recently, miRNAs have emerged as key regulators of keratinocyte biology and disease, acting as conceivable targets for patient-specific treatments. Previous work in our group demonstrated elevated levels of miR-184 in psoriatic lesions where it was thought to modulate the expression of AGO2 (Roberts et al., 2013). Very recent work by Shalom-Feuerstein and colleagues report miR-184 in differentiating keratinocytes (Nagosa et al., 2017). However, despite recent advances in the field, an understanding of the role of miR-184 in keratinocyte biology remains poorly described. With this in mind, the aims of this thesis are:

1. Investigate miR-184 expression during HPEK differentiation and elucidate the regulatory mechanisms.
2. Examine the effects of ectopic miR-184 on HPEK proliferation and differentiation by utilising synthetic miR-184 mimics and miR-184 LNA inhibitors.
3. Investigate miR-184 expression and function during HPEK migration.
4. Explore epidermal AGO dynamics and examine the miR-184:AGO2 axis during HPEK differentiation

## **2. Materials and Methods**

## **2.1. Materials**

Materials and manufactures are listed by technique. All laboratory consumables were provided by Sarstedt, Leicester, UK unless otherwise stated. Pre-designed primers were all purchased from Qiagen, Manchester, UK.

## **2.2. Cell Culture**

### **2.2.1. Isolation**

Human Primary Epidermal Keratinocytes (HPEK) were either purchased from CellnTec, Bern, Switzerland or isolated from normal adult foreskin of multiple donors (Liverpool John Moores University Research Ethics Committee approval number 16/PBS/008). Circumcisions were transported in Dulbeccos Modified Eagle Medium (DMEM) containing 4500 g/L glucose and 500 U/mL Penicillin/Streptomycin (P/S; Sigma-Aldrich, Gillingham, UK) with all further manipulations performed in a sterile type II biological safety cabinet using sterile instruments. To start with, foreskins were transferred to a 10 cm petri dish (Sigma, UK) and were washed in sterile phosphate buffered saline (PBS) containing 500 U/mL P/S. Next, the connective, vascular and adipose tissues were removed using forceps and a scalpel that were kept sterile with 100% ethanol (Sigma, UK) before another wash with sterile PBS plus P/S (Fig. 2.1). In order to separate the epidermis from the dermis, the foreskins were incubated in PBS containing 500 U/mL P/S, 2.5 µg/mL amphotericin B (amp B; Sigma-Aldrich, UK) and 2 mg/mL dispase (Sigma-Aldrich, UK) overnight at 4°C. To increase dispase penetration the skin was scored through the epidermis in a grid pattern every 5 mm prior to incubation. The following day the foreskins were incubated further at room temperature for 1-2 hours before transferring to a sterile 10 cm petri dish (Fig. 2.1). Following this, the epidermis was peeled from the dermis using sterile forceps and added to a 15 ml universal tube containing 5 ml of accutase (CnT-accutase-100; CellnTec, Switzerland) before a 10 minute incubation at 37°C, 5% CO<sub>2</sub> (Fig.

2.1). After incubation, the universal tube was shaken vigorously and the accutase was deactivated using 10 ml of CnT-Prime media (CnT-Pri; CellnTec, Switzerland) prior to centrifugation at 260 Relative Centrifugal Force (RCF) for 5 minutes. Next, the supernatant was removed and the pellet was suspended in 15 ml of CnT-Pri supplemented with CnT-IsoBoost (CnT-ISO-50; CellnTec, Switzerland), 500 U/mL P/S and 2.5 µg/mL amp B before transfer to a T75 tissue culture flask and incubated at 37°C, 5% CO<sub>2</sub> overnight (Fig. 2.1). The following day the media was aspirated and 20 ml of supplemented CnT-Pri was added before incubation at 37°C, 5% CO<sub>2</sub>. Isolated HPEKs were observed daily with supplemented CnT-Pri replaced every 2 days until reaching 70-80% confluence when they were subcultured for either cyrostorage or experimental work (described in 2.1.2).

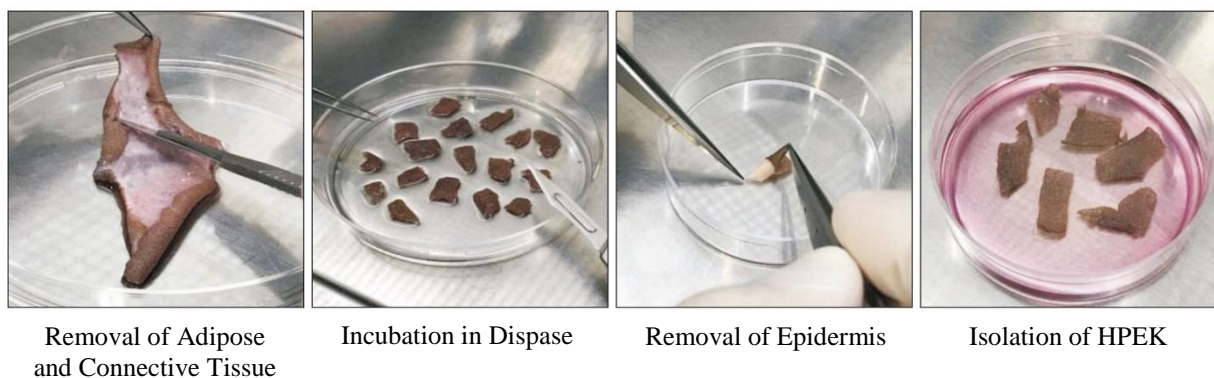


**Figure 2.1: Isolation of HPEK.** Using sterile instruments excess fatty and connective tissue was removed from circumcised human foreskin. Samples were cut into smaller pieces and the epidermis was repeatedly scored before overnight incubation in dispase. The following day, skin samples were incubated in dispase for a further 1-2 hours before separation of the epidermis from the dermis. HPEK were then isolated by disassociation with accutase and growth in a selective epidermal medium. Taken from Choi et al., 2017.

### 2.2.2. General Cultivation

HPEKs from p1-5 were maintained in CnT-Pri without antibiotics/antimycotics and cultured in a sterile type II biological safety cabinet using sterile instruments, pre-warmed media and following aseptic practices. Upon reaching 70-80% confluence HPEKs were passaged as follows: media was aspirated from the T75 flask and the monolayer was washed with 10 ml of PBS (without Calcium or Magnesium) for 3-5 minutes at room temperature to remove any residual media and protein that may affect the effectiveness of accutase. Next, PBS was aspirated and 4 ml of accutase was added to the monolayer with enzymatic dissociation taking place at 37°C, 5% CO<sub>2</sub> for 5-10 minutes. Cell detachment was monitored using a light microscope until around 90% of cells had detached, at which point the accutase was deactivated using 5 ml of CnT-Pri with detachment aided by gentle tapping of the culture vessel. The cell suspension was then centrifuged at 180 RCF for 7 minutes. Following centrifugation, the supernatant was aspirated and the cell pellet was resuspended in 10 ml of CnT-Pri before seeding at a density of 4.0 x10<sup>3</sup> cells/cm<sup>2</sup> and incubating at 37°C, 5% CO<sub>2</sub> in a humidified atmosphere. Culture media was changed every 2-3 days.

For cryostorage, HPEK that had reached 70-80% confluence were passaged as previously described. Cells were made up to a concentration of 2.0 x10<sup>6</sup> cells/mL in CnT-Pri to which an equal volume of cold freezing medium (CnT-CRYO-50; CellnTec, Switzerland) was added dropwise whilst gently swirling the tube to mix. Following this, the suspension was left to osmotically equilibrate on ice for 5 minutes, before transfer to pre-cooled cryovials (Thermofisher Scientific, Runcorn, UK). Finally, cryovials were transferred to a Mr. Frosty (Thermofisher Scientific, UK) and stored at -80°C, before transfer to liquid nitrogen the following day.

For thawing, 10 mL of CnT-Pri was added to a T75 flask and pre-equilibrated in a 37°C, 5% CO<sub>2</sub> incubator. A cryovial was removed from the liquid nitrogen store and immediately

placed in a 37°C water bath to rapidly thaw the cells. To prevent the temperature from reaching over 4°C the cyrovial was gently swirled. Once only a few ice crystals remained the cells were resuspended gently 2-3 times, before adding dropwise to the pre-equilibrated T75 1 mL of CnT-Pri was used to collect any cells remaining in the cyrovial.

### **2.2.3. Differentiation Assay**

HPEK were seeded at a density of  $2-3 \times 10^4$  cells/cm<sup>2</sup>. Usually, after 2-3 days under basal conditions cells would reach 90% confluency, at which point the culture medium was aspirated and the monolayer was washed with PBS for 2-3 minutes at room temperature in order to remove any residual CnT-Pri media. Following this, a differentiation medium (Table 2.1) was added, before incubating at 37°C, 5% CO<sub>2</sub> in a humidified environment for up to 5 days (Fig. 2.2).

### **2.2.4. Scratch Assay**

HPEK were cultured as described in 2.1.2. or nucleofected as described in 2.2. and grown under basal conditions in 6-well dishes (Sarstedt, Leicester, UK) for 2 days in order to approach confluence. Using a p200 pipette tip, held at an angle of 30 degrees to limit width variation, linear scratches were made every 0.5 cm both vertically and horizontally in a lattice formation. Monolayers were then washed in PBS for 2-3 mins at room temperature to remove damaged cells and debris before addition of either basal or differentiation medium. Cells were allowed to migrate into the scratch for up to 5 days.

### **2.2.5. Treatment with SOCE Inhibitors**

Cells were cultured and grown under basal conditions for 2-3 days until around 90% confluency, at which point the medium was aspirated and the cells were washed in PBS for 2-3 minutes at room temperature. Following this, cells were pre-treated for 1 hour with 1 μM of Gd<sup>3+</sup>, a trivalent cation which is a general inhibitor of Ca<sup>2+</sup> influx pathways, or 1 μM BTP2 a pyrazole derivative which is a more potent blocker of Orai. Following treatment, cells were differentiated for up to 5 days by addition of 1.5 mM Ca<sup>2+</sup>. After 2.5 days cells were recharged with inhibitors.

**Table 2.1. Differentiation Medium.** \*CnT-Pri was heat inactivated for 1 hour at 60°C with the aim of deactivating proliferation promoting growth factors

Calcium	Phorbol Myristate Acetate (PMA)
Heat inactivated CnT-Pri*	Heat inactivated CnT-Pri*
1.5 mM CaCl <sub>2</sub>	100 nM PMA
Calcitriol (1,25-dihydroxyvitamin D3)	
Heat inactivated CnT-Pri*	
100 nM Calcitriol	

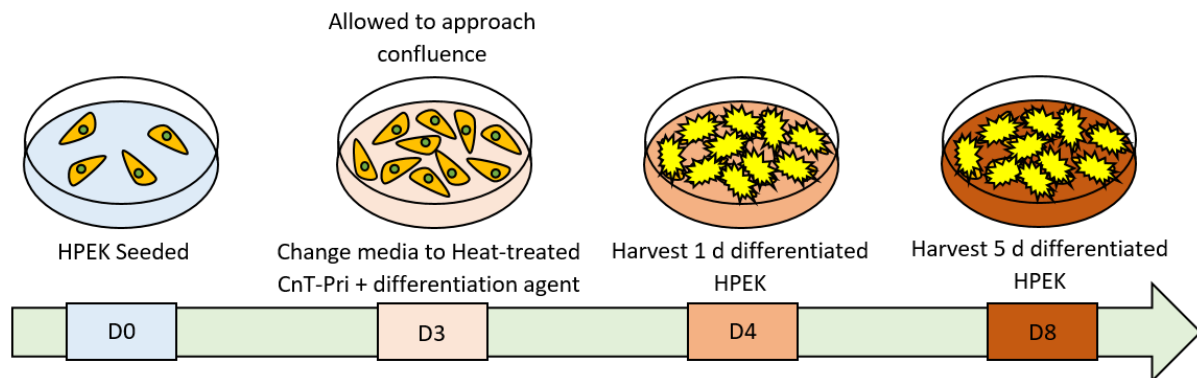


**Figure 2.2: Differentiation of HPEK Schematic.** HPEK were seed at D0 and allowed to approach confluence for 2 days. On D3 media was switched for differentiation medium and cells were left to differentiate until D4 and D8 when 1 d and 5 d time points were harvested for analysis.

### **2.3. Nucleofection**

Transfection is the process of introducing foreign nucleic acid directly into a eukaryotic cell using non-viral methods and can be separated into biological, chemical and physical techniques (Nayerossadat, Maedeh and Ali, 2012). Viral transduction is a biological procedure often grouped with transfection and involves use of viral vectors such as adenovirus and lentivirus resulting in a stably-transfected cell that continuously expresses a gene of interest (Chen and Goncalves, 2016). Non-biological methods tend to be transient resulting in temporary expression of genetic material, which is eventually diluted and lost through mitosis (Nayerossadat, Maedeh and Ali, 2012). Chemical methods including calcium phosphate (Graham and van der Eb, 1973), liposomal e.g. lipofection (Felgner et al., 1987), cationic polymers e.g. DEAE-Dextran (De Smedt, Demeester and Hennink, 2000) and magnetofection (Plank et al., 2003) rely on a similar process whereby chemical:genetic material complexes are attracted to cellular membranes and where uptake occurs via endocytosis. Physical approaches rely on perforating cellular membranes to deliver material and comprise of microinjection (Diacumakos, 1973), biolistics (Klein et al., 1987), electroporation (Wolf et al., 1994) and sonoporation (Bao, Thrall and Miller, 1997). Transfections in this study were performed using nucleofection, a transient, electroporation-based technique that relies upon optimised electrical pulses and cell specific reagents to deliver cargo into hard to transfect cells (Distler et al., 2005). Most non-biological transfection methods deliver nucleic acid directly into the cytoplasm. A significant proportion is either degraded by cytoplasmic nucleases or sequestered by lysosomes before entry to the nucleus. However, it is thought that nucleofection delivers transfection molecules directly into the nucleus, allowing for efficient and quick expression, bypassing the need for cell division, by puncturing both cell and nuclear membranes (Gresch et al., 2004).

Nucleofection reagents, plasmids and consumables were purchased from Lonza, Slough, UK. hsa-miR-184 miRIDIAN miRNA mimic, miRIDIAN miRNA mimic negative

control, siAGO2 ON-TARGETplus siRNA, siORAI1 ON-TARGETplus siRNA and ON-TARGETplus non-targeting siRNA were purchased from Dharmacon, Lafayette, USA. hsa-miR-184 miRCURY Locked Nucleic Acid (LNA) Power Inhibitor and miRCURY LNA Power Inhibitor Negative Control were purchased from Exiqon, UK. AGO2 plasmids were a kind gift from Prof. Tyson Sharp (Queen Mary University of London, UK) .

HPEK of p1-3 were passaged at least 3 days preceding nucleofection, cultured until 70-80% confluent with media being changed every other day. Prior to work supplement was added to P3 nucleofector solution and CnT-Pri (CellnTec, Switzerland) was added to a 6-well plate and pre-equilibrated at 37°C, 5% CO<sub>2</sub> for at least 30 min. HPEKs were enzymatically dissociated by accutase (CellnTec, Switzerland) and enumerated using a haemocytometer. A volume containing 1.0 x10<sup>6</sup> cells was added to a 15 mL universal tube and centrifuged at 260 RCF for 10 minutes at 4°C. The supernatant was aspirated and the resulting pellet was resuspended in 100 µL of P3 Nucleofector solution before transfer to a sterile nucleofection curvette. Prior to transfer the cells were mixed with either pmaxGFP (Green Fluorescent Protein) vector, hsa-miR-184 miRIDIAN miRNA mimic, hsa-miR-184 miRIDIAN miRNA hairpin inhibitor, miRIDIAN miRNA mimic negative control, siAGO2 ON-TARGETplus siRNA, siORAI1 ON-TARGETplus siRNA or ON-TARGETplus non-targeting siRNA at indicated concentrations. A mock control consisting of 1.0 x10<sup>6</sup> cells in 100 µL P3 Nucleofector solution was used to assess the effect of the nucleofection procedure on HPEK. Next, the nucleofection curvette was lightly tapped to ensure the sample covered the bottom before transfer into the 4D-Nucleofectors X unit and by selecting the DS-138 program, nucleofection was performed. Following this, the sample was incubated for 10 minutes at room temperature before 400 µL of pre-equilibrated CnT-Pri was added to the nucleofection curvette. The sample was mixed and removed from the curvette using a dropper pipette and transferred to a 1.5 ml Eppendorf tube (Eppendorf, Stevenage, UK), where it was separated

dependent on experimental seeding requirements. Plates containing nucleofected HPEKs were then incubated at 37°C, 5% CO<sub>2</sub>, with the media changed the following day to remove any dead cells and changed every 2-3 days until harvest.

## **2.4. Real-Time Quantitative Polymerase Chain Reaction (RT-qPCR)**

### **2.4.1. RNA Isolation and Quantification**

Total RNA was isolated from HPEK using reagents purchased from Qiagen, Manchester, UK unless otherwise stated. Psoriasis patient samples (West Midlands, South Birmingham Research Ethics Committee approval number 15/WM/0388) were previously processed and total RNA isolated by Dr. Tyng Han. The following solutions were prepared prior to isolation. Lysis buffer: 20 µL of 2M dithiothreitol (DTT; Sigma-Aldrich, UK) were added to 1 mL of buffer RLT plus. Wash buffers: 44 ml of molecular biology grade 100% ethanol (Thermofisher Scientific, Runcorn, UK) was added to 11 ml of concentrated buffer RPE and 42 ml of isopropanol (Sigma-Aldrich, UK) was added to 14 ml of concentrated buffer FRN. DNase: 550 µL of RNase-free water (Fisher Scientific, UK) was used to dissolve lyophilised DNase I stock (1500 kunitz units) with gentle inversion to mix, before separation into aliquots to prevent freeze-thaw degradation.

For cell lysis, media was completely aspirated from cells grown in 6- or 12-well plates, before addition of PBS (Sigma-Aldrich, UK) to ensure complete removal of any residual media. Next, 350 µL of lysis buffer was added to each sample well and incubated for 1-2 minutes at room temperature. The resulting lysate was collected by scraping the well with a 1 mL pipette tip and rinsing, before transferring to 1.5 mL Eppendorf tubes (Eppendorf, UK).

Eppendorfs containing sample lysates were then vortexed for 1 minute, ensuring no cell clumps remained before either continuing with isolation or storage at -80°C.

For isolation, sample lysates were thawed on ice and briefly vortexed to maintain homogeneity before transfer to an Allprep DNA mini spin column and centrifugation at MAX (16,000) RCF for 30 seconds. The sample that had passed through the column termed flow-through, was then transferred to a 2 mL microcentrifuge tube. 50 µL of proteinase K and 200 µL of 100% ethanol (Fisher Scientific, UK) were added to the lysate and mixed, before incubation for 10 minutes at room temperature. Following incubation, a further 400 µL of 100% ethanol (Fisher Scientific, UK) was added to the lysate and mixed before transfer to RNeasy mini spin columns. The column was then spun for 15 seconds at MAX (16,000) RCF and the flow-through was discarded. Next, 500 µL of buffer RPE was added to the column and centrifuged for 15 seconds at MAX (16,000) RCF with the flow-through discarded. Following this, 10 µL of DNase I stock was diluted in 70 µL of buffer RDD and then added directly to the RNeasy mini spin column membrane, before incubating at room temperature for 15 minutes. After incubation, 500 µL of buffer FRN was added directly to the column membrane and spun at MAX (16,000) RCF for 15 seconds. To ensure isolation of small RNAs, the flow-through was added to the column again with the centrifugation repeated. Following this, a second wash was performed with buffer RPE. Next, 500 µL of 100% ethanol (Fisher Scientific, UK) was added to the column, before centrifugation for 2 minutes at MAX (16,000) RCF. To make sure no ethanol is carried over, the column was added to a new 2 mL collection tube and spun for a further 2 minutes at MAX (16,000) RCF. Finally, the column was transferred to a 1.5 mL RNase-free microcentrifuge tube before adding 30 µL of RNase-free ddH<sub>2</sub>O directly to the column and then centrifuging for 1 minute at 11,600 RCF. To obtain a higher RNA concentration, the eluent were re-added to the column and spun at 11,600 RCF for 1 minute.

The quality and concentration of isolated RNA was determined using a Nanodrop™ 2000 ultraviolet-visible (UV-Vis) spectrophotometer (Thermo Fisher, UK), with optical densities (OD) of 260 and 280 nm averaged from triplicate readings. RNA nucleotides absorb UV light in specific patterns. The absorbency ratio between 260/280 nm was used to determine the quality of the isolated RNA, with ratios of 1.9-2.1 denoting RNA of good quality. Isolated RNA was stored at -80°C until further work.

### **2.4.2. cDNA Synthesis**

Isolated RNA was reverse transcribed into complementary DNA (cDNA) using reagents purchased from Qiagen, Manchester, UK, unless stated otherwise. Template RNA was thawed on ice whilst 10x miScript nucleics mix, RNase-free water and 5x miScript HiFlex Buffer were thawed at room temperature. HiFlex Buffer was chosen as opposed to HiSpec Buffer for the subsequent quantification of mature miRNA and mRNA from the same sample. Next, a master mix was prepared consisting of 4 µL 5x miScript HiFlex Buffer, 2 µL 10x miScript Nucleics Mix, 2 µL miScript Reverse Transcriptase Mix and was scaled up depending on the sample size (Table 2.2). miScript Reverse Transcription Mix was removed from the -20°C freezer just before addition to the master mix. To assess whether any genomic DNA (gDNA) contamination was present in the cDNA preparation, a second master mix was prepared without the presence of miScript Reverse Transcriptase Mix. Following this, 8 µL of the master mixes were aliquoted into 0.2 mL RNase/DNase-free PCR tubes and 400 ng of template RNA was added before making the final volume up to 20 µL with RNase-free water. After this, the samples were centrifuged briefly and incubated at 37°C for 60 minutes. Finally, samples were heated to 95°C for 5 minutes to inactivate miScript Reverse Transcriptase mix and terminate the reaction.

**Table 2.2. Reverse Transcription Mastermix.**

<b>Component</b>	<b>Volume/reaction</b>
5x miScript HiFlex Buffer	4 $\mu$ L
10x miScript Nucleics Mix	2 $\mu$ L
miScript Reverse Transcriptase Mix	2 $\mu$ L
RNase-free water	Variable
Template RNA	Variable
<b>Total Volume</b>	<b>20 <math>\mu</math>L</b>

### 2.4.3. RT-qPCR

Unless otherwise stated RT-qPCR was performed using reagents and consumables bought from Qiagen, Manchester, UK. At all stages of experimental setup, filtered RNase-free pipette tips and RNase-free environment was used. The resultant cDNA from reverse transcription was diluted 10-fold in RNase-free ddH<sub>2</sub>O prior to addition to the RT-qPCR reaction. All PCR reactions were carried out in 0.1 mL PCR strip tubes. RT<sup>2</sup> qPCR Primer assays came as a solution with miScript Primer assays briefly centrifuged and reconstituted in 1.1 mL of TE buffer (Table 2.3). Where primers were supplied by Thermo Fisher, UK the primer mixes were reconstituted in TE buffer to a master stock concentration of 100  $\mu$ M and diluted 10-fold to give a 10  $\mu$ M working stock, in order to minimize freeze/thaw cycles (Table 2.4). All primer products will be referred to as Primer mix.

To start, 2x Quantitect SYBR Green PCR Master Mix, 10x miScript Universal Primer, RNase-free water, template cDNA and Primer mix were thawed on ice before gently mixing to ensure homogeneity. Depending on whether miRNA or mRNA was the target of interest, two PCR master mixes were made. For mRNA, 10  $\mu$ L 2x Quantitect SYBR Green PCR Master

Mix was added to 6  $\mu\text{L}$  of RNase-free water. For miRNA, 10  $\mu\text{L}$  2x Quantitect SYBR Green PCR Master Mix was added to 4  $\mu\text{L}$  of RNase-free water. To either PCR mastermix 2  $\mu\text{L}$  of Primer mix was added. The reactions could be scaled depending on sample size. Where primers provided were by Thermo Fisher, 2  $\mu\text{L}$  of each forward and reverse primers was added to 10  $\mu\text{L}$  of 2x Quantitect SYBR Green PCR Master Mix and 4  $\mu\text{L}$  of RNase-free water. Next, 18  $\mu\text{L}$  of master mix was aliquoted into PCR tubes followed by addition of 2  $\mu\text{L}$  of template cDNA, either manually or using a Qiagility semi-manual liquid handling robot (Qiagen, UK) if there was a large sample size. Reactions were performed in duplicate to protect against run failure and recognise any variances in PCR efficiency. A no template control was added to each run to identify any contaminating DNA in the reaction reagents by substituting template cDNA with 2  $\mu\text{L}$  of RNase-free ddH<sub>2</sub>O.

Following this, the tubes were sealed with caps and transferred to a 72-well rotor-disk which was placed inside of a Rotor-Gene Q real time cycler, supported by Rotor-Gene Q version 2.1.0.9 software (Qiagen, UK). RT-qPCR was set-up as follows: 95°C for 15 mins followed by 40-45 cycles of 94°C for 15 s (Denaturation), 55°C for 30 s (Annealing) and 70°C for 30 s (Extension). SYBR Green is one of the most common fluorescent probes in RT-qPCR. It is thought to intercalate with the minor groove of double-stranded DNA, absorbing blue light at 494 nm and emitting green light at 521 nm. Data was captured when SYBR Green fluorescent signal accumulated enough to cross the background threshold. Cycle threshold (Ct) values were calculated when PCR was in exponential phase during amplification. Upon completion of amplification, melt curve analysis of the product was performed where tubes were subject to a 1°C per second temperature increase starting at 60°C and terminating at 95°C. As the increase in temperature denatures double-stranded DNA causing SYBR green to dissociate, melt curve analysis allows quantification of the resultant loss of fluorescence. The melting temperature (T<sub>m</sub>) varies depending on the base composition of each target DNA,

giving an indication to target specific binding and allowing any anomalies to be removed in further analysis. Results were normalised to a housekeeping gene, whose expression remained relatively stable between samples and experiment. The average Ct for the housekeeping gene was 15.16 ( $\pm 1.14$ , SD) for mRNA data (*GAPDH*) and 23.65 ( $\pm 1.20$ , SD) for miRNA data (*SNORD72*) across all experiments. RT-qPCR data was quantified and depicted relative to the experimental control group using the comparative Ct method,  $2^{-\Delta\Delta Ct}$ . Briefly,  $\Delta\Delta Ct = \Delta Ct_{treated} - \Delta Ct_{untreated}$ .  $\Delta Ct_{treated}$  is the mean Ct of the gene of interest (GOI) minus the mean Ct of the housekeeping control ( $Ct_{GOI} - Ct_{Control}$ ) from duplicate analysis of the experimental treatment groups. Whilst  $\Delta Ct_{untreated}$  is the mean Ct of the GOI minus the mean Ct of the normalisation control ( $Ct_{GOI} - Ct_{Control}$ ) from duplicate analysis of the experimental control group (Schmittgen and Livak, 2008).

**Table 2.3. Pre-designed Qiagen Primers.**

Name	Cat. No.
<i>GAPDH</i>	PPH00150F
<i>LOR</i>	PPH06894F
<i>IVL</i>	PPH01911A
<i>CCNE1</i>	PPH00131A
<i>CCNE2</i>	PPH00955B
<i>CCNB</i>	PPH00126C
<i>AGO1</i>	PPH16729A
<i>AGO2</i>	PPH21840A
<i>AGO3</i>	PPH13995A
<i>AGO4</i>	PPH20751A
SNORD72	MS00033719
SNORD61	MS00033705
miR-26a	MS00029239
miR-184	MS00003640
miR-205	MS00003780
miR-21	MS00009079

**Table 2.4. Thermo Fisher Primers.**

Name	Sequence
<i>CDKN1A (p21)</i>	Forward 5'-TCAGGCTTGGGCTTTCACC-3' Reverse 5'-CCATGCACTTGAATGTGTACCCAGA-3'
<i>ORAI1</i>	Forward 5'-GAGCATGCAAAACAGCCCAGG-3' Reverse 5'-GGCTCATCACCTCGGAGTAACTCT-3'
<i>NFAT2c (NFAT1)</i>	Forward 5'-GGGCTGGGAGATGAACATGAA-3' Reverse 5'-AAATCAATAGCCCAATAGAGGTTCTAGAAAG-3'

## **2.5. Western Blotting**

### **2.5.1. Protein Isolation and Quantification**

Preceding isolation, Radio Immuno Precipitation Assay buffer (RIPA) was prepared as follows: 150 mM sodium chloride, 1.0% Triton X-100, 0.5% sodium deoxycholate, 0.1% sodium dodecyl sulphate (SDS), 50 mM Tris, pH 8.0 and stored at 4°C with 1 mM sodium orthovanadate and 1 complete mini, EDTA-free protease inhibitor cocktail tablet (Sigma-Aldrich, UK) added to 50 mL of RIPA prior to use.

For lysis, cells grown in a 6-well plate were placed on ice and media was aspirated, followed by addition of ice cold PBS for 1-2 minutes to remove residual media. Next, PBS was aspirated and 120 µL of ice cold RIPA buffer was added. The plate kept on ice was then transferred to an orbital shaker to maintain constant agitation for 30 minutes. Following this, cells were scraped with a 1 mL pipette tip and transferred to pre-cooled micro-centrifuge tubes (Eppendorf, UK) before storage at -80°C, until further work.

For quantification, cell lysates were centrifuged at 4°C, 11,600 RCF for 20 minutes with the resulting supernatant transferred to new pre-cooled micro-centrifuge tubes. Cell lysates were then quantified using the Pierce BCA protein assay kit (ThermoFisher scientific, UK) following the manufactures instructions. In brief, a range of bovine serum albumin (BSA) standards were prepared from 0-2000 µg/mL. Working reagent consisting of a highly alkaline bicinchoninic acid (BCA) solution and copper(II) sulphate was made at a ratio of 50:1. 10 µL of BSA standards and unknown samples were pipetted in duplicate into a 96-well plate then 200 µL of working reagent was added to each well, before incubation at 37°C for 30 minutes. The plate was cooled at room temperature and absorbance was measured at 562-590 nm on a CLARIOstar plate reader (BMG Labtech, Aylesbury, UK).

### **2.5.2. Fractional Protein Isolation**

Protein from the cytoplasm and nucleus was separated using reagents from the ab113474-nuclear extraction kit (Abcam, Cambridge, UK), unless otherwise stated. The following solutions were prepared on ice prior to isolation. 1X Pre-extraction buffer: 1 mL of 10X Pre-extraction buffer was diluted in 9 mL of ddH<sub>2</sub>O with addition of 10 µL of 1000X DTT solution and 10 µL of 1000X PIC (protease inhibitor cocktail). Nuclear extraction buffer: 1 µL of 1000X DTT solution and 1 µL of 1000X PIC was added to 998 µL of Extraction buffer.

To start, HPEK grown in 6-well dishes were enzymatically dissociated as previously described in 2.1.2. using appropriate reagent volumes, before centrifugation at 180 RCF for 5 minutes. The supernatant was discarded and the cell pellet was resuspended in 150 µL of ice cold 1X Pre-extraction buffer, before transfer to a micro-centrifuge tube and incubation on ice for 10 minutes. The lysate was then vortexed for 10 seconds before being centrifuged for 1 minute at 11,600 RCF. Following centrifugation, the cytoplasmic extract was carefully removed from the nuclear pellet and transferred to a pre-cooled micro-centrifuge tube. Next, 25 µL of ice cold nuclear extraction buffer was added to the remaining pellet and incubated on ice for 15 minutes, whilst vortexing for 10 seconds every 3 minutes. Following incubation the lysate was vortexed for a further 20 seconds and sonicated for 3 x 10 seconds, before transfer to a -80°C freezer until further work.

### **2.5.3. Western Blotting**

Western blotting was performed using reagents, consumables and equipment purchased from Bio-Rad, Watford, UK unless otherwise stated. The following solutions were prepared prior to western blotting. Running buffer: 25 mM Tris base, 190 mM glycine, 0.1% SDS pH ~8.3. Transfer buffer: 48 mM Tris base, 39 mM glycine, 0.04% SDS, 20% methanol. 10X Tris buffered saline (TBS): 200 mM Tris base, 1500 mM sodium chloride, pH ~7.6. TBS+Tween

20 (TBST): 1:10 dilution of 10X TBS with addition of 0.1% (v/v) Tween20. The pH of solutions were adjusted using 1 M sodium hydroxide or 1 M hydrochloric acid.

For electrophoresis, 20-40  $\mu$ g of sample lysate was diluted in the appropriate amount of 4X Laemmli buffer containing 100 mM DTT, before heating at 95°C for 5 minutes to reduce and denature the sample. Following this, the sample/Laemmli buffer mix was loaded into a well of a 12% polyacrylamide mini-PROTEAN TGX precast gel setup within an electrophoresis chamber filled with running buffer. Precision plus protein kaleidoscope molecular weight marker was loaded into another well. The gel was run at 150 V for 45 minutes or until the migration front reached the bottom of the gel.

For semi-dry protein transfer, a polyvinylidene difluoride (PVDF) membrane was activated for 2 minutes in methanol and equilibrated in ice cold transfer buffer along with the gel for 5 minutes prior to transfer. The gel and membrane was sandwiched between blotting paper (membrane closest to positive electrode) and soaked in transfer buffer before rolling to remove air bubbles. Protein was transferred onto the membrane using Trans-blot turbo transfer apparatus run at 25 V constant and up to 1.0A for 30 minutes. All steps involving the PVDF membrane were performed using tweezers to avoid contamination.

For protein visualisation, the membrane was submerged in 10 mL of blocking buffer (5% (w/v) fat-free milk in TBST), covered and agitated on an orbital shaker for 1 hour at room temperature. Next, the membrane was washed in 10 mL TBST and incubated with primary antibody (Table 2.5), diluted in blocking buffer overnight at 4°C, whilst being kept on a Stuart roller shaker (Cole-Parmer, Staffordshire, UK). The following day, to remove any remaining primary antibody, the membrane was washed in TBST for 5 x 5 minutes, before incubation in horse radish peroxidase (HRP)-conjugated secondary antibody (Table 2.5) diluted with TBST agitated on an orbital shaker at room temperature for 1 hour. Following this, the secondary antibody was removed and to prevent any interference of residual secondary antibody during

the visualisation process, the membrane was washed for 5 x 5 minutes in TBST. Following washing, HRP substrate was prepared by mixing components of the Clarity western ECL substrate kit in a 1:1 ratio (2 ml: 2 ml). This was then added to the protein side of the membrane and incubated for 5 minutes at room temperature. The membrane was then removed from the substrate solution and placed in a ChemiDoc XRS+ digital imager where it was visualised.

**Table 2.5. Western Blotting Antibodies.**

Antigen	Speciation	Reactivity	Clonality	Supplier	Dilution
Involucrin	Mouse	Human	Monoclonal	Abcam	1:1000
Cyclin E1	Rabbit	Human	Monoclonal	Santa Cruz	1:750
Cyclin E2	Mouse	Human	Monoclonal	R&D Systems	1:750
AGO2	Rabbit	Human	Polyclonal	Abcam	1:500
p21	Mouse	Human	Monoclonal	Bio-Rad	1:200
ORAI1	Rabbit	Human	Polyclonal	Bio-Rad	1:200
$\gamma$ H2AX	Mouse	Human	Monoclonal	Millipore	1:500
GAPDH	Rabbit	Human	Monoclonal	Cell signalling technology	1:5000
$\beta$ -Actin	Mouse	Human	Monoclonal	Sigma-Aldrich	1:1000
Anti-Mouse IgG	Goat	Mouse	Polyclonal	Sigma-Aldrich	1:2000
Anti-Rabbit IgG	Donkey	Rabbit	Polyclonal	Thermo Fisher Scientific	1:2000

## 2.6. Proliferation

### 2.6.1. Flow Cytometric Analysis of Cell Cycle

Propidium iodide (PI; Thermo Fisher Scientific, UK), a fluorescent molecule that binds to nucleic acids, was used to analyse the cell cycle. PI binds in proportion to the amount of nucleic acid present within the cell allowing clear distinction between G1 (diploid, 2n), S (DNA synthesis) and G2 (tetraploid, 4n).

HPEKs were nucleofected as previously described in 2.2. and enzymatically disassociated. Following centrifugation, cells were washed in 5 ml of PBS and spun at 260 RCF for 10 minutes. Next, the supernatant was aspirated and 300  $\mu$ L of ddH<sub>2</sub>O was used to resuspend the resultant pellet. To fix, ice cold 100% ethanol was added dropwise, whilst swirling the tube to minimise cell clumping and incubated at 4°C for a minimum of 48 hours, to allow complete dehydration to occur. Following this, samples were centrifuged at 320 RCF for 10 minutes, supernatant removed with the pellet washed in PBS, then samples were centrifuged again under the same conditions. The resultant pellet was resuspended in 100  $\mu$ g/mL PI solution and incubated in the dark for 45 minutes at room temperature, before conducting analysis using a BD Accuri C6 flow cytometer (BD Biosciences, Berkshire, UK). Data was collected for 10,000 gated events using the FL2 channel (488 nm laser and 585/40 nm band pass (BP) filter). Cell debris were excluded using forward scatter (FSC) vs side scatter (SSC) gates with cell aggregates omitted using FSC height (FSC-H) vs FSC area (FSC-A) gates (Fig. 2.3). To minimise cell loss, sample preparation was performed in 15 mL universal tubes and subjected to extended centrifugation (from 5 to 10 minutes) before transfer to 1.5 mL microcentrifuge tubes for analysis. To provide improved accuracy for cell cycle model fitting, data was analysed using the Dean-Jett-Fox (DJF) univariate algorithm on FlowJo version 10.0 (FlowJo, LLC, Ashford, USA). The DJF model, like the common alternative Watson pragmatic model, uses gaussian curves to fit both G1 and G2 stages of the cell cycle, but whereas the

Watson model makes no assumptions for S-phase using a direct fit, the DJF model fits a polynomial curve that can be used to measure S-phase distribution for synchronous cell populations (Fig. 2.3D).

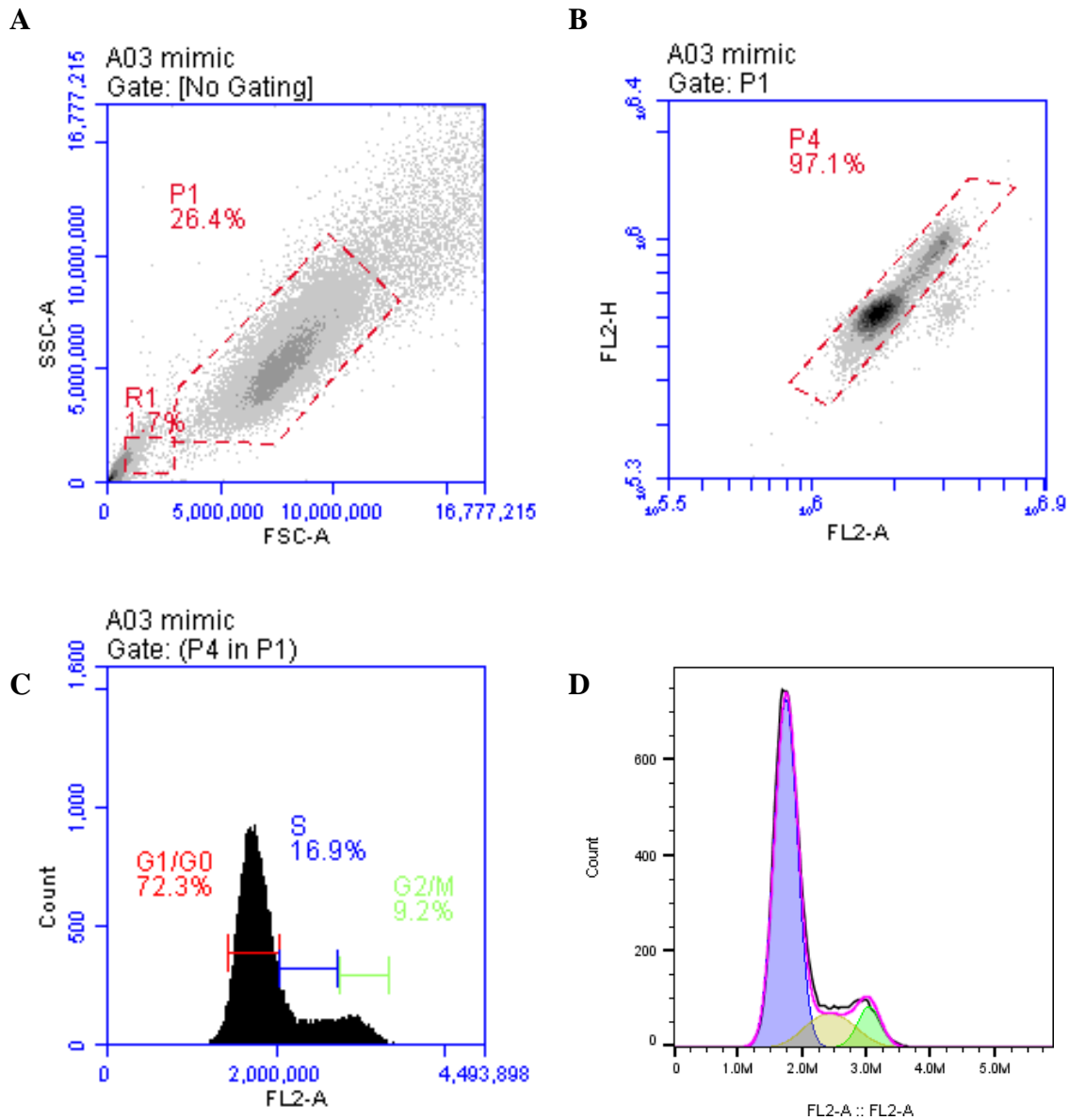


**Figure 2.3: Gating strategies used for flow cytometry data analysis.** The major density of events was captured in P1 (A) before single cells were isolated in P4 (B). Cell cycle data was collected using FL-2A (C) which was gated P4 in P1. R1 (A) was to include for any apoptotic cells which usually shrink during this process and was analysed separately to healthy cells. Cell cycle data was collected and gated before analysis using the univariate Dean-Jett-Fox model on FlowJo v10.0 (D).

## **2.6.2. MTT**

MTT (3-(4,5-dimethylthiazol-2-yl)-2,5-diphenyltetrazolium bromide) provides an indication of cellular metabolic activity and, under defined conditions, a crude representation of cell viability. It relies on the reduction of soluble MTT to insoluble formazan by NADPH-dependent oxidoreductases of which levels are affected by altered proliferation rates. To start, cells were nucleofected as described in 2.2. and seeded in triplicate  $3 \times 10^4$ /well of a 96-well plates for 72 hours. Following this, media was aspirated and 100  $\mu$ L of media along with 10  $\mu$ L of 12 mM MTT was added to each well, before incubating in the dark at 37°C for 4 hours. Next, media was carefully removed so not to disturb the formazan crystals and allowed to air dry for 1-2 minutes. To solubilise, dimethyl sulfoxide (DMSO) was added to each well and mixed gently on an orbital mixer for 5 minutes, before reading the absorbance at 540 nm on a CLARIOstar plate reader (BMG labtech, UK).

## **2.7. Microscopy**

### **2.7.1. Immunofluorescence (IF) Microscopy**

The following solutions were made prior to IF. 4% (w/v) paraformaldehyde (PFA) solution: 4 g of PFA (Sigma Aldrich, UK) was dissolved in 100 mL of ddH<sub>2</sub>O whilst stirring at 60°C, solution was cleared with 1 M sodium hydroxide and the pH adjusted to 7.4. Blocking buffer PBS containing 0.1% Tween20 (PBST) with 10% goat serum. Antibody buffer: PBST containing 2% goat serum.

Cells were cultured on Nunc Lab-Tek permanox 8-well chamber slides (Thermofisher scientific, UK) or glass cover slips before fixation using 4% PFA for 15 minutes at room temperature. Following fixation, cells were washed three times for 5 minutes with PBS (without Ca<sup>2+</sup> or Mg<sup>2+</sup>) before permeabilising in PBS containing 0.2% Triton X-100 for 10 minutes at room temperature. Non-specific antigens were blocked by the addition of blocking

buffer for 1 hour at room temperature. Blocking buffer was removed and primary antibody, diluted in antibody buffer, was added before incubating at 4°C overnight.

The following day, primary antibody was removed and wells were washed three times with PBST for 5 minutes at room temperature. Samples were then incubated with the relevant fluorescently-conjugated secondary antibody diluted in antibody buffer for 1 hour at room temperature in the dark. Following incubation, secondary antibody was aspirated and, to remove any residual antibody, wells were washed 3 x 5 minutes with PBST. Finally, nuclei were counterstained with 4', 6-diamidino-2-phenylindole (DAPI; Ex358, Em461) for 5 minutes at room temperature, before mounting with Fluoromount-G mounting medium (Southern Biotech, Birmingham, USA). Images were collected from at least 5 fields of view per sample condition using a fluorescent microscope (Leica DMI6000B, Leica, London, UK). For DNA damage, images of  $\gamma$ H2AX stained samples were captured from 10 fields of view containing at least 20 cells, before analysis and quantification by Dr. Carlos Rubbi (University of Liverpool, Liverpool, UK) using proprietary software.

**Table 2.6. Immunofluorescent Antibodies.**

Antigen	Speciation	Reactivity	Clonality	Supplier	Dilution
AGO2	Rabbit	Human	Polyclonal	Abcam	1:500
$\gamma$ H2AX	Mouse	Human	Monoclonal	Millipore	1:500
Alexa Fluor 647	Goat	Mouse	Polyclonal	Invitrogen	1:1000
Alexa Fluor 488	Goat	Rabbit	Polyclonal	Invitrogen	1:1000

### **2.7.2. Live Cell-Imaging**

Prior to live cell-imaging experiments, a stage incubator attached to a Leica DMI6000B inverted microscope was equilibrated to 37°C, 5% CO<sub>2</sub> whilst maintaining humidity. Cells were seeded in 6-well plates in accordance with experimental requirements at least 1 d prior to imaging. Plates were transferred carefully into the microscope incubator and placed onto the microscope stage. Using the Mark & Find function on LAS X software at least four locations from around each individual well was selected and saved. Time-lapse images were then automatically taken at each pre-selected location every 30 min for 3 days.

## **2.8. Statistical Analysis**

Experiments were conducted in biological triplicate on three independent occasions. All data is presented as mean  $\pm$  SEM unless otherwise stated. Data was assessed for normality. Statistical analysis was carried out using GraphPad Prism 6 software (California, USA). Unless otherwise stated, unpaired students t-test was utilised when 2 groups were present with one-way analysis of variance (ANOVA) used when more than 2 groups were present. to correct for multiple comparisons, Tukey's post hoc test was applied when using ANOVA in order to compare all groups. A p value of  $p < 0.05$  determined significance.

### **3. Investigation of miR-184 Expression in HPEKs and Psoriasis**

### 3.1. Introduction

The most commonly used technique to trigger keratinocyte differentiation *in vitro* is a calcium switch, whereby the levels of extracellular  $\text{Ca}^{2+}$  in the growth medium are elevated. Early work on epidermal mouse keratinocytes by Hennings and colleagues documented that levels of calcium  $<0.1$  mM suppress differentiation and allow keratinocytes to proliferate rapidly, whereas high concentrations ( $>1.0$  mM) induce terminal differentiation at varying rates (Hennings et al., 1980). As keratinocytes undergo terminal differentiation, they express specialised differentiation markers such as involucrin (IVL) and loricrin (LOR) which form part of the protective cornified envelope (Candi, Schmidt and Melino, 2005; Eckert et al., 2005). Studies have also shown that inhibiting mediators of calcium-induced differentiation such as protein PKC (Lee et al., 1997) result in a considerable reduction in the levels of these differentiation makers. Strict control of the cell cycle is an important feature of keratinocyte differentiation, and recent work by Freije and colleagues has shown that cyclin E accumulation causes growth arrest, re-replication and DNA damage. This results in the onset of differentiation by inhibiting mitotic regulators such as cyclin B and cdk1, as well as activating the p21/p53 pathway (Freije et al., 2012).

Several miRNAs have been shown to play key roles in keratinocyte differentiation including miR-205 (Wang et al., 2013), miR-203 (Lena et al., 2008; Yi et al., 2008b), miR-24 (Amelio et al., 2012). Moreover, a comprehensive analysis by Hildebrand and colleagues indicates that at least 55 miRNAs are upregulated in human epidermal keratinocytes treated with 1 mM  $\text{Ca}^{2+}$  for 7 days, although miR-184 was not listed (Hildebrand et al., 2011). More recently, miR-184 was shown to be present in reconstituted human epidermis (RHE) with levels modulated by the pro-inflammatory cytokines, IL-22 and Oncostatin M (OSM), suggesting that miR-184 may play a role in keratinocyte stratification (Roberts et al., 2013). In addition, a very recent report, published following the inception of this work, has shown

presence of miR-184 in the suprabasal layers of neonatal mouse epidermis as well as in cultured human keratinocytes (Nagosa et al., 2017).

An indispensable form of  $\text{Ca}^{2+}$  entry in epidermal keratinocytes is called SOCE. Recent work by Vandenberghe and colleagues demonstrates the importance of SOCE to normal keratinocyte biology with disruption of CRAC channels leading to disrupted keratinocyte migration and differentiation (Vandenberghe et al., 2013). A common CRAC channel protein is ORAI1, consisting of three dimeric subunit pairs which together form a hexamer channel complex. Intermembrane coupling with the  $\text{Ca}^{2+}$ -sensor STIM protein following ER  $\text{Ca}^{2+}$  depletion activates ORAI1, consequently opening the central pore and allowing  $\text{Ca}^{2+}$  entry (Prakriya and Lewis, 2015). The NFAT signalling pathway is key downstream effector of SOCE. Following elevated  $[\text{Ca}^{2+}]$ , the serine/threonine protein phosphatase, CaN is activated by CaM and consequently dephosphorylates NFAT, which in turn localises to the nucleus where it regulates gene expression (Rumi-Masante et al., 2012; Mognol et al., 2016). Despite its vital role in keratinocyte biology little is known about SOCE as a regulatory miRNA pathway.

Psoriasis is a chronic inflammatory cutaneous disorder involving complex pathological processes between keratinocytes and immune cells that affects around 2% of the UK population, with the first link between miRNAs and its pathogenesis occurring over a decade ago (Sonkoly et al., 2007). As recently reviewed by Hawkes and colleagues, several miRNAs have been shown to be upregulated in psoriasis, including miR-184 (Hawkes et al., 2016). Recent work by Roberts and co-workers has shown elevated levels of primary and mature miR-184 in psoriatic lesions, albeit with a small sample size (Roberts et al., 2013). Evidence suggest that miR-184 is involved in the regulation of other miRNAs through targeting a central protein of the RISC complex known as AGO2 (Roberts et al., 2013).

Previous evidence confirms that miR-184 regulates ocular keratinocyte systems. However, despite recent attempts by Nagosa and co-workers indicating elevated levels of miR-184 within differentiating mouse epidermal keratinocytes, little is known about the mechanisms of miR-184 induction or miR-184 expression patterns and how these change in psoriasis (Nagosa et al., 2017).

## 3.2. Aims

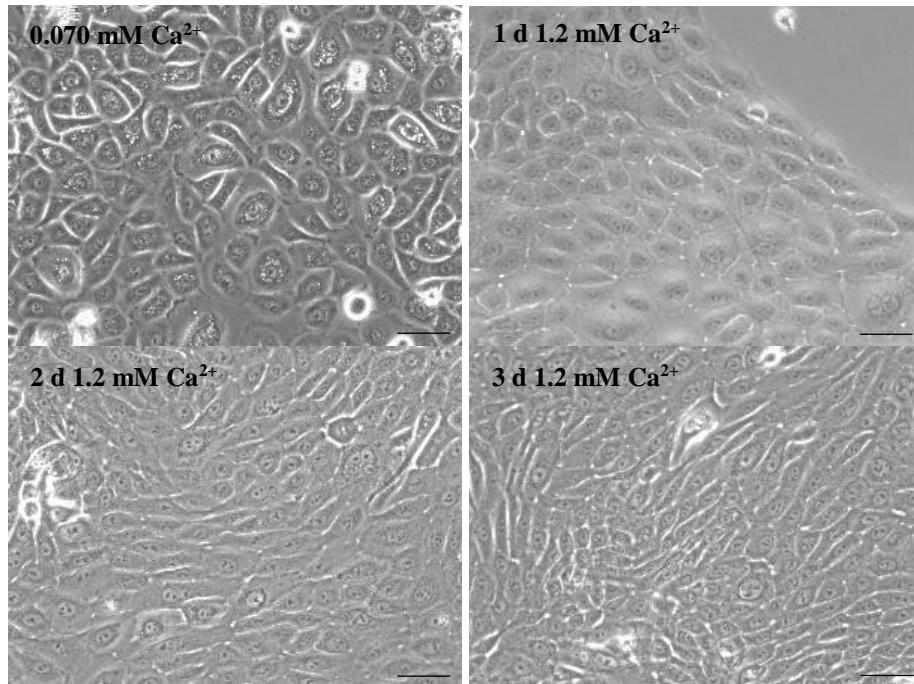
- To optimise calcium-dependent HPEK differentiation
- Investigate expression of miR-184 during HPEK differentiation in response to  $\text{Ca}^{2+}$  and other differentiation agents
- Examine the impact of SOCE on miR-184 expression
- Assess expression of miR-184 in psoriatic lesions

## 3.3. Results

### 3.3.1. Optimisation of HPEK Differentiation

Initially, based on work by Hennings et al., HPEKs were stimulated with 1.2 mM  $\text{Ca}^{2+}$  for 3 days (Hennings et al., 1980). As shown in Figure 3.1A, expression of *IVL* was increased 6.8-fold ( $\pm 4.1$ ) over 3 days, with no considerable change in *LOR*. However, errors were inconsistent suggesting that 3 d at 1.2 mM  $\text{Ca}^{2+}$  is insufficient to promote adequate differentiation of HPEK. However, transmitted light microscope observations revealed varied morphologies over 3 days suggesting that a mix of proliferating and differentiating HPEK may have been present (Fig. 3.1B), although to validate this claim visualisation of markers for basal cells (K1) and early differentiated cells (K10) could be performed.

**A**



**B**

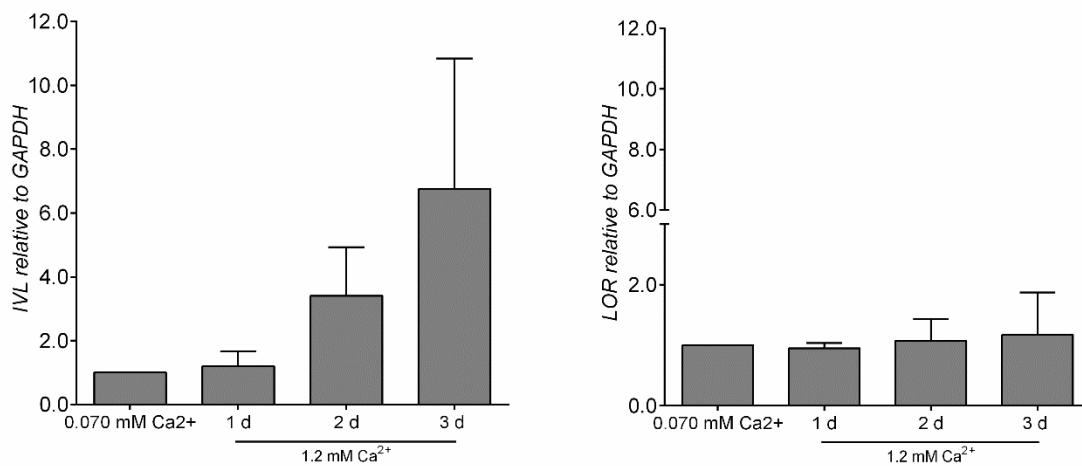


**Figure 3.1: Effect of stimulation with 1.2 mM Ca<sup>2+</sup> for 3 days on HPEKs.** (A) Phase contrast or bright field images were captured for a period of 1-3 days at x200 magnification (objective plus eyepiece). Scale represents 100  $\mu$ m. (B) RT-qPCR analysis of *IVL* (left) and *LOR* (right) in HPEKs treated with 1.2 mM Ca<sup>2+</sup> for 1-3 days. Values were normalised to GAPDH and depicted relative the basal control. Data is pooled from three independent experiments (+SEM).

Given that 1.2 mM of  $\text{Ca}^{2+}$  caused insufficient induction of both differentiation markers, the concentration was increased to 1.5 mM and the stimulation time was extended from 3 days to 5 days. After 5 days of 1.5 mM  $\text{Ca}^{2+}$ , HPEKs showed a strong induction of *IVL* at 42.3-fold ( $\pm 14.9$ ) higher than basal HPEKs. *LOR* showed an induction of 54.8-fold ( $\pm 31.3$ ) higher than basal HPEK, although expression levels between repeats were inconsistent (Fig. 3.2A). Transmitted light microscopy images show a substantial morphological change between basal and 5 d 1.5 mM treated HPEKs indicative of terminal differentiation (Fig. 3.2B).

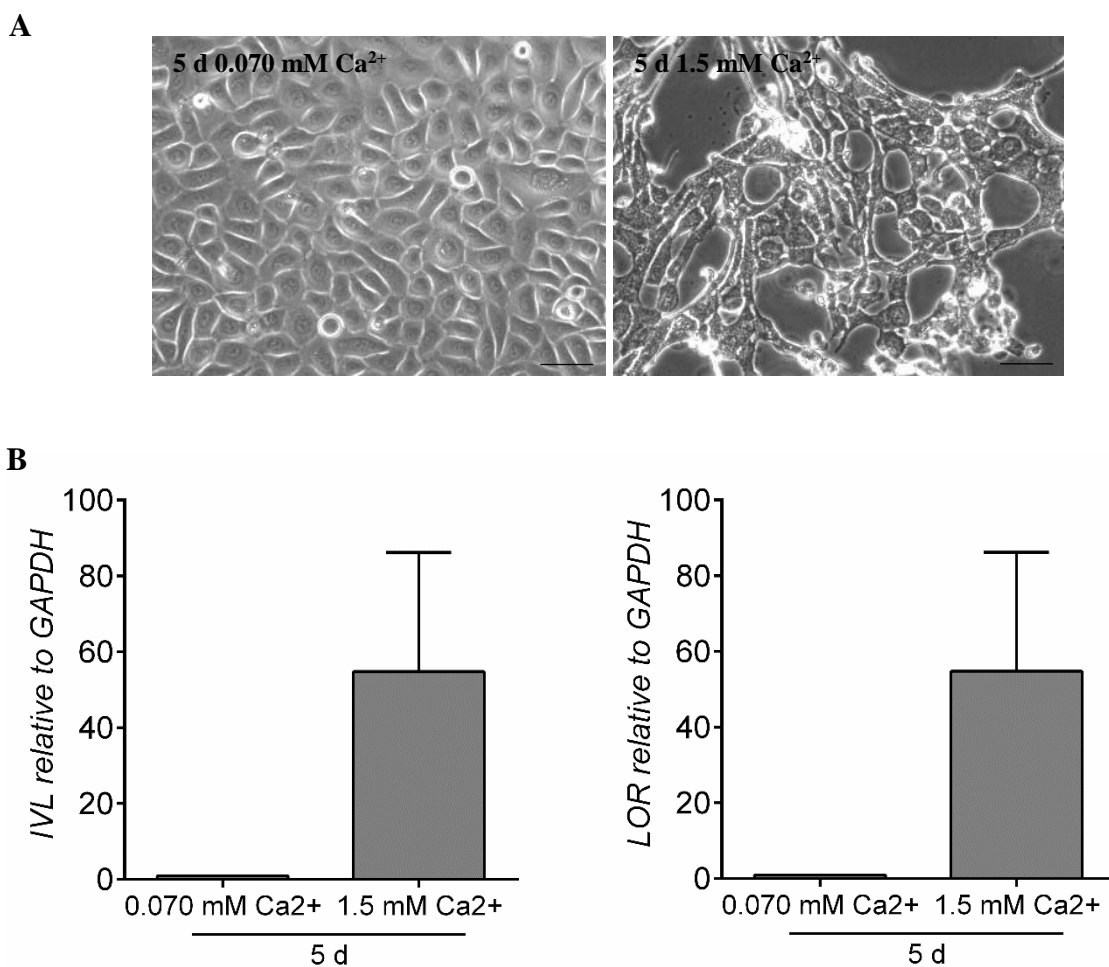


**Figure 3.2: Effect of stimulation with 1.5 mM  $\text{Ca}^{2+}$  for 5 days on HPEKs.** (A) Phase contrast images captured after a period of 5 days at x200 magnification (objective plus eyepiece). Scale represents 100  $\mu\text{m}$ . (B) RT-qPCR analysis of *IVL* (left) and *LOR* (right) in HPEKs treated with 1.5 mM  $\text{Ca}^{2+}$  for 5 days. Values were normalised to GAPDH and depicted relative to the basal control. Data is pooled from three independent experiments ( $\pm$ SEM).

The cell cycle is commonly dysregulated during differentiation and a hallmark of suprabasal cells is the accumulation of cyclin E. Therefore, the expression of G1/S phase cyclin E1 (*CCNE1*) and cyclin E2 (*CCNE2*), as well as the mitotic cyclin B (*CCNB*), was analysed in differentiating HPEKs. As shown in Figure 3.3, following 1 d exposure to 1.5 mM  $\text{Ca}^{2+}$ , levels of both *CCNE1* and *CCNE2* were unchanged. However, after 5 days a 2.0- and 2.4-fold increase in the expression of both *CCNE1* and *CCNE2* was observed. Expression of *CCNB* transcript 1 d post calcium switch was elevated ~2-fold before decreasing considerably to 0.26-fold over 5 days.

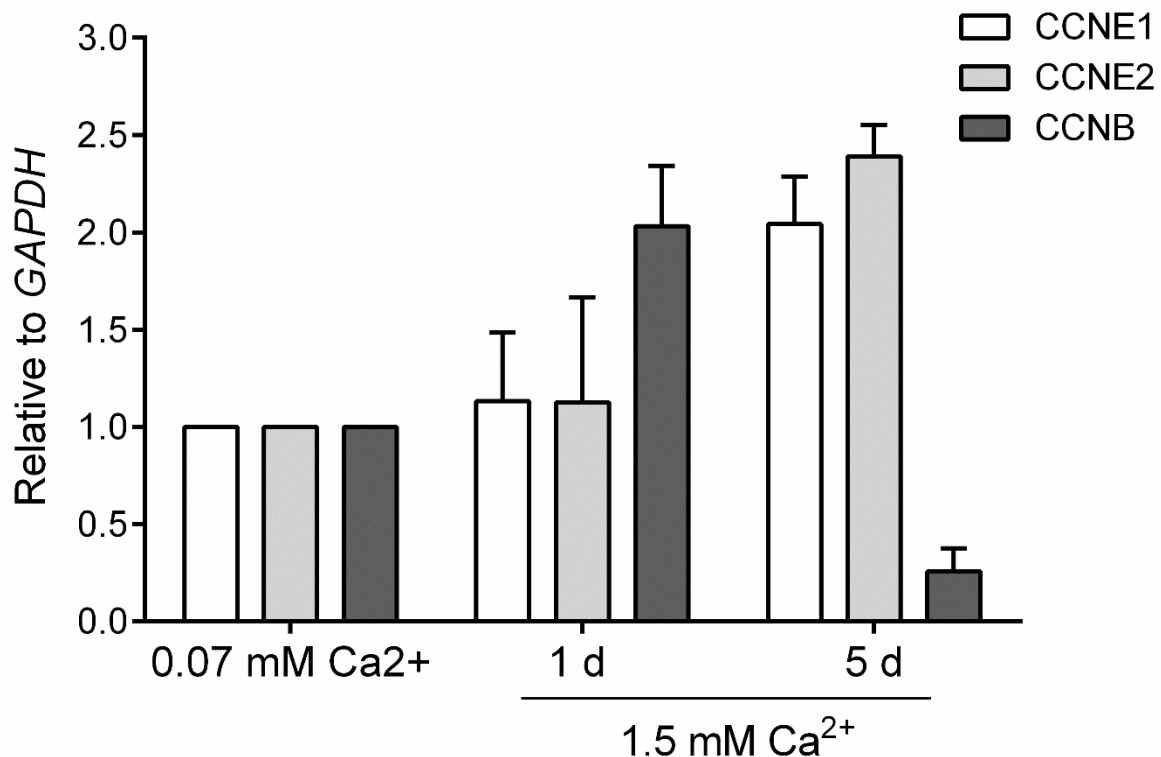


**Figure 3.3: Impact of differentiation on cyclin E1, E2 and B transcript expression.** RT-qPCR analysis of *CCNE1*, *CCNE2* and *CCNB* in HPEKs treated with 1.5 mM  $\text{Ca}^{2+}$  for 5 days. Values were normalised to *GAPDH* and depicted relative to the proliferating control. Data was pooled from three independent experiments ( $\pm$ SEM)

As recently reviewed by Lui and colleagues, transcript levels by themselves are not enough to predict protein expression (Liu, Beyer and Aebersold, 2016). Therefore, to determine whether elevated transcript levels translate into increased protein, involucrin and cyclin E proteins were analysed by western blot. A strong time-dependent increase of both involucrin and cyclin E was observed following treatment with 1.5 mM Ca<sup>2+</sup> for 5 days when compared with basal conditions (Fig. 3.4). Taken together, these results confirm commitment of HPEK to terminal differentiation.

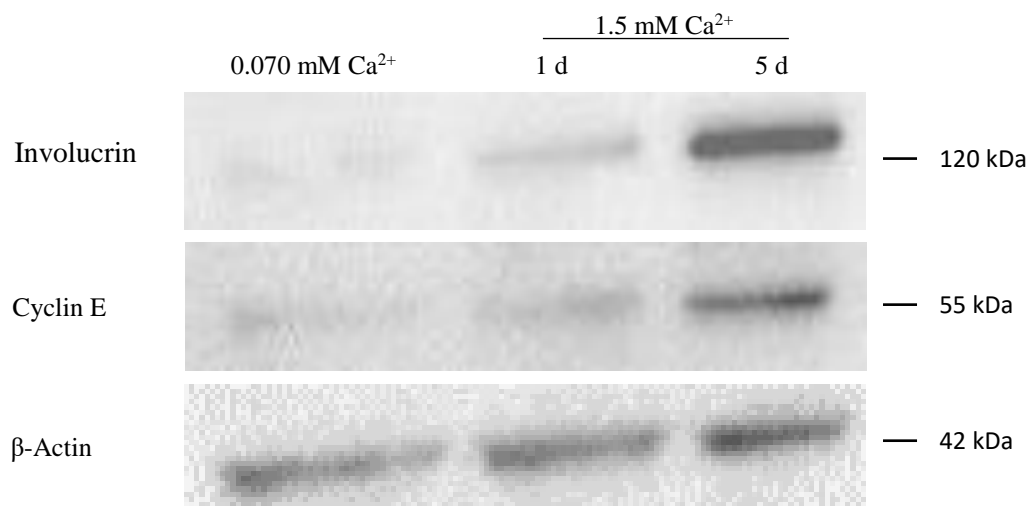


**Figure 3.4: Effect of differentiation on involucrin and cyclin E protein expression.** Western blot analysis of HPEKs under basal conditions or treated with 1.5 mM Ca<sup>2+</sup> for 1-5 days. Whole cell lysates (40 µg) were examined using primary antibodies for Involucrin and Cyclin E with β-Actin used as a loading control.

### 3.3.2. Effect of HPEK Differentiation on Expression of miR-184

Although miR-184 was not detected in proliferating HPEK monolayers in early work (Ryan, Oliveira-Fernandes and Lavker, 2006), it was found in RHE suggesting a role for miR-184 in epidermal stratification (Roberts et al., 2013). We therefore hypothesised that miR-184 also plays a role HPEK differentiation. Therefore, the expression of miR-184 in basal HPEKs and those stimulated with common differentiation agents was investigated.

Initially, miR-184 expression was examined in HPEKs differentiated with 1.2 mM Ca<sup>2+</sup> for 3 days. After 1 day a 2-fold ( $\pm 0.2$ ) induction was observed. The expression of miR-184 then returned to basal levels before a strong reduction to 0.3-fold ( $\pm 0.2$ ) following 3 days of 1.2 mM Ca<sup>2+</sup> stimulation (Fig. 3.5).

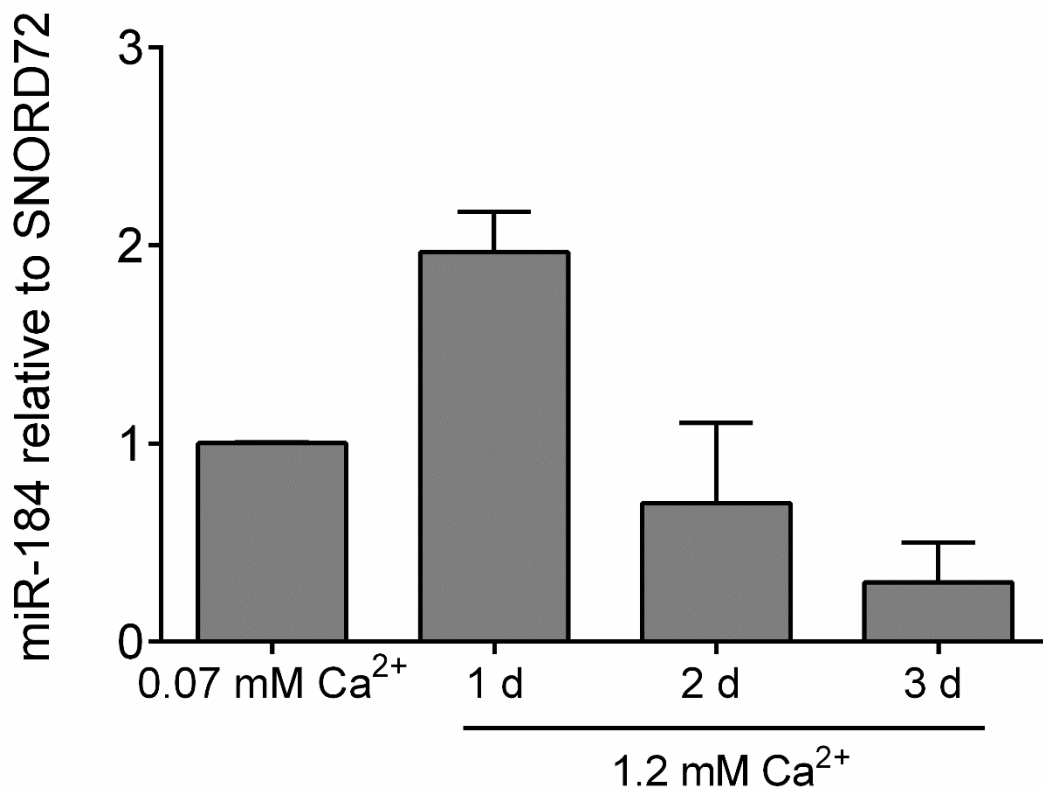


**Figure 3.5: Effect of 1.2 mM Ca<sup>2+</sup> treatment on miR-184 expression.** RT-qPCR analysis of miR-184 in HPEKs treated with 1.2 mM Ca<sup>2+</sup> for 3 days. Values were normalised to SNORD72 and depicted relative to HPEK grown in 0.07 mM Ca<sup>2+</sup> for 3 days. Data was pooled from three independent experiments ( $\pm$ SEM).

Since treatment with 1.2 mM Ca<sup>2+</sup> for 3 days did not promote adequate differentiation (Fig. 3.1), miR-184 expression was analysed in HPEK differentiated for 5 days with 1.5 mM Ca<sup>2+</sup>. A striking 26-fold ( $\pm 1.3$ ) induction of miR-184 with a 2.8-fold ( $\pm 1.7$ ) induction at 1 d was observed, consistent with work by Nagosa and colleagues (Nagosa et al., 2017) (Fig. 3.6).

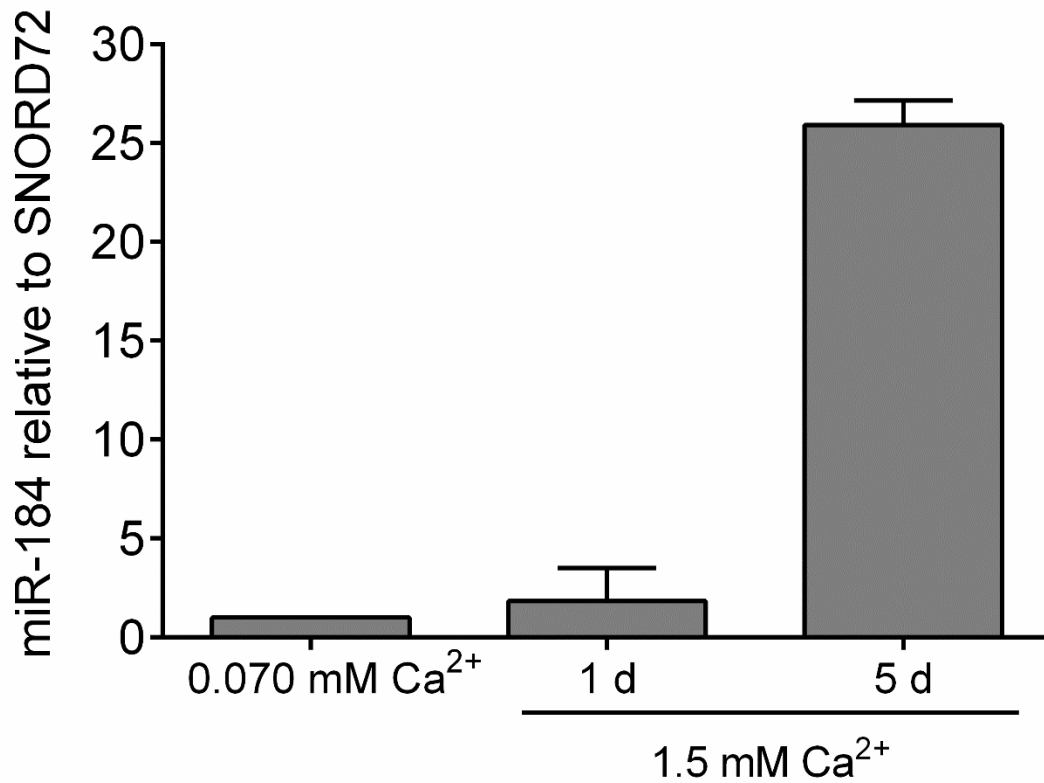


**Figure 3.6: Effect of 5 days 1.5 mM Ca<sup>2+</sup> treatment on miR-184 expression.** RT-qPCR analysis of miR-184 in HPEKs treated with 1.5 mM Ca<sup>2+</sup> for 5 days. Values were normalised to SNORD72 and depicted relative to HPEK grown in 0.07 mM Ca<sup>2+</sup> for 3 days. Data was pooled from three independent experiments ( $\pm$ SEM).

To assess the impact of calcium-independent keratinocyte differentiation on miR-184 expression the effect of three other common differentiation agents, interferon gamma (IFN- $\gamma$ ) (Karlsson, Vahlquist and Torma, 2010), vitamin D (1,25(OH)D<sub>3</sub>) (Bikle, 2004) and phorbol myristate acetate (PMA) (Karlsson, Vahlquist and Torma, 2010) was examined. Following stimulation for 5 days with 100 nM of PMA, following work by Torma and colleagues, despite a robust induction of *IVL* (Fig. 3.7A), miR-184 expression was relatively unchanged (Fig. 3.7B).

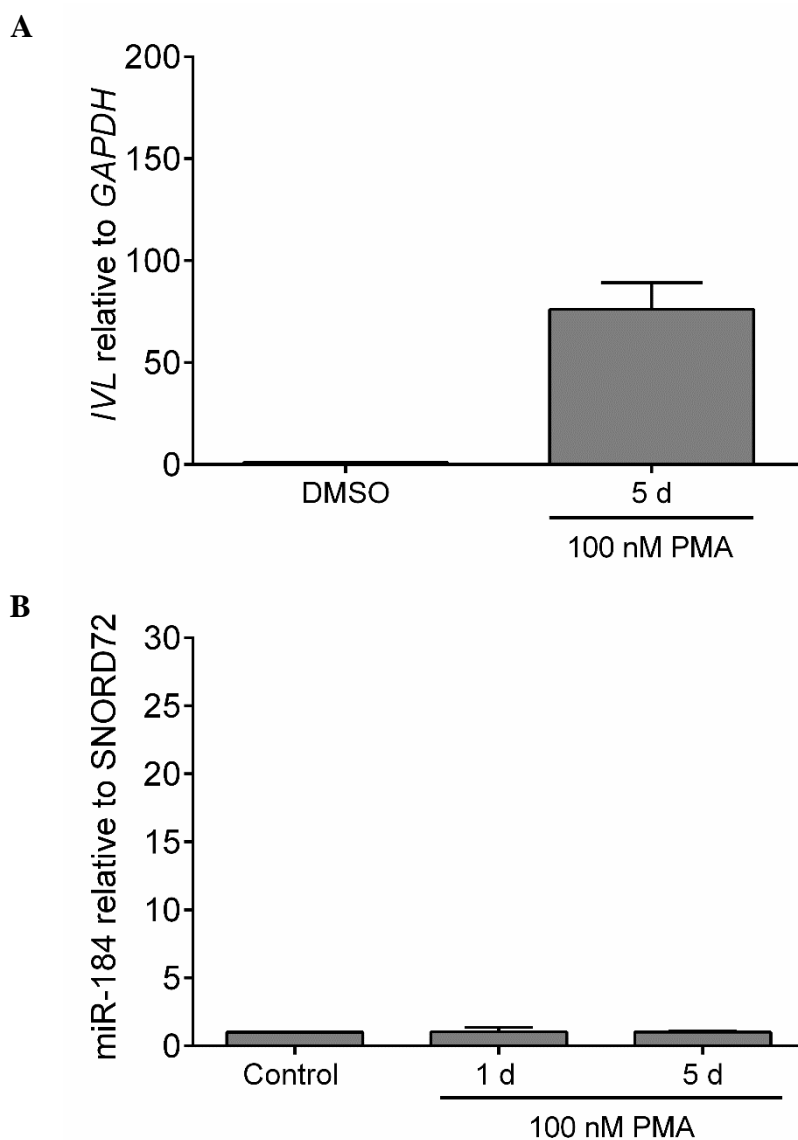


**Figure 3.7: Impact of PMA treatment on miR-184 expression.** RT-qPCR analysis of (A) *IVL* or (B) miR-184 in HPEKs treated with 100 nM PMA for 5 days. Values were normalised to SNORD72 for miR-184 or *GAPDH* for *IVL* and depicted relative to HPEK grown in 0.01% DMSO for 5 days. Data was pooled from three independent experiments ( $\pm$ SEM).

Contrastingly, based on work by Hill and co-workers, 100 nM 1,25(OH)D<sub>3</sub> provided a notable decrease in expression of miR-184 to 0.4-fold ( $\pm 0.2$ ; Fig. 3.8B), with a similar induction of *IVL* (Fig. 3.8A). However, treatment with IFN- $\gamma$  (10 ng/ml) failed to show any induction of miR-184, with low levels detected within basal HPEK reduced to an undetectable level. Collectively, these results suggest that the induction of miR-184 observed after 5 days of stimulation with 1.5 mM Ca<sup>2+</sup> seems to be associated with Ca<sup>2+</sup>-dependent pathways and not simply the process of keratinocyte differentiation.

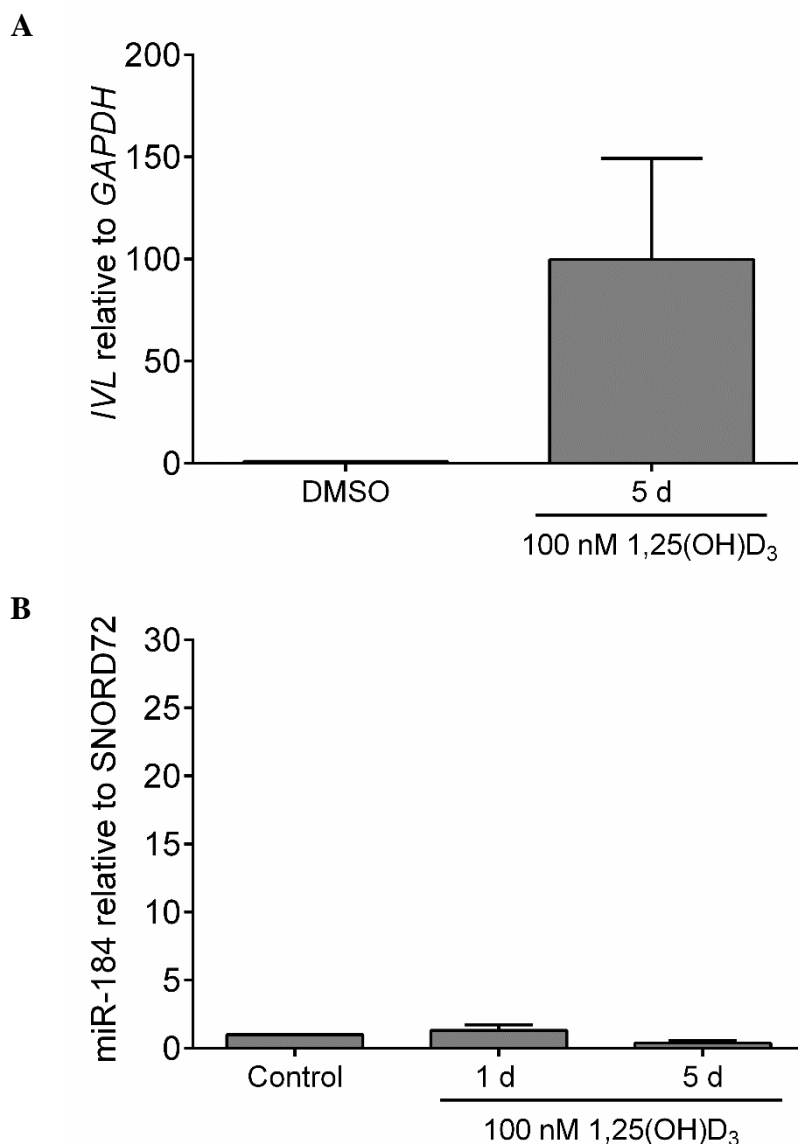


**Figure 3.8: Effect of 1,25(OH)D<sub>3</sub> on miR-184 expression.** RT-qPCR analysis of (A) *IVL* or (B) miR-184 in HPEKs treated with 100 nM 1,25(OH)D<sub>3</sub> for 5 days. Values were normalised to SNORD72 for miR-184 or *GAPDH* for *IVL* and depicted relative to HPEK grown in 0.07 mM Ca<sup>2+</sup> for 5 days. Data was pooled from three independent experiments ( $\pm$ SEM).

### 3.3.3. Effect of SOCE Inhibition on Ca<sup>2+</sup>-dependent miR-184 Induction

The Ca<sup>2+</sup> sensor STIM1 and Ca<sup>2+</sup> channel ORAI facilitates SOCE and maintain epidermal homeostasis. Since the miR-184 induction observed during keratinocyte differentiation was dependent upon Ca<sup>2+</sup>, the relationship between SOCE and Ca<sup>2+</sup>-dependent miR-184 induction was examined. The expression of miR-184 was therefore analysed in HPEKs maintained for 5 days in 1.5 mM Ca<sup>2+</sup> and treated with the SOCE blocker, Gd<sup>3+</sup> or the ORAI1 specific pharmacologic inhibitor, BTP2.

The trivalent cation, Gd<sup>3+</sup> is a non-selective ion channel inhibitor that blocks ORAI1-dependent Ca<sup>2+</sup> entry at 1–5  $\mu$ M (Putney, 2010). Pre-treatment with 1  $\mu$ M Gd<sup>3+</sup> prior to stimulation with 1.5 mM Ca<sup>2+</sup> significantly reduced miR-184 expression by 80% to 0.2-fold ( $\pm$ 0.03), as depicted in Fig. 3.9A. Furthermore, pre-treatment of differentiating HPEKs with the ORAI1 inhibitor, BTP2, suppressed expression of miR-184 by 70% to 0.3-fold ( $\pm$ 0.05; Fig. 3.10A). The levels of *IVL* transcript was analysed in Gd<sup>3+</sup> and BTP2 treated HPEK. A ~50% decrease was observed when compared with the control (Fig. 3.9B and 3.10B).

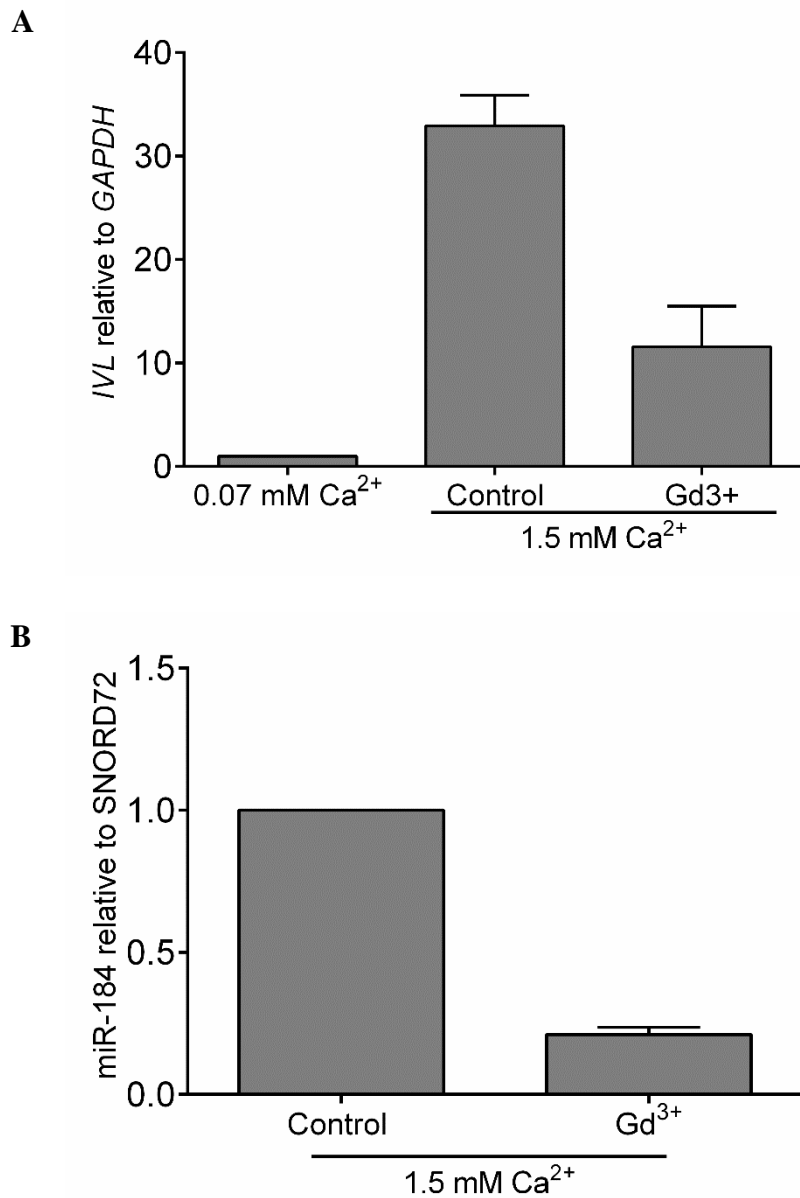


**Figure 3.9: Effect of Gd<sup>3+</sup> on miR-184 expression during calcium induced differentiation.** RT-qPCR analysis of (A) *IVL* and (B) miR-184 from HPEKs pre-treated for 1 hour with 1  $\mu$ M Gd<sup>3+</sup> followed by stimulation with 1.5 mM Ca<sup>2+</sup> for 5 days. Values were normalised to SNORD72 for miR-184 or *GAPDH* for *IVL* and depicted relative to the appropriate control. Data is pooled from three independent experiments (+SEM) for miR-184 analysis and two for *IVL* analysis.

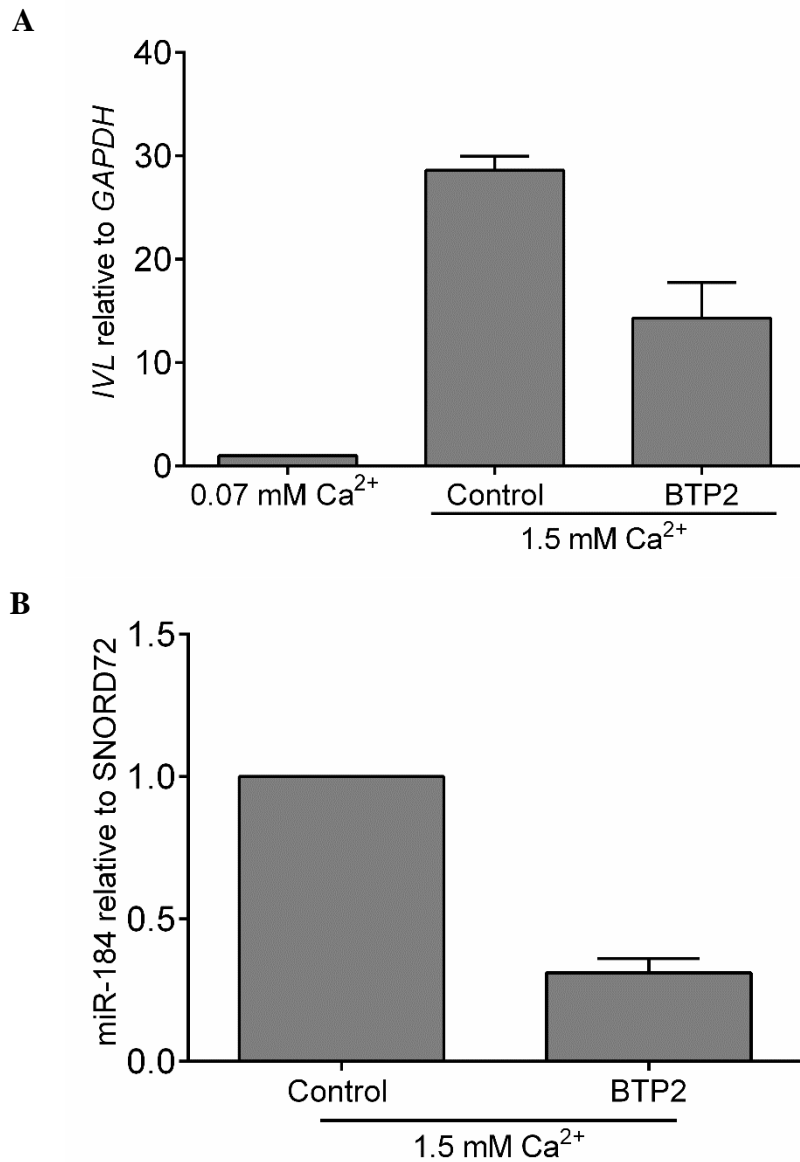


**Figure 3.10: Effect of BTP2 on miR-184 expression during calcium induced differentiation.** RT-qPCR analysis of (A) miR-184 and (B) *IVL* from HPEKs pre-treated for 1 hour with 1  $\mu$ M BTP2 followed by stimulation with 1.5 mM Ca<sup>2+</sup> for 5 days. Values were normalised to SNORD72 for miR-184 or *GAPDH* for *IVL* and depicted relative to the appropriate control. Data is pooled from three independent experiments (+SEM) for miR-184 analysis and two for *IVL* analysis.

To confirm the observations from the SOCE inhibitors, siORAI1 was nucleofected into HPEK and the levels of miR-184 were analysed (Prakriya et al., 2006). A strong decrease of miR-184 expression to 0.3-fold ( $\pm 0.07$ ) was observed in 5 d differentiated HPEKs introduced to 100 nM siORAI1 when compared to HPEKs treated with 100 nM of control oligonucleotide. Similarly to the SOCE inhibitors, levels of *IVL* were reduced by around 50% in differentiated HPEK transfected with siORAI1.

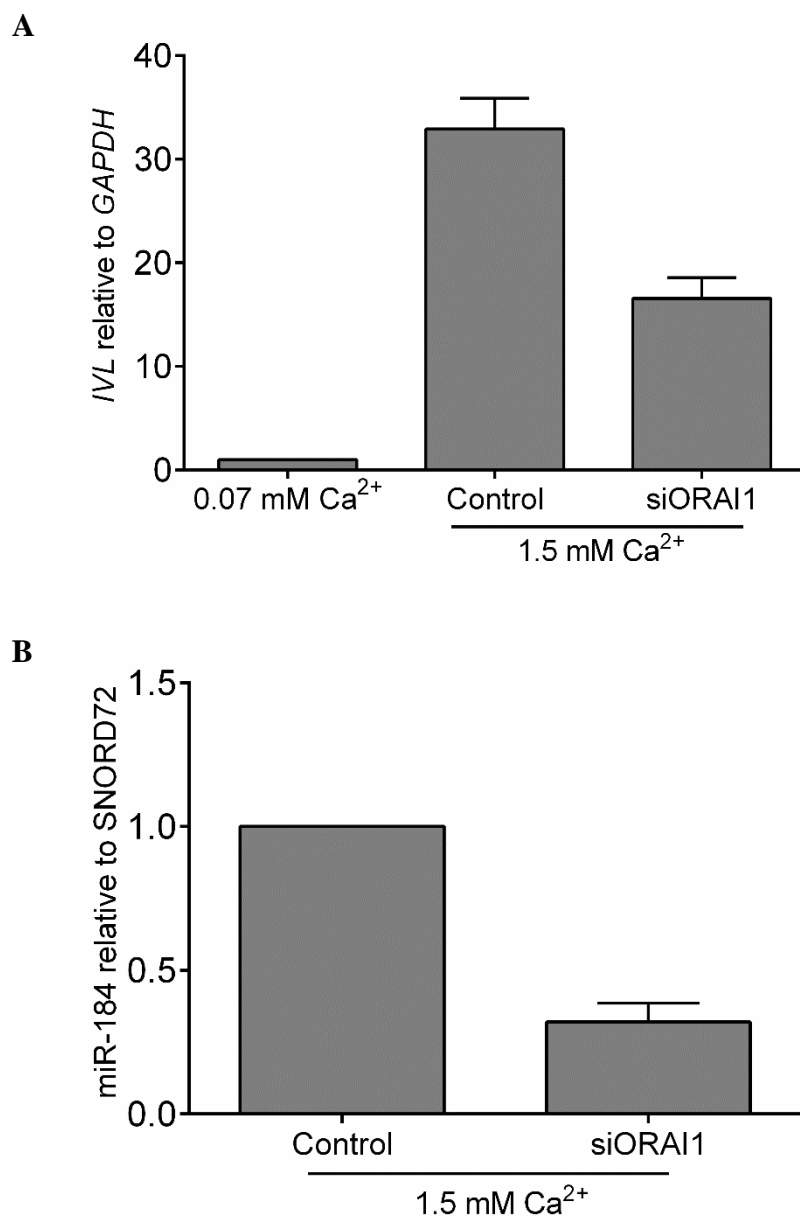


**Figure 3.11: Impact of ORAI1 knockdown on miR-184 expression during calcium induced differentiation.** RT-qPCR analysis of miR-184 and *IVL* from HPEKs nucleofected with 100 nM of siORAI1 followed by stimulation with 1.5 mM  $Ca^{2+}$  for 5 days. Values were normalised to SNORD72 for miR-184 or *GAPDH* for *IVL* and depicted relative to the appropriate control. Data is pooled from three independent experiments (+SEM).

To investigate the influence of downstream SOCE effectors upon miR-184 induction, the calcineurin inhibitor, CsA, was used to impede NFAT function. Pre-treatment with 1  $\mu$ M CsA resulted in a reduction of miR-184 expression to 0.3-fold ( $\pm$ 0.1) when compared with the control (Fig. 3.12). Taken together, these results suggest the miR-184 induction observed during  $\text{Ca}^{2+}$ -dependent differentiation is reliant upon SOCE and the downstream transcriptional activity of the calcineurin/NFAT axis.

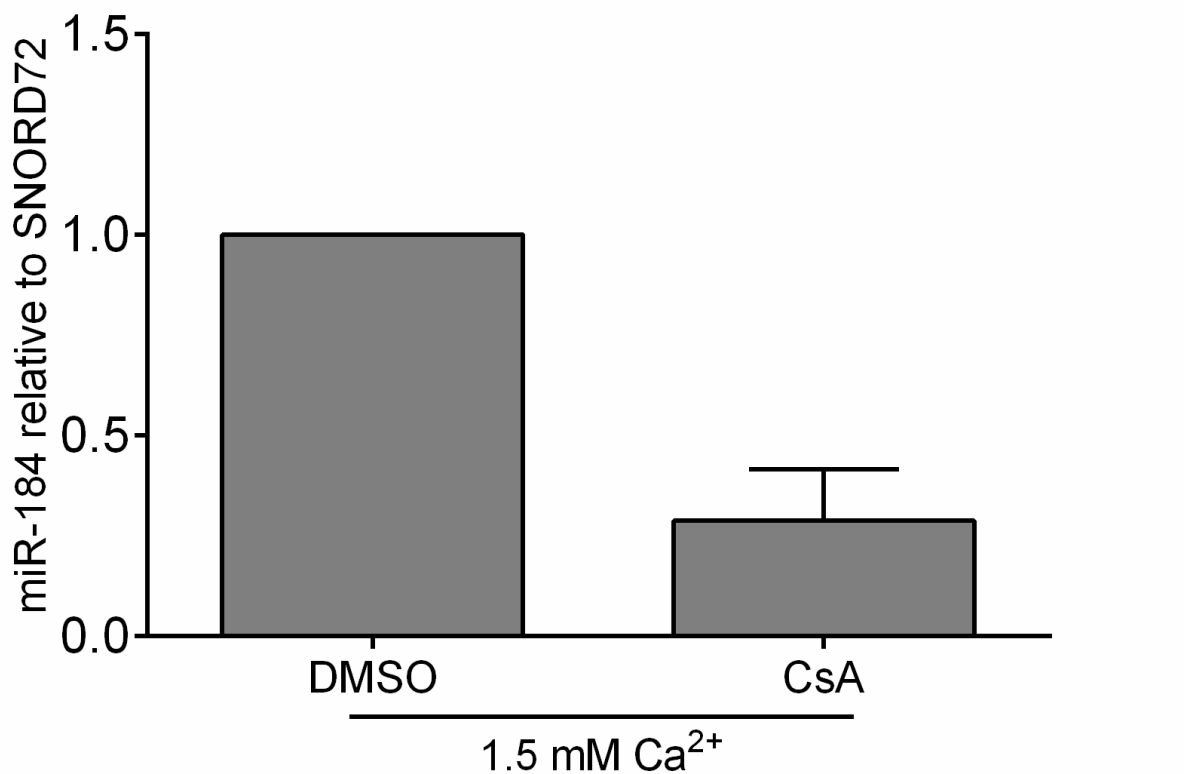


**Figure 3.12: Effect of NFAT1 inhibition on miR-184 expression during calcium induced differentiation.** RT-qPCR analysis of miR-184 from HPEKs treated with 1  $\mu$ M CsA followed by stimulation with 1.5 mM  $\text{Ca}^{2+}$  for 5 days. Values were normalised to SNORD72 for miR-184 depicted relative to the DMSO control. Data is pooled from three independent experiments (+SEM).

Finally, the levels of *ORAI1* was assessed primarily as a control for siORAI knockdown, but also to evaluate whether *ORAI1* inhibitors interfere with the channels expression levels over 5 days of inhibition. Following inhibition of SOCE for 5 days under basal condition,  $Gd^{3+}$  reduced levels of *ORAI1* transcript by around 45% (Fig. 3.13A), although this could be down to the non-specific actions of  $Gd^{3+}$  as BTP2 caused little effect on *ORAI1* expression (Fig. 3.14A). Encouragingly, following 5 days of inhibition with exposure to 1.5 mM  $Ca^{2+}$  neither  $Gd^{3+}$  (Fig. 3.13B) nor BTP2 (Fig. 3.14B) caused any notable change in *ORAI1* transcript levels. As expected, *ORAI1* expression following treatment with 100 nM siORAI1 was reduced by 71% to 0.29-fold ( $\pm 0.11$ ; Fig. 3.15A) in proliferating HPEK and by 55% to 0.45-fold ( $\pm 0.01$ ; Fig. 3.15B) in differentiated cells.

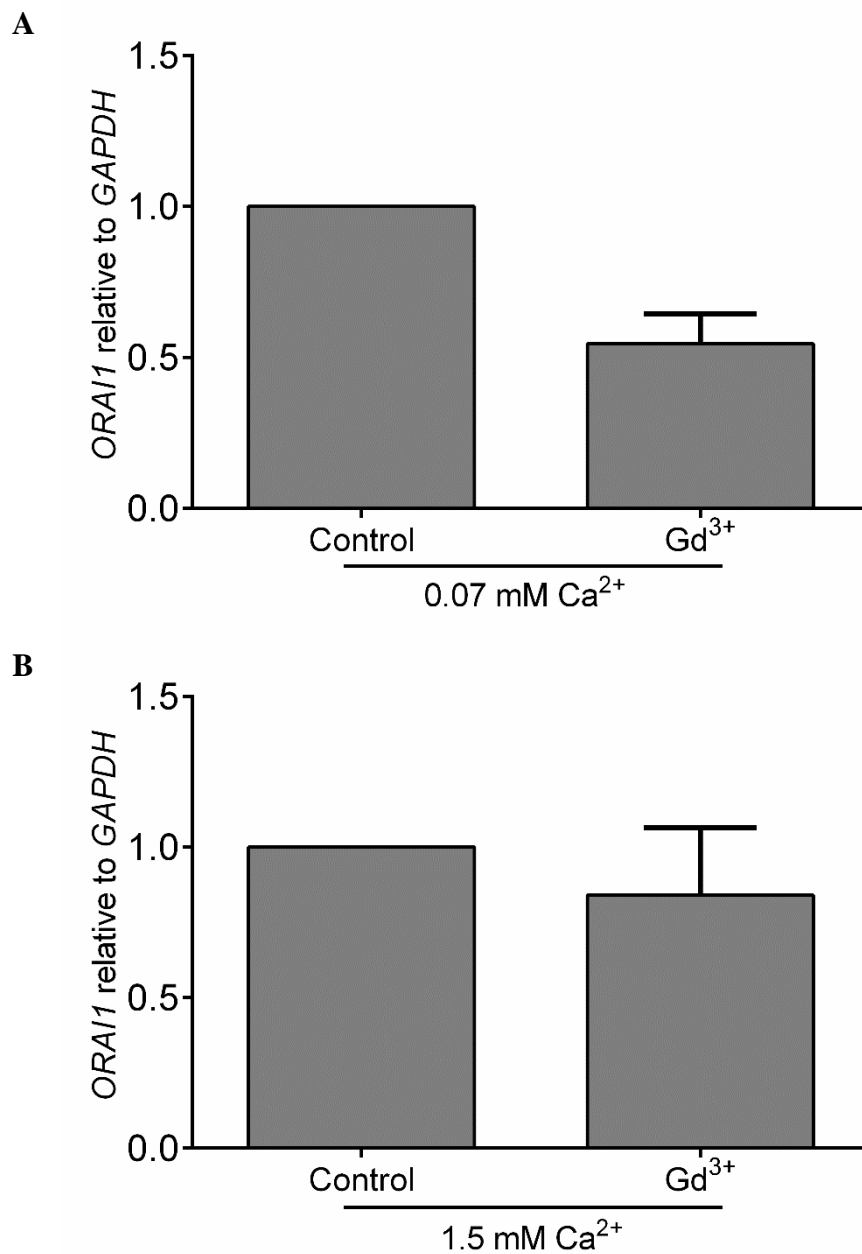


**Figure 3.13: Effect of Gd<sup>3+</sup> treatment on *ORAI1* transcript expression.** RT-qPCR analysis of *ORAI1* in HPEKs pre-treated for 1 hour with 1  $\mu$ M Gd<sup>3+</sup> before differentiating with 1.5 mM Ca<sup>2+</sup> for 5 days. Values were normalised to *GAPDH* and depicted relative to the vehicle control (Water). Data is pooled from three independent experiments ( $\pm$ SEM).

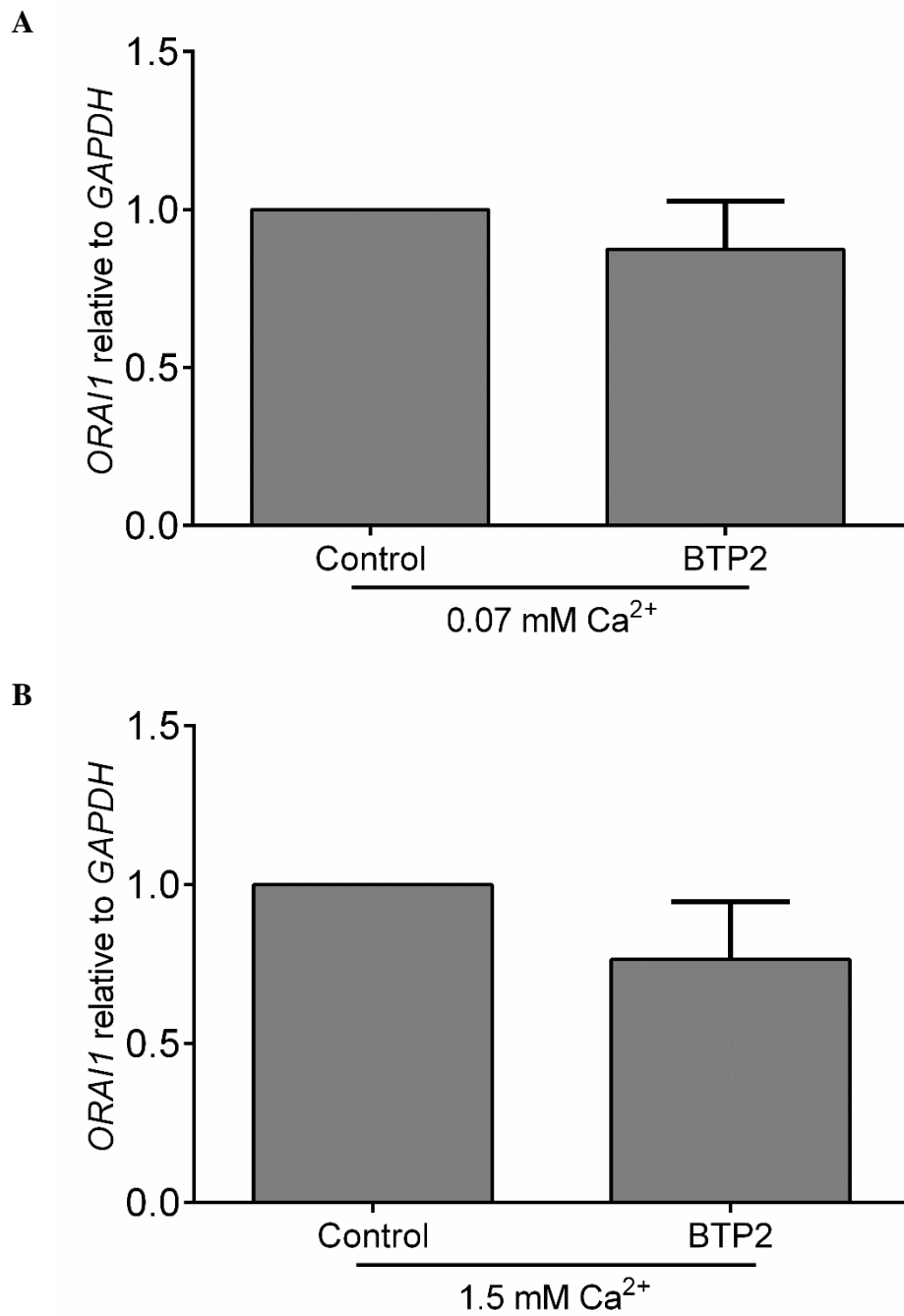


**Figure 3.14: Effect of BTP2 treatment on *ORAI1* expression.** RT-qPCR analysis of *ORAI1* in HPEKs pre-treated for 1 hour with 1  $\mu$ M BTP2 before treatment with 1.5 mM Ca<sup>2+</sup> for 5 days. Values were normalised to *GAPDH* and depicted relative to the vehicle control (DMSO). Data is pooled from three independent experiments ( $\pm$ SEM).

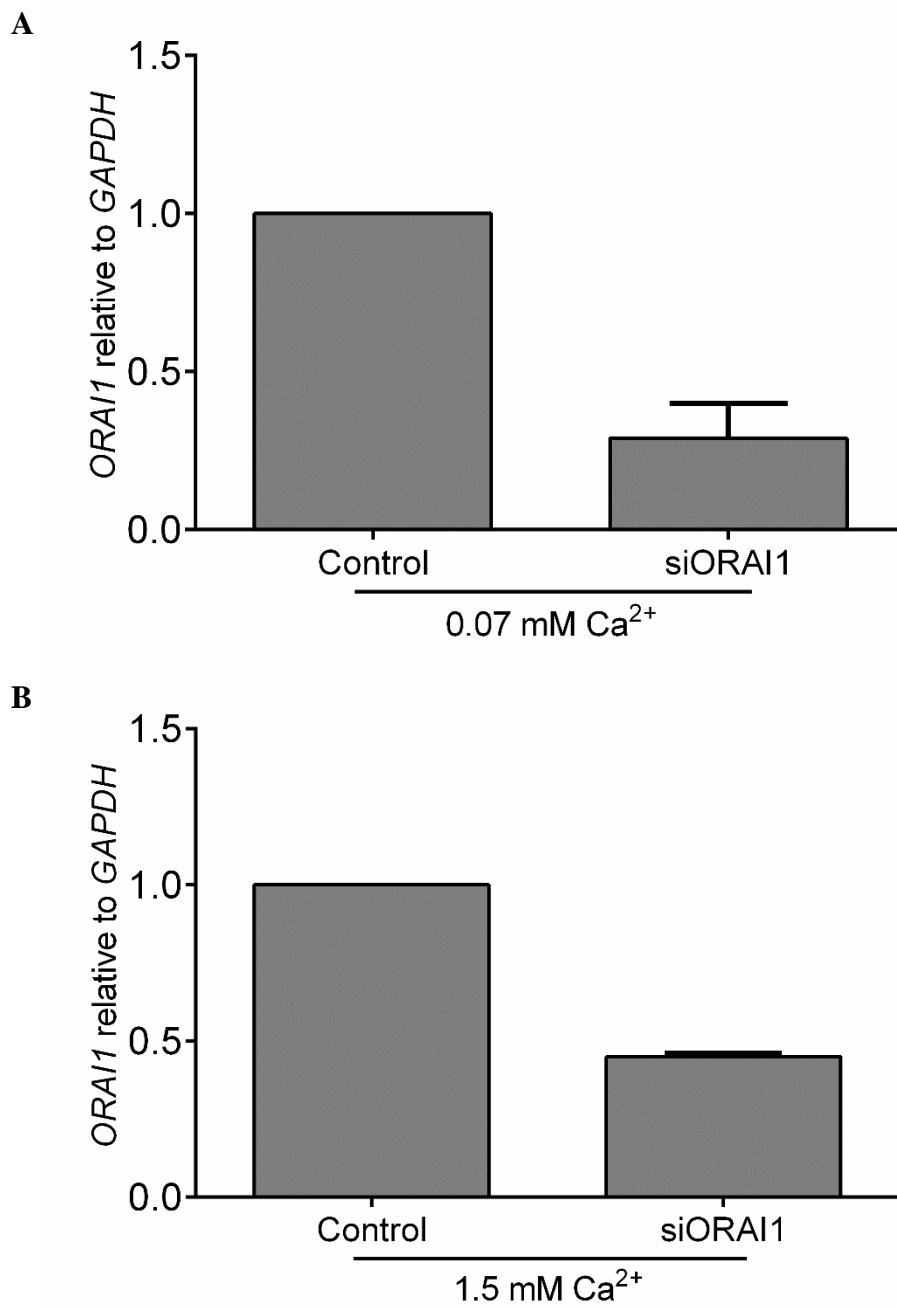


**Figure 3.15: Impact of siORAI1 nucleofection on *ORAI1* transcript expression.** RT-qPCR analysis of *ORAI1* in HPEKs nucleofected with 100 nM siORAI1 before stimulation with 1.5 mM Ca<sup>2+</sup> for 5 days. Values were normalised to *GAPDH* and depicted relative to the control oligo. Data is pooled from three independent experiments ( $\pm$ SEM).

### 3.3.4. Expression of miR-184 in Psoriatic Lesions

Expression of miR-184 in psoriasis has previously been reported (Joyce et al., 2011; Roberts et al., 2013). However, the role of miR-184 in psoriasis remains poorly described. Therefore, expression of mature miR-184 was examined by RT-qPCR in non-lesional (PN) and lesional (PP) areas from the skin of patients with psoriasis.

Initially, mature miR-184 expression was examined from eight patients and data was presented as mean expression. A 4-fold ( $\pm 0.9$ ) increase of miR-184 was observed in PP biopsies when compared to PN however this method of analysis fails to clearly show inherent patient variance.

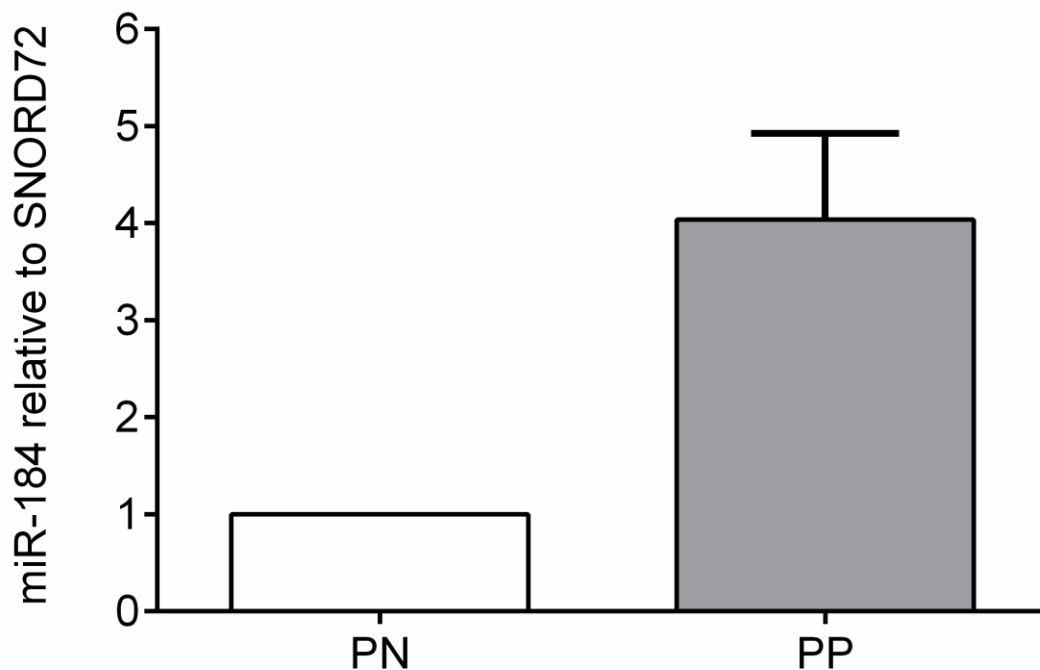


**Figure 3.16: Mean expression of miR-184 in psoriatic lesions.** Levels of mature miR-184 was analysed by RT-qPCR in psoriatic non-lesional (PN) and lesional (PP) biopsies. Values were normalised to SNORD72 and depicted relative PN. Data is pooled from eight independent biopsies ( $\pm$ SEM).

Therefore, to better depict this variance, miR-184 levels previously recorded from eight patient biopsies were reanalysed. As shown in figure 3.17A, miR-184 was upregulated in every PP sample when compared to PN ranging from 1.4-fold higher (patient number 02) to 8.1-fold higher (patient number 04). Although still upregulated, observations here do not emulate the substantial 40-10,000-fold increase detected by Roberts and colleagues (Roberts et al., 2011). To show the range present within PN and PP samples, box and whiskers charts were used. When plotting normalised Ct values known as  $-\Delta Ct$  ( $Ct_{miR-184} - Ct_{SNORD72}$ ) there is a significant increase of miR-184 (decrease in  $-\Delta Ct$ ) with a median of 8.8 in PP when compared with the median of 10.5 in PN. There is large variance present amongst PP samples when compared to PN, with minimum values of 6.1 and 8.9 in addition to maximum values of 10.4 and 10.9 respectively (Fig. 3.17A).

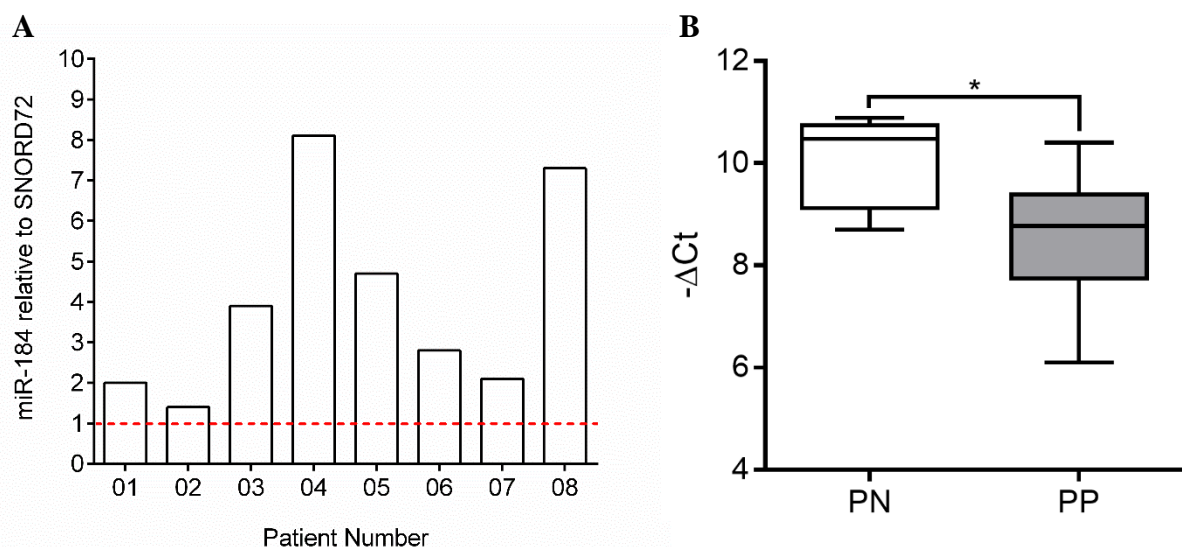


**Figure 3.17: Patient variation of miR-184 expression in psoriatic lesions.** Levels of mature miR-184 was analysed by RT-qPCR from psoriatic non-lesional (PN) and lesional (PP) biopsies taken from eight patients. Values were normalised to SNORD72 and plotted relative to their corresponding PN values (red line; A). Box and whiskers were plotted using  $-\Delta Ct$  ( $Ct_{miR-184} - Ct_{SNORD72}$ ) The top and bottom of each box represent the 75th and 25th percentile and the middle line represents the median value with the extended lines depicting the range (B). \* represents  $p \leq 0.05$ .

## 3.4. Discussion

### 3.4.1. Differentiation of HPEKs

The first aim of this thesis was to establish a model for *in vitro* epidermal keratinocyte differentiation. Keratinocyte differentiation can be induced by adjusting the concentration of  $\text{Ca}^{2+}$  in the media with Hennings and colleagues demonstrating that 1.2 mM of  $\text{Ca}^{2+}$  for 3 days is sufficient (Hennings et al., 1980). Conflictingly, in initial experiments differentiation associated genes such as *IVL* were inconsistently induced by 1.2 mM  $\text{Ca}^{2+}$  after 3 days (Fig. 3.2). Later work demonstrated that elevated  $\text{Ca}^{2+}$  along with extended exposure times provides a more consistent approach to reproducible differentiation (Borowiec et al., 2013).

Consistently, involucrin was induced at both mRNA and protein level using 1.5 mM  $\text{Ca}^{2+}$  for 5 d. Loricrin, on the other hand, was less reproducible (Fig. 3.2B). However, other differentiation markers could have been assessed such as K1, K10 and filaggrin. In addition to the induction of differentiation-associated genes, cell cycle changes are important to keratinocyte differentiation, supporting their enlargement through re-replication and promotion of growth arrest (Zanet et al., 2010). Work by Freije and colleagues has shown that cyclin E accumulates in suprabasal keratinocytes where it causes DNA damage, consequently activating p53/p21 DDR pathways, which in turn inhibits mitotic regulators such as cyclin B and cdk1, ultimately leading to growth arrest and terminal differentiation (Freije et al., 2012). Taken together, our data is consistent with this study whereby we show elevated cyclin E at both transcript and protein level, in addition to severely diminished cyclin B mRNA levels following 5 days of  $\text{Ca}^{2+}$ -induced differentiation.

### 3.4.2. Induction of miR-184 During HPEK Differentiation

Expression of miR-184 was induced during terminal differentiation, and this induction was only observed when stimulated with  $\text{Ca}^{2+}$ . An early mouse study found that miR-184 was undetectable in the epidermis and only present in ocular keratinocytes (Ryan, Oliveira-Fernandes and Lavker, 2006). However, recent work has implicated miR-184 in epidermal keratinocyte differentiation, reporting a 4-fold increase of miR-184 levels in primary human keratinocytes following 7 days of high  $\text{Ca}^{2+}$ . This is consistent with our finding, as we both report elevated levels of miR-184 in human epidermal keratinocytes following  $\text{Ca}^{2+}$ -induced differentiation. However, we observed a much stronger induction of miR-184 at around 25-fold, but the differentiation conditions used by Nagosa and colleagues were poorly defined, i.e.  $\text{Ca}^{2+}$  concentration, with the disparity between levels of miR-184 likely arising from differences in experimental design (Nagosa et al., 2017).

Our data show the exclusive ability of elevated extracellular  $\text{Ca}^{2+}$  to promote miR-184 expression. The other common differentiation agents, PMA and  $1,25(\text{OH})\text{D}_3$ , failed to induce miR-184. Contrastingly, previous work by Sonkoly and co-workers have demonstrated that levels of miR-203, can be elevated by treatment with  $\text{Ca}^{2+}$ ,  $1,25(\text{OH})\text{D}_3$  and a phorbol ester analogue similar to PMA (Sonkoly et al., 2010). Both  $\text{Ca}^{2+}$  and PMA are potent activators of PKC. By activating PKC independent of  $\text{Ca}^{2+}$ , PMA promotes keratinocyte differentiation (Matsui et al., 1993). This suggests that induction of miR-184 observed following  $\text{Ca}^{2+}$  stimulation is somewhat uncoupled from PKC and AP-1 pathways. However, further work including inhibition of PKC/AP-1 activity during  $\text{Ca}^{2+}$ -induced differentiation, as well as activation of PKC/AP-1 in basal cells could be performed to validate this finding.

### 3.4.3. SOCE Facilitates Induction of miR-184

The ability of SOCE to regulate epidermal homeostasis has been assessed (Vandenberghe et al., 2013). The putative miRNAs induced specifically by SOCE has not been defined. Conversely, the regulation of miRNA expression by SOCE is unknown. Moreover, a link between miRNAs and SOCE in epidermal keratinocytes has not yet been reported. We have shown that miR-184 is induced during HPEK differentiation and that this induction is dependent on  $\text{Ca}^{2+}$ . SOCE is a predominant form of  $\text{Ca}^{2+}$  entry in keratinocytes.

Our data indicates that SOCE mediates the induction of miR-184 observed during  $\text{Ca}^{2+}$ -dependent differentiation, whereby levels of miR-184 are considerably reduced when factors important to SOCE activity are inhibited. Previous work has demonstrated the importance of miRNAs in the regulation of SOCE activity, with a recent study indicating that Dicer, a major miRNA biogenesis protein, is vital for SOCE function with its ablation in CD4+ T cells leading to downregulation of ORAI1, and consequently reduced  $\text{Ca}^{2+}$  entry, through SOCE-dependent mechanisms (Zhang et al., 2016). However, this is the first time to our knowledge that SOCE has been shown to directly regulate the expression of a miRNA. Additionally, it is the first time a link between miRNAs and SOCE in keratinocytes has been demonstrated. SOCE activity varies in proliferating and differentiating keratinocytes, suggesting that SOCE and its downstream pathways are key to the induction and fine-tuning of differentiation-associated miRNA expression. Although as of yet, there is little evidence to support this claim and therefore it could represent an exciting separate study, whereby miRNA profiling in keratinocytes with perturbed SOCE activity, could illuminate other miRNAs regulated in this fashion.

The transcription factor NFAT, is a major downstream effector of SOCE and a recent computational study has predicted that NFAT promotes the expression of 32 miRNAs, 12 of which overlap miRNAs expressed during *in vitro* epidermal keratinocyte differentiation

(Hildebrand et al., 2011; Kannambath, 2016). Nevertheless, miR-184 was not mentioned in either study. However, we show inhibition of NFAT using CsA, an inhibitor of the NFAT activator called calcineurin, leads to a striking reduction of miR-184 in keratinocytes following 5 days of high  $\text{Ca}^{2+}$ . This suggests that miR-184 expression during epidermal keratinocyte differentiation is highly dependent on NFAT activity.

When HPEKs were treated with SOCE inhibitors the induction of involucrin observed 5 days post calcium switch is severely diminished. Only a few studies have analysed involucrin expression in differentiating epidermal keratinocytes following inhibition of SOCE. Vandenberghe and co-workers report a striking increase of involucrin in primary human keratinocytes exposed to siORAI1 following a 24 h  $\text{Ca}^{2+}$  switch (Vandenberghe et al., 2013). However, our data, demonstrating reduced levels of involucrin in 5 d differentiated HPEK pre-transfected with siORAI1, is in opposition with this work, although the differences in time points used between studies prevents a direct comparison. Recent work by Numaga-Tomita and Putney partially supports our finding showing a similar reduction in differentiation-associated genes, specifically the early differentiation marker K1, in keratinocytes with diminished ORAI1 activity after 7 days of  $\text{Ca}^{2+}$  (Numaga-Tomita and Putney, 2013). Taken together this suggests a possible regulatory role for ORAI1 in the progression from early to late differentiation. Furthermore, this data raises the question of whether it is reduced SOCE activity that is directly responsible for the reduction of miR-184 expression, or whether it is simply as a result of a dampened differentiation response.

#### **3.4.4. miR-184 is Elevated in Psoriatic Lesions**

Consistent with the literature, our data show that miR-184 expression was elevated in psoriasis. We observed a ~4-fold increase of miR-184 in PP samples when compared with PN. Contrastingly, a deep sequencing study by Joyce and co-workers describes an increase of miR-184 in psoriatic samples when compared with healthy skin (Joyce et al., 2011). Interestingly, levels of miR-184 between PP and PN were relatively the same. This could be down to differences in chosen methods, with Joyce et al., employing a next generation sequencing (NGS) approach and our data representing RT-qPCR (Joyce et al., 2011). Additionally, recent work has demonstrated elevated levels of miR-184 in the epidermis of psoriatic lesions when compared with non-lesional skin (Roberts et al., 2013). Moreover, miR-184 can be upregulated in HaCaTs and RHE by pro-inflammatory cytokines implicated in psoriasis, such as IL-22 (Roberts et al., 2013). Given that miR-184 was induced during HPEK differentiation, the elevated levels of miR-184 observed in psoriasis and following IL-22 stimulation may be a compensatory mechanism to recover a differentiated phenotype.

## **4. Function of miR-184 During HPEK**

### **Differentiation**

## 4.1. Introduction

The ability of miR-184 to regulate the balance between proliferation and differentiation has been reported in a variety of cell types over the past decade. An early study has shown that miR-184 prevented differentiation of adult neural stem cells, with those overexpressing miR-184 differentiating into ~30% less astrocytes and neurons (Liu et al., 2010). Work on hepatocellular carcinoma cell lines implicated miR-184 in proliferation. With ectopic expression of miR-184 leading to increased cell colonies, enhanced MTT signal and an elevated number of cells present in S phase accompanied by reduced G1/G0 percentages (Wu et al., 2014). A recent study on mice by Tattikota and colleagues uncovered a role for miR-184 in pancreatic  $\beta$ -cell proliferation, where miR-184 suppressed expression of Ago2 resulting in reduced  $\beta$ -cell islet mass and consequently decreased levels of circulating insulin (Tattikota et al., 2014).

Lavker and co-workers proposed a role for miR-184 in the regulation of corneal keratinocytes when they detected high levels of miR-184 in mouse corneal epithelium but not in foot-pad epithelium (Ryan, Oliveira-Fernandes and Lavker, 2006). They later found miR-184 modulates proliferation of corneal epithelium by indirectly elevating SHIP2. This in turn acts as a negative regulator of Akt signalling leading to decreased cellular growth and survival. However, they did not detect miR-184 in epidermal keratinocytes (Yu et al., 2008). In contrast, work by Ross and colleagues showed miR-184 in RHE and HaCaTs (Roberts et al., 2013). Furthermore, a very recent study by Nagosa and co-workers showed miR-184 was significantly elevated in the suprabasal layers of mouse epidermis (Nagosa et al., 2017). Furthermore, through use of loss- and gain-of-function mouse models Shalom-Feuerstein and co-workers, were able to show that miR-184 maintains the equilibrium between proliferation and differentiation by direct regulation of the Notch and p63 pathways (Nagosa et al., 2017).

Early work by Missero and colleagues in p21 null mice revealed that early p21 expression is required to commit keratinocytes to terminal differentiation (Missero et al., 1996). E-type cyclins are components of core cell cycle machinery and consist of two functionally redundant proteins, cyclin E1 and cyclin E2, encoded by *CCNE1* (ch.19q12) and *CCNE2* genes (ch.8q22.1). Cyclin E1 is the most abundant protein form and herein represents cyclin E in protein analysis. During keratinocyte differentiation, cyclin E accumulation causes DNA damage predominately through activation of p21/p53 pathways and this DNA damage is vital for successful keratinocyte stratification (Freije et al., 2012; Freije et al., 2014). Although we and others have shown miR-184 in differentiating epidermal keratinocytes, the role of miR-184 within the proliferation: differentiation switch has remained relatively unexplored.

## 4.2. Aims

- To optimise miR-184 nucleofection of HPEKs
- Investigate the impact of perturbed miR-184 activity on keratinocyte growth
- Examine the effect of dysregulated miR-184 upon differentiation

## 4.3. Results

### 4.3.1. Optimisation of Nucleofection

To determine nucleofection efficiencies, HPEKs were nucleofected with 2 µg of pmaxGFP vector and the expression levels were investigated after 2 and 5 days. When quantified the proportion of GFP-positive cells exhibited a modest increase from 29.7% ( $\pm 0.5\%$ ) at 2 days to 34.8% ( $\pm 1.0\%$ ;  $P=0.012$ ) at 5 days (Figure 4.1), suggesting some cells that had taken up the plasmid, but those which were not expressing GFP at day 2, were able to express GFP at a later

time point. The morphology of the cells appeared normal, suggesting that nucleofection did not have adverse effects (Fig. 4.1A-D).

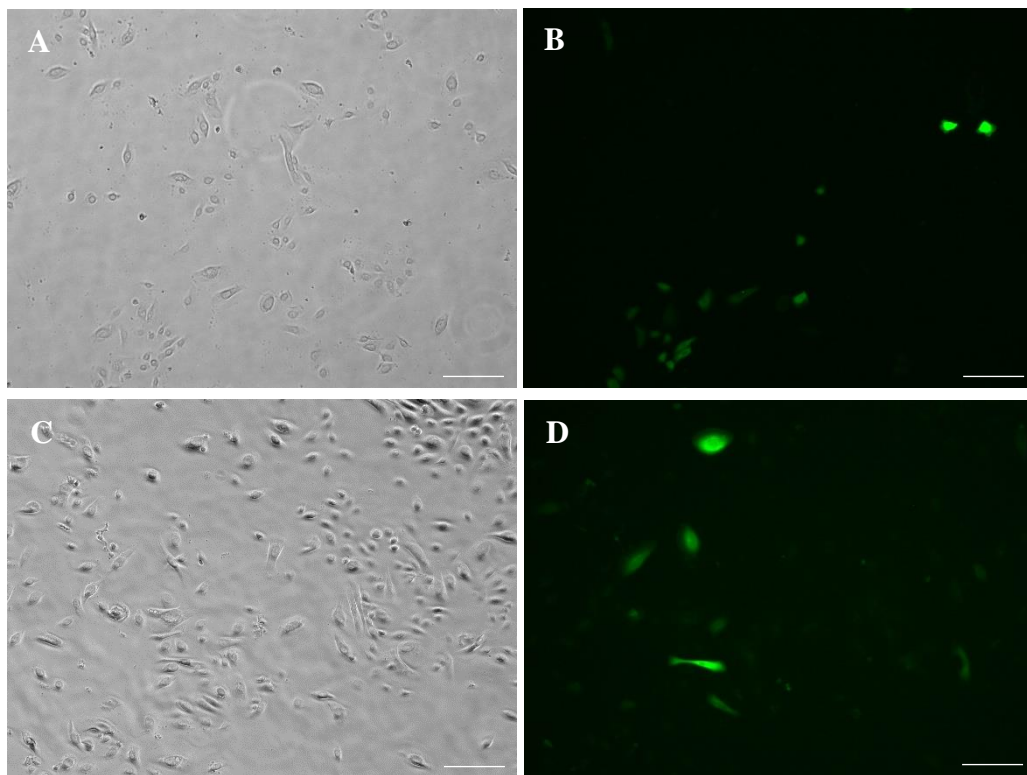


**Figure 4.1: Effect of time on GFP expressing HPEKs.** HPEKs 2 days (A-B) or 5 days (C-D) post-nucleofection. A and C phase contrast images, same field of view. B and D fluorescent images of pmaxGPF vector, same field of view. Scale represents 100  $\mu$ M. Chart (Bottom) represents percentages of GFP-positive cells quantified using ImageJs cell counting tool. Data represents averages from four fields of view taken from three independent experiments. (+SEM). \* represents  $p \leq 0.05$ .

Nucleofection with small synthetic oligonucleotides such as miRNA mimics or siRNA is thought to have increased efficiencies when compared with GFP. Therefore, the levels of mature miR-184 following nucleofection with miR-184 mimic were analysed by RT-qPCR. Initially, HPEK were nucleofected with 20 nM of miR-184 mimic which elevated expression of mature miR-184 by 3.9-fold ( $\pm 1.8$ ) when compared with the control, although the variance between replicates was high (Fig.4.2A). To further elevate the levels of miR-184, HPEKs were exposed to the upper limit of miR-184 mimic used by Ross and colleagues at 100 nM, resulting in a striking 4787-fold ( $\pm 1618$ ) increase (Fig. 4.2B) (Roberts et al., 2013).

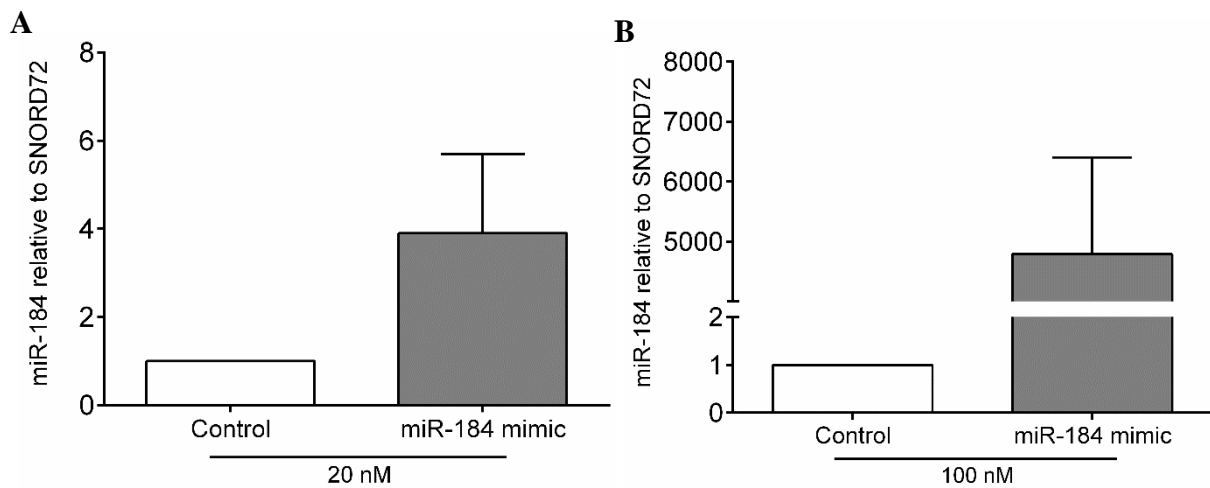


**Figure 4.2: Effect of miR-184 mimic on basal miR-184 expression.** HPEKs nucleofected with 20 nM (A) or 100 nM (B) of control oligonucleotide or miR-184 mimic and grown 0.07 mM  $\text{Ca}^{2+}$  for 1 day before analysis by RT-qPCR. Values were normalised to SNORD72 and depicted relative to the control oligo. Data represents two independent experiments (+SEM).

To examine the longevity of synthetic miR-184, nucleofected HPEKs were grown for extended periods of time before analysis by RT-qPCR. As expected 3 days post nucleofection the levels of mature miR-184 remained elevated at 1386-fold when compared with the control oligonucleotide (Fig. 4.3A). Interestingly, when compared with 1 d nucleofection (Fig. 4.2B), miR-184 levels were reduced by ~70%. As shown in Figure 4.3B, the expression of miR-184 following 5 days of growth was further reduced to 68.8-fold when compared with the control oligonucleotide. Even though nucleofection with miR-184 mimic displayed a reduction over 5 days, supraphysiological levels would still be present with amounts at 5 days at least 2-fold higher than the uppermost biological levels during differentiation (Fig. 3.6).

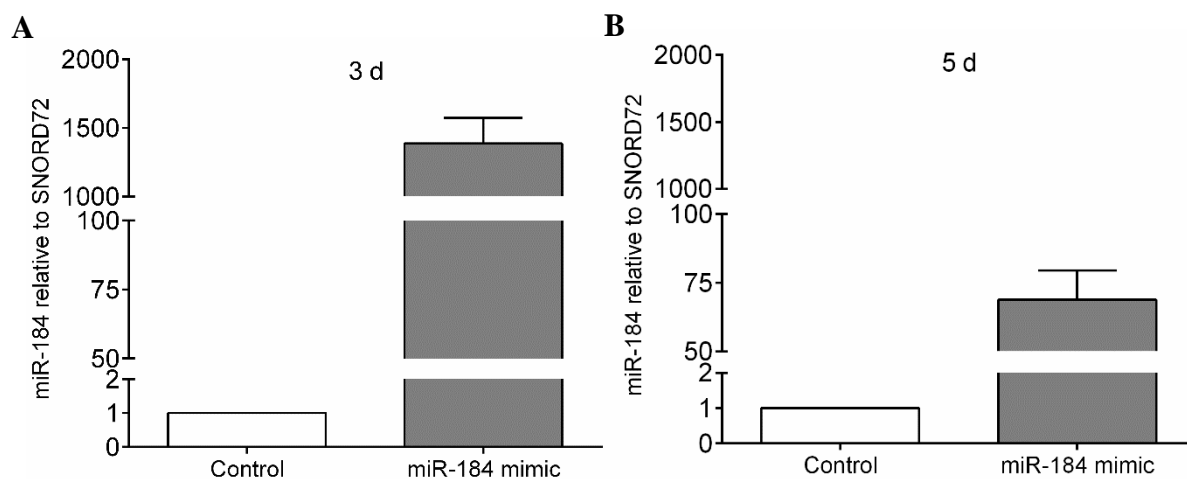


**Figure 4.3: Impact of miR-184 mimic on miR-184 expression over 5 days.** HPEKs nucleofected with either 100 nM control oligonucleotide (white bars) or 100 nM miR-184 mimic (grey bars) and grown in 0.07 mM  $\text{Ca}^{2+}$  for either 3 d (A) or 5 days (B) before analysis by RT-qPCR. Values were normalised to SNORD72 and depicted relative to the control oligo. Data represents two independent experiments (+SEM).

### 4.3.2. The Effects of miR-184 on Keratinocyte Growth

miR-184 has been shown to suppress cell viability and growth in several cell types (Tattikota et al., 2014; Tung et al., 2016; Wang et al., 2017). Therefore, HPEK were transfected with 100 nM of miR-184 mimic. Cell viability and growth were measured by MTT and trypan blue exclusion assays. Nucleofection with miR-184 mimic showed a decrease in MTT signal with a ~40% reduction compared with the control, though this failed to reach significance ( $p=0.06$ ; fig. 4.4B). In trypan blue assays, miR-184 mimic reduced cell viability by 16.2% to 83.8% (+0.4%;  $p\leq 0.0001$ ) compared to the control oligonucleotide. Taken together data suggests that introduction of miR-184 mimic may have a toxic effect on HPEK reducing cellular viability.

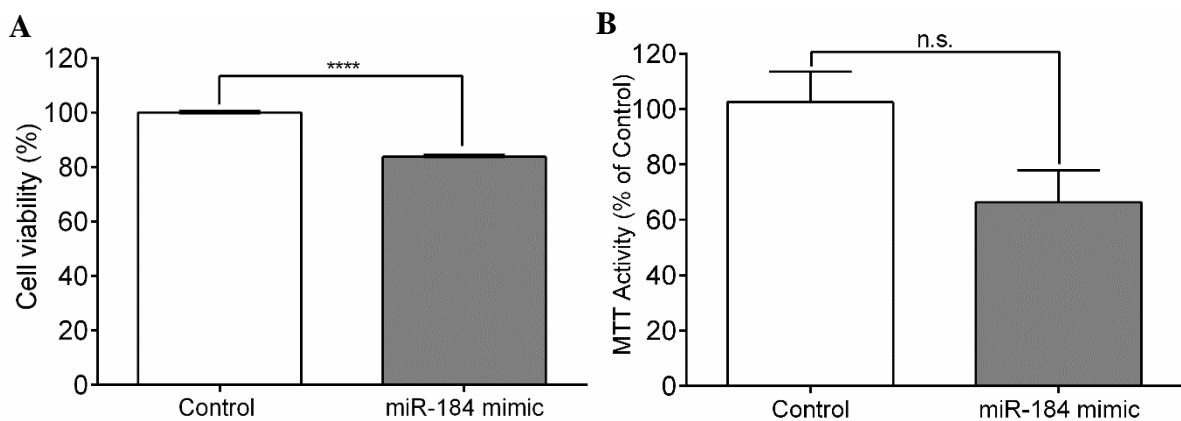


**Figure 4.4: Effect of miR-184 on cellular health.** HPEKs were nucleofected with 100 nM of control oligonucleotide or miR-184 mimic grown and grown in 0.07 mM  $\text{Ca}^{2+}$  for 2 days before analysis by either exclusion trypan blue (A) or MTT (B). Values were depicted relative to the control. Data represents three independent experiments (+SEM). \*\*\*\* depicts significance  $p\leq 0.0001$ . n.s. indicates no significance.

Given that miR-184 reduces cell viability it was hypothesised that miR-184 would have an impact on cell cycle progression in epidermal keratinocytes. HPEKs loaded with miR-184 were stained with the DNA-binding dye propidium iodide (PI) and analysed by flow cytometry. The proportion of cells in G1-phase was 76.7% when loaded with miR-184 mimic, compared with 63.4% of the control oligonucleotide. A corresponding drop from 21.6% to 16% during S-phase and 13.4% to 7.4% in G2 was also observed in cells with elevated miR-184 (Fig. 4.5). This suggests that miR-184 causes cells to accumulate and/or arrest in G1-phase of the cell cycle.

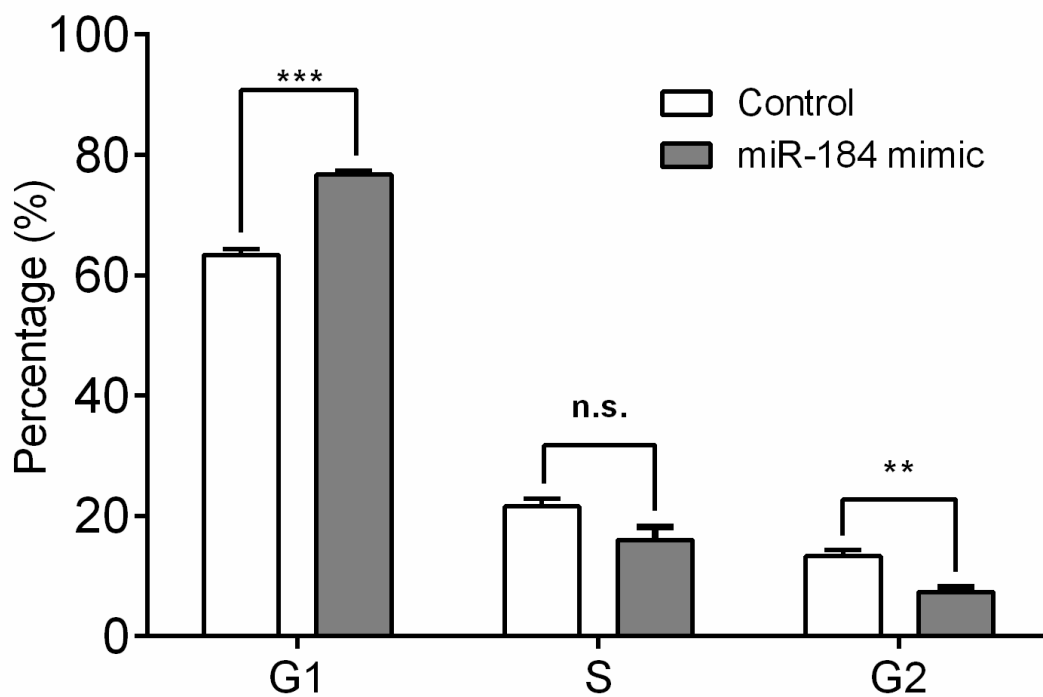


**Figure 4.5: The effect of miR-184 on cell cycle dynamics.** HPEKs were transfected with 100 nM of either control oligonucleotide or miR-184 mimic and grown under basal conditions for 2 days before staining with 100 ug/ml propidium iodide for 45 minutes and analysed by flow cytometry. Data represents three independent repeats (+SEM). \*\*\*\* depicts significance  $p \leq 0.0001$  and \* indicates significance  $p \leq 0.05$ .

### 4.3.3. The Effects of miR-184 on Keratinocyte Differentiation

#### 4.3.3.1. Impact of miR-184 on Involucrin

To assess the effect of miR-184 on differentiation markers, involucrin was analysed by RT-qPCR. When proliferating HPEK are loaded with synthetic miR-184, *IVL* transcript is reduced in a dose dependent manner, with 20 nM leading to a modest reduction in *IVL* levels to 0.75-fold (Fig. 4.6A). Strikingly, 100 nM led to a 75% reduction when compared with the control oligonucleotide (Fig. 4.6B).

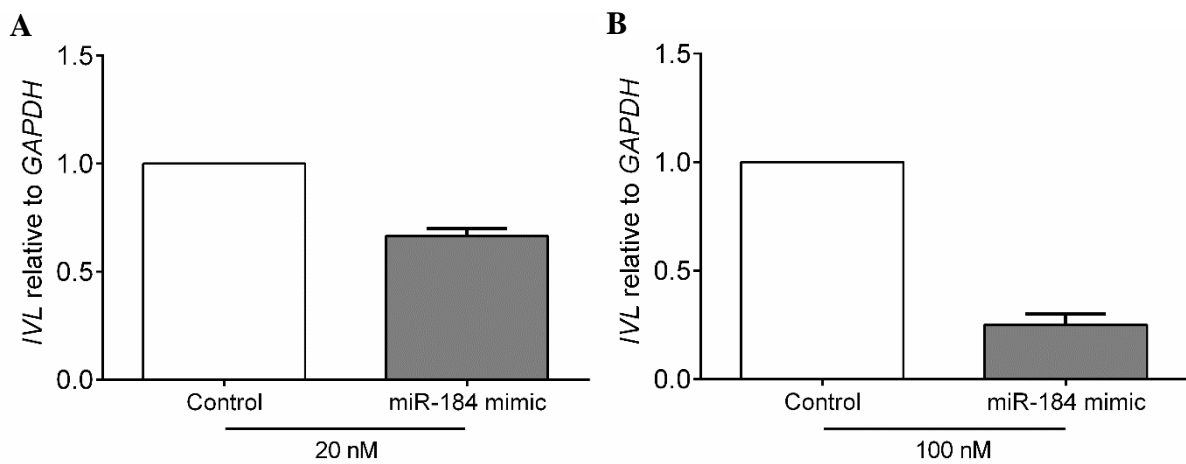


**Figure 4.6: Effect of miR-184 on involucrin transcript expression in HPEKs.** HPEKs were nucleofected with either 20 (A) or 100 (B) nM of control oligonucleotide or miR-184 mimic grown in 0.07 mM  $\text{Ca}^{2+}$  for 2 days before analysis by RT-qPCR. Values were normalised to *GAPDH* and depicted relative to the 0.07 mM  $\text{Ca}^{2+}$  control. Data represents two repeats (+SEM).

Next, to evaluate translational activity, involucrin protein levels were determined by western blot in cells overexpressing miR-184. Ectopic miR-184 induced a 3.4-fold ( $\pm 0.5$ ) elevation of involucrin after 5 days (Fig. 4.7A) and represented 79.5% of the overall chemiluminescent signal compared to 20.5% of the control oligonucleotide (Fig. 4.7B).

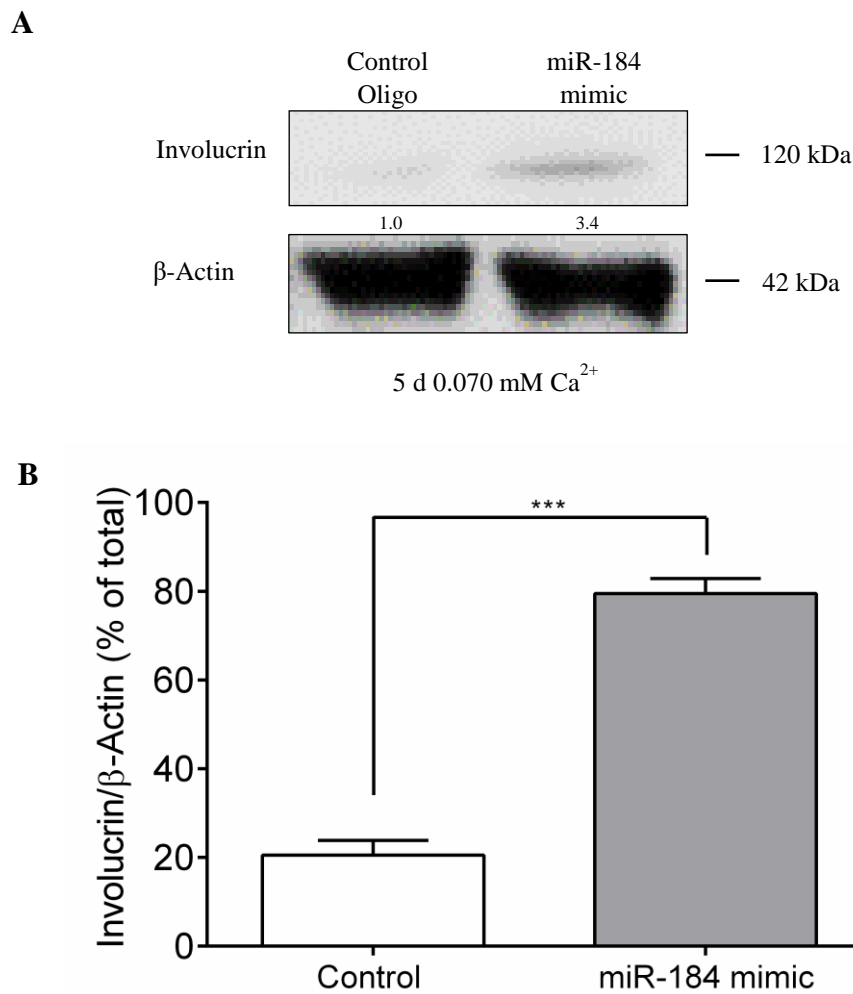


**Figure 4.7: Impact of miR-184 overexpression on Involucrin in HPEKs.** HPEKs were nucleofected with 100 nM of control oligonucleotide or miR-184 mimic and grown in 0.07 mM  $\text{Ca}^{2+}$  for 5 days before analysis by western blot (A). Values were normalised to  $\beta$ -Actin and density proportions were calculated from the total densities of the samples (B). Data represents three independent experiments (+SEM). \*\*\* depicts significance were  $p \leq 0.001$ .

### 4.3.3.2. Impact of Ectopic miR-184 on Cyclin E

Cyclin E plays a vital role in keratinocyte differentiation (Freije et al., 2012). When compared with the control oligonucleotide both *CCNE1* and *CCNE2* transcripts remained unchanged in basal HPEKs possessing miR-184 (Fig. 4.8, 4.9). At the protein level, cyclin E in proliferating cells exposed to 100 nM miR-184 mimic was 3.1-fold ( $\pm 0.7$ ) higher when compared with the control oligonucleotide (Fig. 4.10).

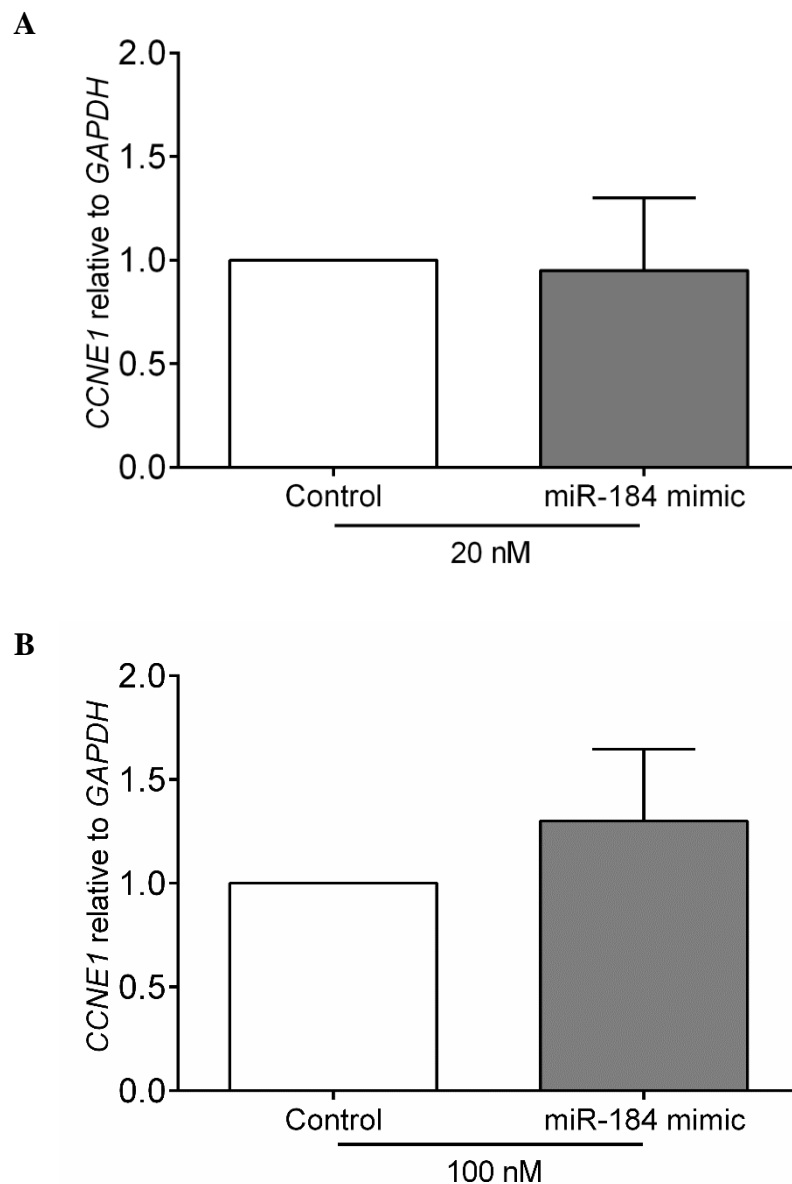


**Figure 4.8: Effect of miR-184 on cyclin E1 transcript expression in HPEKs.** HPEKs were nucleofected with either 20 (A) or 100 (B) nM of control oligonucleotide or miR-184 mimic grown in 0.07 mM  $\text{Ca}^{2+}$  for 5 days before analysis by RT-qPCR. Values were normalised to *GAPDH* and depicted relative to the 0.07 mM  $\text{Ca}^{2+}$  control. Data represents three independent experiments (+SEM).

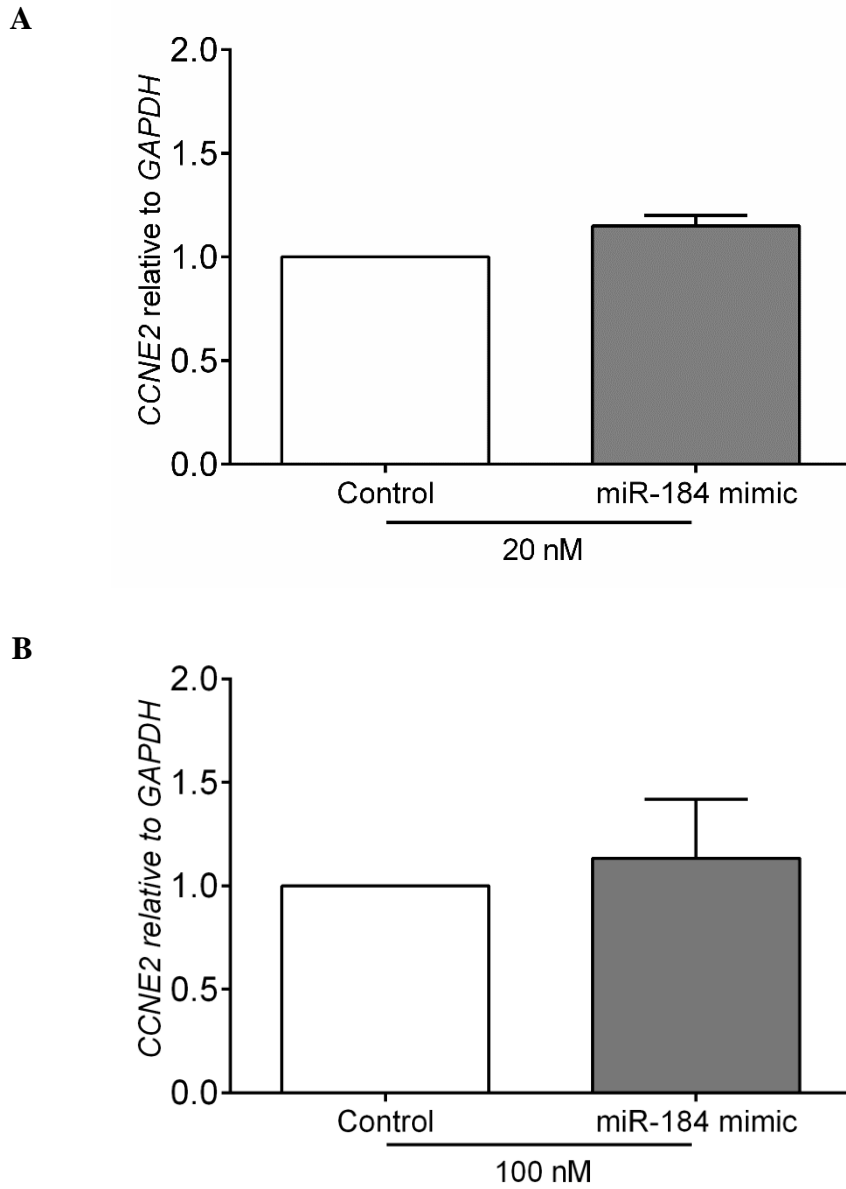
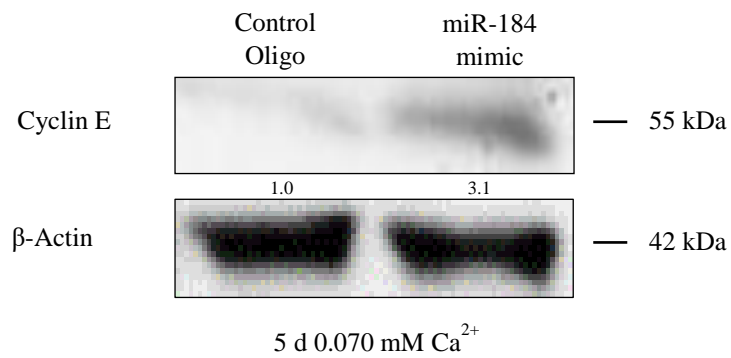


**Figure 4.9: Effect of miR-184 on cyclin E2 transcript expression in HPEKs.** HPEKs were nucleofected with either 20 (A) or 100 (B) nM of control oligonucleotide or miR-184 mimic grown in 0.07 mM  $\text{Ca}^{2+}$  for 5 days before analysis by RT-qPCR. Values were normalised to *GAPDH* and depicted relative to the 0.07 mM  $\text{Ca}^{2+}$  control. Data represents three independent experiments (+SEM).

**A**



**B**

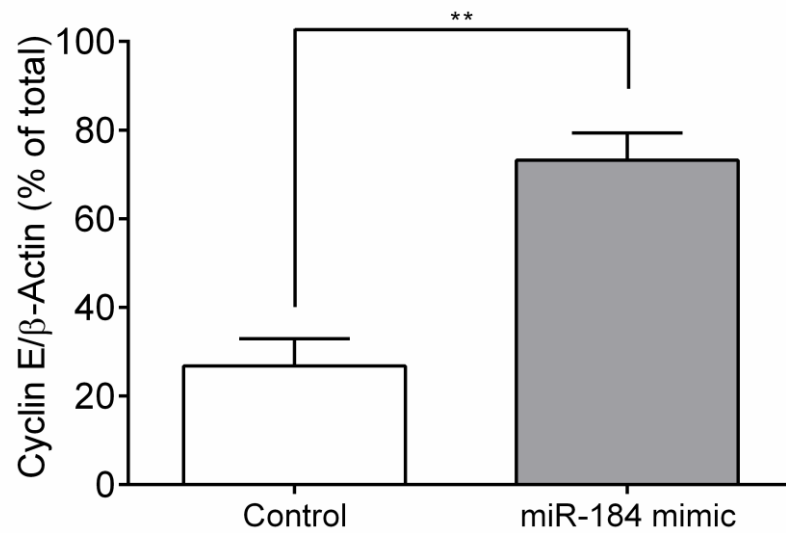


**Figure 4.10: Effect of miR-184 on Cyclin E protein in HPEKs.** HPEKs were nucleofected with 100 nM of control oligonucleotide or miR-184 mimic and grown in 0.07 mM Ca<sup>2+</sup> for 5 days before analysis by western blot with fold changes worked out based on density and normalised to  $\beta$ -Actin (A). Values were normalised to  $\beta$ -Actin and density proportions were calculated from the total densities of the samples (B). Data represents three independent experiments (+SEM). \*\* depicts significance were  $p \leq 0.01$ .

### 4.3.3.3. The Effects of ectopic miR-184 on p21

p21, an inhibitor of cyclin E, plays an important role in the regulation of keratinocyte proliferation and differentiation (Missero et al., 1996; Devgan et al., 2006; Freije et al., 2014). Consequently, the expression of *p21* transcript in HPEK treated with miR-184 mimic was analysed. As shown in Figure 4.11, following introduction of synthetic miR-184, *p21* levels were elevated 2.5-fold when compared to the control oligonucleotide.

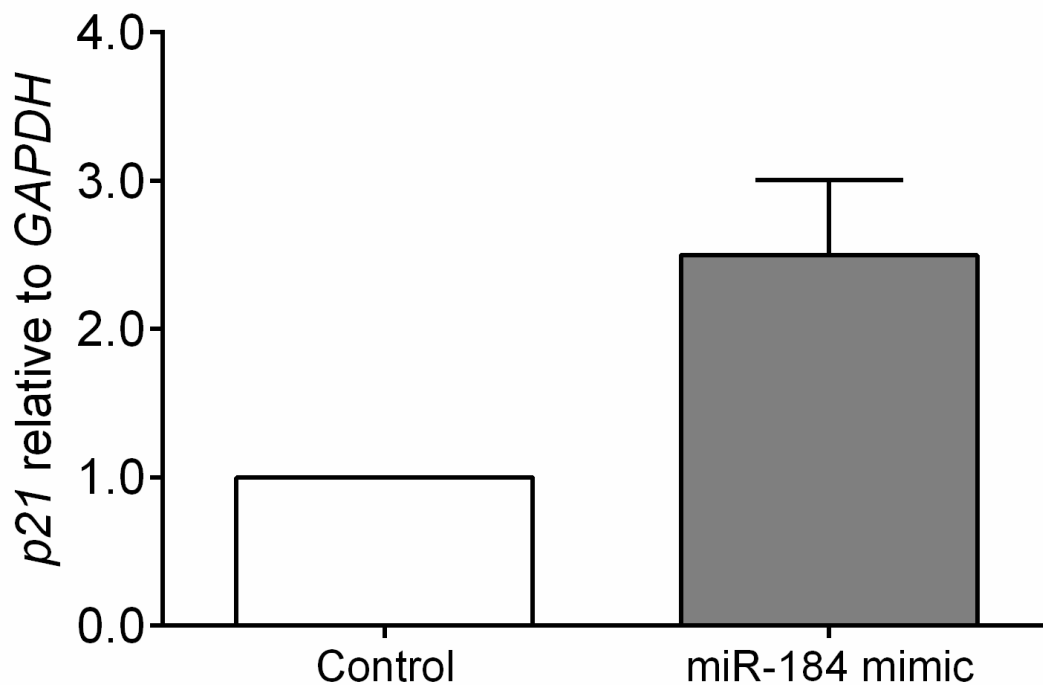


**Figure 4.11: Impact of miR-184 on p21 transcript in HPEKs.** HPEKs were nucleofected with 100 nM of control oligonucleotide or miR-184 mimic grown in 0.07 mM  $\text{Ca}^{2+}$  for 2 days before analysis by RT-qPCR. Values were normalised to *GAPDH* and depicted relative to the 0.07 mM  $\text{Ca}^{2+}$  control. Data represents two repeats ( $\pm$ SEM).

As with *p21* transcript levels it was believed that p21 protein would also be elevated. To determine this lysates from proliferating HPEKs exposed to 100 nM of miR-184 were analysed by western blot. A 2.0-fold ( $\pm 0.1$ ) induction of p21 was observed in cells transfected with synthetic miR-184 (Fig. 4.12). Taken together, elevated involucrin (Fig. 4.8), cyclin E (Fig. 4.10) and p21 (Fig. 4.12) all point to a differentiation phenotype.

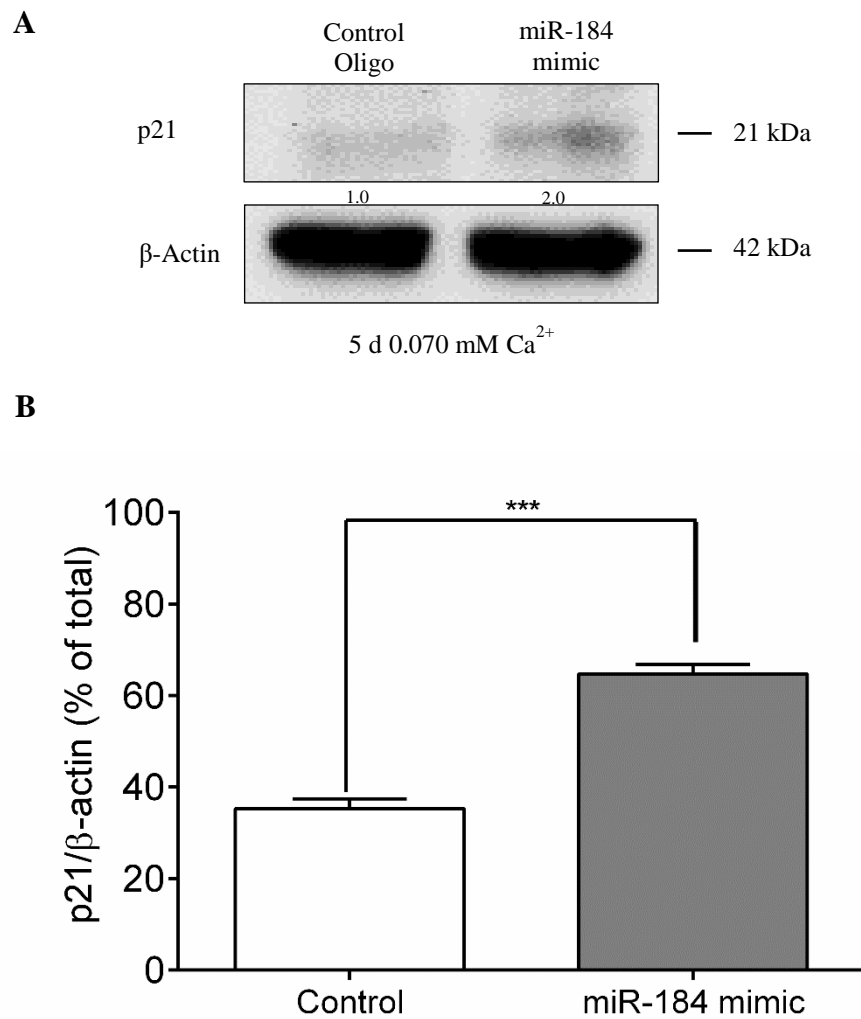


**Figure 4.12: Impact of miR-184 on p21 protein in HPEKs.** HPEKs were nucleofected with 100 nM of control oligonucleotide or miR-184 mimic and grown in 0.07 mM Ca<sup>2+</sup> for 5 days before analysis by western blot (A). Values were normalised to  $\beta$ -Actin and density proportions were calculated from the total densities of the samples (B). Data represents three independent experiments (+SEM). \*\*\* depicts significance were  $p \leq 0.001$ .

#### **4.3.3.4. Impact of miR-184 Inhibition on HPEK Differentiation**

Ectopic miR-184 causes induction of cyclin E, p21 and involucrin in proliferating HPEKs (Fig. 4.7-4.12). Given that miR-184 was induced during HPEK differentiation (Fig. 3.6) the effects of miR-184 inhibition were examined. To ascertain the role of miR-184 during differentiation, physiological miR-184 induction was repressed by loading HPEKs with a miR-184 targeting LNA inhibitor before differentiation with 1.5 mM Ca<sup>2+</sup> for 5 days. As revealed in Figure 4.13, expression of involucrin was significantly reduced by 60% to 0.4-fold when physiological miR-184 was inhibited. Cyclin E was also significantly reduced by 90% in miR-184 inhibitor samples to 0.1-fold when compared with the control oligonucleotide (Fig. 4.14). Levels of cyclin E inhibiting p21 were reduced by 50% to 0.5-fold in cells with inhibited miR-184 (Fig. 4.15). Taken together, suppression of involucrin (Fig. 4.13), cyclin E (Fig. 4.14) and p21 (Fig. 4.15) by inhibition of physiological miR-184 confirms a role in the regulation of proteins related differentiation.

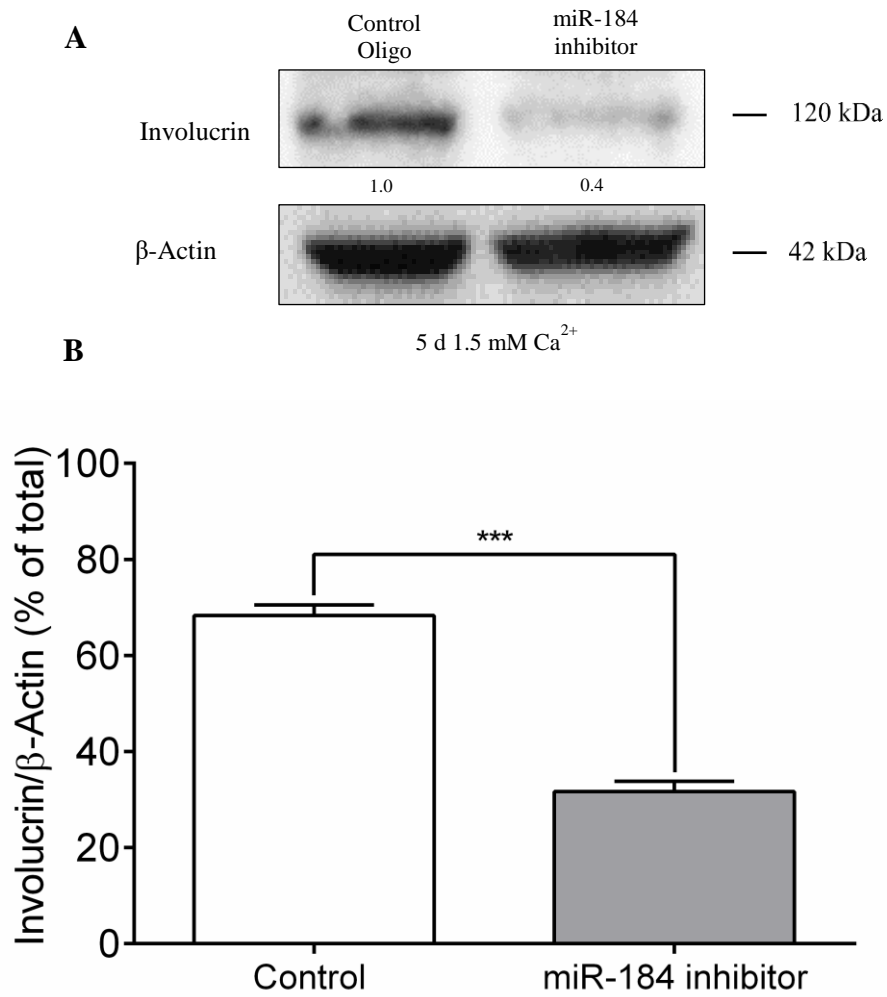


**Figure 4.13: Impact of miR-184 inhibition on involucrin in HPEKs.** HPEKs were nucleofected with 100 nM of control oligonucleotide or miR-184 inhibitor and grown in 0.07 mM Ca<sup>2+</sup> for 5 days before analysis by western blot (A). Values were normalised to  $\beta$ -Actin densitometry was performed (B). Data represents three independent experiments (+SEM). \*\*\* depicts significance were  $p \leq 0.001$ .

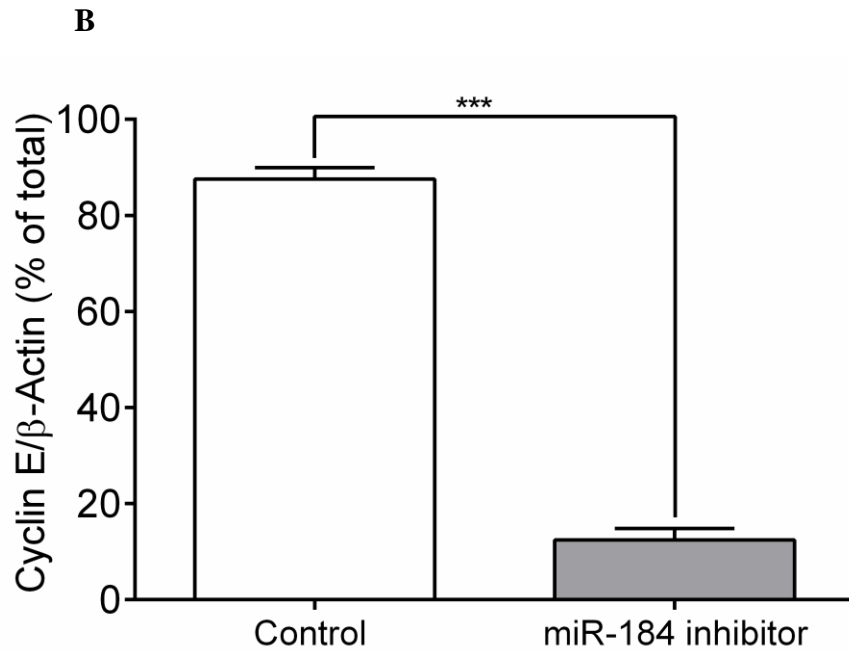
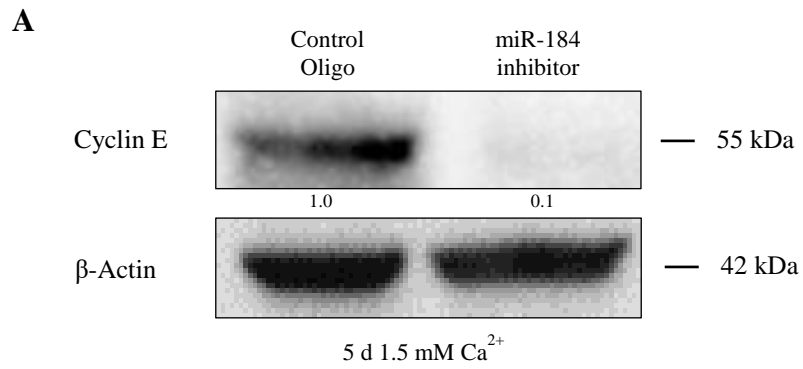


**Figure 4.14: Effect of miR-184 inhibition on Cyclin E in HPEKs.** HPEKs were nucleofected with 100 nM of control oligonucleotide or miR-184 inhibitor and grown in 0.07 mM Ca<sup>2+</sup> for 5 days before analysis by western blot (A). Values were normalised to  $\beta$ -Actin densitometry was performed (B). Data represents three independent experiments (+SEM). \*\*\* depicts significance were  $p \leq 0.001$ .

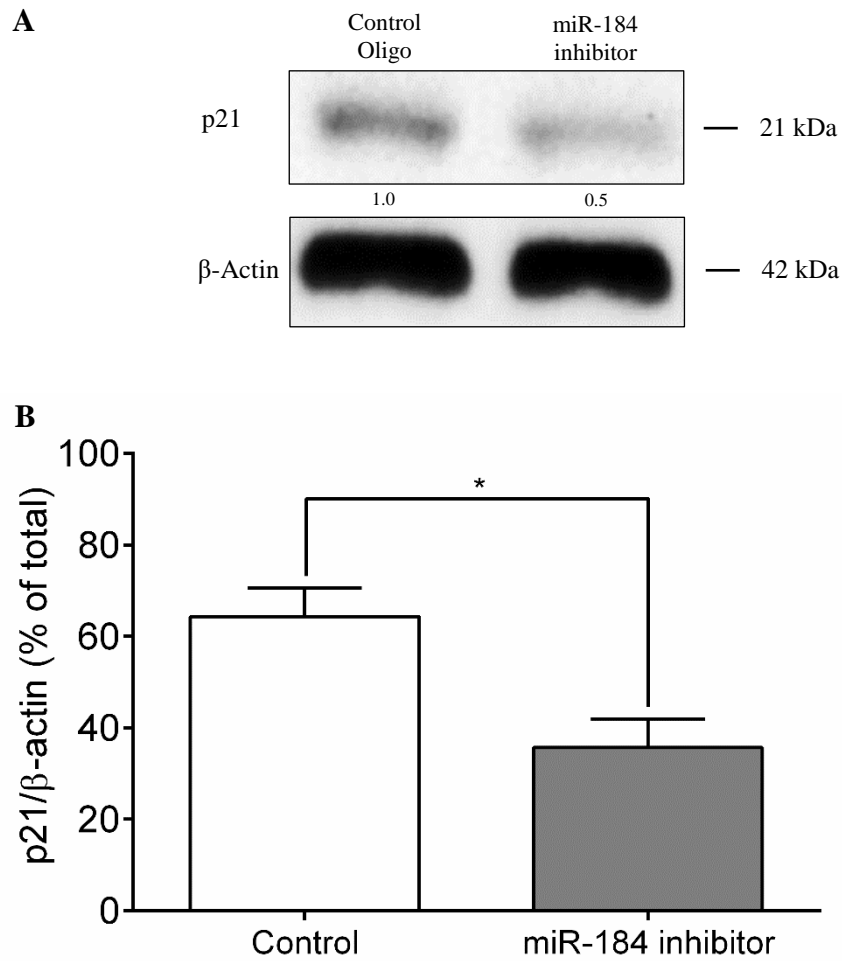


**Figure 4.15: Effect of miR-184 inhibition on p21 in HPEKs.** HPEKs were nucleofected with 100 nM of control oligonucleotide or miR-184 inhibitor and grown in 0.07 mM  $\text{Ca}^{2+}$  for 5 days before analysis by western blot (A). Values were normalised to  $\beta$ -Actin densitometry was performed (B). Data represents three independent experiments (+SEM). \* depicts significance were  $p \leq 0.05$ .

#### **4.3.3.5. The Effects of miR-184 on DNA damage**

DNA damage is a key feature of terminal differentiation and previous work has indicated the role cyclin E/p21 has in promoting genomic damage and growth arrest. Both cyclin E and p21 protein were upregulated in cells loaded with miR-184 suggesting that miR-184 encourages differentiation through cyclin E/p21-related DNA damage. To investigate whether miR-184 causes DNA damage, expression and activity levels of phosphorylated H2AX ( $\gamma$ H2AX), a histone marker that localises to double stranded breaks and promotes recruitment of DNA repair factors was measured (Bonner et al., 2008). Proliferating cells transfected with miR-184 mimic were examined by western blot, with the levels of  $\gamma$ H2AX quantified. Cells loaded with miR-184 had significantly elevated levels of  $\gamma$ H2AX at 1.8-fold when compared to the control oligonucleotide (Fig. 4.16). In contrast, levels of  $\gamma$ H2AX were modestly reduced to 0.7-fold when physiological miR-184 was inhibited (Fig. 4.17).

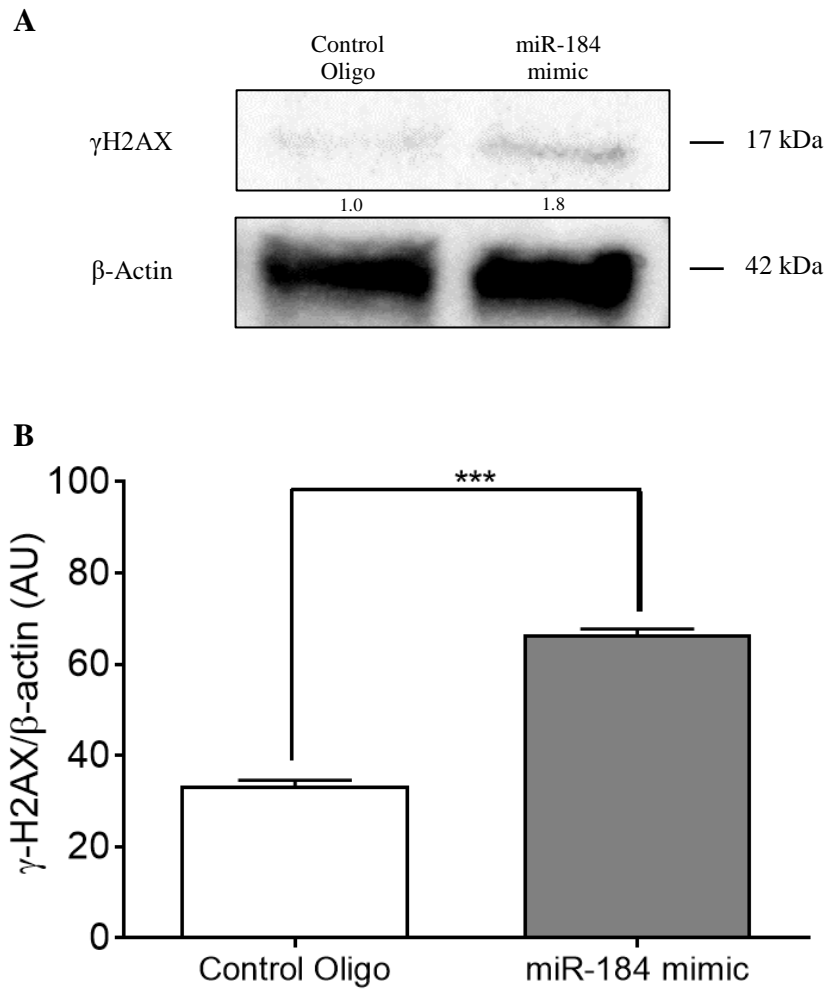


**Figure 4.16: Effect of miR-184 mimic on  $\gamma$ H2AX levels in HPEKs.** HPEKs were nucleofected with 100 nM of control oligonucleotide or miR-184 mimic and grown in 0.07 mM  $\text{Ca}^{2+}$  for 5 days before analysis by western blot (A). Values were normalised to  $\beta$ -Actin densitometry was performed (B). Data represents three independent experiments ( $\pm$ SEM). \*\*\* depicts significance were  $p \leq 0.001$ .

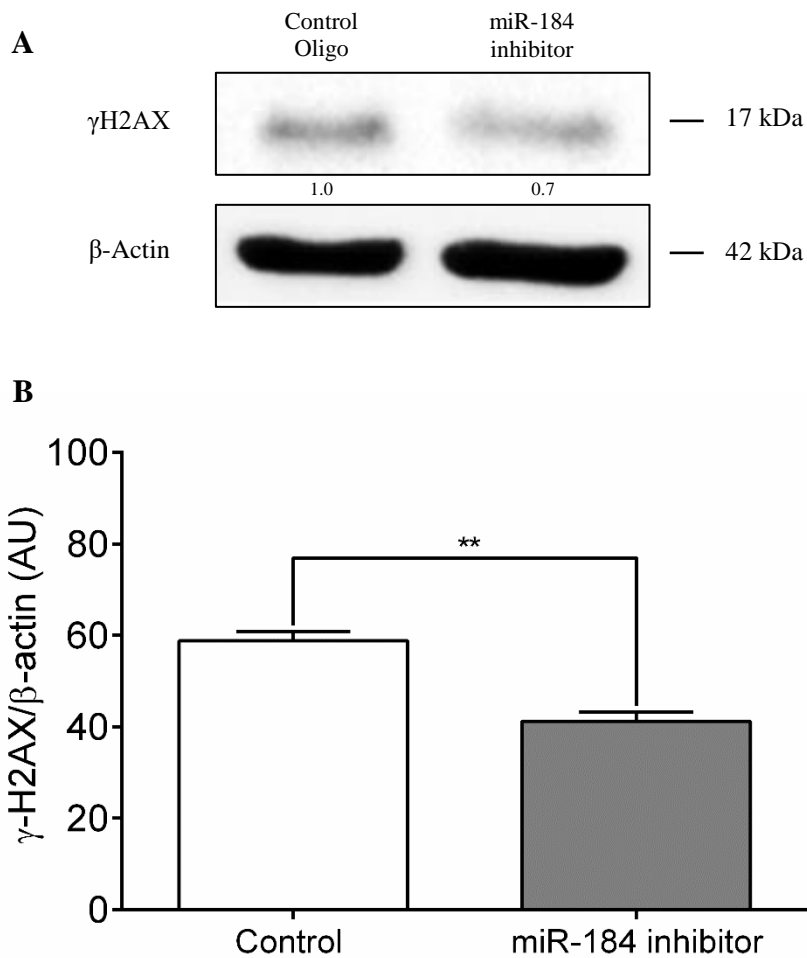


**Figure 4.17: Effect of miR-184 Inhibitor on  $\gamma$ H2AX levels in HPEKs.** HPEKs were nucleofected with 100 nM of control oligonucleotide or miR-184 inhibitor and grown in 1.5 mM  $\text{Ca}^{2+}$  for 5 days before analysis by western blot (A). Values were normalised to  $\beta$ -Actin densitometry was performed (B). Data represents three independent experiments ( $\pm$ SEM). \*\* depicts significance were  $p \leq 0.001$ .

To confirm increased levels of  $\gamma$ H2AX was associated with characteristic DNA damage foci, fluorescent images of HPEK with ectopic miR-184 were captured before quantification of  $\gamma$ H2AX foci. On average, cells transfected with miR-184 had over double the amount of fluorescent  $\gamma$ H2AX foci at 7.6 compared to 3.6 present in the control oligonucleotide samples (Fig. 4.19A) with a clear difference between images (Fig. 4.18). When miR-184 was inhibited in differentiating cells, the levels of  $\gamma$ H2AX foci remained relatively unchanged, suggesting that DNA damage cannot readily be reduced beyond physiological levels (Fig. 4.19B).

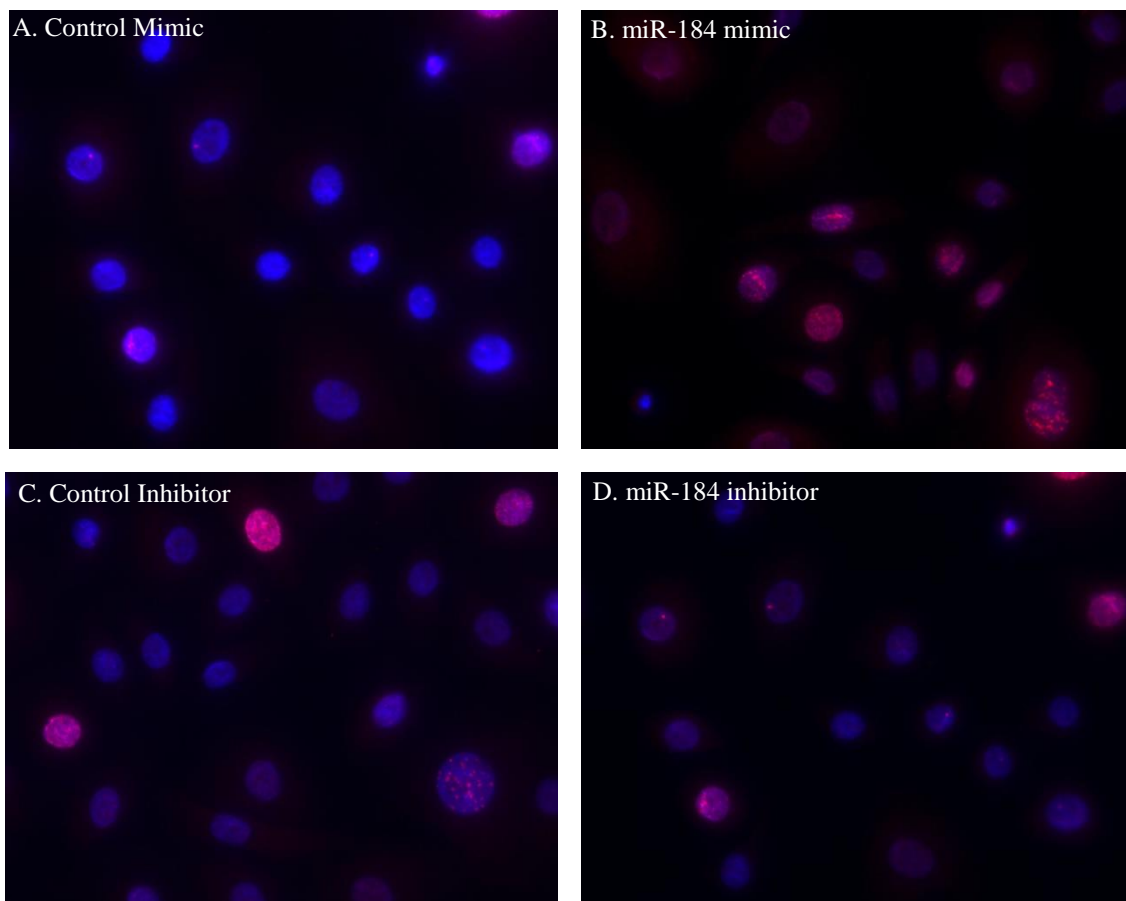


**Figure 4.18: Impact of miR-184 overexpression upon  $\gamma$ H2AX foci.** HPEKs were nucleofected with 100 nM of miR-184 mimic (B) or miR-184 inhibitor (D) along with the corresponding controls (A, C) before growth in either 0.07 mM (A-B) or 1.5 mM (C-D)  $\text{Ca}^{2+}$  for 5 days followed by  $\gamma$ H2AX staining and nuclear counterstaining with DAPI. Fluorescent images were taken at 20x magnification from 10 fields of view per sample.

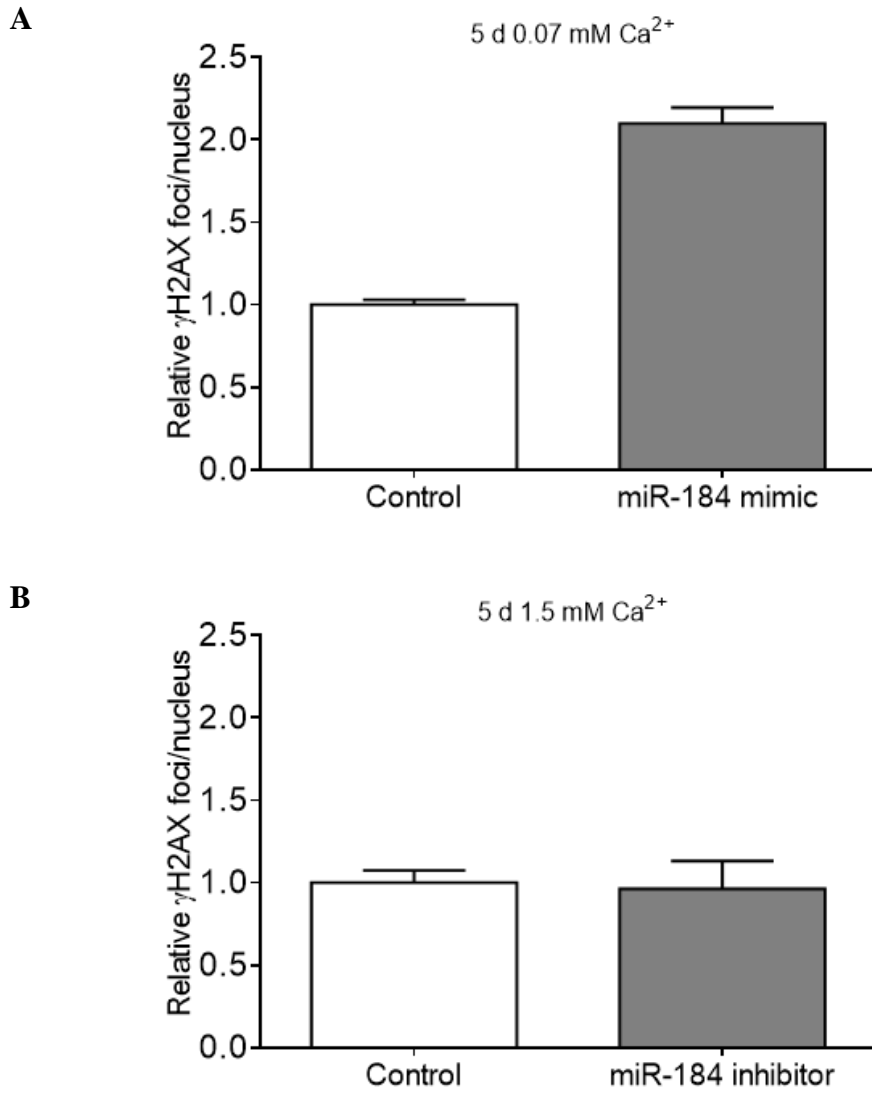


**Figure 4.19: Quantification of fluorescent  $\gamma$ H2AX foci.** HPEKs were nucleofected with either 100 nM of miR-184 mimic (A), miR-184 inhibitor (B) or respective controls and grown in 0.07 mM Ca<sup>2+</sup> (A) or 1.5 mM Ca<sup>2+</sup> (B) for 5 days before staining with  $\gamma$ H2AX. Fluorescent images were taken from 10 fields of view at 20x magnification from control (white) and miR-184 mimic (grey) samples. Data represents relative foci per nucleus (+SEM) quantified from three independent experiments.

## 4.4. Discussion

### 4.4.1. Nucleofection Optimisation

The first aim of this chapter was to optimise transfection of HPEK in order to manipulate levels of miR-184. Taken together our data gives important insights into the levels of miR-184 following transfection of HPEKs with miR-184 mimic and how long miR-184 mimic persists in the cell. Primary human keratinocytes are notoriously hard to transfect, especially when compared to immortalised cell lines such as HaCaTs (Distler et al., 2005). In addition to being more susceptible to toxic reagents, where any damage can cause irreversible differentiation primary cells are thought to degrade exogenous RNA at an elevated rate (Hunt et al., 2010). Our data shows that nucleofection with a GFP plasmid was successful, although transfection efficiencies at 35% were lower than the 56% reported by Distler and colleagues (Fig. 4.1) (Distler et al., 2005). Several factors may contribute to lower transfection efficiencies, such as keratinocyte donor variation and nucleofector condition/solution differences, though it is important to note that GFP expression was not lost over the course of 5 days.

RNAi activity relies on binding of delivered cargo to the RISC complex. The levels of miR-184 in HPEKs following transient transfection are relatively undescribed. However, very recent work on nasopharyngeal carcinoma cell lines has demonstrated ~500-fold increase of miR-184 2 days after transfection with miR-184 mimic (Zhu et al., 2018). Our data shows that nucleofection with a synthetic miR-184 mimic increased levels of mature miR-184 in a dose dependent manner, with 100 nM providing a more consistent elevation up to ~4800-fold after 1 d (Fig. 4.2). A recent review by Jin and colleagues has highlighted the pitfalls of using miRNA mimics, showing that transfection of synthetic miRNAs at high concentrations increases miRNA levels by a factor of several hundred, leads to accumulation of high molecular weight RNA and ultimately results in non-specific changes in gene expression (Jin et al., 2015). We used cel-miR-67, a non-targeting control isolated from *C. elegans* known to have minimal

sequence identity with miRNAs in humans, to allow differentiation between mimic activity and non-specific background effects. However, cel-miR-67 still causes accumulation of RNA species and therefore a miR-184 mimic with a mutant seed region could have been used throughout to validate specific effects from the active miR-184 mimic (Jin et al., 2015). Furthermore, although miR-184 was still present at elevated levels, there was a drastic reduction observed over the course of 5 days. This may suggest that miR-184 is reduced through cellular division or that excess free-floating miR-184 mimic not bound to the RISC complex is rapidly degraded.

#### **4.4.2. miR-184 Modulates Keratinocyte Proliferation**

The regulation of normal keratinocyte proliferation is critical in the maintenance of the epidermis. Previous studies have demonstrated that miR-184 plays an important role in the regulation of proliferation, acting as both tumour suppressor and onco-miR in several cell types. Early work by Stallings and co-workers demonstrated that overexpression of miR-184 reduces viability and proliferation in human glioma cell lines (Chen and Stallings, 2007). Moreover, a very recent study has shown that miR-184 reduces proliferation by promoting apoptosis in human colon cancer cell lines (Wang et al., 2017). In contrast, work on hepatocellular carcinoma lines has shown that miR-184 promotes proliferation through direct targeting of SRY-Box 7 (SOX7) (Wu et al., 2014). In addition, a very recent study has supported this role with overexpression of miR-184 in tongue squamous carcinoma cell lines promoting proliferation through targeting of SOX7 (Chen et al., 2018). It is evident that miR-184 plays a context-dependent role in human cancer proliferation. In epidermal keratinocytes, recent work has demonstrated that miR-184 modulates growth with miR-184-null mice exhibiting epidermal hyperplasia. The same study also shows that forced tetracycline-inducible expression of miR-184 reduces proliferation by activation of Notch signalling resulting in epidermal hypoplasia (Nagosa et al., 2017)

We have shown that HPEKs loaded with miR-184 mimic have reduced MTT signal although this failed to reach significance. A major pitfall of the MTT assay is the metabolic state of the cell whereby any changes in MTT signal may be directly proportional to cell number but equally could reflect metabolic changes induced by addition of external stimuli. To confirm changes in HPEK growth and to complement MTT data, trypan blue exclusion was performed. Our data indicates that when transfected with synthetic miR-184 cell viability was significantly reduced (Fig. 4.4A). To our knowledge, there is no literature evaluating the effect of miR-184 on cells by trypan blue exclusion assay although, it has been demonstrated that the

membranes of terminally differentiating keratinocytes become permeable to trypan blue (Parkinson and Emmerson, 1982). Given that miR-184 induces the differentiation marker, involucrin (Fig. 4.7), this suggests that the HPEKs loaded with miR-184 have an elevated population of terminally differentiated cells.

Cell cycle regulation is vitally important for every aspect of keratinocyte growth, not only maintaining normal proliferation but also supporting growth arrest at the onset of differentiation (Zanet et al., 2010). Our data indicates that miR-184 causes proliferating HPEK to accumulate in G1-phase of the cell cycle, consequently decreasing S and G2 proportions (Fig. 4.5). Recent work by Nagosa and colleagues on epidermal keratinocytes from miR-184-null mice validates our finding, reporting accumulation of cells in S- and G2-phases in addition to a reduced G1-phase proportion (Nagosa et al., 2017). Consistent with our finding, a recent study in glioma cell lines show that cells loaded with miR-184 accumulate in G1-phase of the cell cycle (Cheng et al, 2015). Contrastingly, work on hepatocellular carcinoma cell lines has shown that miR-184 differentially regulates the cell cycle, causing a shift in cycling dynamics and elevating levels of S-phase cells (Wu et al., 2014). Taken all together, we have demonstrated for the first time in monolayer HPEKs, a potential role for miR-184 in the regulation of proliferation, relying predominately on shifted cell cycle dynamics. However, with the limitations of the methods used, to confirm the role of miR-184 in the control of proliferation additional work evaluating proliferation markers for example Ki67, proliferating cell nuclear antigen (PCNA) and K5/K14 or assessing changes in proliferation further, using techniques such as BrdU incorporation assay, could be performed. Moreover, although recent work has illuminated the role of miR-184 in the proliferation of murine epidermis, further work using human organotypic models could provide an interesting insight into the effects of miR-184 in a fully stratified human system.

### 4.4.3. miR-184 Promotes Early Differentiation

Precise, co-ordination of keratinocyte proliferation and differentiation is essential to epidermal homeostasis. Early work detected miR-184 in RHE but not monolayers suggesting that miR-184 may play a role in keratinocyte stratification (Roberts et al., 2013). Very recent work has described expression patterns of miR-184 in murine epidermis, reporting none in both basal and terminally differentiated compartments and high amounts in early-differentiated layers (Nagosa et al., 2017). Moreover, they demonstrate  $\text{Ca}^{2+}$ -dependent induction of miR-184 during primary human keratinocyte differentiation where it targets Notch1 signalling to support differentiation (Nagosa et al., 2017).

Our data shows that levels of involucrin can be regulated in proliferating and differentiating HPEKs by perturbation of miR-184 levels (Fig. 4.7, 4.13). A recent study optimising keratinocyte differentiation conditions have reported elevated expression of both p21 and involucrin following sustained treatment with high  $\text{Ca}^{2+}$  (Borowiec et al., 2013). Furthermore, it has been demonstrated in HPEKs that overexpression of cyclin E leads to induction of involucrin (Freije et al., 2012). Consistent with the literature, we have shown concomitant induction of involucrin with cyclin E and p21, in differentiating HPEKs loaded with control oligonucleotide. We also show that miR-184 can induce involucrin in proliferating HPEKs (Fig. 4.7), suggesting that miR-184 alone is sufficient to trigger a differentiation response in the absence of high  $\text{Ca}^{2+}$  or other differentiation reagents. Interestingly, levels of involucrin transcript did not parallel its respective protein amounts, with a reduction in transcript, coupled with elevated protein, being observed in cells with elevated levels of miR-184. In contrast, recent work reported a significant increase of involucrin transcript in primary human keratinocytes, following transfection with synthetic miR-184, though protein levels were not assessed (Nagosa et al., 2017). However, this observed increase of involucrin transcript was in differentiating keratinocytes loaded with miR-184 mimic, preventing a direct

comparison with our data. In contrast, we show upregulated levels of both p21 mRNA and protein (Fig. 4.11-12) in proliferative HPEKs treated with miR-184, though there is not always a proportional relationship between transcript and protein levels (Liu, Beyer and Aebersold, 2016). Although miR-184 was not described, previous work has demonstrated that miRNAs can upregulate translation of certain mRNAs in mammalian cells (Bukhari, Truesdell and Vasudevan, 2018). Conceivably, miR-184 plays a potential regulatory role in the translation of involucrin, that differs between proliferative and differentiated HPEKs or *IVL* transcription is not as dynamic as other transcripts, especially in monolayer HPEKs where naturally some cells have elevated levels of involucrin mRNA. Further experiments such as fractional sequencing, whereby interaction of miR-184 with *IVL* transcripts could be analysed in both unbound and ribosomal bound pools of mRNA, would be required for further investigation of these ideas. In contrast, our data shows that the induction of involucrin protein observed in differentiating HPEKs, can be inhibited by antagonising normal miR-184 activity (Fig. 4.13). Recent work is consistent with this finding showing that inhibition of miR-184 during primary human keratinocyte differentiation reduces levels of involucrin transcript (Nagosa et al., 2017).

Our data shows that loading proliferating HPEKs with miR-184 mimic results in upregulation of cyclin E (Fig. 4.10). Given that cyclin E is a regulator of G1/S-phase transition, this may explain the ability of miR-184 to promote accumulation of G1-phase cells. Conversely, inhibition of physiological miR-184 during HPEK differentiation results in a drastic reduction (Fig. 4.14). A previous study on murine epidermis has shown that cyclin E accumulates in suprabasal layers supporting cellular enlargement through endoreplication (Zanet et al., 2010). Similarly, an *in vitro* study demonstrated that cyclin E accumulates in differentiating HPEKs where it induces mitosis failure and differentiation (Freije et al., 2012). This suggests that elevated levels of cyclin E in proliferating HPEKs loaded with miR-184 is a similar differentiation response. Both studies by Zanet et al., 2010 and Freije et al., 2012

suggest that primary keratinocytes accumulate in G2- not G1-phase when undergoing differentiation. However, they use the proto oncogene, c-myc, to differentiate keratinocytes and their data represents terminally differentiated and not early differentiating cells. To our knowledge a link between miR-184 and cyclin E has not yet been reported. However, miR-184 is known to inhibit NFAT1 in umbilical cord CD4+ T-lymphocytes. Given that NFAT1 acts as a repressor of G1/S-phase effectors such as cyclin E in several cell types it may be speculated that miR-184 targets NFAT1 in HPEKs allowing for accumulation of cyclin E (Baksh, DeCaprio and Burakoff, 2000; Horsley et al., 2008; Weitzel et al., 2009; Teixeira et al., 2016). Although there is little evidence to support this and as such it could represent an interesting further study.

Elevation of cyclin E is normally coupled with induction of its inhibitor, p21. An increase of p21 was observed in basal HPEKs loaded with miR-184 (Fig. 4.12). Conversely, p21 induction during Ca<sup>2+</sup>-dependent HPEK differentiation was reduced in the presence of miR-184 inhibitor (Fig. 4.15). Studies from the Gandarillas laboratory have demonstrated that p21 is induced during the onset of keratinocyte differentiation and is associated with cyclin E accumulation. Moreover, overexpression of cyclin E was sufficient to induce expression of p21 (Freije et al., 2012; Freije et al., 2014). Consistent with the literature, our data show that miR-184 mediates the induction of p21 observed during differentiation. Multiple cyclin/cdk complexes are targets for p21 inhibition, with a recent study reporting that immunodepletion of p21, at the onset of differentiation, results in removal of mitotic cyclin A with significant amounts of cyclin E remaining (Freije et al., 2012). Therefore, our data suggests that miR-184-dependent p21 induction acts to support differentiation by inhibiting mitotic cyclins rather than cyclin E, although evaluation of cyclin A levels in HPEKs with perturbed miR-184 would further support this idea. Consistent with our observations, overexpression of miR-184 induces expression of p21, which in turn supports growth arrest of lung cancer cell lines (Liu et al.,

2014). Likewise, later work has demonstrated that miR-184 causes growth arrest in glioma and breast cancer cell lines in part due to an induction of p21 (Feng and Dong, 2015).

Emerging evidence suggests that DNA damage is an important factor in keratinocyte differentiation. Overexpression of cyclin E has been shown to promote DNA damage to an irreversible threshold, inducing a mitosis block and ultimately leading to terminal differentiation (Freije et al., 2012). In our work, HPEKs loaded with miR-184 seem to undergo differentiation by inducing cyclin E, p21 and involucrin. Given the ability of cyclin E to induce genomic damage we predicted that this miR-184-induced differentiation occurs in a DNA damage-dependent manner. Our data shows that miR-184 induces DNA damage as measured by elevated expression and activity of  $\gamma$ H2AX. To our knowledge, this is the first time a direct link between miR-184 and DNA damage has been reported and it expands our understanding of miR-184s functional activity within epidermal keratinocytes. We have shown that miR-184 upregulates expression of cyclin E, which has previously been shown to induce phosphorylation of  $\gamma$ H2AX indicative of DNA damage (Freije et al., 2012). Moreover, we have shown that expression of the DNA damage effector, p21 is elevated in cells loaded with miR-184. Sustained miR-184-dependent accumulation of cyclin E may result in the induction of the DDR pathway, of which p21 is a component, leading to the expression of differentiation markers like involucrin. In contrast, inhibition of physiological miR-184 during keratinocyte differentiation has little effect on  $\gamma$ H2AX activity, suggesting that levels of cyclin E and/or DNA damage cannot be reduced beyond endogenous levels. Although speculative, further work evaluating DDRs in depth, using comet assays, observing miR-184 induced changes in other DNA damage markers or assessing DNA damage in cyclin E deficient HPEKs loaded with miR-184 could validate these findings.

Taken together, we have provided evidence that miR-184 promotes differentiation by concomitant induction of cyclin E, p21 and involucrin. Furthermore, we propose (Fig. 4.20)

that miR-184 induced differentiation is dependent on DNA damage whereby cyclin E hyperactivity results in accumulation of activated  $\gamma$ H2AX, which in turn leads to a p21 DDR, growth arrest and early differentiation by means of involucrin.

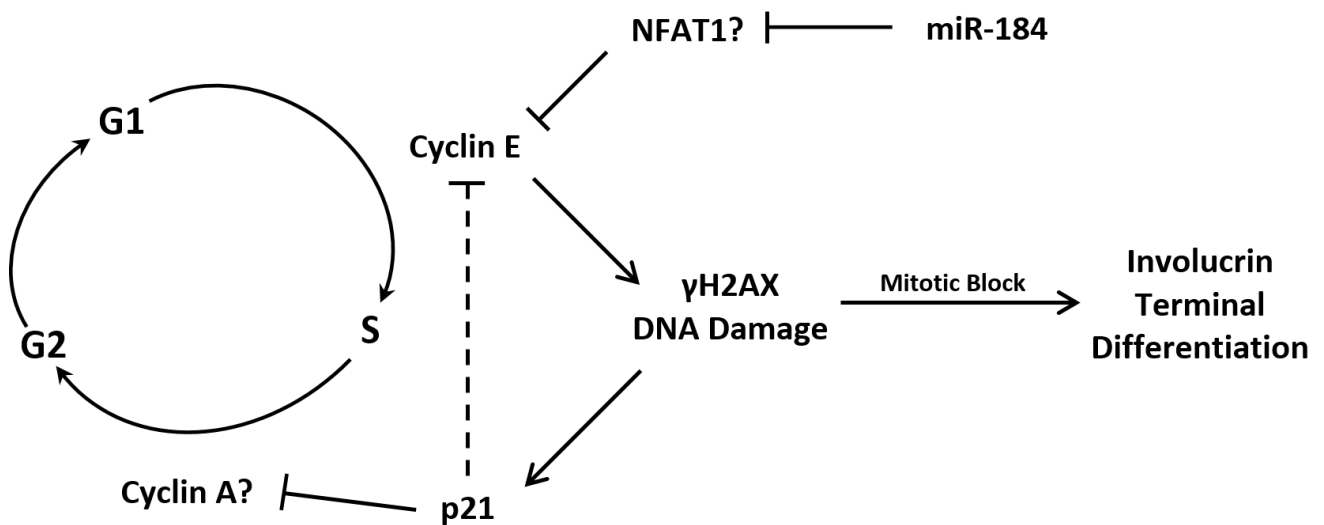


**Figure 4.20: Schematic Representation of Proposed miR-184: Differentiation Pathway.** miR-184 causes accumulation of Cyclin E possibly through direct inhibition of NFAT1. Cyclin E leads to hyperactive cell cycle progression consequently resulting in replicative stress and DNA damage. DNA damage activates DNA damage responses including p21 that in turn inhibits mitotic Cyclin A. Sustained DNA damage and growth arrest reaches an irreversible threshold and triggers keratinocyte differentiation. Based on Fig. 1.6 from Gandarillas, 2012.

# **5. The Effect of miR-184 on HPEK Migration**

## 5.1. Introduction

Following cutaneous injury, a large array of processes which facilitate tissue repair take place, with the migration of keratinocytes from the wound edge into the denuded wound surface central to successful reepithelization and restoration of barrier function. A popular method for assessing collective cell migration is the wound healing or scratch assay. A cell-free zone is created by mechanical damage that consequently promotes migration of surrounding cells. The scratch assay is a cheap and relatively simple way to screen treatment conditions on overall cell migration. A major limitation of the scratch assay is reproducibility; unless methods are described in sufficient detail, other groups can struggle to emulate results (Liang et al., 2007).

The roles of miRNAs in keratinocyte migration and wound healing have begun to surface. Recent work by Li and colleagues has shown miR-132 to be down regulated in chronic wounds and also that replenishment reduced inflammation and promoted wound closure (Li et al., 2017). Work on murine wound biopsies have shown considerably raised levels of miR-21 present within the wound edge 7 days post wounding (Yang et al., 2011). Human wound biopsies have shown significantly elevated levels of miR-31 7 days following injury (Li et al., 2015). Conversely, expression of miR-198 is heavily downregulated over 24 hours of wound healing in organotypic culture (Sundaram et al., 2013). Likewise, in human primary keratinocytes, expression of miR-200c is significantly reduced during *in vitro* scratch wound assay. Moreover, the same study describes severely reduced levels of miR-200c in the epidermis of mice following 7 days of wounding (Aunin et al., 2017). In contrast, work by Amelio and colleagues show that migration can be blocked by miR-24 causing actin remodelling through suppression of cytoskeletal modulators (Amelio et al., 2012). Furthermore, overexpression of miR-483-3p inhibits keratinocyte migration through modulation of proliferation-associated proteins (Bertero et al., 2011). More recently, work by

Wu and colleagues has found the microRNA Let-7b to inhibit keratinocyte migration by modulating insulin-like growth factor (IGF) expression (Wu et al., 2017).

Despite its emerging roles in migration of various cell types, the function of miR-184 in epidermal keratinocyte migration has not been evaluated. Early work by Robert Lavkers group suggests that miR-184 impairs keratinocyte migration in corneal epithelium (Yu et al., 2010). Recent work by Zhoa and colleagues demonstrated that miR-184 reduced migration rates over 72 hours in an epithelial retinal pigment cell line (Jiang et al., 2016). Conversely, inhibition of miR-184 in mouse lens epithelial cells suppresses cell migration (Hoffmann et al., 2012). Furthermore, transfection of miR-184 into human glioma cell lines results in enhanced migration (Yuan et al., 2014). Migration plays a role in keratinocyte differentiation where keratinocytes migrate upwards from the basal layer. The ability of miR-184 to regulate keratinocyte biology by promoting early differentiation has been shown in chapter 4 and by Nagosa et al., 2017 (Nagosa et al., 2017).

In recent years, studies have emerged suggesting that a group of RNA molecules around 200 nt in length with no protein coding capacity, termed long non-coding RNAs (lncRNAs), play a role in cellular migration. Of these the lncRNA, Urothelial cancer associated 1 (UCA1), has received particular attention as it has been shown to impact migration of several cell/tissue types (Wang et al., 2008; Fan et al., 2014; Zuo et al., 2017). The interesting property of this particular lncRNA is the ability to inhibit miR-184 function, effectively acting as a miR-184 sponge (Zhou et al., 2017). A recent RNA profiling study has demonstrated that expression of UCA1 is relatively low in HPEKs and elevated considerably in HaCaTs. In contrast, the same study shows negative expression values of UCA1 in skin samples (Katayama et al., 2015). Therefore, we hypothesised that UCA1 may contribute to processes vital to keratinocyte biology, such as migration.

## 5.2. Aims

- Examine expression of miR-184 in HPEKs following scratch assay
- Elucidate the impact of SOCE on miR-184 expression
- Inspect UCA1 expression following scratching
- Investigate the effects of perturbed miR-184 activity on migration

## 5.3. Results

### 5.3.1. The Effect of Scratching on miR-184 Expression

To evaluate the impact of wounding on miR-184, expression was analysed in basal and differentiated keratinocytes subjected to scratch assays. When cultured in low  $\text{Ca}^{2+}$  for 5 days, scratching promoted a 47-fold induction of miR-184 compared with the unwounded control where miR-184 was barely detectable. Conversely, wounded differentiated keratinocytes cultured for 5 days in high  $\text{Ca}^{2+}$  exhibited a modest 11-fold increase of miR-184 when compared with the unscratched control (Fig. 5.1). As high  $\text{Ca}^{2+}$  promotes miR-184 expression (Fig. 3.6), this suggests that keratinocytes may already be desensitised to miR-184 inducing stimuli upon wounding, or the induction observed may be dampened by the pre-existing high levels of miR-184.

Given that, induction of miR-184 during differentiation is dependent on SOCE (Fig. 3.9-12), we hypothesised that SOCE would also impact miR-184 levels during wounding. Treatment with the SOCE inhibitors,  $\text{Gd}^{3+}$  and BTP2, in proliferating keratinocytes eliminated the induction of miR-184 during wounding, with  $\text{Gd}^{3+}$  presenting similar levels (Fig. 5.1C) and BTP2 reducing miR-184 beyond basal levels by around 50% (Fig. 5.1D) when compared with the unscratched control.

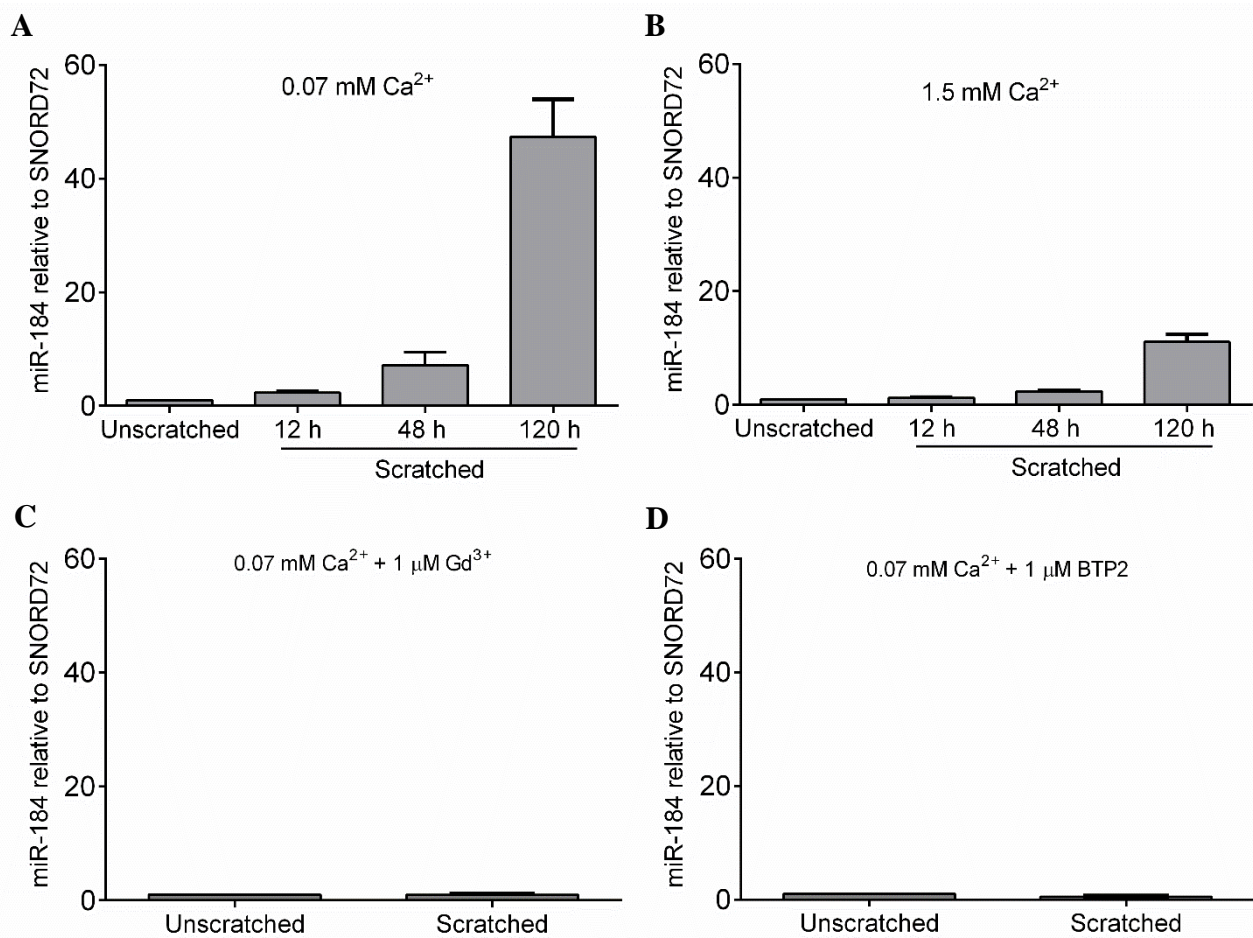


**Figure 5.1: Impact of HPEK wounding on expression of miR-184.** HPEKs were scratched and maintained in either 0.07 mM Ca<sup>2+</sup> (A) or 1.5 mM Ca<sup>2+</sup> (B) for 5 days. To inhibit SOCE, HPEK were pre-treated with Gd<sup>3+</sup> (C) or BTP2 (D) and maintain in low Ca<sup>2+</sup> for 5 days. Levels of miR-184 were assessed by RT-qPCR. Values were normalised to SNORD72 and depicted relative to the corresponding 5 day unscratched control. Data is pooled from three independent experiments (+SEM).

### 5.3.2. The Effect of Scratch Assay on Expression of UCA1

The lncRNA UCA1 acts as a sponge for miR-184 and has also been reported to regulate migration in several cell types. Given that miR-184 was induced during HPEK migration (Fig. 5.1), the effects of scratch assay on the levels of UCA1 in HPEKs was also investigated. Keratinocytes scratch-wounded and maintained in basal conditions for 5 days had 11-fold higher levels of UCA1 than their unscratched counterparts (Fig. 5.2). Thus, UCA1 seems to be co-induced with its miR-184 target.

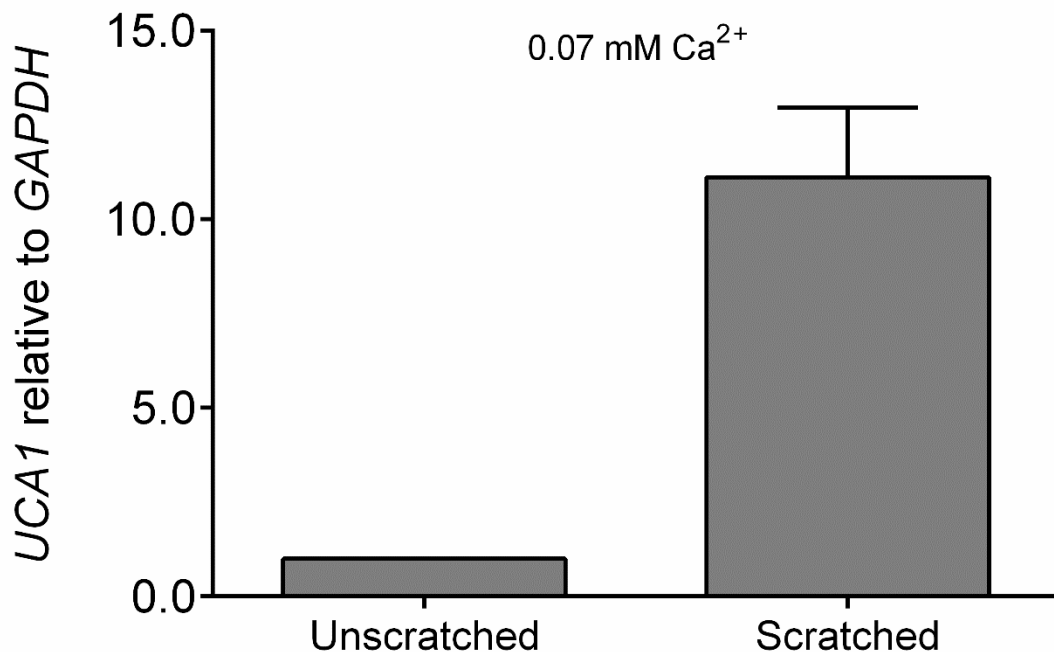


**Figure 5.2: Impact of HPEK wounding on expression of UCA1.** HPEKs were scratched and maintained in 0.07 mM Ca<sup>2+</sup> for 5 days before analysis by RT-qPCR. Values were normalised to *GAPDH* and depicted relative to the corresponding 5 day unscratched control. Data is pooled from three independent experiments (+SEM).

To determine whether the observed UCA1 induction was also dependent on SOCE, levels of UCA1 in keratinocytes treated with  $Gd^{3+}$  or BTP2 were analysed. UCA1 expression seems to be SOCE-dependent, as when treated with SOCE inhibitors UCA1 levels are effectively halved to 5-fold in both  $Gd^{3+}$  (Fig. 5.3A) and BTP2 (Fig. 5.3B).

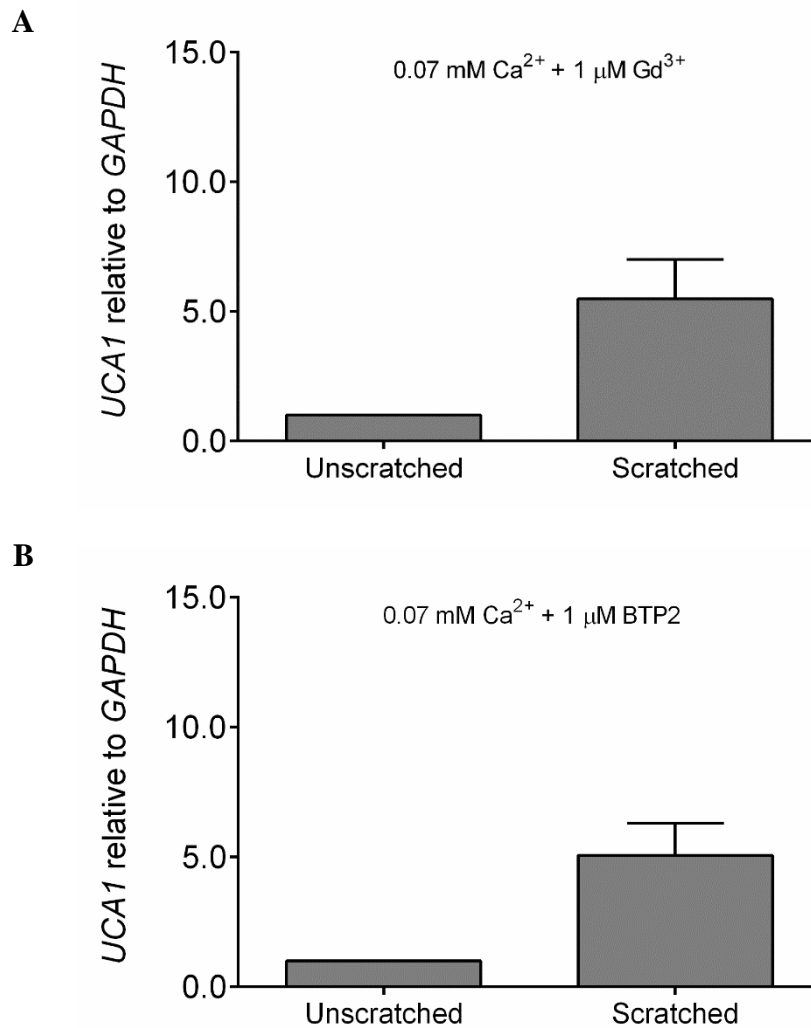


**Figure 5.3: Effect of SOCE inhibitors on UCA1 expression during wounding.** HPEKs were pre-treated with  $Gd^{3+}$  (A) or BTP2 (B) for 1 h before scratching with cultures maintained in 0.07 mM  $Ca^{2+}$  for 5 days before analysis by RT-qPCR. Values were normalised to *GAPDH* and depicted relative to the corresponding 5 day unscratched control. Data is pooled from three independent experiments (+SEM).

### **5.3.3. Impact of Perturbed miR-184 Levels on Wound Healing**

Given the induction of miR-184 observed during wound healing (Fig. 5.1) the effects of perturbed miR-184 activity on keratinocyte migration were examined. To assess this, a synthetic miR-184 mimic was transferred into keratinocytes prior to scratch assay. Migration was assessed over the course of 72 h with images captured every 30 min. Images of scratched keratinocyte monolayers were divided into three sections and the cells that breached the middle section were quantified over the entire time course (Fig. 5.4).

Exogenous miR-184 led to a striking 3-fold increase in the rate of migration after 12 hours when compared with the 12 h control oligonucleotide. At 24, 36 and 48 h timepoints migration continued to increase at 11-, 15- and 20-fold higher, respectively, when compared with the same 12 h control. When compared with the equivalent control time points, the rate of migration in miR-184 treated cells was 50-75% higher (Fig. 5.9). However, at 72 h in monolayers overexpressing miR-184, artificial wounds were completely closed when compared with cells nucleofected with control oligonucleotide (Fig. 5.5-5.6), therefore these timepoints were not included in analysis (Fig. 5.9).

Next, the impact of miR-184 inhibition on wound closure was assessed by using a LNA miR-184 inhibitor and assessing migration over 72 h. Blockade of miR-184 activity at 12 h did not affect migration when compared with the control inhibitor. At 24, 36 and 48 h time points and when compared with the same 12 h control inhibitor, migration increased marginally at 1.4-, 1.8- and 3.9-fold, respectively. Although, when compared with the control oligonucleotide at the respective 24, 36 and 48 h time points a substantial reduction in migration rates of at least 50% was observed in cells treated with miR-184 inhibitor (Fig. 5.9).

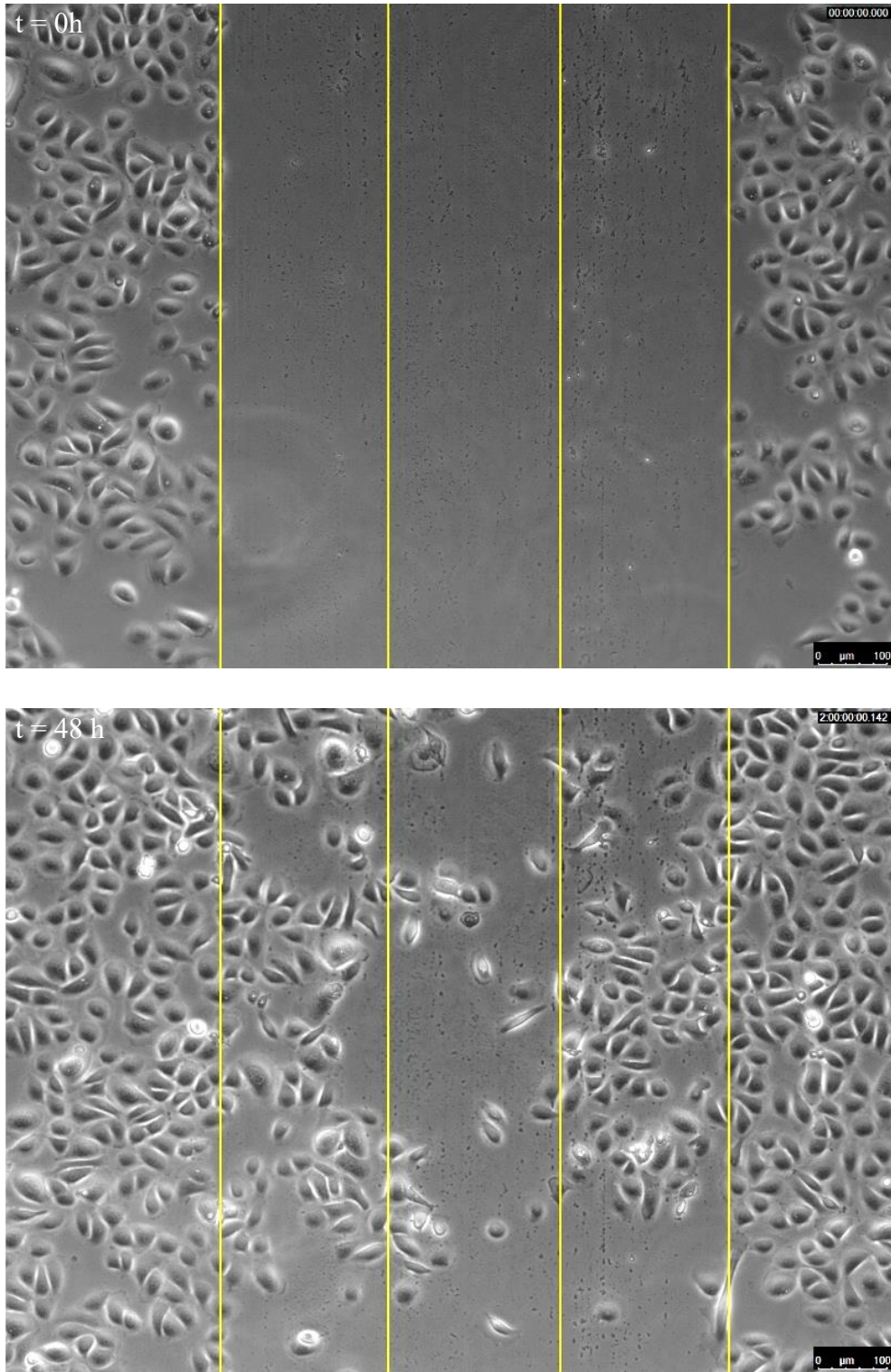


**Figure 5.4: Example analysis of live cell images of scratched HPEKs.** HPEKs were nucleofected and cultured in 0.07 mM  $\text{Ca}^{2+}$  with light microscopy images (20x) taken every 30 min for up to 3 days. Analysis was performed by creating three sections of equal width starting from the edges of the wound with cells breaching the middle section quantified.

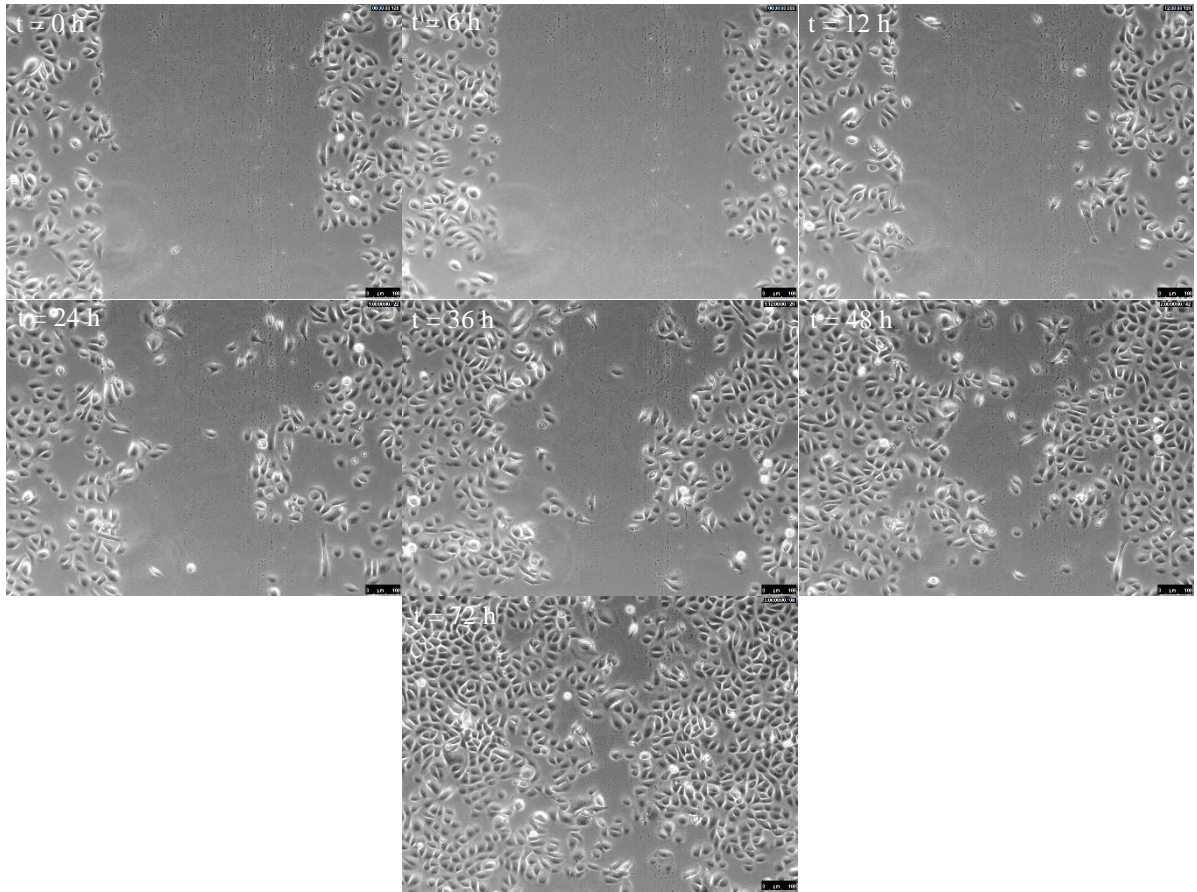


**Figure 5.5: Impact of control oligonucleotide upon wounded keratinocytes.** Cells were loaded with 100 nM of control oligonucleotide and cultured for 3 days in low  $\text{Ca}^{2+}$  with light microscopy (20x) images took every 30 min.

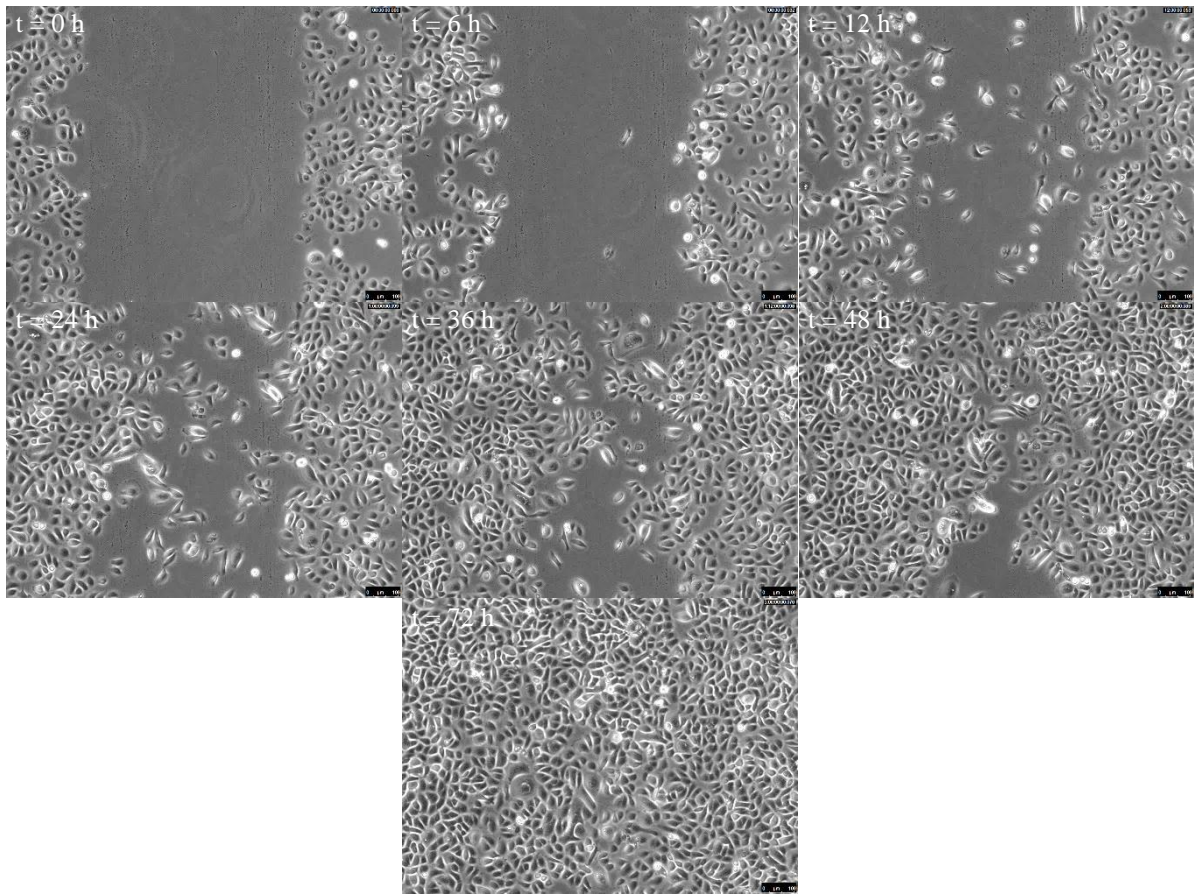


**Figure 5.6: Effect of miR-184 mimic on wounded HPEKs.** Cells were nucleofected with 100 nM of miR-184 mimic and cultured for 3 days in low  $\text{Ca}^{2+}$  with light microscopy (20x) images took every 30 min.

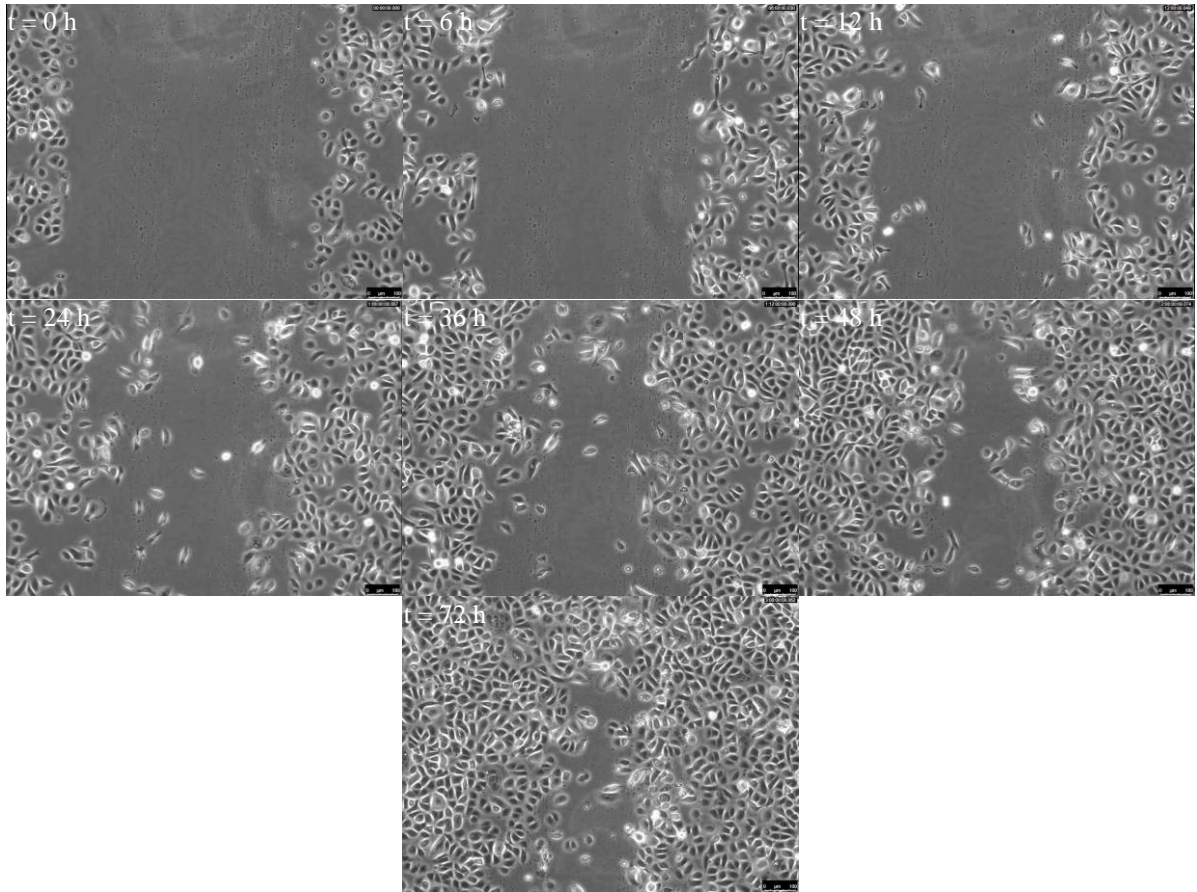


**Figure 5.7: Effect of control inhibitor on wounded HPEKs.** Cells were loaded with 100 nM of miR-184 mimic and cultured for 3 days in low  $\text{Ca}^{2+}$  with light microscopy (20x) images took every 30 min.

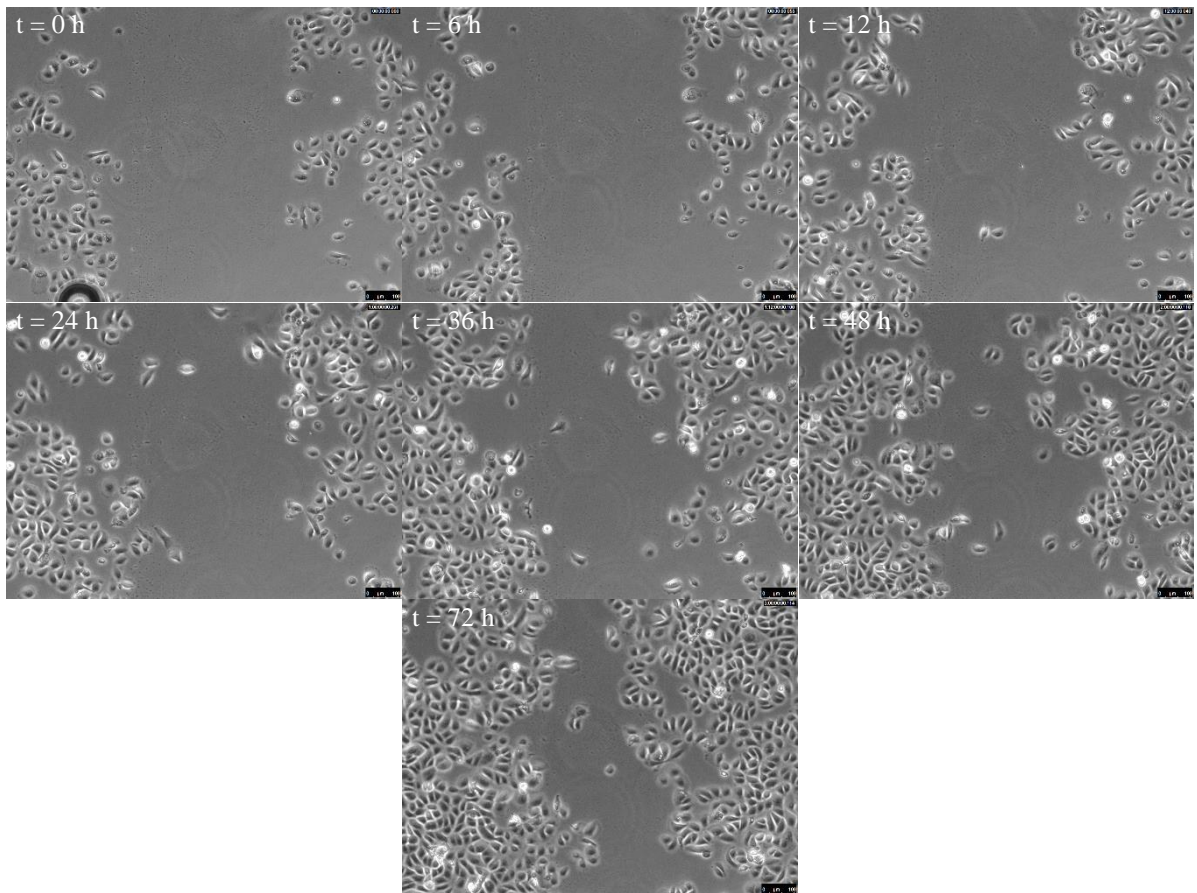


**Figure 5.8: Effect of miR-184 inhibitor on wounded HPEKs.** HPEKs were nucleofected with 100 nM of miR-184 mimic and cultured for 3 days in low  $\text{Ca}^{2+}$  with light microscopy (20x) images took every 30 min.

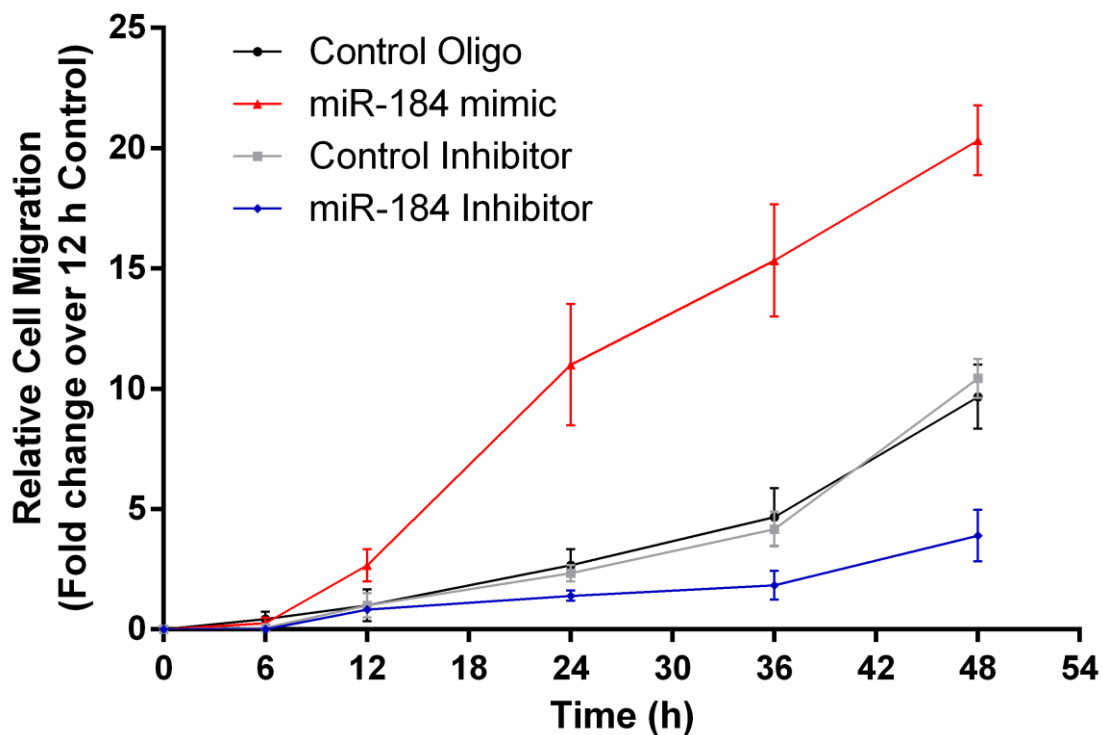


**Figure 5.9: Effect of miR-184 perturbation on wound closure.** Cells were exposed to 100 nM of either control oligonucleotide (black), miR-184 mimic (red), control inhibitor (grey) or miR-184 inhibitor (blue). Cells were scratch upon approaching confluence and cultured for 2 days in low  $\text{Ca}^{2+}$  with light microscopy (20x) images took every 30 min. Migration rates were normalised to the number of cells breaching the middle section at 12 h. Data represents three independent experiments.

## **5.4. Discussion**

### **5.4.1. SOCE-Dependent miR-184 Induction During HPEK Migration**

Keratinocyte migration is of vital importance to both successful stratification, where keratinocytes migrate upwards from the basal layer, and efficient wound repair, where keratinocytes migrate into the denuded wound surface. A recent review has highlighted the importance of miRNAs to the migration of keratinocytes (Mulholland, Dunne and McCarthy, 2017). We have shown that miR-184 regulates keratinocyte differentiation (Chapter 4) and with migration playing a role in epidermal stratification we hypothesised that miR-184 may also regulate keratinocyte migration. Therefore, our first aim for this chapter was to determine miR-184 levels in proliferating and differentiating HPEKs following scratching.

Our data shows that miR-184 was induced in both proliferating and differentiating HPEKs (Fig. 5.1). However, this induction was less profound in differentiated cells, presumably as endogenous miR-184 has already desensitised HPEKs to miR-184-inducing stimuli or that comparisons made against unscratched HPEK with high pre-existing miR-184 dulls fold-change differences. Interestingly, an early study by Lavker and co-workers implicated miR-184 in the migration of corneal keratinocytes, where it impaired actin-based motility pathways by repressing miR-205 activity (Yu et al., 2010). However, they failed to report endogenous miR-184 levels during a scratch wound assay hence whether levels of miR-184 induction in wounded epidermal and corneal keratinocyte monolayer are similar remains to be determined.

SOCE has previously been shown to regulate migration of epidermal keratinocytes. A study by Reynolds and colleagues has demonstrated that inhibition of SOCE, using siRNA for STIM1 or downstream inhibition of NFAT using CsA, leads to reduced migration in response to pro-migratory stimuli (Jans et al., 2013). In contrast, very recent work has shown that

ablation of STIM1 in mice elevates long-term wound healing abilities, seemingly due to dampened immune responses and elevated activated keratinocytes (Putney et al., 2017). We have shown that induction of miR-184 during HPEK differentiation is reliant on SOCE (Fig. 3.9-3.12). Therefore, we anticipated that the induction of miR-184 observed following scratching would also be dependent on SOCE. Our data shows that induction of miR-184 during keratinocyte migration occurs in a SOCE-dependent fashion (Fig. 5.1). This is the first time to our knowledge that SOCE has been implicated in the expression of miRNAs during keratinocyte migration. Moreover, this finding supports our previous data (Fig. 3.9-3.12), suggesting a role for SOCE in the regulation of miR-184 in the context of keratinocyte biology.

#### **5.4.2. Migration Induces UCA1 Expression in a SOCE-Dependent Manner**

Emerging evidence suggests that the lncRNA, UCA1, is dysregulated in several cell types, whereby it seems to support migration (Wang et al., 2008; Fang et al., 2014; Zhou et al., 2017). We have shown that miR-184 was induced by scratching (Fig. 5.1) and with UCA1 acting as a sponge for miR-184 we anticipated that it may be co-induced with its miR-184 target. Moreover, with miR-184 induced in a SOCE-dependent manner during both HPEK differentiation (Fig. 3.9-3.12) and migration (Fig. 5.1) we predicted that changes in UCA1 levels might also be reliant on SOCE.

Indeed, we found that UCA1 was induced in basal HPEKs following scratching and that this induction was impaired by treatment with inhibitors of SOCE (Fig. 5.2-5.3). Consistent with the literature (Wang et al., 2008; Fang et al., 2014; Zhou et al., 2017) we show that UCA1 was upregulated during migration. This is the first time to our knowledge that UCA1 has been described in migration of keratinocytes. Similar to Katayama and colleagues who showed low levels of UCA1 in epidermal keratinocytes, we also demonstrate relatively low levels of UCA1 in unscratched proliferating HPEKs (Katayama et al., 2015). Both elevated UCA1 and miR-184 was observed following 5 days of scratching. However, to what extent the two interact is

still unclear. Further work examining interactions of UCA1 with miR-184 using methods such as luciferase assays, would help understand this relationship in the context of keratinocyte migration.

### **5.4.3. miR-184 Promotes Keratinocyte Migration**

Previous work has demonstrated that miR-184 reduces migration in several cell types. In human glioma cell lines, transfection with miR-184 mimic reduces migration into an artificial scratch by 50%, whereas inhibition of miR-184 effectively doubles migration rates (Cheng et al., 2015). Similarly, in human umbilical cord vein endothelial cells (HUVEC) treatment with miR-184 mimic results in significantly less coverage of the wound surface compared with the control when assessed by scratch assay (Zong et al., 2016). Likewise, nasopharyngeal carcinoma cell lines loaded with miR-184 exhibit severely diminished migration rates during wounding (Zhu et al., 2018). We have shown that miR-184 was induced in HPEKs following scratch wounding (Fig. 5.1). It was unclear whether miR-184 was promoting migration or the induction was a compensatory response by the cell to reduce the migratory actions of keratinocytes.

Therefore, we loaded keratinocytes with miR-184 mimic and observed significantly elevated migration over 48 h when assessed by a scratch wound assay. Conversely, inhibition of endogenous miR-184 using a LNA miR-184 inhibitor during scratch wound healing resulted in severely reduced HPEK migration (Fig. 5.9). This is the first time to our knowledge that miR-184 has been shown to regulate migration of epidermal keratinocytes. Early work by Yu and colleagues has shown that miR-184 can modulate migration of human corneal epithelial keratinocytes by antagonising miR-205 activity, consequently impairing actin-based migration pathways (Yu et al., 2010). This suggests a differential role for miR-184 within epidermal keratinocytes although further work utilising transcriptomic and proteomic approaches could help delineate the migration pathways modulated by miR-184 in HPEKs.

## **6. Epidermal Argonaute Dynamics**

## 6.1. Introduction

Argonaute proteins form the catalytic core of the RISC complex, and as the RISC is essential to miRNA function are indispensable to cell homeostasis. AGO2 is the only AGO in humans that possesses endonuclease activity and for this reason receives the most attention, with remarkably little consideration paid to other AGOs. Initially Argonaute proteins were implicated in development. Early work by Bohmert and colleagues observed an altered phenotype in the developing leaves of AGO1 mutated *Arabidopsis thaliana* (Bohmert et al., 1998). Furthermore, mutation of Argonaute orthologs in *C. elegans* results in a reduced viable progeny (Grishok et al., 2001). In mice, deletion of AGO2 causes embryonic death post implantation whereas deletion of AGO2, 3 and 4 results in viable embryos (Cheloufi et al., 2010; Modzelewski et al., 2012). However, the ability of the AGO to regulate other cellular functions such as differentiation is now apparent. AGO1 or AGO2 overexpression induces spontaneous differentiation of neuroblastoma cell lines (Parisi et al., 2011). Similarly, in human monocytes inhibition of AGO2 activity results in perturbed differentiation (Iosue et al., 2013). In the skin, a study has highlighted AGO2 as the most abundant mammalian AGO, associating with the largest pool of miRNAs in both mouse epidermis and human melanoma cells. Furthermore, ablation of AGO2 led to a ~30% reduction of global miRNA levels with co-ablation of AGO1 and AGO2 leading to an 80% decrease and causing severe epidermal thickening (Wang et al., 2012).

The majority of studies assume AGO function is based entirely in the cytoplasm. However, emerging work demonstrates the functional activity of AGO within the nucleus. A prominent study by Bischof and co-workers has shown that AGO2 accumulates in the nucleus of aging fibroblasts repressing genes related to growth (Benhamed et al., 2012). Likewise, recent work demonstrates dominant nuclear AGO2 activity in primary keratinocyte cultures

and human epidermis (Sharma et al., 2016). Nonetheless, the mechanisms of AGO2 localisation in HPEK have received little attention.

Analysis of the miRNAome in psoriasis revealed expression of miR-184 to be upregulated in psoriatic lesions (Joyce et al., 2011). We show that miR-184 levels on average are 4-fold higher in psoriatic lesions (Fig 3.6). Previous work in our group showed that miR-184 directly targets and represses AGO2 in both HaCaTs and HPEKs, and this has been confirmed in pancreatic  $\beta$  cells (Roberts et al., 2013; Tattikota et al., 2014). Ross and colleagues also demonstrated AGO2 insufficiency coupled with miR-184 overexpression in psoriasis (Roberts et al., 2013). Despite this surprisingly little is known about the expression of AGO1-4 in psoriasis.

## **6.2. Aims**

- To examine the expression of AGO1-4 during HPEK differentiation
- Study Argonaute levels in psoriatic lesions
- Investigate AGO2 function during differentiation

## 6.3. Results

### 6.3.1. Investigation of Argonaute Expression in HPEKs

Several miRNAs have been implicated in keratinocyte differentiation. Work on mice has demonstrated the vital role AGOs play in epidermal homeostasis with co-ablation of AGO1 and AGO2 resulting in 80% less miRNA levels (Wang et al., 2012). Given that, AGOs are essential to miRNA function we hypothesised that their expression patterns would change over the course of differentiation. Therefore, the expression of *AGO1-4* in basal and differentiating HPEKs was examined. We and others have shown that miR-184 is induced during keratinocyte differentiation (Fig.3.6) (Nagosa et al., 2017) and so particular interest was paid to AGO2.

Initially, levels of *AGO2* were examined in HPEKs differentiated for 3 days with 1.2 mM  $\text{Ca}^{2+}$ . However, expression of *AGO2* was relatively unchanged at all time points (Fig. 6.1A). Since stimulation for 3 days with 1.2 mM  $\text{Ca}^{2+}$  did not promote an adequate differentiation response (Fig. 3.1), levels of *AGO2* was assessed during differentiation with 1.5 mM  $\text{Ca}^{2+}$  for 5 days. Although, variance between experiments was large, after 1 day a 2-fold induction was observed. However, *AGO2* levels then returned to those similar to proliferating HPEK at both 4 and 5 days (Fig. 6.1B).

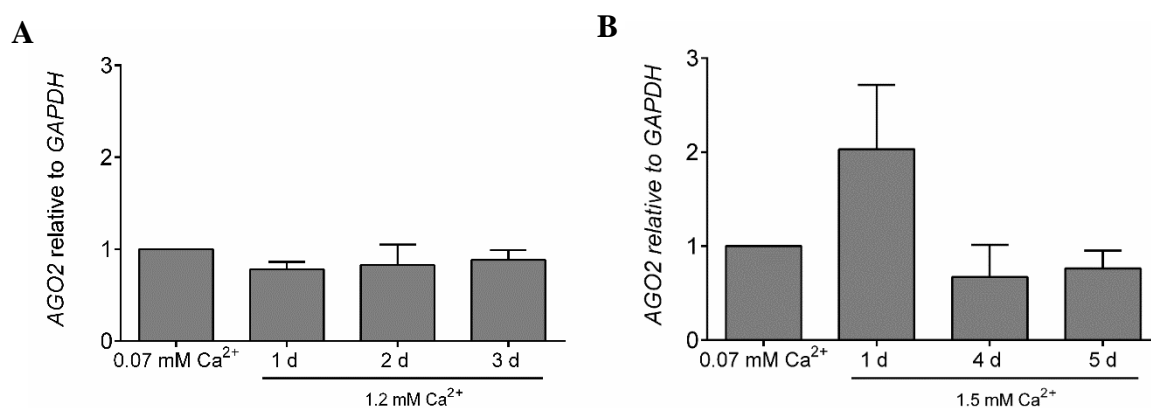


**Figure 6.1: Effect of differentiation on AGO2 expression.** HPEKs were grown in 0.07 mM, 1.2 mM (A) and 1.5 mM (B)  $\text{Ca}^{2+}$  for up to 5 days before analysis by RT-qPCR. Values were normalised to *GAPDH* and depicted relative to the proliferating control. Data represents three independent experiments (+SEM).

Next, expression of *AGO1*, *AGO2* and *AGO4* was analysed in HPEKs treated with 1.5 mM  $\text{Ca}^{2+}$  for up to 5 days. Levels of *AGO1* transcript were relatively unaffected by  $\text{Ca}^{2+}$ -induced HPEK differentiation or any effect was concealed by large variations in SEM (Fig. 6.2A). However, expression of *AGO3* displayed an upwards trend in expression to 2-fold at 4 days before reducing to 1.5-fold at 5 days (Fig. 6.2B). Expression of *AGO4* exhibited a modest downwards trend with levels reduced by 60% to 0.4-fold at 5 days following treatment with 1.5 mM  $\text{Ca}^{2+}$  (Fig. 6.2C).

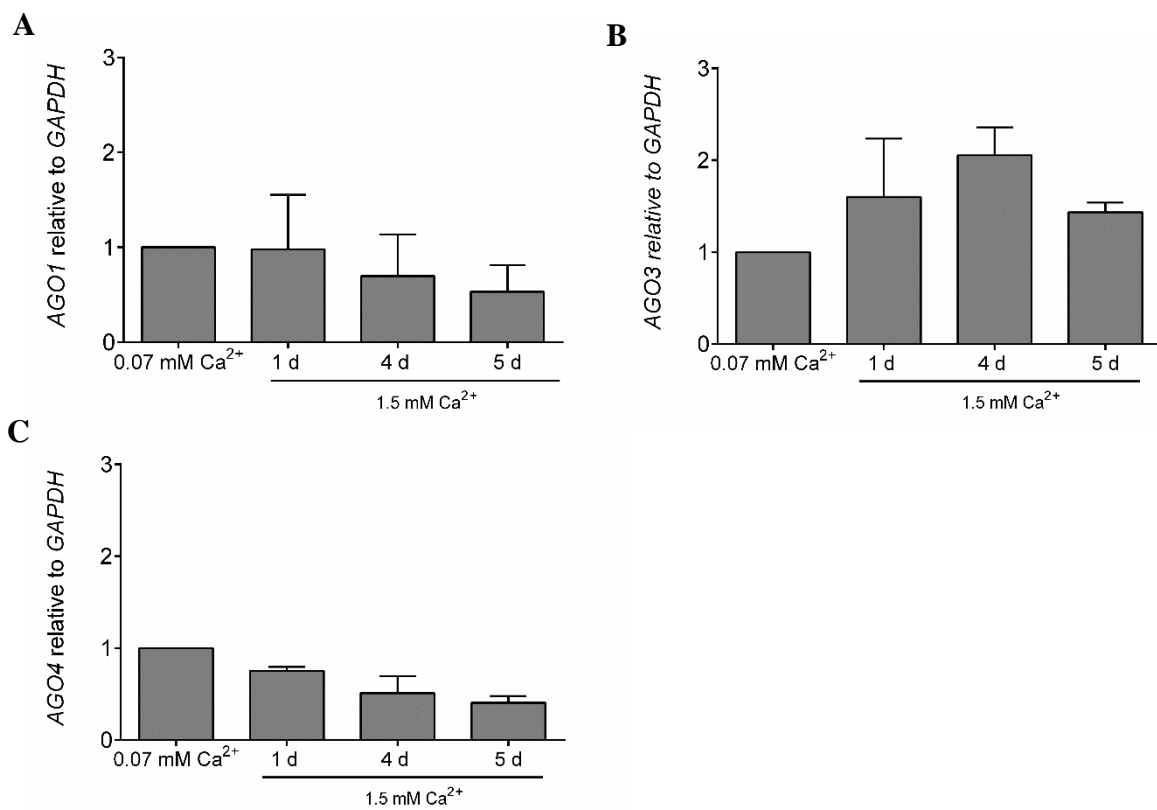


**Figure 6.2: Impact of differentiation on AGO1, AGO3 and AGO4 expression.** HPEKs were grown in 0.07 mM or 1.5 mM  $\text{Ca}^{2+}$  for up to 5 days before levels of AGO1 (A), AGO3 (B) and AGO4 (C) were analysed by RT-qPCR. Values were normalised to *GAPDH* and depicted relative to the proliferating control. Data represents three independent experiments (+SEM).

To gain insight into the relative expression of the four AGOs during HPEK differentiation, the data was re-evaluated to determine AGO expression levels in relation to each other during differentiation. As depicted in figure 6.3, when compared with the weakly expressed *AGO3* levels observed in cells maintained in 0.07 mM  $\text{Ca}^{2+}$ , levels of *AGO4* were 34-fold higher than *AGO3*, compared to *AGO2* which was only 3-fold higher. Differentiation did not have a significant effect on *AGO4* levels. Expression of *AGO2* increased to 7-fold following 1 day of 1.5 mM  $\text{Ca}^{2+}$  stimulation before returning to normal 3-fold expression at 4 and 5 days when compared with proliferating *AGO3* levels. Expression of both *AGO1* and *AGO3* were comparable at all time points. Taken together these results suggest that *AGO4* is the most abundant transcript in monolayer HPEKs and is most effected during differentiation.

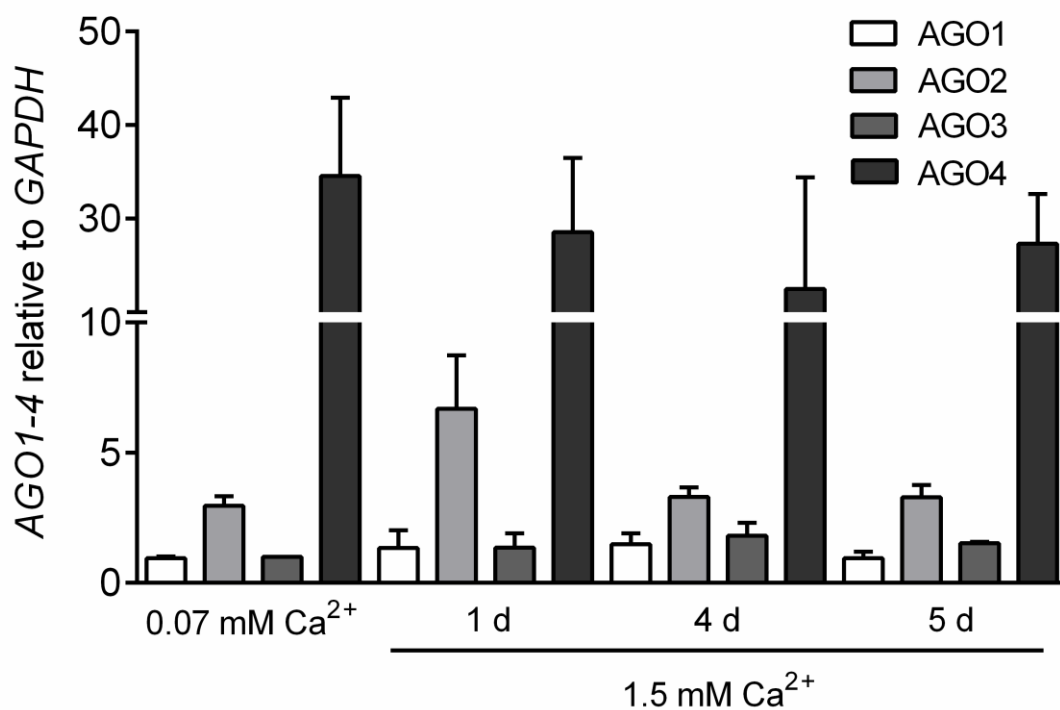


**Figure 6.3: Effect of Differentiation on AGO Expression.** HPEKs were grown in 0.07 mM or 1.5 mM  $\text{Ca}^{2+}$  for up to 5 days before analysis by RT-qPCR. Values were normalised to *GAPDH* and depicted relative *AGO3* levels in 0.07 mM  $\text{Ca}^{2+}$ . Data pooled from three independent experiments (+SEM).

### 6.3.2. Argonaute Expression in Psoriasis

A recent review by Hawke and colleagues has described multiple miRNAs as dysregulated in psoriasis (Hawkes et al., 2016). Moreover, a very recent study has shown that factors involved in miRNA biogenesis such as Dicer are upregulated in psoriatic lesions (Rostami Mogaddam et al., 2017). Work by Roberts and colleagues have shown that AGO2 was downregulated in psoriasis possibly in response to upregulation of miR-184 (Roberts et al., 2013). Despite this the levels of AGOs expressed in psoriasis is relatively unclear. Therefore, expression of *AGO1-4* was assessed in lesional (PP) and non-lesional (PN) psoriasis.

As shown in figure 6.4, when compared with their corresponding PN sample, expression of *AGO1* in PP samples was reduced below 0.4-fold in 4 out of 8 patient samples, elevated at 3.5-fold in 1 out of 8 patients and relatively unchanged in the remaining 3 lesional samples (Fig. 6.4A). In order to compare PN and PP side-by-side and to better assess variation within the dataset, box and whisker charts were used. When plotting  $-\Delta Ct (Ct_{AGO1} - Ct_{GAPDH})$ , there is a significant decrease of *AGO1* in PP samples when compared with PN with medians of 7.3 and 5.4 respectively, although expression variation was elevated in the PP samples demonstrated by minimum values of 4.7 and maximum values of 7.8 compared with 4.0 and 5.9 of PN (Fig. 6.4B). When compared with their relative PN sample, expression of *AGO2* in PP samples was decreased below 0.5-fold in 4 out of 8 patients, elevated 4-6-fold in 2 out of 8 patients and relatively unchanged in the remaining 2 samples (Fig. 6.5A). However, when all 8 patients were compared, there was no significant difference detected in *AGO2* between PP and PN samples presumably due to elevated variation in both PP and PN between patients.

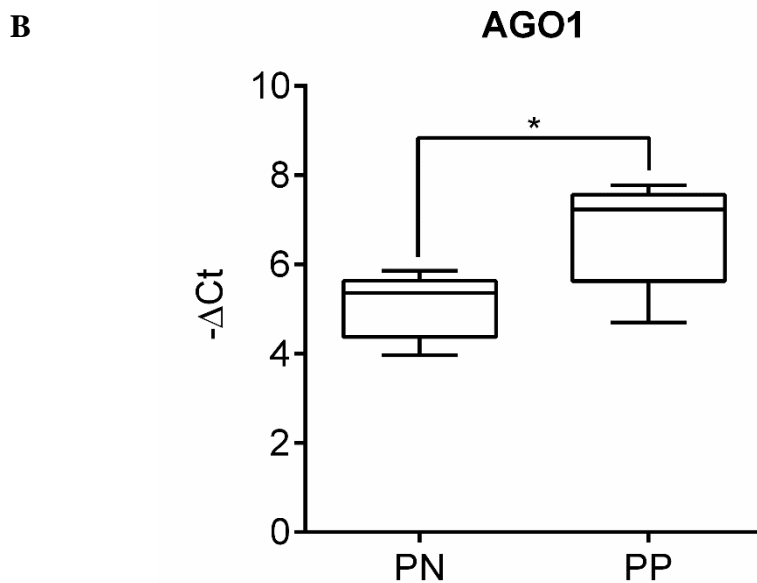
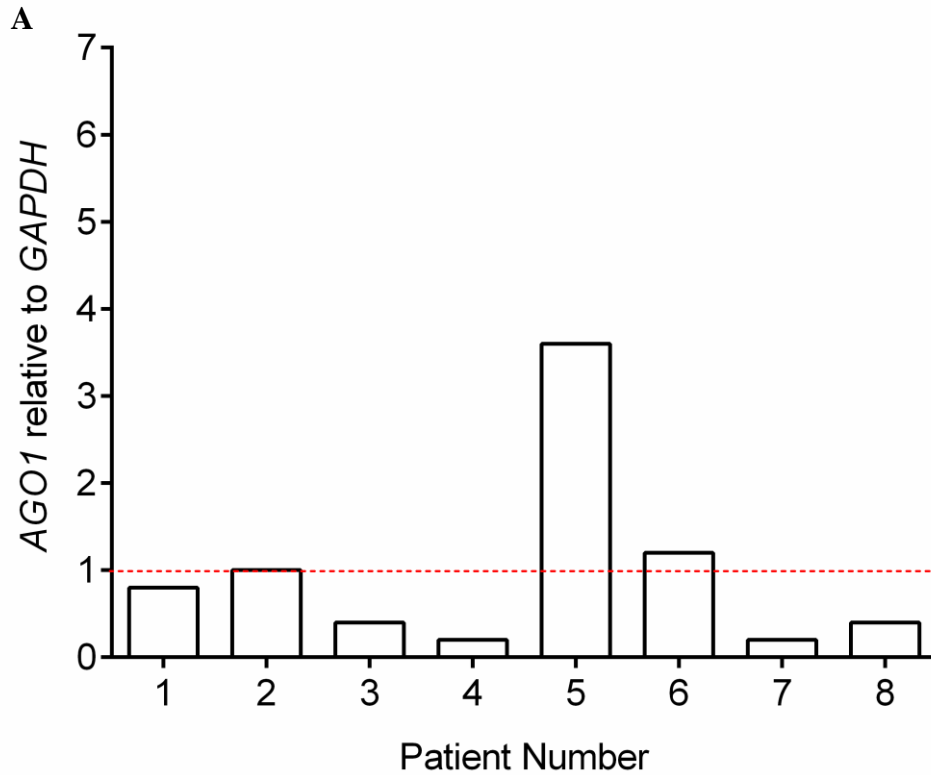


**Figure 6.4: Expression of AGO1 in Psoriatic Lesions.** Levels of AGO1 from psoriatic non-lesional (PN) and lesional (PP) biopsies taken from eight patients were analysed by RT-qPCR. Values were normalised to *GAPDH* and plotted relative to their corresponding PN values (red line; A). Box and whiskers were plotted using  $-\Delta Ct$  ( $Ct_{AGO1} - Ct_{GAPDH}$ ). The top and bottom of each box represent the 75th and 25th percentile and the middle line represents the median value with the extended lines depicting the range (B). \* represents  $p \leq 0.05$ .

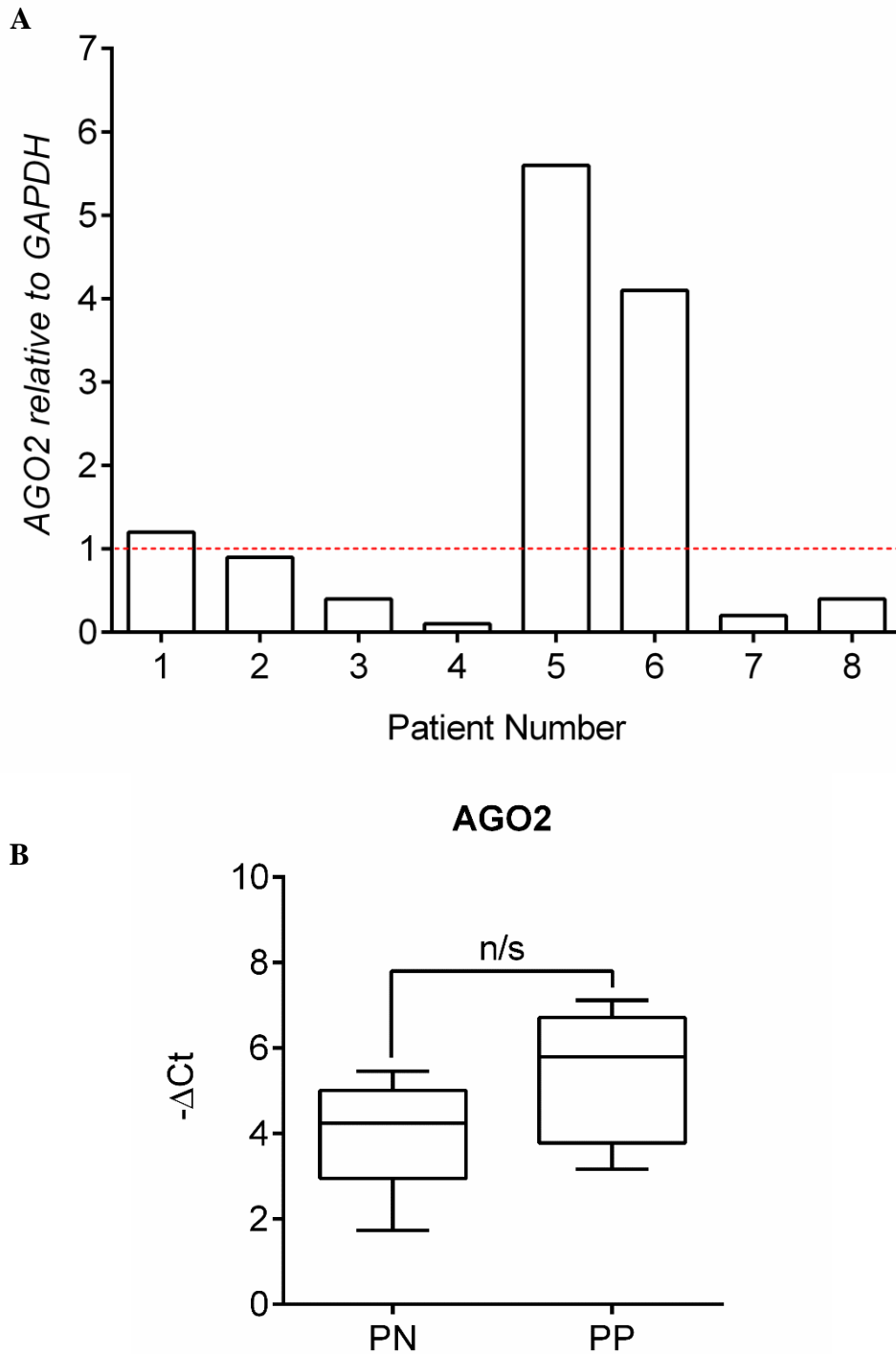


**Figure 6.5: Expression of AGO2 in Psoriatic Lesions.** Levels of AGO2 from psoriatic non-lesional (PN) and lesional (PP) biopsies taken from eight patients were analysed by RT-qPCR. Values were normalised to *GAPDH* and plotted relative to their corresponding PN values (red line; A). Box and whiskers were plotted using  $-\Delta Ct$  ( $Ct_{AGO2} - Ct_{GAPDH}$ ). The top and bottom of each box represent the 75th and 25th percentile and the middle line represents the median value with the extended lines depicting the range (B). \* represents  $p \leq 0.05$ .

Expression of *AGO3* in PP samples was decreased below 0.5-fold in 5 out of 8 patients, elevated 2-3-fold 2 out of 8 patients and somewhat unaffected in the remaining sample (Fig. 6.6A). However, there was no significant difference between pooled PP and PN  $-\Delta$ Cts (Fig. 6.6B). *AGO4* expression was reduced below 0.5-fold in all but one PP sample, which was elevated by 2.8-fold (Patient 6), when compared with relative PN samples (Fig. 6.7A). When  $-\Delta$ Cts from PP and PN were compared there was significantly decreased levels of *AGO4* present within PP samples with a median of 3.6 compared to 1.7 observed in PN. Variation between patient samples was low and consistent in both PN and PP with minimum values of 0.6 and 2.8 in addition to maximum values of 3.0 and 5.2 respectively (Fig. 6.7B)

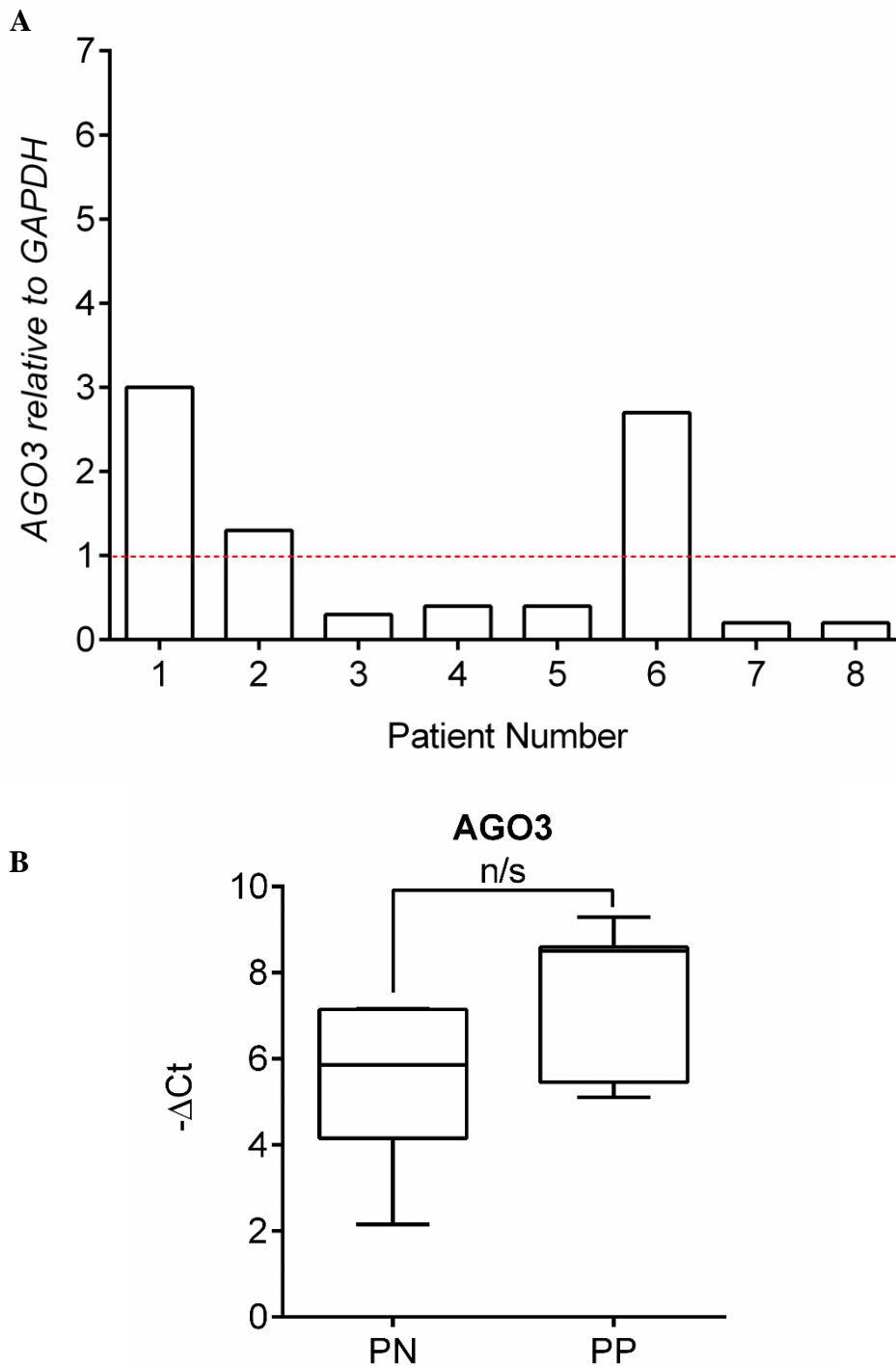


**Figure 6.6: Expression of AGO3 in Psoriatic Lesions.** Levels of AGO3 from psoriatic non-lesional (PN) and lesional (PP) biopsies taken from eight patients were analysed by RT-qPCR. Values were normalised to *GAPDH* and plotted relative to their corresponding PN values (red line; A). Box and whiskers were plotted using  $-\Delta Ct$  ( $Ct_{AGO3} - Ct_{GAPDH}$ ). The top and bottom of each box represent the 75th and 25th percentile and the middle line represents the median value with the extended lines depicting the range (B). \* represents  $p \leq 0.05$ .

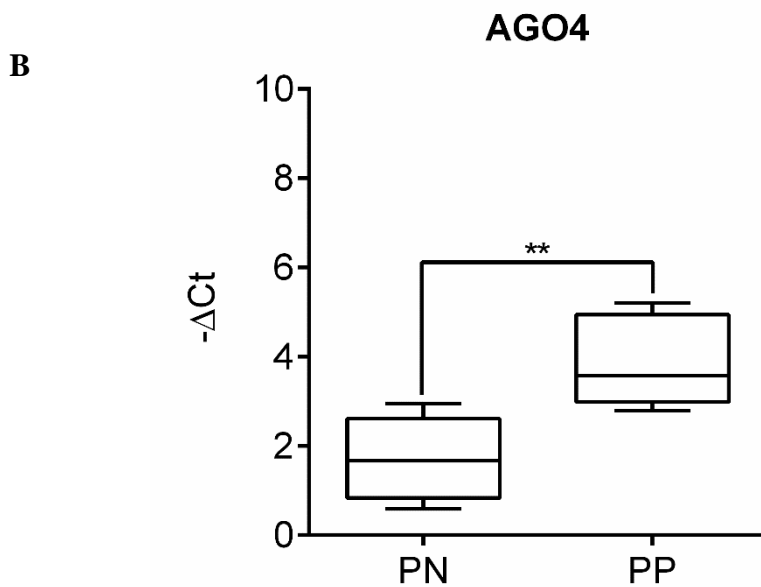
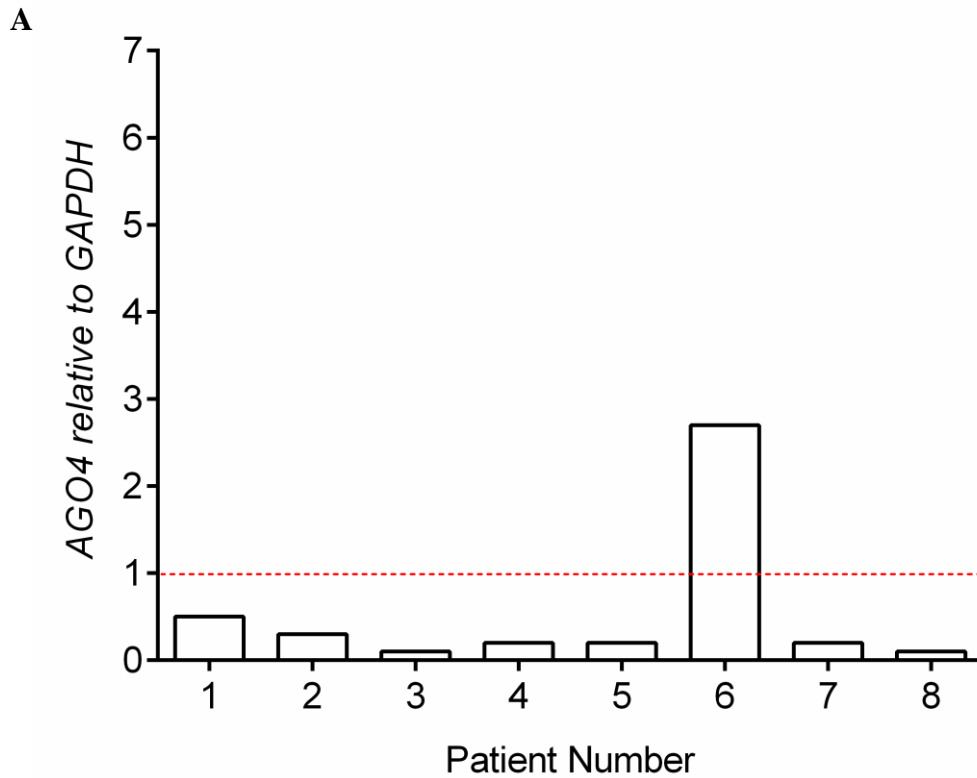


**Figure 6.7: Expression of AGO4 in Psoriatic Lesions.** Levels of AGO4 from psoriatic non-lesional (PN) and lesional (PP) biopsies taken from eight patients were analysed by RT-qPCR. Values were normalised to *GAPDH* and plotted relative to their corresponding PN values (red line; A). Box and whiskers were plotted using  $-\Delta Ct$  ( $Ct_{AGO4} - Ct_{GAPDH}$ ). The top and bottom of each box represent the 75th and 25th percentile and the middle line represents the median value with the extended lines depicting the range (B). \*\* represents  $p \leq 0.01$ .

### 6.3.3. The Effects of AGO2 Perturbation on HPEK Differentiation

AGO2 associates with most miRNAs and plays an essential role in epidermal growth (Wang et al., 2012). Previous work has shown that miR-184 targets AGO2 and given that we have shown miR-184 induction during  $\text{Ca}^{2+}$ -dependent HPEK differentiation, we anticipated that AGO2 may play a role in the differentiation of HPEKs. Therefore, the expression of cyclin E and involucrin transcripts was assessed in differentiating HPEKs loaded with siAGO2.

Initially, to assess the ability and longevity of siAGO2, expression of *AGO2* was analysed in siAGO2-loaded proliferating and differentiating HPEKs. When compared with the siControl, levels of *AGO2* were downregulated by 80% to 0.2-fold in proliferating HPEKs introduced to siAGO2 (Fig. 6.8A). When HPEKs were differentiated for 1 day in 1.5 mM  $\text{Ca}^{2+}$ , levels of *AGO2* increased in those pre-treated with siControl at 2.8-fold when compared with the proliferating siControl. However, this induction of *AGO2* was diminished in cells loaded with siAGO2 were levels remained comparable to those found in the proliferating siControl (Fig.6.8). After 5 days of differentiation, expression of *AGO2* in the siControl returned to basal levels whereas in cells loaded with siAGO2 levels reduced by 50% to 0.5-fold (Fig. 6.8A). To evaluate the specificity of siAGO2, expression of *AGO4* was examined in proliferating and differentiating HPEKs pre-treated with siAGO2. Positively, levels of *AGO4* were relatively unchanged between siControl and siAGO2 at all time points (6.8B).

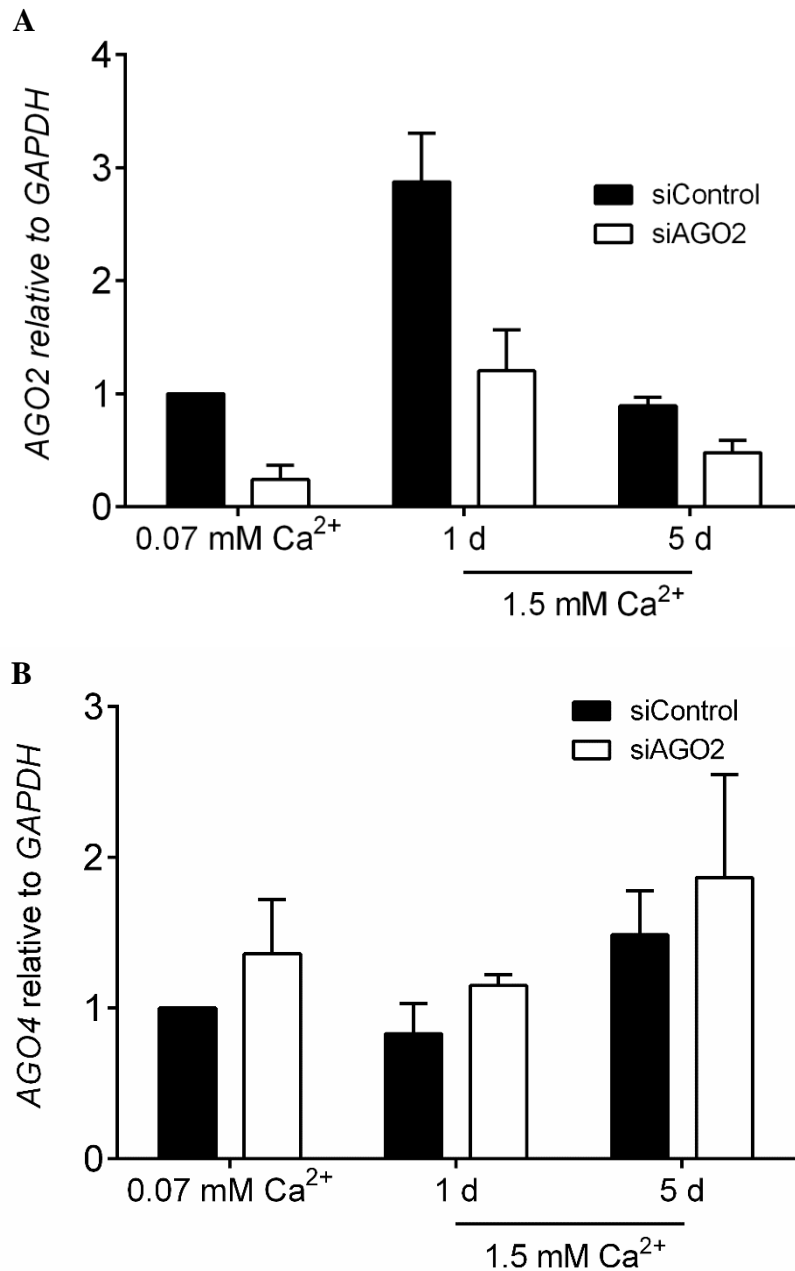


**Figure 6.8: Effect of siAGO2 on Expression of AGO2 and AGO4 During Differentiation.** HPEKs nucleofected 100 nM of siControl or siAGO2 and grown 0.07 mM or 1.5 mM Ca<sup>2+</sup> for up to 5 days. Levels of *AGO2* (A) and *AGO4* (B) were analysed by RT-qPCR. Values were normalised to *GAPDH* and depicted relative to proliferating siControl. Data represents three independent experiments (+SEM).

AGO2 has been shown to regulate cell cycle factors such as cyclin E (Benhamed et al., 2012). Control of the cell cycle during early commitment to terminal differentiation is an essential process with strong evidence suggesting that cyclin E is somewhat responsible (Zanet et al., 2010; Freije et al., 2012). Therefore, both *CCNE1* and *CCNE2* expression was analysed in proliferating and differentiating HPEKs loaded with siAGO2. In proliferating HPEKs, *CCNE1* (Fig. 6.9A) and *CCNE2* (Fig. 6.9B) were considerably elevated in cells loaded with siAGO2 at 4.0- and 3.0-fold respectively when compared with the proliferating siControl. As expected, when HPEKs were differentiated with 1.5 mM Ca<sup>2+</sup> for 5 days both *CCNE1* (Fig. 6.9A) and *CCNE2* (Fig. 6.9B) were elevated in siControl at 1.7- and 3.0-fold respectively. Conversely, in cells loaded with siAGO2 a strong decrease in *CCNE2* to 0.3-fold was observed although *CCNE1* exhibited a more moderate reduction at 0.6-fold after 5 days of 1.5 mM Ca<sup>2+</sup>. After 1 day of Ca<sup>2+</sup> stimulation, a moderate 2-fold increase in *CCNE1* and a modest decrease in *CCNE2* to 0.7-fold was observed in cells treated with siAGO2. In cells treated with siControl, no change was observed in *CCNE1* with a 1-5-fold increase observed in *CCNE2* (Fig. 6.9). These findings suggest that AGO2 regulates cyclin E and this regulatory role differs between proliferating and differentiating states.

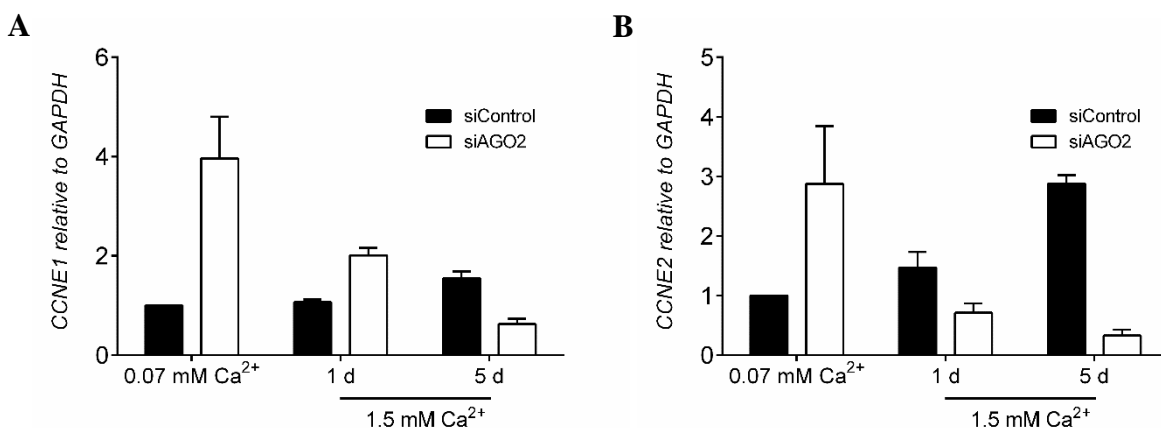


**Figure 6.9: Effect of siAGO2 on Cyclin E Expression During Differentiation.** HPEKs nucleofected 100 nM of siControl or siAGO2 and grown 0.07 mM or 1.5 mM Ca<sup>2+</sup> for up to 5 days. Levels of Cyclin E1 (*CCNE1*; A) and Cyclin E2 (*CCNE2*; B) were analysed by RT-qPCR. Values were normalised to *GAPDH* and depicted relative to proliferating siControl. Data represents three independent experiments (+SEM).

Next, the effect of reduced *AGO2* levels on the keratinocyte differentiation marker, involucrin was assessed. In proliferating HPEKs loaded with siAGO2, a 50% reduction of *IVL* transcript to 0.5-fold was observed when compared with the siControl. However, when differentiated with 1.5 mM  $\text{Ca}^{2+}$ , *IVL* expression was relatively unchanged in HPEKs loaded with siAGO2 when compared with the siControl at both 1 and 5 d time points (Fig. 6.10).

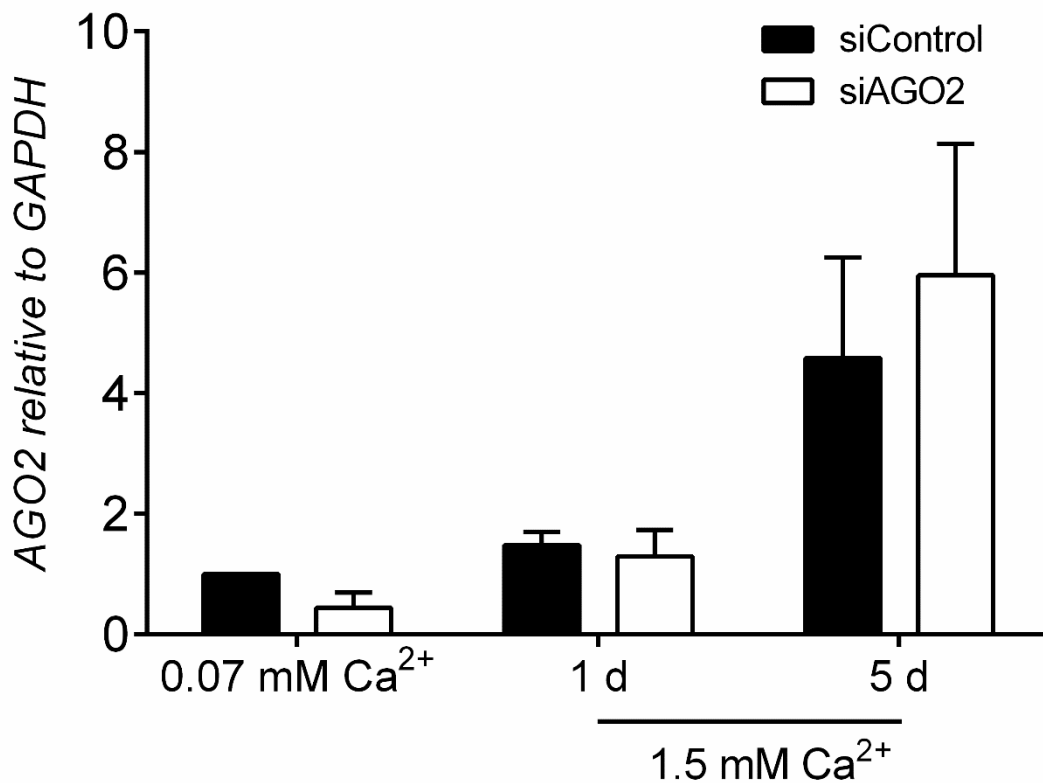


**Figure 6.10: Impact of siAGO2 on Expression of Involucrin During Differentiation.** HPEKs nucleofected 100 nM of siControl or siAGO2 and grown 0.07 mM or 1.5 mM  $\text{Ca}^{2+}$  for up to 5 days. Levels of *IVL* were analysed by RT-qPCR. Values were normalised to *GAPDH* and depicted relative to proliferating siControl. Data represents three independent experiments (+SEM).

Finally, given that AGO2 is vital to the function of the RISC, levels of miRNAs implicated with keratinocyte biology were analysed in HPEKs that had reduced levels of AGO2. Levels of both miR-21 and miR-205 were decreased by around 50% to 0.5-fold in differentiating HPEK nucleofected with siAGO2 when compared with those nucleofected with siControl. Interestingly, levels of miR-184 were reduced by 70% to 0.3-fold (Fig. 6.11).

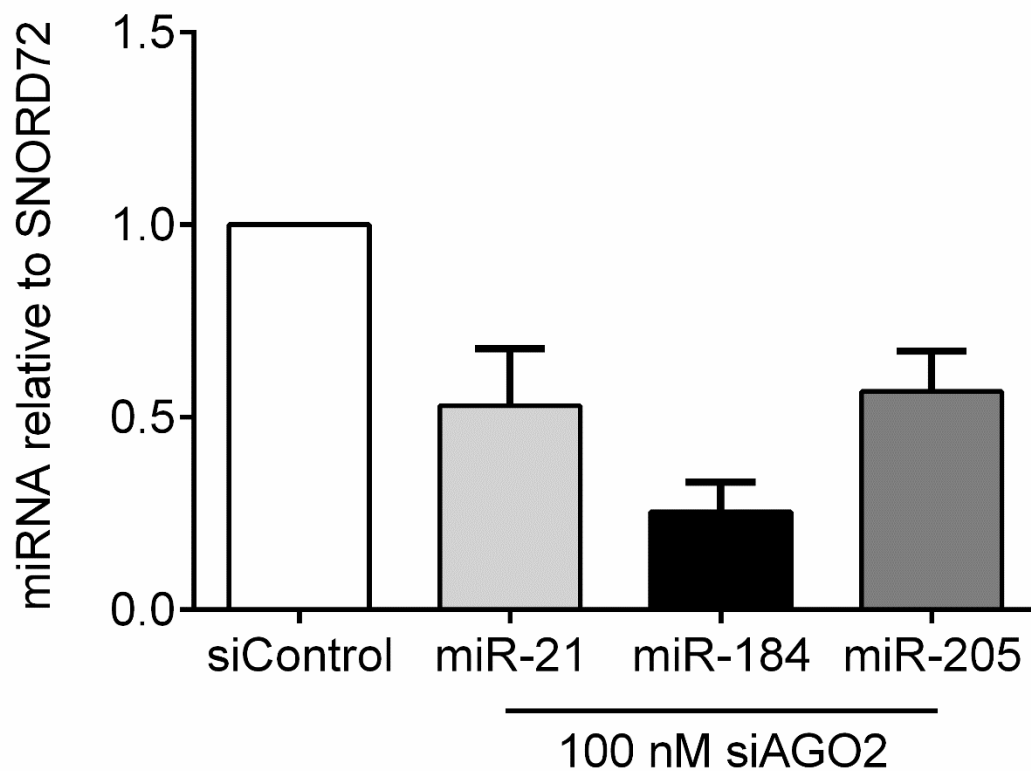
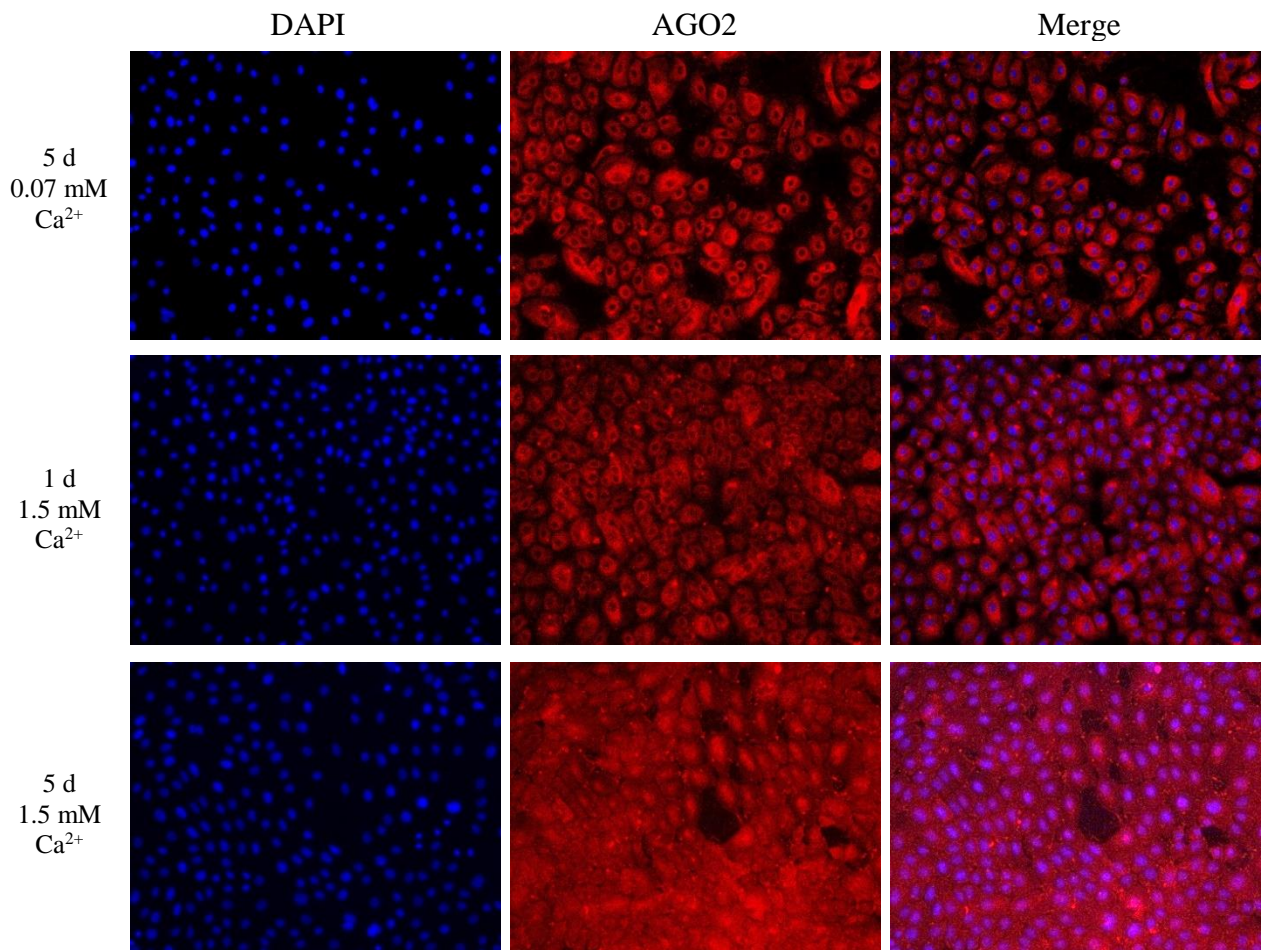


**Figure 6.11: Effect of siAGO2 on Expression of miRNAs.** HPEKs nucleofected 100 nM of siControl or siAGO2 and grown 1.5 mM for 5 days. Levels of miR-21, miR-184 and miR-205 were analysed by RT-qPCR. Values were normalised to SNORD72 and depicted relative to proliferating siControl. Data represents three independent experiments (+SEM).

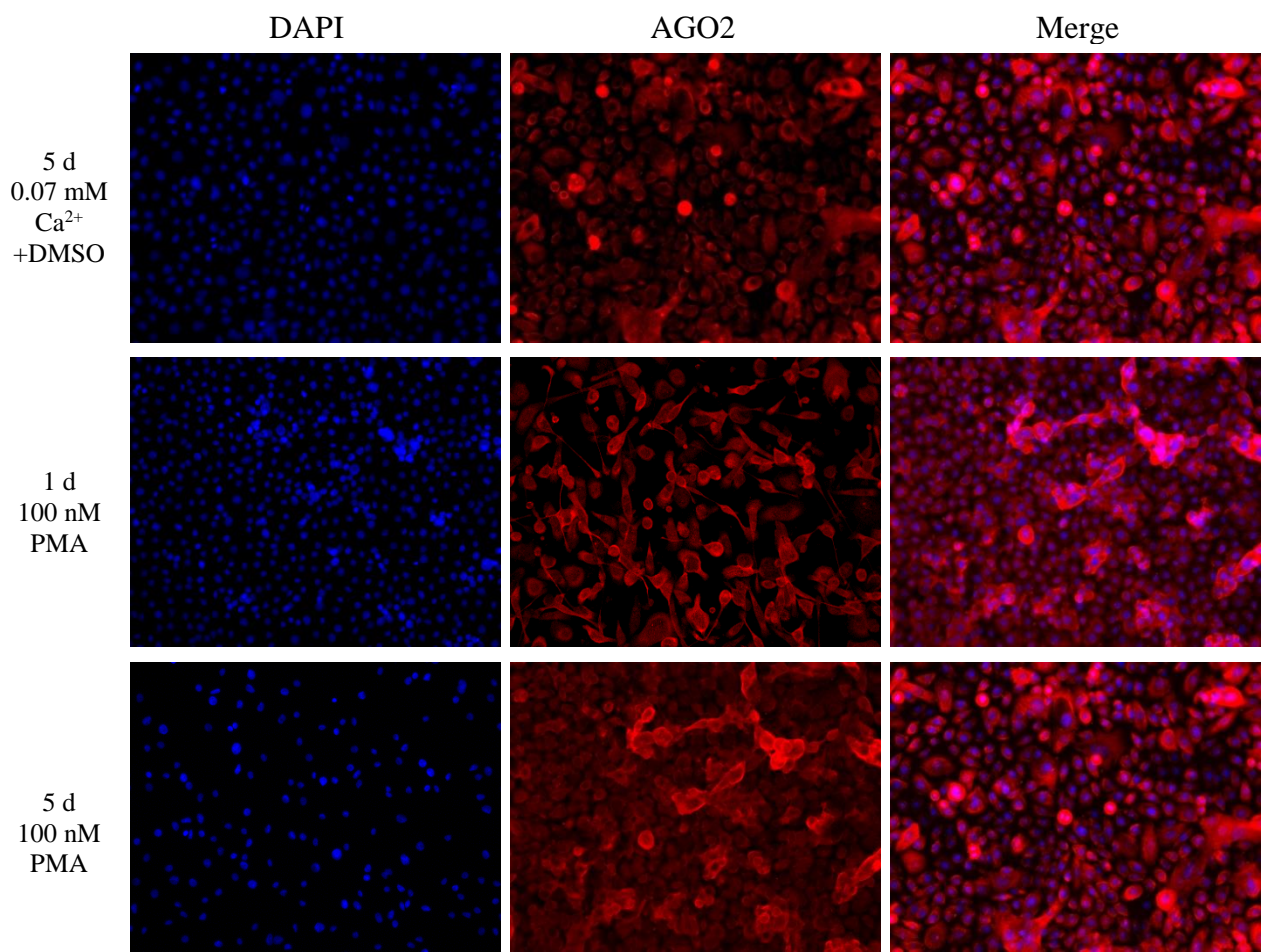
#### 6.3.4. Subcellular Location of AGO2

AGO2 accumulates in the nucleus of senescent fibroblasts where it regulates proliferation linked genes (Benhamed et al., 2012). Very recent work has reported AGO2 as predominately nuclear in both human skin and human primary keratinocyte monolayer and organotypic cultures (Sharma et al., 2016). Therefore, we anticipated that AGO2 may localise to the nucleus of differentiating HPEKs. Consequently, we analysed AGO2 subcellular location in proliferating HPEK and those stimulated with common differentiation reagents.

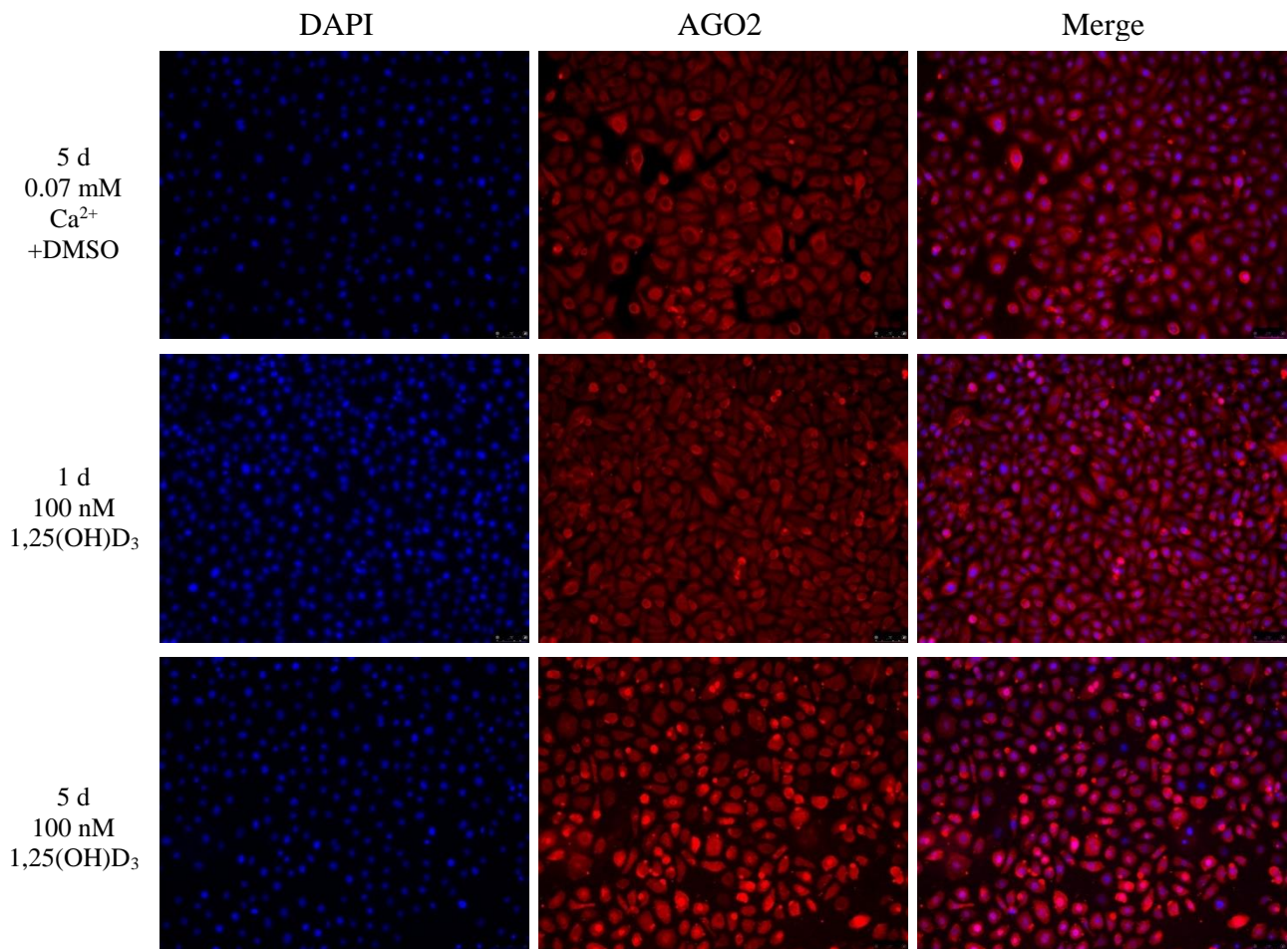
As shown in Figure 6.12, when HPEKs were maintained in low  $\text{Ca}^{2+}$  for 5 days, AGO2 was perinuclear with almost none present within the nucleus. Following stimulation with 1.5 mM  $\text{Ca}^{2+}$ , AGO2 seemed relatively unchanged after 1 d, remaining predominately perinuclear although nuclei appear less defined which might suggest some nuclear AGO2. After 5 d of 1.5 mM  $\text{Ca}^{2+}$ , there appears to be a striking accumulation of AGO2 in the nucleus although some remains in the cytoplasm (Fig. 6.12). Following treatment with 100 nM PMA, AGO2 localisation seemed relatively unchanged at both 1 d and 5 d time points (Fig. 6.13). When stimulated with 100 nM of  $1,25(\text{OH})\text{D}_3$  for 5 days the subcellular location of AGO2 appeared more dispersed throughout the whole cell suggesting some nuclear AGO2 though this could be due to DMSO (Fig. 6.14).



**Figure 6.12: Impact of Ca<sup>2+</sup> Induced Differentiation on AGO2 Subcellular Location.** HPEKs were grown in 0.07 mM or 1.5 mM Ca<sup>2+</sup> for up to 5 days before AGO2 staining and nuclear counterstaining with DAPI. Fluorescent images were taken at 20x magnification from proliferating cells in addition to 1 d and 5 d differentiated HPEKs.

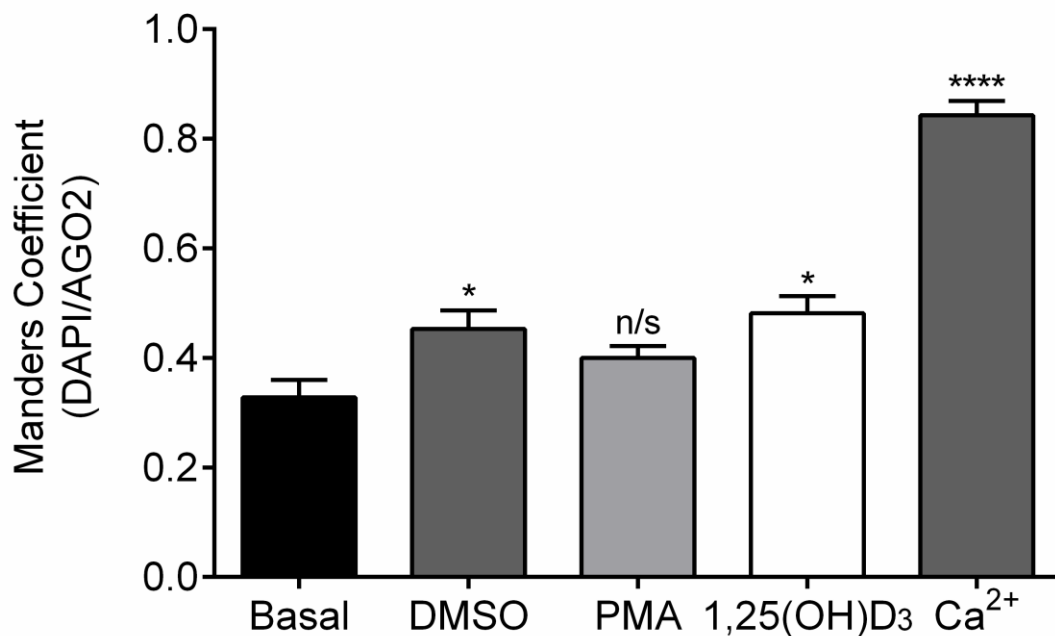


**Figure 6.13: Effect of PMA Induced Differentiation on AGO2 Subcellular Location.** HPEKs were grown in 0.07 mM Ca<sup>2+</sup> or 100 nM of PMA for up to 5 days before AGO2 staining and nuclear counterstaining with DAPI. Fluorescent images were taken at 20x magnification from proliferating cells in addition to 1 d and 5 d differentiated HPEKs.



**Figure 6.14: Impact of 1,25(OH)D<sub>3</sub> Induced Differentiation on AGO2 Subcellular Location.** HPEKs were grown in 0.07 mM Ca<sup>2+</sup> with DMSO or 100 nM of 1,25(OH)D<sub>3</sub> for up to 5 days before AGO2 staining and nuclear counterstaining with DAPI. Fluorescent images were taken at 20x magnification from proliferating cells in addition to 1 d and 5 d differentiated HPEKs.

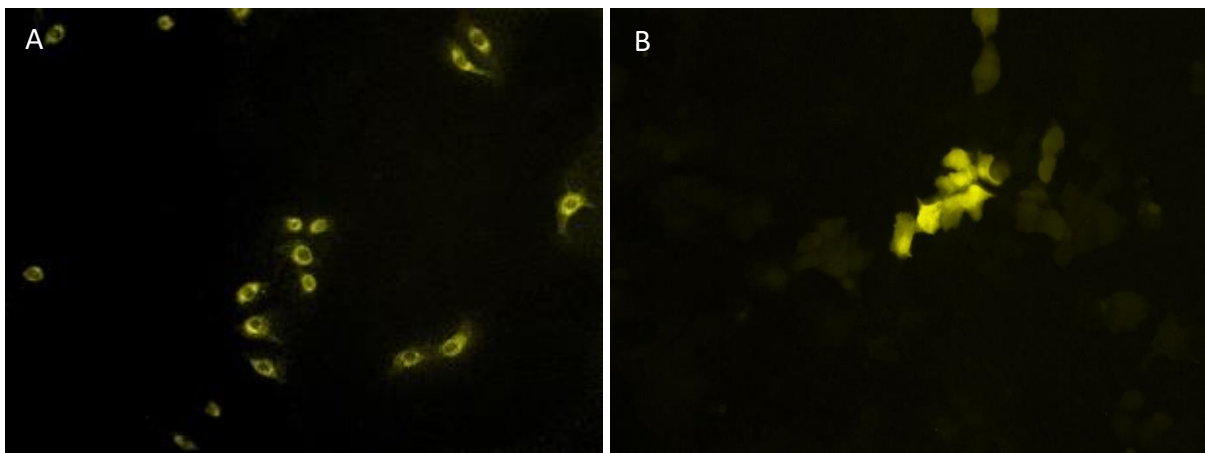
To quantify changes in subcellular location Manders overlap coefficient was used, which in its most simplistic form measures overlapping pixels with perfect overlap described as 1.0. Values were comparable between proliferating cells and those treated with 0.1% DMSO, 100 nM PMA and 100 nM 1,25(OH)D<sub>3</sub> respectively suggesting weak to moderate co-localisation (Fig. 6.15). Changes in PMA was not significant but both DMSO and 1,25(OH)D<sub>3</sub> reached significance although, DMSO is likely responsible for the changes exhibited by 1,25(OH)D<sub>3</sub>. In contrast, when treated with 1.5 mM Ca<sup>2+</sup> there was a significant increase to around 0.85 when compared with proliferating control indicative of very strong co-localisation (Fig. 6.15).



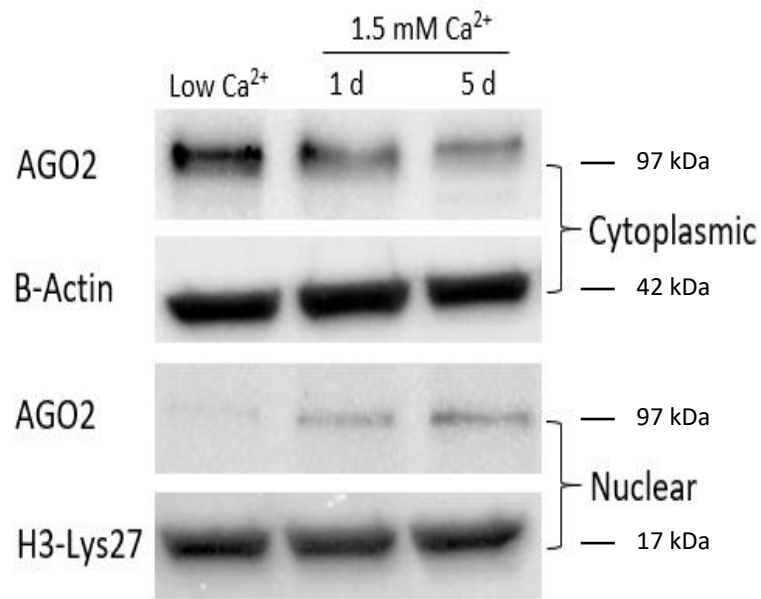
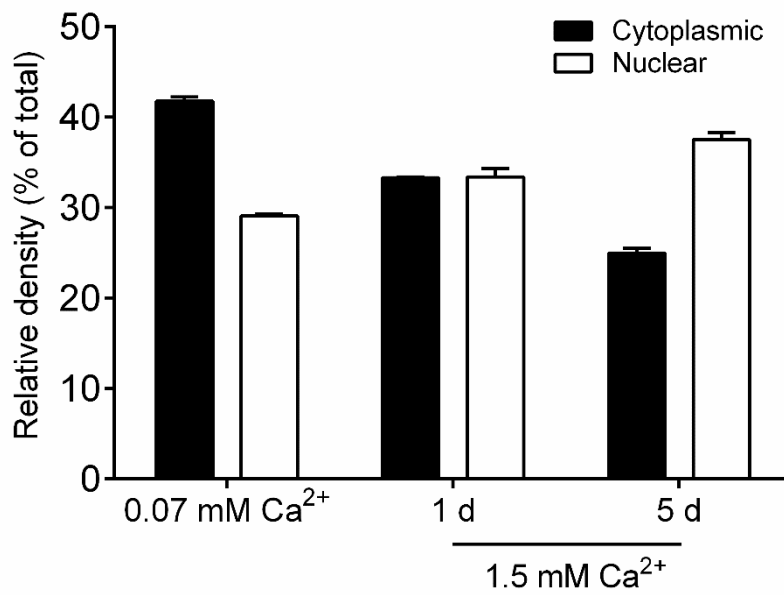
**Figure 6.15: Manders Colocalisation Coefficient Analysis.** Colocalisation analysis between basal HPEKs, Vehicle (DMSO) and HPEKs differentiated for 5 days with PMA, 1,25(OH)D<sub>3</sub> and Ca<sup>2+</sup> using Fiji/ImageJ. Stained for AGO2 and counterstained for the nucleus using DAPI. Manders coefficients were calculated for each sample, the means from four fields of view from three independent experiments were pooled into a bar graph (+SEM). \* represents  $p \leq 0.05$ , \*\*\*\* represents  $p \leq 0.0001$ .

To confirm these observations in living cells, HPEKs were nucleofected with a plasmid encoding enhanced yellow fluorescent protein (EYFP) tagged AGO2. Consistent with the immunofluorescent images, when maintained in low  $\text{Ca}^{2+}$ , EYFP tagged AGO2 appeared perinuclear with little to no presence in the nucleus. Upon stimulation with 1.5 mM  $\text{Ca}^{2+}$  for 5 days, EYFP-AGO2 appeared more disperse throughout the cell (Fig. 6.16).

Finally, to confirm AGO2 nuclear localisation during HPEK differentiation, fractional western blotting was performed. In proliferating cells, levels of cytoplasmic AGO2 were high representing 42% of the total cytoplasmic densitometric proportion. Following addition of 1.5 mM  $\text{Ca}^{2+}$  levels of AGO2 present within the cytoplasm were almost halved after 5 days.  $\beta$ -Actin was used as a cytoplasmic control with expression stable throughout (Fig. 6.17). In contrast, levels of nuclear AGO2 in proliferating HPEKs were very low representing 29% based on chemiluminescent density. When stimulated with 1.5 mM  $\text{Ca}^{2+}$  the amount of AGO2 present in the nucleus increased, with a total nuclear densitometric proportion of 33% and 38% for 1 and 5 d respectively (Fig. 6.17).



**Figure 6.16: Impact of  $\text{Ca}^{2+}$  Induced Differentiation on YFP-AGO2 Subcellular Location.** HPEKs nucleofected with 2  $\mu\text{g}$  of EYFP-AGO2 were grown in 0.07 mM (A) or 1.5 mM  $\text{Ca}^{2+}$  (B) for 5 days. Fluorescent images were taken at 20x magnification.

**A****B**

**Figure 6.17: Fractional Western Blotting for AGO2 Following Differentiation.** HPEKs were grown in 0.07 mM or 1.5 mM Ca<sup>2+</sup> for 5 days. Cytoplasmic and nuclear fractions were separated and probed for AGO2 (A). Values were normalised to the respective loading control and densitometry was performed (B). Data represents two independent experiments (+SEM).

## 6.4. Discussion

### 6.4.1. Effect of HPEK Differentiation on Argonaute Expression

As a key part of the RISC complex, regulation of AGOs is likely a tightly controlled process that underpins cellular proliferation and differentiation. Work by Wang and colleagues identified that AGO2 is the most abundant AGO and binds to most miRNAs within the epidermis of mice (Wang et al., 2012). A study has identified that miR-184 targets AGO2 in HPEKs and HaCaTs, with recent work confirming this observation in pancreatic  $\beta$  cells (Roberts et al., 2013). In neuroblastoma cell lines, overexpression of either AGO1 or AGO2 can induce differentiation independent of stimulation with differentiation reagents (Parisi et al., 2011). We have previously shown that miR-184 is induced during  $\text{Ca}^{2+}$ -dependent HPEK differentiation, suggesting that elevated levels of miR-184 may reduce AGO2 during differentiation (Fig. 3.6). However, little is known about the expression patterns and abundancies of AGO1-4 during human epidermal keratinocyte differentiation. Therefore, the first aim of this chapter was to evaluate expression of AGO1-4 during  $\text{Ca}^{2+}$ -induced *in vitro* HPEK differentiation.

We have shown that expression of *AGO* transcripts do not change substantially during HPEK differentiation with *AGO1* remaining relatively unchanged, *AGO2* displaying a slight increase at 1 d, *AGO3* exhibiting a modest increase at 4 d and *AGO4* downregulated over the 5 days, though this was not at a statistically significant level. Given that we have demonstrated induction of miR-184 during keratinocyte differentiation and that miR-184 targets AGO2 we anticipated a reduction in *AGO2* during differentiation. Surprisingly, we observed no reduction in *AGO2* expression after 5 days of differentiation suggesting that the induction of miR-184 is insufficient to cause noticeable inhibition of *AGO2* or that *AGO2* transcripts are not targeted for degradation and instead translationally repressed. To our knowledge this is the first time individual *AGO* expression has been assessed in differentiating monolayer HPEKs. To provide

contrast, expression of AGO2 is increased in human myeloblastic and monocytic cell lines during terminal differentiation into granulocytes (Iosue et al., 2013). Conversely, in mouse embryonic stem cells, expression of AGO2 protein is reduced following differentiation (Ngondo et al., 2018). Suggesting that changes in AGO during differentiation occurs in a tissue/cell type dependent fashion with substantial changes in AGO levels not required for HPEK differentiation or that the slight fluctuations in AGO transcripts observed may effectively perturb protein levels. Although we did not evaluate protein expression and may provide interesting further work.

When levels of *AGO1-4* were compared in proliferating and differentiating HPEK, *AGO4* was the most abundant transcript at every time point followed by *AGO2* with both *AGO1* and *AGO3* comparably low. Conversely, recent work evaluating AGO expression in human skin has demonstrated that *AGO1* is the most abundant transcript followed by *AGO2* and consistent with our data they show that *AGO3* is the least abundant AGO transcript (Völler et al., 2016). We show that *AGO4* is the most abundant transcript in HPEK monolayers suggesting that stratification has different AGO expression requirements than monolayer HPEK cultures, although protein levels were not assessed in either studies, work on organotypic cultures could provide a stratified *in vitro* model to bridge the gap between monolayer and skin. In contrast, work by Yi and colleagues on mouse epidermis, employing shotgun proteomics and AGO-Immunoprecipitation methods, have demonstrated that Ago2 is most abundant at the protein level, followed by Ago1 with both Ago3 and Ago4 expressed at significantly low levels (Wang et al., 2012). We only assessed expression of AGO transcripts preventing a direct comparison. However, comparative analysis between human and mouse skin transcriptomes demonstrates that only ~30% of genes overlap of which AGOs were not included suggesting that their expression could be differential between mouse and human skin (Gerber Peter et al., 2014).

### 6.4.2. Argonuates in the Psoriatic Epidermis

Upregulation of cutaneous AGO1 and AGO2 has been linked to squamous cell carcinoma, basal cell carcinoma and actinic keratosis (Sand et al., 2012). In contrast, overall expression of AGO1-4 is severely reduced in melanoma cell lines with AGO2 most effected (Völler et al., 2016). Recent work has showed perturbed expression of miRNA biogenesis enzymes in psoriasis, demonstrating that levels of *Dicer* and *Drosha* transcripts are significantly higher in psoriatic lesions when compared with both non-lesional and healthy samples (Rostami Mogaddam et al., 2017). Moreover, a study by Roberts and colleagues found a significant reduction of *AGO2* in psoriatic lesions (Roberts et al., 2013). Given the strong dysregulation of miRNAs and their biogenesis proteins observed in psoriasis, surprisingly little is known about the expression of *AGO1-4*.

Our analysis of a small set of 8 lesional and non-lesional psoriatic epidermis samples show that *AGO1* and *AGO4* transcripts were significantly downregulated in psoriatic lesions. Additionally, expression of both *AGO2* and *AGO3* seems patient specific with downregulation more commonly observed (Fig. 6.4-6.7). Surprisingly, to our knowledge this is the first time *AGO1-4* expression in psoriasis has been reported together. Conversely, recent work reported a significant decrease of *AGO2* in psoriasis although their sample size was small at five clinical samples (Roberts et al., 2013). However, in our data set expression of *AGO2* from two out of eight PP samples was severely upregulated by 4 to 6-fold which may mask any significance. Nonetheless, reporting a slightly elevated number of samples suggests that expression of *AGO2* is more patient specific than previously considered although additional psoriatic samples would be required to confirm this suggestion. Conversely, a recent study demonstrated significantly upregulated *AGO2* in PP samples when compared with PN (Zhou et al., 2016). However, consistent with our data, the same study shows a reduction of *AGO1* in psoriatic lesions, though their findings represent gene expression data derived from RNA-sequencing without validation

by RT-qPCR. We have showed that *AGO3* was expressed in very low levels in HPEK and others reported low levels of *AGO3* present in human skin (Völler et al., 2016). Hence, unsurprisingly, *AGO3* expression was relatively unchanged between PP and PN samples, suggesting that the other *AGOs* are favoured over *AGO3* by epidermal keratinocytes. Interestingly, *AGO4* the most abundant AGO transcript we found in HPEK was the most heavily downregulated in psoriatic lesions, suggesting that *AGO4* may play an unidentified role in epidermal keratinocyte biology and providing an interesting area for further study. Conceivably, elevated levels of miRNAs produced by upregulated Dicer/Drosha put *AGOs* under functional strain or that mechanisms which may or may not be miRNA dependent directly affect AGO expression.

#### **6.4.3. siAGO2 Impacts Expression of Differentiation-associated Genes**

The epidermis consists of a dynamic relationship between proliferating and differentiating keratinocytes with tight spatial and temporal control required to maintain normal skin homeostasis. *AGOs* are essential in maintaining tissue homeostasis by regulating expression of epidermal miRNAs. Given that double knockout of cutaneous *Ago1* and *Ago2* in mice can upset this homeostasis, resulting in hyper thickened epidermis likely down to a reduction of global miRNA levels, the effects of *AGO2* perturbation on factors associated with differentiation of human keratinocytes is relatively unstudied (Wang et al., 2012). Therefore, changes in the differentiation associated effectors, cyclin E and involucrin, were examined in proliferating and differentiating HPEK loaded with siAGO2.

In proliferating HPEK loaded with siAGO2 both *CCNE1* and *CCNE2* were elevated when compared with the controls (Fig. 6.9). Given that, miR-184 induces cyclin E protein (Fig. 4.8) but has no effect on both *CCNE1* and *CCNE2* transcript levels (Fig. 4.6-4.7), this may suggest that *AGO2* is not a target for miR-184 in the context of miR-184 induced

differentiation. To our knowledge this is the first time AGO2 has been linked to the regulation of cyclin E transcripts in HPEKs. Previous work in human fibroblasts, has shown that AGO2 represses E2F target genes such as cyclin E whereby they show overexpression of AGO2 reduces cyclin E promoter activity by 50% (Benhamed et al., 2012). Suggesting that elevated cyclin E in response to reduced AGO2 activity might be due to derepression of E2F genes. Both *CCNE1* and *CCNE2* transcripts consistently induced in differentiating HPEKs (Fig. 3.3). However, in cells loaded with siAGO2 this induction was severely diminished compared to cells loaded with control siRNA (Fig. 6.9). This could be a compensatory mechanism by the cell, whereby elevated levels of cyclin E transcript are present within proliferating HPEKs treated with siAGO2 and accumulation of more transcript is not required.

In both proliferating and differentiating HPEKs loaded with siAGO2 we have shown that *IVL* levels are relatively unchanged when compared with the control, although an increase was observed over 5 days indicative of differentiation (fig. 6.10). Yi and colleagues have shown that knockout of both Ago1 and Ago2 has a severe effect on the skin of mice, resulting in a hyper thickened epidermis and more apoptotic basal keratinocytes (Wang et al., 2012). Taken together with the minimal effect of siAGO2 on the expression of the differentiation marker, *IVL*, this may suggest that cyclin E is responsible for the development defects observed in the skin of mice with ablated Ago1/Ago2 and would provide an interesting avenue of further investigation.

#### **6.4.4. siAGO2 Effects Expression of miR-205, miR-184 and miR-21**

Consistent with the literature our data shows that levels of miRNAs associated with epidermal development and disease, including miR-205 (Wang et al., 2013) and miR-21 (Guinea-Viniegra et al., 2014), are down regulated in HPEKs treated with siAGO2 (Fig. 6.11). Previous work has shown that global expression of mature miRNAs is reduced by 40% in embryonic fibroblasts derived from AGO2 knockout mice (Diederichs and Haber, 2007). A study on the skin of Ago2 knockout mice has shown that global miRNA expression is reduced on average by 30% (Wang et al., 2012). Interestingly, our data shows that levels of miR-184 are reduced more than the other miRNAs tested, suggesting that miR-184 is less stable than both miR-21 and miR-205 when the pool of AGO2 molecules is limited.

#### **6.4.5. AGO2 Accumulates in the Nucleus During Differentiation with Ca<sup>2+</sup>**

AGO2 is a central part of the RISC complex and through miRNA-dependent inhibition, acts as an influential regulator of mRNA translation in the cytoplasm of mammalian cells. However, emerging evidence suggests that AGO2 also has functional activity within the nucleus where it can regulate processes such as alternative splicing and TGS (Benhamed et al., 2012; Taliaferro et al., 2013). Work by Bischof and colleagues has shown that AGO2 accumulates in the nucleus of human lung fibroblasts undergoing an irreversible form of growth arrest called senescence (Benhamed et al., 2012). Moreover, later work demonstrates a substantial presence of nuclear AGO2 in several cell types including HeLa, A459 and human breast cancer cell lines (Gagnon et al., 2014). Recent work showed strong nuclear AGO2 in human skin and keratinocyte cultures (Sharma et al., 2016). Taken together, nuclear localisation of AGO2 does not seem to be dependent on cell type. Therefore, our final aim of this study was to evaluate subcellular localisation of AGO2 in basal and differentiated HPEKs using several common differentiation agents.

In proliferating HPEKs our data indicates that little to no AGO2 was present within the nucleus with most distributed in a perinuclear fashion. In contrast, when differentiation was induced, AGO2 appeared to localise to the nucleus in a  $\text{Ca}^{2+}$  specific fashion (Fig. 6.12-6.14). Relevant work by Sharma and colleagues partially supports our work, describing AGO2 as predominantly nuclear in parabasal differentiating layers of human epidermis as well as suprabasal layers of organotypic cultures. Contradictory, the same study also reports nuclear AGO2 within monolayer cultures in addition to basal cells of skin and organotypic cultures (Sharma et al., 2016). However, the proliferative or differentiated state of these monolayer cultures were not well described. Previous work suggests that 2% fetal bovine serum (FBS) is enough to trigger terminal differentiation in keratinocytes (Borowiec et al., 2013). Consequently, the addition of 5% FBS to low  $\text{Ca}^{2+}$  media by this study most likely triggered differentiation of HPEK monolayers although they provided no information describing differentiation marker expression. Therefore, the nuclear AGO2 reported by Sharma et al., 2016 in apparently proliferating keratinocytes may be due to FBS.

Perinuclear distributions of AGO2 are a common feature in human cells whereby processing of miRNAs occurs just outside of the nucleus. We show perinuclear localisation of AGO2 in proliferating cells, to our knowledge this has not been previously described in keratinocytes (Fig. 6.12-6.16). Consistently, in a hepatocarcinoma cell line called Huh7, AGO2 is distributed in a similar perinuclear fashion (Berezhna et al., 2011). Likewise, a very recent study has observed AGO2 in the perinuclear region of HeLa cells (Castanotto et al., 2018). This could suggest that in keratinocytes the majority of non-coding RNA maturation occurs within close proximity to the nucleus.

For the first time to our knowledge, we have shown  $\text{Ca}^{2+}$ -dependent AGO2 nuclear localisation during keratinocyte differentiation (Fig. 6.12, 6.15 and 6.16). In contrast, both PMA and  $1,25(\text{OH})\text{D}_3$  failed to trigger substantial nuclear AGO2 shifts (Fig. 6.13 and 6.14).

Given that AGO2 localises to the nucleus of senescent lung fibroblasts where it regulates proliferation-associated genes (Benhamed et al., 2012), a hallmark of keratinocyte differentiation is growth arrest therefore, AGO2 may have a nuclear role during  $\text{Ca}^{2+}$ -dependent keratinocyte differentiation.

## **7. Conclusion**

MiRNAs are vitally important to epidermal homeostasis with a plethora of cutaneous diseases arising from dysregulated miRNA expression. With this in mind, a growing body of research has sought to elucidate the molecular mechanisms behind miRNA-dependent regulation of keratinocyte biology. A specific miRNA, miR-184, has been shown to modulate AGO2 activity in epidermal keratinocytes (Roberts et al., 2013). However, despite recent advances, the understanding of miR-184 in the context of human epidermal keratinocyte biology has remained poorly described. Thus, the aims of this thesis were:

1. Investigate miR-184 expression during HPEK differentiation and elucidate the regulatory mechanisms.
2. Examine the effects of ectopic miR-184 on HPEK proliferation and differentiation by utilising synthetic miR-184 mimics and miR-184 LNA inhibitors.
3. Investigate miR-184 expression and function during HPEK migration.
4. And finally, explore epidermal AGO dynamics and examine the miR-184:AGO2 axis during HPEK differentiation

In chapter 3, the expression of miR-184 was examined in HPEKs differentiated with the common differentiation agents,  $\text{Ca}^{2+}$ , PMA and Vitamin D. The results have shown that miR-184 is induced during HPEK differentiation in a mechanism that is dependent on  $\text{Ca}^{2+}$  and the major keratinocyte  $\text{Ca}^{2+}$  entry pathway SOCE. Moreover, levels of miR-184 were upregulated in psoriatic lesions when compared to non-lesional skin. A very recent study reported elevated levels of miR-184 in differentiating epidermal keratinocytes (Nagosa et al., 2017). However, this is the first time to our knowledge that SOCE has been implicated in the regulation of miRNAs and may provide a basis for further work investigating other miRNAs regulated in this fashion. Limitations of this chapter are not evaluating the expression of miR-184 in a stratified system such as human epidermis or organotypic cultures as well as not using

additional techniques such as fluorescent *in situ* hybridization to explore expression and specificity of miR-184 in both proliferating and differentiating HPEK.

To realise aim 2, chapter 4 investigated the effects of perturbed miR-184 levels on HPEK proliferation and differentiation. We report that following introduction of a synthetic miR-184 mimic, HPEKs accumulate in G1-phase of the cell cycle and promote expression of key effectors associated with growth arrest, cyclin E (Freije et al., 2012) and p21 (Santini et al., 2001) in addition to the differentiation marker, involucrin (Borowiec et al., 2013). Importantly, inhibition of physiological miR-184 during keratinocyte differentiation impaired the normal expression of involucrin, cyclin E and p21 typically observed during HPEK differentiation. A recent study has shown accumulation of cyclin E in differentiating keratinocytes causes DNA damage (Freije et al., 2012). However, this chapter shows for the first time to our knowledge that miR-184 causes sustained DNA damage, likely from cyclin E accumulation, which may explain induction of the DNA damage effector, p21. We propose that miR-184 leads to cyclin E induced DNA damage and induction of a p21 DDR consequently leading to growth arrest and commitment to differentiation through expression of involucrin.

For the first time, chapter 5 shows the induction of miR-184 in scratched monolayers. Furthermore, we support the apparent role of SOCE in the regulation of miR-184 in epidermal keratinocytes. This chapter also shows the induction of the miR-184 sponge, UCA1, in wounded monolayers. One of the most exciting findings from this research was the modulation of keratinocyte migration by perturbation of miR-184 levels, whereby migration was stimulated in HPEKs loaded with miR-184 whilst inhibition of miR-184 reduced migration. However, by not identifying miR-184 targets in both differentiating and migrating HPEK, chapter 4 and 5 share a major limitation. We anticipated a role for AGO2, which has previously been shown to be a target for miR-184 (Roberts et al., 2013; Tattikota et al., 2014). Nonetheless, a putative link between AGO2 and miR-184 was not found in the context of miR-184 induced

differentiation. However, we have shown cause and effect with ectopic miR-184 modulating the differentiation and migration of HPEK. With science based fundamentally on observations these findings could lead to further work utilising genome wide expression profiling, as well as transcriptomic and proteomic analysis to expand our knowledge of miR-184 targets in keratinocyte differentiation and migration, facilitating the development of miRNA-based dermaceuticals for treatment of chronic wounds and cutaneous diseases such as psoriasis.

In chapter 6, we report for the first time independent expression profiles for *AGO1-4* in differentiating HPEK monolayers. Bosserhoff and colleagues show *AGO1* as the most abundant AGO transcript in human skin (Völler et al., 2016). However, our data has shown that *AGO4* was most abundant in HPEK monolayers. Moreover, evaluation of *AGO2* in differentiating HPEKs revealed no reduction in response to enhanced physiological miR-184. Interestingly, both *AGO1* and *AGO4* were downregulated in psoriatic patients. Finally, it was established that in differentiating HPEK, AGO2 localises to the nucleus in a process that is reliant on  $Ca^{2+}$ , pointing to a nuclear role for AGO2 during differentiation and representing an interesting area of further study to demystify the role of nuclear AGO2 in epidermal keratinocyte differentiation.

## References

- Aggarwal, S., Ghilardi, N., Xie, M.H., de Sauvage, F.J. and Gurney, A.L. (2003) Interleukin-23 promotes a distinct CD4 T cell activation state characterized by the production of interleukin-17. *J Biol Chem*, 278 (3), 1910-1914.
- Ahmed, M.I., Alam, M., Emelianov, V.U., Poterlowicz, K., Patel, A., Sharov, A.A., Mardaryev, A.N. and Botchkareva, N.V. (2014) MicroRNA-214 controls skin and hair follicle development by modulating the activity of the Wnt pathway. *J Cell Biol*, 207 (4), 549-567.
- Al-Daraji, W.I., Grant, K.R., Ryan, K., Saxton, A. and Reynolds, N.J. (2002) Localization of calcineurin/NFAT in human skin and psoriasis and inhibition of calcineurin/NFAT activation in human keratinocytes by cyclosporin A. *J Invest Dermatol*, 118 (5), 779-788.
- Alam, M. and Ratner, D. (2001) Cutaneous squamous-cell carcinoma. *N Engl J Med*, 344 (13), 975-983.
- Ambros, V., Bartel, B., Bartel, D.P., Burge, C.B., Carrington, J.C., Chen, X., Dreyfuss, G., Eddy, S.R., Griffiths-Jones, S., Marshall, M., Matzke, M., Ruvkun, G. and Tuschl, T. (2003) A uniform system for microRNA annotation. *RNA*, 9 (3), 277-279.
- Amelio, I., Lena, A.M., Viticchie, G., Shalom-Feuerstein, R., Terrinoni, A., Dinsdale, D., Russo, G., Fortunato, C., Bonanno, E., Spagnoli, L.G., Aberdam, D., Knight, R.A., Candi, E. and Melino, G. (2012) miR-24 triggers epidermal differentiation by controlling actin adhesion and cell migration. *J Cell Biol*, 199 (2), 347-363.
- Arwert, E.N., Hoste, E. and Watt, F.M. (2012) Epithelial stem cells, wound healing and cancer. *Nat Rev Cancer*, 12 (3), 170-180.
- Aunin, E., Broadley, D., Ahmed, M.I., Mardaryev, A.N. and Botchkareva, N.V. (2017) Exploring a Role for Regulatory miRNAs In Wound Healing during Ageing: Involvement of miR-200c in wound repair. *Scientific Reports*, 7 (1), 3257.
- Auyeung, V.C., Ulitsky, I., McGeary, S.E. and Bartel, D.P. (2013) Beyond secondary structure: primary-sequence determinants license pri-miRNA hairpins for processing. *Cell*, 152 (4), 844-858.
- Baek, D., Villen, J., Shin, C., Camargo, F.D., Gygi, S.P. and Bartel, D.P. (2008) The impact of microRNAs on protein output. *Nature*, 455 (7209), 64-71.
- Baksh, S., DeCaprio, J.A. and Burakoff, S.J. (2000) Calcineurin regulation of the mammalian G0/G1 checkpoint element, cyclin dependent kinase 4. *Oncogene*, 19 (24), 2820-2827.
- Bang, C., Batkai, S., Dangwal, S., Gupta, S.K., Foinquinos, A., Holzmann, A., Just, A., Remke, J., Zimmer, K., Zeug, A., Ponimaskin, E., Schmiedl, A., Yin, X., Mayr, M., Halder, R., Fischer, A., Engelhardt, S., Wei, Y., Schober, A., Fiedler, J. and Thum, T. (2014) Cardiac fibroblast-derived

microRNA passenger strand-enriched exosomes mediate cardiomyocyte hypertrophy. *J Clin Invest*, 124 (5), 2136-2146.

Bao, S., Thrall, B.D. and Miller, D.L. (1997) Transfection of a reporter plasmid into cultured cells by sonoporation in vitro. *Ultrasound Med Biol*, 23 (6), 953-959.

Barbollat-Boutrand, L., Joly-Tonetti, N., Dos Santos, M., Metral, E., Boher, A., Masse, I., Berthier-Vergnes, O., Bertolino, P., Damour, O. and Lamartine, J. (2017) MicroRNA-23b-3p regulates human keratinocyte differentiation through repression of TGIF1 and activation of the TGF- $\beta$ -SMAD2 signalling pathway. *Exp Dermatol*, 26 (1), 51-57.

Bartel, D.P. (2004) MicroRNAs: genomics, biogenesis, mechanism, and function. *Cell*, 116 (2), 281-297.

Bartel, D.P. (2009) MicroRNAs: target recognition and regulatory functions. *Cell*, 136 (2), 215-233.

Baskerville, S. and Bartel, D.P. (2005) Microarray profiling of microRNAs reveals frequent coexpression with neighboring miRNAs and host genes. *RNA*, 11 (3), 241-247.

Behm-Ansmant, I., Rehwinkel, J., Doerks, T., Stark, A., Bork, P. and Izaurralde, E. (2006) mRNA degradation by miRNAs and GW182 requires both CCR4:NOT deadenylase and DCP1:DCP2 decapping complexes. *Genes Dev*, 20 (14), 1885-1898.

Benhamed, M., Herbig, U., Ye, T., Dejean, A. and Bischof, O. (2012) Senescence is an endogenous trigger for microRNA-directed transcriptional gene silencing in human cells. *Nat Cell Biol*, 14 (3), 266-275.

Berezhna, S.Y., Supekova, L., Sever, M.J., Schultz, P.G. and Deniz, A.A. (2011) Dual regulation of hepatitis C viral RNA by cellular RNAi requires partitioning of Ago2 to lipid droplets and P-bodies. *RNA (New York, N.Y.)*, 17 (10), 1831-1845.

Berezikov, E., Chung, W.J., Willis, J., Cuppen, E. and Lai, E.C. (2007) Mammalian mirtron genes. *Mol Cell*, 28 (2), 328-336.

Bertero, T., Gastaldi, C., Bourget-Ponzio, I., Imbert, V., Loubat, A., Selva, E., Busca, R., Mari, B., Hofman, P., Barbry, P., Meneguzzi, G., Ponzio, G. and Rezzonico, R. (2011) miR-483-3p controls proliferation in wounded epithelial cells. *FASEB J*, 25 (9), 3092-3105.

Bikle, D.D. (2004) Vitamin D regulated keratinocyte differentiation. *J Cell Biochem*, 92 (3), 436-444.

Bikle, D.D. (2011) Vitamin D metabolism and function in the skin. *Mol Cell Endocrinol*, 347 (1-2), 80-89.

Bikle, D.D., Xie, Z. and Tu, C.L. (2012) Calcium regulation of keratinocyte differentiation. *Expert Rev Endocrinol Metab*, 7 (4), 461-472.

Boele, J., Persson, H., Shin, J.W., Ishizu, Y., Newie, I.S., Søkilde, R., Hawkins, S.M., Coarfa, C., Ikeda, K., Takayama, K.-i., Horie-Inoue, K., Ando, Y., Burroughs, A.M., Sasaki, C., Suzuki, C., Sakai, M., Aoki, S., Ogawa, A., Hasegawa, A., Lizio, M., Kaida, K., Teusink, B., Carninci, P., Suzuki, H., Inoue, S., Gunaratne, P.H., Rovira, C., Hayashizaki, Y. and de Hoon, M.J.L. (2014) PAPD5-mediated 3' adenylation and subsequent degradation of miR-21 is disrupted in proliferative disease. *Proceedings of the National Academy of Sciences*, 111 (31), 11467.

Bohmert, K., Camus, I., Bellini, C., Bouchez, D., Caboche, M. and Benning, C. (1998) AGO1 defines a novel locus of Arabidopsis controlling leaf development. *EMBO J*, 17 (1), 170-180.

Boland, A., Huntzinger, E., Schmidt, S., Izaurralde, E. and Weichenrieder, O. (2011) Crystal structure of the MID-PIWI lobe of a eukaryotic Argonaute protein. *Proc Natl Acad Sci U S A*, 108 (26), 10466-10471.

Bonner, W.M., Redon, C.E., Dickey, J.S., Nakamura, A.J., Sedelnikova, O.A., Solier, S. and Pommier, Y. (2008) GammaH2AX and cancer. *Nat Rev Cancer*, 8 (12), 957-967.

Bootman, M.D. (2012) Calcium signaling. *Cold Spring Harb Perspect Biol*, 4 (7), a011171.

Borowiec, A.S., Delcourt, P., Dewailly, E. and Bidaux, G. (2013) Optimal differentiation of in vitro keratinocytes requires multifactorial external control. *PLoS One*, 8 (10), e77507.

Bowcock, A.M. and Krueger, J.G. (2005) Getting under the skin: the immunogenetics of psoriasis. *Nat Rev Immunol*, 5 (9), 699-711.

Brennecke, J., Stark, A., Russell, R.B. and Cohen, S.M. (2005) Principles of microRNA-target recognition. *PLoS Biol*, 3 (3), e85.

Bridge, K.S., Shah, K.M., Li, Y., Foxler, D.E., Wong, S.C.K., Miller, D.C., Davidson, K.M., Foster, J.G., Rose, R., Hodgkinson, M.R., Ribeiro, P.S., Aboobaker, A.A., Yashiro, K., Wang, X., Graves, P.R., Plevin, M.J., Lagos, D. and Sharp, T.V. (2017) Argonaute Utilization for miRNA Silencing Is Determined by Phosphorylation-Dependent Recruitment of LIM-Domain-Containing Proteins. *Cell Rep*, 20 (1), 173-187.

Bronevetsky, Y., Villarino, A.V., Easley, C.J., Barbeau, R., Barczak, A.J., Heinz, G.A., Kremmer, E., Heissmeyer, V., McManus, M.T., Erle, D.J., Rao, A. and Ansel, K.M. (2013) T cell activation induces proteasomal degradation of Argonaute and rapid remodeling of the microRNA repertoire. *J Exp Med*, 210 (2), 417-432.

Bukhari, S.I.A., Truesdell, S.S. and Vasudevan, S. (2018) Analysis of MicroRNA-Mediated Translation Activation of In Vitro Transcribed Reporters in Quiescent Cells. *Methods Mol Biol*, 1686, 251-264.

Cai, X., Hagedorn, C.H. and Cullen, B.R. (2004) Human microRNAs are processed from capped, polyadenylated transcripts that can also function as mRNAs. *RNA*, 10 (12), 1957-1966.

Candi, E., Schmidt, R. and Melino, G. (2005) The cornified envelope: a model of cell death in the skin. *Nat Rev Mol Cell Biol*, 6 (4), 328-340.

Carmell, M.A., Xuan, Z., Zhang, M.Q. and Hannon, G.J. (2002) The Argonaute family: tentacles that reach into RNAi, developmental control, stem cell maintenance, and tumorigenesis. *Genes Dev*, 16 (21), 2733-2742.

Carthew, R.W. and Sontheimer, E.J. (2009) Origins and Mechanisms of miRNAs and siRNAs. *Cell*, 136 (4), 642-655.

Castanotto, D., Zhang, X., Alluin, J., Zhang, X., Rüger, J., Armstrong, B., Rossi, J., Riggs, A. and Stein, C.A. (2018) A stress-induced response complex (SIRC) shuttles miRNAs, siRNAs, and oligonucleotides to the nucleus. *Proceedings of the National Academy of Sciences*, 115 (25), E5756.

Chang, K.W., Kao, S.Y., Wu, Y.H., Tsai, M.M., Tu, H.F., Liu, C.J., Lui, M.T. and Lin, S.C. (2013) Passenger strand miRNA miR-31\* regulates the phenotypes of oral cancer cells by targeting RhoA. *Oral Oncol*, 49 (1), 27-33.

Cheloufi, S., Dos Santos, C.O., Chong, M.M. and Hannon, G.J. (2010) A dicer-independent miRNA biogenesis pathway that requires Ago catalysis. *Nature*, 465 (7298), 584-589.

Chen, D., Li, J., Li, S., Han, P., Li, N., Wang, Y. and Du, S. (2018) miR-184 promotes cell proliferation in tongue squamous cell carcinoma by targeting SOX7. *Oncol Lett*, 16 (2), 2221-2228.

Chen, X. and Goncalves, M.A. (2016) Engineered Viruses as Genome Editing Devices. *Mol Ther*, 24 (3), 447-457.

Chen, Y. and Stallings, R.L. (2007) Differential patterns of microRNA expression in neuroblastoma are correlated with prognosis, differentiation, and apoptosis. *Cancer Res*, 67 (3), 976-983.

Chendrimada, T.P., Gregory, R.I., Kumaraswamy, E., Norman, J., Cooch, N., Nishikura, K. and Shiekhattar, R. (2005) TRBP recruits the Dicer complex to Ago2 for microRNA processing and gene silencing. *Nature*, 436 (7051), 740-744.

Cheng, Z., Wang, H.Z., Li, X., Wu, Z., Han, Y., Li, Y., Chen, G., Xie, X., Huang, Y., Du, Z. and Zhou, Y. (2015) MicroRNA-184 inhibits cell proliferation and invasion, and specifically targets TNFAIP2 in Glioma. *J Exp Clin Cancer Res*, 34, 27.

Cho, Y.S., Bae, J.M., Chun, Y.S., Chung, J.H., Jeon, Y.K., Kim, I.S., Kim, M.S. and Park, J.W. (2008) HIF-1 $\alpha$  controls keratinocyte proliferation by up-regulating p21(WAF1/Cip1). *Biochim Biophys Acta*, 1783 (2), 323-333.

Choi, M., Park, M., Lee, S., Lee, J.W., Cho, M.C., Noh, M. and Lee, C. (2017) Establishment of Immortalized Primary Human Foreskin Keratinocytes and Their Application to Toxicity Assessment and Three Dimensional Skin Culture Construction. *Biomolecules & therapeutics*, 25 (3), 296-307.

Chu, Y., Yue, X., Younger, S.T., Janowski, B.A. and Corey, D.R. (2010) Involvement of argonaute proteins in gene silencing and activation by RNAs complementary to a non-coding transcript at the progesterone receptor promoter. *Nucleic Acids Res*, 38 (21), 7736-7748.

Connor, C.J., Liu, V. and Fiedorowicz, J.G. (2015) Exploring the Physiological Link between Psoriasis and Mood Disorders. *Dermatol Res Pract*, 2015, 409637.

Dale, B.A., Holbrook, K.A., Fleckman, P., Kimball, J.R., Brumbaugh, S. and Sybert, V.P. (1990) Heterogeneity in harlequin ichthyosis, an inborn error of epidermal keratinization: variable morphology and structural protein expression and a defect in lamellar granules. *J Invest Dermatol*, 94 (1), 6-18.

Davidovici, B.B., Sattar, N., Prinz, J., Puig, L., Emery, P., Barker, J.N., van de Kerkhof, P., Stahle, M., Nestle, F.O., Girolomoni, G. and Krueger, J.G. (2010) Psoriasis and systemic inflammatory diseases: potential mechanistic links between skin disease and co-morbid conditions. *J Invest Dermatol*, 130 (7), 1785-1796.

Davis, B.N., Hilyard, A.C., Lagna, G. and Hata, A. (2008) SMAD proteins control DROSHA-mediated microRNA maturation. *Nature*, 454 (7200), 56-61.

De Smedt, S.C., Demeester, J. and Hennink, W.E. (2000) Cationic polymer based gene delivery systems. *Pharm Res*, 17 (2), 113-126.

Decker, C.J. and Parker, R. (2012) P-bodies and stress granules: possible roles in the control of translation and mRNA degradation. *Cold Spring Harb Perspect Biol*, 4 (9), a012286.

Devgan, V., Mammucari, C., Millar, S.E., Brisken, C. and Dotto, G.P. (2005) p21WAF1/Cip1 is a negative transcriptional regulator of Wnt4 expression downstream of Notch1 activation. *Genes Dev*, 19 (12), 1485-1495.

Devgan, V., Nguyen, B.C., Oh, H. and Dotto, G.P. (2006) p21WAF1/Cip1 suppresses keratinocyte differentiation independently of the cell cycle through transcriptional up-regulation of the IGF-I gene. *J Biol Chem*, 281 (41), 30463-30470.

Di Meglio, P., Villanova, F. and Nestle, F.O. (2014) Psoriasis. *Cold Spring Harb Perspect Med*, 4 (8).

Diacumakos, E.G. (1973) Methods for micromanipulation of human somatic cells in culture. *Methods Cell Biol*, 7, 287-311.

Diederichs, S. and Haber, D.A. (2007) Dual Role for Argonautes in MicroRNA Processing and Posttranscriptional Regulation of MicroRNA Expression. *Cell*, 131 (6), 1097-1108.

Distler, J.H., Jungel, A., Kurowska-Stolarska, M., Michel, B.A., Gay, R.E., Gay, S. and Distler, O. (2005) Nucleofection: a new, highly efficient transfection method for primary human keratinocytes\*. *Exp Dermatol*, 14 (4), 315-320.

Eckert, R.L. (1989) Structure, function, and differentiation of the keratinocyte. *Physiol Rev*, 69 (4), 1316-1346.

Eckert, R.L., Crish, J.F. and Robinson, N.A. (1997) The epidermal keratinocyte as a model for the study of gene regulation and cell differentiation. *Physiol Rev*, 77 (2), 397-424.

Eckert, R.L., Sturniolo, M.T., Broome, A.M., Ruse, M. and Rorke, E.A. (2005) Transglutaminases in epidermis. *Prog Exp Tumor Res*, 38, 115-124.

Eckhart, L., Lippens, S., Tschachler, E. and Declercq, W. (2013) Cell death by cornification. *Biochim Biophys Acta*, 1833 (12), 3471-3480.

Elias, P.M. (1983) Epidermal lipids, barrier function, and desquamation. *J Invest Dermatol*, 80 (1 Suppl), 44s-49s.

Elkayam, E., Kuhn, C.D., Tocilj, A., Haase, A.D., Greene, E.M., Hannon, G.J. and Joshua-Tor, L. (2012) The structure of human argonaute-2 in complex with miR-20a. *Cell*, 150 (1), 100-110.

Elkayam, E., Faehnle, C. R., Morales, M., Sun, J., Li, H., & Joshua-Tor, L. (2017). Multivalent Recruitment of Human Argonaute by GW182. *Molecular cell*, 67(4), 646-658.e3.

Eming, S.A., Martin, P. and Tomic-Canic, M. (2014) Wound repair and regeneration: mechanisms, signaling, and translation. *Sci Transl Med*, 6 (265), 265sr266.

Ender, C. and Meister, G. (2010) Argonaute proteins at a glance. *J Cell Sci*, 123 (Pt 11), 1819-1823.

Eulalio, A., Behn-Ansmant, I., Schweizer, D. and Izaurralde, E. (2007) P-Body Formation Is a Consequence, Not the Cause, of RNA-Mediated Gene Silencing. *Mol Cell Bio*, 27 (11), 3970-3981.

Fabian, M.R., Mathonnet, G., Sundermeier, T., Mathys, H., Zipprich, J.T., Svitkin, Y.V., Rivas, F., Jinek, M., Wohlschlegel, J., Doudna, J.A., Chen, C.Y., Shyu, A.B., Yates, J.R., 3rd, Hannon, G.J., Filipowicz, W., Duchaine, T.F. and Sonenberg, N. (2009) Mammalian miRNA RISC recruits CAF1 and PABP to affect PABP-dependent deadenylation. *Mol Cell*, 35 (6), 868-880.

Fan, Y., Shen, B., Tan, M., Mu, X., Qin, Y., Zhang, F. and Liu, Y. (2014) Long non-coding RNA UCA1 increases chemoresistance of bladder cancer cells by regulating Wnt signaling. *FEBS J*, 281 (7), 1750-1758.

Fang, Z., Wu, L., Wang, L., Yang, Y., Meng, Y. and Yang, H. (2014) Increased expression of the long non-coding RNA UCA1 in tongue squamous cell carcinomas: a possible correlation with cancer metastasis. *Oral Surg Oral Med Oral Pathol Oral Radiol*, 117 (1), 89-95.

Feingold, K.R. and Elias, P.M. (2014) Role of lipids in the formation and maintenance of the cutaneous permeability barrier. *Biochim Biophys Acta*, 1841 (3), 280-294.

Felgner, P.L., Gadek, T.R., Holm, M., Roman, R., Chan, H.W., Wenz, M., Northrop, J.P., Ringold, G.M. and Danielsen, M. (1987) Lipofection: a highly efficient, lipid-mediated DNA-transfection procedure. *Proc Natl Acad Sci U S A*, 84 (21), 7413-7417.

Feng, R. and Dong, L. (2015) Inhibitory effect of miR-184 on the potential of proliferation and invasion in human glioma and breast cancer cells in vitro. *Int J Clin Exp Pathol*, 8 (8), 9376-9382.

Freije, A., Ceballos, L., Coisy, M., Barnes, L., Rosa, M., De Diego, E., Blanchard, J.M. and Gandarillas, A. (2012) Cyclin E drives human keratinocyte growth into differentiation. *Oncogene*, 31 (50), 5180-5192.

Freije, A., Molinuevo, R., Ceballos, L., Cagigas, M., Alonso-Lecue, P., Rodriguez, R., Menendez, P., Aberdam, D., De Diego, E. and Gandarillas, A. (2014) Inactivation of p53 in Human Keratinocytes Leads to Squamous Differentiation and Shedding via Replication Stress and Mitotic Slippage. *Cell Rep*, 9 (4), 1349-1360.

Friedlander, M.R., Lizano, E., Houben, A.J., Bezdán, D., Banez-Coronel, M., Kudla, G., Mateu-Huertas, E., Kagerbauer, B., Gonzalez, J., Chen, K.C., LeProust, E.M., Marti, E. and Estivill, X. (2014) Evidence for the biogenesis of more than 1,000 novel human microRNAs. *Genome Biol*, 15 (4), R57.

Friedman, R.C., Farh, K.K., Burge, C.B. and Bartel, D.P. (2009) Most mammalian mRNAs are conserved targets of microRNAs. *Genome Res*, 19 (1), 92-105.

Fromm, B., Billipp, T., Peck, L.E., Johansen, M., Tarver, J.E., King, B.L., Newcomb, J.M., Sempere, L.F., Flatmark, K., Hovig, E. and Peterson, K.J. (2015) A Uniform System for the Annotation of Vertebrate microRNA Genes and the Evolution of the Human microRNAome. *Annu Rev Genet*, 49, 213-242.

Fujita, S., Ito, T., Mizutani, T., Minoguchi, S., Yamamichi, N., Sakurai, K. and Iba, H. (2008) miR-21 Gene expression triggered by AP-1 is sustained through a double-negative feedback mechanism. *J Mol Biol*, 378 (3), 492-504.

Fukunaga, R., Colpan, C., Han, B.W. and Zamore, P.D. (2014) Inorganic phosphate blocks binding of pre-miRNA to Dicer-2 via its PAZ domain. *EMBO J*, 33 (4), 371-384.

Furie, M. and Kadono, T. (2017) "Inflammatory skin march" in atopic dermatitis and psoriasis. *Inflamm Res*, 66 (10), 833-842.

- Gagnon, K.T., Li, L., Janowski, B.A. and Corey, D.R. (2014) Analysis of nuclear RNA interference in human cells by subcellular fractionation and Argonaute loading. *Nature protocols*, 9 (9), 2045-2060.
- Gandarillas, A. (2012) The mysterious human epidermal cell cycle, or an oncogene-induced differentiation checkpoint. *Cell Cycle*, 11 (24), 4507-4516.
- Gerber Peter, A., Buhren Bettina, A., Schrupf, H., Homey, B., Zlotnik, A. and Hevezi, P. (2014) *The top skin-associated genes: a comparative analysis of human and mouse skin transcriptomes.* *Biological Chemistry*. 395: 577.
- Ghatak, S., Chan, Y.C., Khanna, S., Banerjee, J., Weist, J., Roy, S. and Sen, C.K. (2015) Barrier Function of the Repaired Skin Is Disrupted Following Arrest of Dicer in Keratinocytes. *Mol Ther*, 23 (7), 1201-1210.
- Gladman, D.D., Antoni, C., Mease, P., Clegg, D.O. and Nash, P. (2005) Psoriatic arthritis: epidemiology, clinical features, course, and outcome. *Ann Rheum Dis*, 64 Suppl 2, ii14-17.
- Golden, R. J., Chen, B., Li, T., Braun, J., Manjunath, H., Chen, X., Wu, J., Schmid, V., Chang, T. C., Kopp, F., Ramirez-Martinez, A., Tagliabracci, V. S., Chen, Z. J., Xie, Y. and Mendell, J. T. (2017). An Argonaute phosphorylation cycle promotes microRNA-mediated silencing. *Nature*, 542(7640), 197-202.
- Graham, F.L. and van der Eb, A.J. (1973) A new technique for the assay of infectivity of human adenovirus 5 DNA. *Virology*, 52 (2), 456-467.
- Greb, J.E., Goldminz, A.M., Elder, J.T., Lebwohl, M.G., Gladman, D.D., Wu, J.J., Mehta, N.N., Finlay, A.Y. and Gottlieb, A.B. (2016) Psoriasis. *Nat Rev Dis Primers*, 2, 16082.
- Gregory, R.I., Yan, K.P., Amuthan, G., Chendrimada, T., Doratotaj, B., Cooch, N. and Shiekhattar, R. (2004) The Microprocessor complex mediates the genesis of microRNAs. *Nature*, 432 (7014), 235-240.
- Gresch, O., Engel, F.B., Nestic, D., Tran, T.T., England, H.M., Hickman, E.S., Korner, I., Gan, L., Chen, S., Castro-Obregon, S., Hammermann, R., Wolf, J., Muller-Hartmann, H., Nix, M., Siebenkotten, G., Kraus, G. and Lun, K. (2004) New non-viral method for gene transfer into primary cells. *Methods*, 33 (2), 151-163.
- Grimson, A., Farh, K.K., Johnston, W.K., Garrett-Engele, P., Lim, L.P. and Bartel, D.P. (2007) MicroRNA targeting specificity in mammals: determinants beyond seed pairing. *Mol Cell*, 27 (1), 91-105.
- Grishok, A., Pasquinelli, A.E., Conte, D., Li, N., Parrish, S., Ha, I., Baillie, D.L., Fire, A., Ruvkun, G. and Mello, C.C. (2001) Genes and mechanisms related to RNA interference regulate expression of the small temporal RNAs that control *C. elegans* developmental timing. *Cell*, 106 (1), 23-34.

- Guinea-Viniegra, J., Jiménez, M., Schonhaler, H.B., Navarro, R., Delgado, Y., José Concha-Garzón, M., Tschachler, E., Obad, S., Daudén, E. and Wagner, E.F. (2014) Targeting miR-21 to Treat Psoriasis. *Science Translational Medicine*, 6 (225), 225re221.
- Guo, H., Ingolia, N.T., Weissman, J.S. and Bartel, D.P. (2010) Mammalian microRNAs predominantly act to decrease target mRNA levels. *Nature*, 466 (7308), 835-840.
- Ha, H.L., Wang, H., Pisitkun, P., Kim, J.C., Tassi, I., Tang, W., Morasso, M.I., Udey, M.C. and Siebenlist, U. (2014) IL-17 drives psoriatic inflammation via distinct, target cell-specific mechanisms. *Proc Natl Acad Sci U S A*, 111 (33), E3422-3431.
- Hammond, S.M. (2005) Dicing and slicing: the core machinery of the RNA interference pathway. *FEBS Lett*, 579 (26), 5822-5829.
- Han, J., Lee, Y., Yeom, K.H., Nam, J.W., Heo, I., Rhee, J.K., Sohn, S.Y., Cho, Y., Zhang, B.T. and Kim, V.N. (2006) Molecular basis for the recognition of primary microRNAs by the Drosha-DGCR8 complex. *Cell*, 125 (5), 887-901.
- Hawkes, J.E., Nguyen, G.H., Fujita, M., Florell, S.R., Callis Duffin, K., Krueger, G.G. and O'Connell, R.M. (2016) microRNAs in Psoriasis. *J Invest Dermatol*, 136 (2), 365-371.
- Henderson, I.R., Zhang, X., Lu, C., Johnson, L., Meyers, B.C., Green, P.J. and Jacobsen, S.E. (2006) Dissecting Arabidopsis thaliana DICER function in small RNA processing, gene silencing and DNA methylation patterning. *Nat Genet*, 38 (6), 721-725.
- Hennings, H., Michael, D., Cheng, C., Steinert, P., Holbrook, K. and Yuspa, S.H. (1980) Calcium regulation of growth and differentiation of mouse epidermal cells in culture. *Cell*, 19 (1), 245-254.
- Hessam, S., Sand, M., Skrygan, M. and Bechara, F.G. (2017) The microRNA effector RNA-induced silencing complex in hidradenitis suppurativa: a significant dysregulation within active inflammatory lesions. *Arch Dermatol Res*, 309 (7), 557-565.
- Hildebrand, J., Rutze, M., Walz, N., Gallinat, S., Wenck, H., Deppert, W., Grundhoff, A. and Knott, A. (2011) A comprehensive analysis of microRNA expression during human keratinocyte differentiation in vitro and in vivo. *J Invest Dermatol*, 131 (1), 20-29.
- Hock, J. and Meister, G. (2008) The Argonaute protein family. *Genome Biol*, 9 (2), 210.
- Hoffmann, A., Huang, Y., Suetsugu-Maki, R., Ringelberg, C.S., Tomlinson, C.R., Del Rio-Tsonis, K. and Tsonis, P.A. (2012) Implication of the miR-184 and miR-204 competitive RNA network in control of mouse secondary cataract. *Mol Med*, 18, 528-538.
- Horman, S.R., Janas, M.M., Litterst, C., Wang, B., MacRae, I.J., Sever, M.J., Morrissey, D.V., Graves, P., Luo, B., Umesalma, S., Qi, H.H., Miraglia, L.J., Novina, C.D. and Orth, A.P. (2013)

Akt-mediated phosphorylation of argonaute 2 downregulates cleavage and upregulates translational repression of MicroRNA targets. *Mol Cell*, 50 (3), 356-367.

Horsley, V., Aliprantis, A.O., Polak, L., Glimcher, L.H. and Fuchs, E. (2008) NFATc1 balances quiescence and proliferation of skin stem cells. *Cell*, 132 (2), 299-310.

Huang, V., Place, R.F., Portnoy, V., Wang, J., Qi, Z., Jia, Z., Yu, A., Shuman, M., Yu, J. and Li, L.C. (2012) Upregulation of Cyclin B1 by miRNA and its implications in cancer. *Nucleic Acids Res*, 40 (4), 1695-1707.

Humphreys, D.T., Westman, B.J., Martin, D.I. and Preiss, T. (2005) MicroRNAs control translation initiation by inhibiting eukaryotic initiation factor 4E/cap and poly(A) tail function. *Proc Natl Acad Sci U S A*, 102 (47), 16961-16966.

Hunt, M.A., Currie, M.J., Robinson, B.A. and Dachs, G.U. (2010) Optimizing transfection of primary human umbilical vein endothelial cells using commercially available chemical transfection reagents. *J Biomol Tech*, 21 (2), 66-72.

Hutvagner, G., McLachlan, J., Pasquinelli, A.E., Balint, E., Tuschl, T. and Zamore, P.D. (2001) A cellular function for the RNA-interference enzyme Dicer in the maturation of the let-7 small temporal RNA. *Science*, 293 (5531), 834-838.

Hutvagner, G. and Simard, M.J. (2008) Argonaute proteins: key players in RNA silencing. *Nat Rev Mol Cell Biol*, 9 (1), 22-32.

Hwang, H.C. and Clurman, B.E. (2005) Cyclin E in normal and neoplastic cell cycles. *Oncogene*, 24 (17), 2776-2786.

Iosue, I., Quaranta, R., Masciarelli, S., Fontemaggi, G., Batassa, E.M., Bertolami, C., Ottone, T., Divona, M., Salvatori, B., Padula, F., Fatica, A., Lo-Coco, F., Nervi, C. and Fazi, F. (2013) Argonaute 2 sustains the gene expression program driving human monocytic differentiation of acute myeloid leukemia cells. *Cell Death & Disease*, 4, e926.

Iwasaki, S., Kobayashi, M., Yoda, M., Sakaguchi, Y., Katsuma, S., Suzuki, T. and Tomari, Y. (2010) Hsc70/Hsp90 chaperone machinery mediates ATP-dependent RISC loading of small RNA duplexes. *Mol Cell*, 39 (2), 292-299.

Janowski, B.A., Huffman, K.E., Schwartz, J.C., Ram, R., Nordsell, R., Shames, D.S., Minna, J.D. and Corey, D.R. (2006) Involvement of AGO1 and AGO2 in mammalian transcriptional silencing. *Nat Struct Mol Biol*, 13 (9), 787-792.

Jans, R., Mottram, L., Johnson, D.L., Brown, A.M., Sikkink, S., Ross, K. and Reynolds, N.J. (2013) Lysophosphatidic acid promotes cell migration through STIM1- and Orai1-mediated Ca<sup>2+</sup>(i) mobilization and NFAT2 activation. *J Invest Dermatol*, 133 (3), 793-802.

Jiang, C., Qin, B., Liu, G., Sun, X., Shi, H., Ding, S., Liu, Y., Zhu, M., Chen, X. and Zhao, C. (2016) MicroRNA-184 promotes differentiation of the retinal pigment epithelium by targeting the AKT2/mTOR signaling pathway. *Oncotarget*, 7 (32), 52340-52353.

Jin, H.Y., Gonzalez-Martin, A., Miletic, A.V., Lai, M., Knight, S., Sabouri-Ghomi, M., Head, S.R., Macauley, M.S., Rickert, R.C. and Xiao, C. (2015) Transfection of microRNA Mimics Should Be Used with Caution. *Front Genet*, 6, 340.

Jinek, M. and Doudna, J.A. (2009) A three-dimensional view of the molecular machinery of RNA interference. *Nature*, 457 (7228), 405-412.

Joyce, C.E., Zhou, X., Xia, J., Ryan, C., Thrash, B., Menter, A., Zhang, W. and Bowcock, A.M. (2011) Deep sequencing of small RNAs from human skin reveals major alterations in the psoriasis miRNAome. *Human Molecular Genetics*, 20 (20), 4025-4040.

Kalinin, A.E., Kajava, A.V. and Steinert, P.M. (2002) Epithelial barrier function: assembly and structural features of the cornified cell envelope. *Bioessays*, 24 (9), 789-800.

Kannambath, S. (2016) Micro-RNA Feedback Loops Modulating the Calcineurin/NFAT Signaling Pathway. *Noncoding RNA*, 2 (2).

Karlsson, T., Vahlquist, A. and Torma, H. (2010) Keratinocyte differentiation induced by calcium, phorbol ester or interferon-gamma elicits distinct changes in the retinoid signalling pathways. *J Dermatol Sci*, 57 (3), 207-213.

Kataoka, Y., Takeichi, M. and Uemura, T. (2001) Developmental roles and molecular characterization of a Drosophila homologue of Arabidopsis Argonaute1, the founder of a novel gene superfamily. *Genes Cells*, 6 (4), 313-325.

Katayama, S., Skoog, T., Jouhilahti, E.M., Siitonen, H.A., Nuutila, K., Tervaniemi, M.H., Vuola, J., Johnsson, A., Lonnerberg, P., Linnarsson, S., Elomaa, O., Kankuri, E. and Kere, J. (2015) Gene expression analysis of skin grafts and cultured keratinocytes using synthetic RNA normalization reveals insights into differentiation and growth control. *BMC Genomics*, 16, 476.

Khvorova, A., Reynolds, A. and Jayasena, S.D. (2003) Functional siRNAs and miRNAs exhibit strand bias. *Cell*, 115 (2), 209-216.

Kim, D.H., Saetrom, P., Snove, O., Jr. and Rossi, J.J. (2008) MicroRNA-directed transcriptional gene silencing in mammalian cells. *Proc Natl Acad Sci U S A*, 105 (42), 16230-16235.

Kim, V.N. (2004) MicroRNA precursors in motion: exportin-5 mediates their nuclear export. *Trends Cell Biol*, 14 (4), 156-159.

Klein, T.M., Wolf, E.D., Wu, R. and Sanford, J.C. (1987) High-velocity microprojectiles for delivering nucleic acids into living cells. *Nature*, 327, 70.

- Koga, Y., Jinnin, M., Ichihara, A., Fujisawa, A., Moriya, C., Sakai, K., Fukushima, S., Inoue, Y. and Ihn, H. (2014) Analysis of expression pattern of serum microRNA levels in patients with psoriasis. *Journal of Dermatological Science*, 74 (2), 170-171.
- Koster, M.I. and Roop, D.R. (2007) Mechanisms regulating epithelial stratification. *Annu Rev Cell Dev Biol*, 23, 93-113.
- Krueger, J.G. and Bowcock, A. (2005) Psoriasis pathophysiology: current concepts of pathogenesis. *Ann Rheum Dis*, 64 Suppl 2, ii30-36.
- Kuhn, C.D. and Joshua-Tor, L. (2013) Eukaryotic Argonautes come into focus. *Trends Biochem Sci*, 38 (5), 263-271.
- Kurinna, S., Schäfer, M., Ostano, P., Karouzakis, E., Chiorino, G., Bloch, W., Bachmann, A., Gay, S., Garrod, D., Lefort, K., Dotto, G.-P., Beer, H.-D. and Werner, S. (2014) A novel Nrf2-miR-29-desmocollin-2 axis regulates desmosome function in keratinocytes. *Nature Communications*, 5, 5099.
- Lagos-Quintana, M., Rauhut, R., Lendeckel, W. and Tuschl, T. (2001) Identification of novel genes coding for small expressed RNAs. *Science*, 294 (5543), 853-858.
- Lau, N.C., Lim, L.P., Weinstein, E.G. and Bartel, D.P. (2001) An abundant class of tiny RNAs with probable regulatory roles in *Caenorhabditis elegans*. *Science*, 294 (5543), 858-862.
- Lau, P.W., Guiley, K.Z., De, N., Potter, C.S., Carragher, B. and MacRae, I.J. (2012) The molecular architecture of human Dicer. *Nat Struct Mol Biol*, 19 (4), 436-440.
- Lee, H.Y., Zhou, K., Smith, A.M., Noland, C.L. and Doudna, J.A. (2013) Differential roles of human Dicer-binding proteins TRBP and PACT in small RNA processing. *Nucleic Acids Res*, 41 (13), 6568-6576.
- Lee, R.C. and Ambros, V. (2001) An extensive class of small RNAs in *Caenorhabditis elegans*. *Science*, 294 (5543), 862-864.
- Lee, R.C., Feinbaum, R.L. and Ambros, V. (1993) The *C. elegans* heterochronic gene *lin-4* encodes small RNAs with antisense complementarity to *lin-14*. *Cell*, 75 (5), 843-854.
- Lee, Y., Ahn, C., Han, J., Choi, H., Kim, J., Yim, J., Lee, J., Provost, P., Radmark, O., Kim, S. and Kim, V.N. (2003) The nuclear RNase III Drosha initiates microRNA processing. *Nature*, 425 (6956), 415-419.
- Lee, Y., Hur, I., Park, S.Y., Kim, Y.K., Suh, M.R. and Kim, V.N. (2006) The role of PACT in the RNA silencing pathway. *EMBO J*, 25 (3), 522-532.
- Lee, Y., Kim, M., Han, J., Yeom, K.H., Lee, S., Baek, S.H. and Kim, V.N. (2004) MicroRNA genes are transcribed by RNA polymerase II. *EMBO J*, 23 (20), 4051-4060.

Lee, Y.S., Dlugosz, A.A., McKay, R., Dean, N.M. and Yuspa, S.H. (1997) Definition by specific antisense oligonucleotides of a role for protein kinase C alpha in expression of differentiation markers in normal and neoplastic mouse epidermal keratinocytes. *Mol Carcinog*, 18 (1), 44-53.

Lena, A.M., Shalom-Feuerstein, R., Rivetti di Val Cervo, P., Aberdam, D., Knight, R.A., Melino, G. and Candi, E. (2008) miR-203 represses 'stemness' by repressing DeltaNp63. *Cell Death Differ*, 15 (7), 1187-1195.

Li, D., Li, X.I., Wang, A., Meisgen, F., Pivarcsi, A., Sonkoly, E., Stahle, M. and Landen, N.X. (2015) MicroRNA-31 Promotes Skin Wound Healing by Enhancing Keratinocyte Proliferation and Migration. *J Invest Dermatol*, 135 (6), 1676-1685.

Li, L.C., Okino, S.T., Zhao, H., Pookot, D., Place, R.F., Urakami, S., Enokida, H. and Dahiya, R. (2006) Small dsRNAs induce transcriptional activation in human cells. *Proc Natl Acad Sci U S A*, 103 (46), 17337-17342.

Li, X., Li, D., Wang, A., Chu, T., Lohcharoenkal, W., Zheng, X., Grunler, J., Narayanan, S., Eliasson, S., Herter, E.K., Wang, Y., Ma, Y., Ehrstrom, M., Eidsmo, L., Kasper, M., Pivarcsi, A., Sonkoly, E., Catrina, S.B., Stahle, M. and Xu Landen, N. (2017) MicroRNA-132 with Therapeutic Potential in Chronic Wounds. *J Invest Dermatol*, 137 (12), 2630-2638.

Lippens, S., Lefebvre, S., Gilbert, B., Sze, M., Devos, M., Verhelst, K., Vereecke, L., Mc Guire, C., Guerin, C., Vandenabeele, P., Pasparakis, M., Mikkola, M.L., Beyaert, R., Declercq, W. and van Loo, G. (2011) Keratinocyte-specific ablation of the NF-kappaB regulatory protein A20 (TNFAIP3) reveals a role in the control of epidermal homeostasis. *Cell Death Differ*, 18 (12), 1845-1853.

Liu, C., Teng, Z.Q., Santistevan, N.J., Szulwach, K.E., Guo, W., Jin, P. and Zhao, X. (2010) Epigenetic regulation of miR-184 by MBD1 governs neural stem cell proliferation and differentiation. *Cell Stem Cell*, 6 (5), 433-444.

Liu, J., Rivas, F.V., Wohlschlegel, J., Yates, J.R., 3rd, Parker, R. and Hannon, G.J. (2005) A role for the P-body component GW182 in microRNA function. *Nat Cell Biol*, 7 (12), 1261-1266.

Liu, Y., Beyer, A. and Aebersold, R. (2016) On the Dependency of Cellular Protein Levels on mRNA Abundance. *Cell*, 165 (3), 535-550.

Liu, Z., Mai, C., Yang, H., Zhen, Y., Yu, X., Hua, S., Wu, Q., Jiang, Q., Zhang, Y., Song, X. and Fang, W. (2014) Candidate tumour suppressor CCDC19 regulates miR-184 direct targeting of C-Myc thereby suppressing cell growth in non-small cell lung cancers. *J Cell Mol Med*, 18 (8), 1667-1679.

Loffler, D., Brocke-Heidrich, K., Pfeifer, G., Stocsits, C., Hackermuller, J., Kretzschmar, A.K., Burger, R., Gramatzki, M., Blumert, C., Bauer, K., Cvijic, H., Ullmann, A.K., Stadler, P.F. and Horn, F. (2007) Interleukin-6 dependent survival of multiple myeloma cells involves the

Stat3-mediated induction of microRNA-21 through a highly conserved enhancer. *Blood*, 110 (4), 1330-1333.

Loschke, F., Seltmann, K., Bouameur, J.E. and Magin, T.M. (2015) Regulation of keratin network organization. *Curr Opin Cell Biol*, 32, 56-64.

Lowes, M.A., Bowcock, A.M. and Krueger, J.G. (2007) Pathogenesis and therapy of psoriasis. *Nature*, 445 (7130), 866-873.

Lu, L.-F., Boldin, M.P., Chaudhry, A., Lin, L.-L., Taganov, K.D., Hanada, T., Yoshimura, A., Baltimore, D. and Rudensky, A.Y. (2010) Function of miR-146a in controlling Treg cell-mediated regulation of Th1 responses. *Cell*, 142 (6), 914-929.

Lund, E., Guttinger, S., Calado, A., Dahlberg, J.E. and Kutay, U. (2004) Nuclear export of microRNA precursors. *Science*, 303 (5654), 95-98.

Lytle, J.R., Yario, T.A. and Steitz, J.A. (2007) Target mRNAs are repressed as efficiently by microRNA-binding sites in the 5' UTR as in the 3' UTR. *Proc Natl Acad Sci U S A*, 104 (23), 9667-9672.

MacRae, I.J., Zhou, K. and Doudna, J.A. (2007) Structural determinants of RNA recognition and cleavage by Dicer. *Nat Struct Mol Biol*, 14 (10), 934-940.

Macrae, I.J., Zhou, K., Li, F., Repic, A., Brooks, A.N., Cande, W.Z., Adams, P.D. and Doudna, J.A. (2006) Structural basis for double-stranded RNA processing by Dicer. *Science*, 311 (5758), 195-198.

Martinez, I., Hayes, K.E., Barr, J.A., Harold, A.D., Xie, M., Bukhari, S.I.A., Vasudevan, S., Steitz, J.A. and DiMaio, D. (2017) An Exportin-1-dependent microRNA biogenesis pathway during human cell quiescence. *Proc Natl Acad Sci U S A*, 114 (25), E4961-E4970.

Matsuda, S. and Koyasu, S. (2000) Mechanisms of action of cyclosporine. *Immunopharmacology*, 47 (2), 119-125.

Matsui, M.S., Illarda, I., Wang, N. and DeLeo, V.A. (1993) Protein kinase C agonist and antagonist effects in normal human epidermal keratinocytes. *Exp Dermatol*, 2 (6), 247-256.

Meisgen, F., Xu, N., Wei, T., Janson, P.C., Obad, S., Broom, O., Nagy, N., Kauppinen, S., Kemény, L., Stähle, M., Pivarcsi, A. and Sonkoly, E. (2012) MiR-21 is up-regulated in psoriasis and suppresses T cell apoptosis. *Experimental Dermatology*, 21 (4), 312-314.

Menon, G.K. (2002) New insights into skin structure: scratching the surface. *Adv Drug Deliv Rev*, 54 Suppl 1, S3-17.

Menon, G.K., Lee, S.E. and Lee, S.H. An Overview of Epidermal Lamellar Bodies: Novel roles in biological adaptations and secondary barriers. *Journal of Dermatological Science*.

- Miller, S.J. (1991) Biology of basal cell carcinoma (Part I). *J Am Acad Dermatol*, 24 (1), 1-13.
- Missero, C., Di Cunto, F., Kiyokawa, H., Koff, A. and Dotto, G.P. (1996) The absence of p21Cip1/WAF1 alters keratinocyte growth and differentiation and promotes ras-tumor progression. *Genes Dev*, 10 (23), 3065-3075.
- Miyoshi, K., Tsukumo, H., Nagami, T., Siomi, H. and Siomi, M.C. (2005) Slicer function of Drosophila Argonautes and its involvement in RISC formation. *Genes Dev*, 19 (23), 2837-2848.
- Modzelewski, A.J., Holmes, R.J., Hilz, S., Grimson, A. and Cohen, P.E. (2012) AGO4 regulates entry into meiosis and influences silencing of sex chromosomes in the male mouse germline. *Dev Cell*, 23 (2), 251-264.
- Mognol, G.P., Carneiro, F.R., Robbs, B.K., Faget, D.V. and Viola, J.P. (2016) Cell cycle and apoptosis regulation by NFAT transcription factors: new roles for an old player. *Cell Death Dis*, 7, e2199.
- Morizane, S. and Gallo, R.L. (2012) Antimicrobial peptides in the pathogenesis of psoriasis. *J Dermatol*, 39 (3), 225-230.
- Mulholland, E.J., Dunne, N. and McCarthy, H.O. (2017) MicroRNA as Therapeutic Targets for Chronic Wound Healing. *Mol Ther Nucleic Acids*, 8, 46-55.
- Murray, A.W. (2004) Recycling the cell cycle: cyclins revisited. *Cell*, 116 (2), 221-234.
- Nagosa, S., Leesch, F., Putin, D., Bhattacharya, S., Altshuler, A., Serror, L., Amitai-Lange, A., Nasser, W., Aberdam, E., Rouleau, M., Tattikota, S.G., Poy, M.N., Aberdam, D. and Shalom-Feuerstein, R. (2017) microRNA-184 Induces a Commitment Switch to Epidermal Differentiation. *Stem Cell Reports*, 9 (6), 1991-2004.
- Nayerossadat, N., Maedeh, T. and Ali, P.A. (2012) Viral and nonviral delivery systems for gene delivery. *Adv Biomed Res*, 1, 27.
- Nestle, F.O., Kaplan, D.H. and Barker, J. (2009) Psoriasis. *N Engl J Med*, 361 (5), 496-509.
- Ngondo, R.P., Cirera-Salinas, D., Yu, J., Wischniewski, H., Bodak, M., Vandormael-Pournin, S., Geiselmann, A., Wettstein, R., Luitz, J., Cohen-Tannoudji, M. and Ciaudo, C. (2018) Argonaute 2 Is Required for Extra-embryonic Endoderm Differentiation of Mouse Embryonic Stem Cells. *Stem Cell Reports*, 10 (2), 461-476.
- Nguyen, T.A., Jo, M.H., Choi, Y.G., Park, J., Kwon, S.C., Hohng, S., Kim, V.N. and Woo, J.S. (2015) Functional Anatomy of the Human Microprocessor. *Cell*, 161 (6), 1374-1387.
- Nilsen, B.M. and Paulsen, B.S. (1990) Isolation and characterization of a glycoprotein allergen, Art v II, from pollen of mugwort (*Artemisia vulgaris* L.). *Mol Immunol*, 27 (10), 1047-1056.

Noland, C.L., Ma, E. and Doudna, J.A. (2011) siRNA repositioning for guide strand selection by human Dicer complexes. *Mol Cell*, 43 (1), 110-121.

Numaga-Tomita, T. and Putney, J.W. (2013) Role of STIM1- and Orai1-mediated Ca<sup>2+</sup> entry in Ca<sup>2+</sup>-induced epidermal keratinocyte differentiation. *J Cell Sci*, 126 (Pt 2), 605-612.

O'Brien, J., Hayder, H., Zayed, Y., & Peng, C. (2018). Overview of MicroRNA Biogenesis, Mechanisms of Actions, and Circulation. *Frontiers in endocrinology*, 9, 402.

O'Connell, R.M., Rao, D.S. and Baltimore, D. (2012) microRNA Regulation of Inflammatory Responses. *Annual Review of Immunology*, 30 (1), 295-312.

Orom, U.A., Nielsen, F.C. and Lund, A.H. (2008) MicroRNA-10a binds the 5'UTR of ribosomal protein mRNAs and enhances their translation. *Mol Cell*, 30 (4), 460-471.

Parisi, C., Giorgi, C., Batassa, E.M., Braccini, L., Maresca, G., D'Agnano, I., Caputo, V., Salvatore, A., Pietrolati, F., Cogoni, C. and Catalanotto, C. (2011) Ago1 and Ago2 differentially affect cell proliferation, motility and apoptosis when overexpressed in SH-SY5Y neuroblastoma cells. *FEBS Letters*, 585 (19), 2965-2971.

Park, J.E., Heo, I., Tian, Y., Simanshu, D.K., Chang, H., Jee, D., Patel, D.J. and Kim, V.N. (2011) Dicer recognizes the 5' end of RNA for efficient and accurate processing. *Nature*, 475 (7355), 201-205.

Parkinson, E.K. and Emmerson, A. (1982) The effects of tumour promoters on the multiplication and morphology of cultured human epidermal keratinocytes. *Carcinogenesis*, 3 (5), 525-531.

Pasquinelli, A.E., Reinhart, B.J., Slack, F., Martindale, M.Q., Kuroda, M.I., Maller, B., Hayward, D.C., Ball, E.E., Degan, B., Muller, P., Spring, J., Srinivasan, A., Fishman, M., Finnerty, J., Corbo, J., Levine, M., Leahy, P., Davidson, E. and Ruvkun, G. (2000) Conservation of the sequence and temporal expression of let-7 heterochronic regulatory RNA. *Nature*, 408 (6808), 86-89.

Petrie, R.J. and Yamada, K.M. (2012) At the leading edge of three-dimensional cell migration. *J Cell Sci*, 125 (Pt 24), 5917-5926.

Plank, C., Schillinger, U., Scherer, F., Bergemann, C., Remy, J.S., Krotz, F., Anton, M., Lausier, J. and Rosenecker, J. (2003) The magnetofection method: using magnetic force to enhance gene delivery. *Biol Chem*, 384 (5), 737-747.

Prakriya, M., Feske, S., Gwack, Y., Srikanth, S., Rao, A. and Hogan, P.G. (2006) Orai1 is an essential pore subunit of the CRAC channel. *Nature*, 443 (7108), 230-233.

Prakriya, M. and Lewis, R.S. (2015) Store-Operated Calcium Channels. *Physiol Rev*, 95 (4), 1383-1436.

Primo, M.N., Bak, R.O., Schibler, B. and Mikkelsen, J.G. (2012) Regulation of pro-inflammatory cytokines TNF $\alpha$  and IL24 by microRNA-203 in primary keratinocytes. *Cytokine*, 60 (3), 741-748.

Proksch, E., Folster-Holst, R. and Jensen, J.M. (2006) Skin barrier function, epidermal proliferation and differentiation in eczema. *J Dermatol Sci*, 43 (3), 159-169.

Putney, J.W. (2010) Pharmacology of store-operated calcium channels. *Mol Interv*, 10 (4), 209-218.

Putney, J.W., Steinckwich-Besancon, N., Numaga-Tomita, T., Davis, F.M., Desai, P.N., D'Agostin, D.M., Wu, S. and Bird, G.S. (2017) The functions of store-operated calcium channels. *Biochim Biophys Acta Mol Cell Res*, 1864 (6), 900-906.

Qi, H.H., Ongusaha, P.P., Myllyharju, J., Cheng, D., Pakkanen, O., Shi, Y., Lee, S.W., Peng, J. and Shi, Y. (2008) Prolyl 4-hydroxylation regulates Argonaute 2 stability. *Nature*, 455 (7211), 421-424.

Quévillon Huberdeau, M., Zeitler, D. M., Hauptmann, J., Bruckmann, A., Fressigné, L., Danner, J., Piquet, S., Strieder, N., Engelmann, J. C., Jannot, G., Deutzmann, R., Simard, M. J. and Meister, G. (2017). Phosphorylation of Argonaute proteins affects mRNA binding and is essential for microRNA-guided gene silencing *in vivo*. *The EMBO journal*, 36 (14), 2088-2106.

Ray-Jones, H., Eyre, S., Barton, A. and Warren, R.B. (2016) One SNP at a Time: Moving beyond GWAS in Psoriasis. *J Invest Dermatol*, 136 (3), 567-573.

Rebane, A., Runnel, T., Aab, A., Maslovskaja, J., Rückert, B., Zimmermann, M., Plaas, M., Kärner, J., Treis, A., Pihlap, M., Haljasorg, U., Hermann, H., Nagy, N., Kemeny, L., Erm, T., Kingo, K., Li, M., Boldin, M.P. and Akdis, C.A. (2014) MicroRNA-146a alleviates chronic skin inflammation in atopic dermatitis through suppression of innate immune responses in keratinocytes. *Journal of Allergy and Clinical Immunology*, 134 (4), 836-847.e811.

Reinhart, B.J. and Bartel, D.P. (2002) Small RNAs correspond to centromere heterochromatic repeats. *Science*, 297 (5588), 1831.

Reinhart, B.J., Slack, F.J., Basson, M., Pasquinelli, A.E., Bettinger, J.C., Rougvie, A.E., Horvitz, H.R. and Ruvkun, G. (2000) The 21-nucleotide let-7 RNA regulates developmental timing in *Caenorhabditis elegans*. *Nature*, 403 (6772), 901-906.

Ribas, J., Ni, X., Castanares, M., Liu, M.M., Esopi, D., Yegnasubramanian, S., Rodriguez, R., Mendell, J.T. and Lupold, S.E. (2012) A novel source for miR-21 expression through the alternative polyadenylation of VMP1 gene transcripts. *Nucleic Acids Res*, 40 (14), 6821-6833.

Roberson, E.D. and Bowcock, A.M. (2010) Psoriasis genetics: breaking the barrier. *Trends Genet*, 26 (9), 415-423.

Roberts, J.C., Warren, R.B., Griffiths, C.E. and Ross, K. (2013) Expression of microRNA-184 in keratinocytes represses argonaute 2. *J Cell Physiol*, 228 (12), 2314-2323.

Rodriguez, A., Griffiths-Jones, S., Ashurst, J.L. and Bradley, A. (2004) Identification of mammalian microRNA host genes and transcription units. *Genome Res*, 14 (10A), 1902-1910.

Rostami Mogaddam, M., Safavi Ardabili, N., Shafaei, Y., Maleki, N., Jafari, N. and Jafari, A. (2017) Overexpression of Drosha, DiGeorge syndrome critical region gene 8 (DGCR8), and Dicer mRNAs in the pathogenesis of psoriasis. *J Cosmet Dermatol*, 16 (4), e48-e53.

Rudel, S., Wang, Y., Lenobel, R., Korner, R., Hsiao, H.H., Urlaub, H., Patel, D. and Meister, G. (2011) Phosphorylation of human Argonaute proteins affects small RNA binding. *Nucleic Acids Res*, 39 (6), 2330-2343.

Rumi-Masante, J., Rusinga, F.I., Lester, T.E., Dunlap, T.B., Williams, T.D., Dunker, A.K., Weis, D.D. and Creamer, T.P. (2012) Structural basis for activation of calcineurin by calmodulin. *J Mol Biol*, 415 (2), 307-317.

Ryan, D.G., Oliveira-Fernandes, M. and Lavker, R.M. (2006) MicroRNAs of the mammalian eye display distinct and overlapping tissue specificity. *Mol Vis*, 12, 1175-1184.

Sakamoto, S., Aoki, K., Higuchi, T., Todaka, H., Morisawa, K., Tamaki, N., Hatano, E., Fukushima, A., Taniguchi, T. and Agata, Y. (2009) The NF90-NF45 complex functions as a negative regulator in the microRNA processing pathway. *Mol Cell Biol*, 29 (13), 3754-3769.

Sand, M., Skrygan, M., Georgas, D., Arenz, C., Gambichler, T., Sand, D., Altmeyer, P. and Bechara, F.G. (2012) Expression levels of the microRNA maturing microprocessor complex component DGCR8 and the RNA-induced silencing complex (RISC) components argonaute-1, argonaute-2, PACT, TARBP1, and TARBP2 in epithelial skin cancer. *Mol Carcinog*, 51 (11), 916-922.

Sandilands, A., Sutherland, C., Irvine, A.D. and McLean, W.H. (2009) Filaggrin in the frontline: role in skin barrier function and disease. *J Cell Sci*, 122 (Pt 9), 1285-1294.

Santini, M.P., Talora, C., Seki, T., Bolgan, L. and Dotto, G.P. (2001) Cross talk among calcineurin, Sp1/Sp3, and NFAT in control of p21(WAF1/CIP1) expression in keratinocyte differentiation. *Proc Natl Acad Sci U S A*, 98 (17), 9575-9580.

Schmittgen, T.D. and Livak, K.J. (2008) Analyzing real-time PCR data by the comparative C(T) method. *Nat Protoc*, 3 (6), 1101-1108.

Selbach, M., Schwanhausser, B., Thierfelder, N., Fang, Z., Khanin, R. and Rajewsky, N. (2008) Widespread changes in protein synthesis induced by microRNAs. *Nature*, 455 (7209), 58-63.

- Sharma, N.R., Wang, X., Majerciak, V., Ajiro, M., Kruhlak, M., Meyers, C. and Zheng, Z.M. (2016) Cell Type- and Tissue Context-dependent Nuclear Distribution of Human Ago2. *J Biol Chem*, 291 (5), 2302-2309.
- Shekar, P.C., Naim, A., Sarathi, D.P. and Kumar, S. (2011) Argonaute-2-null embryonic stem cells are retarded in self-renewal and differentiation. *J Biosci*, 36 (4), 649-657.
- Shen, J., Xia, W., Khotskaya, Y.B., Huo, L., Nakanishi, K., Lim, S.O., Du, Y., Wang, Y., Chang, W.C., Chen, C.H., Hsu, J.L., Wu, Y., Lam, Y.C., James, B.P., Liu, X., Liu, C.G., Patel, D.J. and Hung, M.C. (2013) EGFR modulates microRNA maturation in response to hypoxia through phosphorylation of AGO2. *Nature*, 497 (7449), 383-387.
- Sherman, M.H., Bassing, C.H. and Teitell, M.A. (2011) Regulation of cell differentiation by the DNA damage response. *Trends Cell Biol*, 21 (5), 312-319.
- Sherr, C.J. and Roberts, J.M. (2004) Living with or without cyclins and cyclin-dependent kinases. *Genes Dev*, 18 (22), 2699-2711.
- Sheu-Gruttadauria, J. and MacRae, I.J. (2018) Phase Transitions in the Assembly and Function of Human miRISC. *Cell*, 173 (4), 946-957.E16.
- Simpson, C.L., Patel, D.M. and Green, K.J. (2011) Deconstructing the skin: cytoarchitectural determinants of epidermal morphogenesis. *Nat Rev Mol Cell Biol*, 12 (9), 565-580.
- Sonkoly, E., Wei, T., Janson, P.C., Saaf, A., Lundeberg, L., Tengvall-Linder, M., Norstedt, G., Alenius, H., Homey, B., Scheynius, A., Stähle, M. and Pivarcsi, A. (2007) MicroRNAs: novel regulators involved in the pathogenesis of psoriasis? *PLoS One*, 2 (7), e610.
- Sonkoly, E., Wei, T., Pavez Loriè, E., Suzuki, H., Kato, M., Törmä, H., Stähle, M. and Pivarcsi, A. (2010) Protein Kinase C-Dependent Upregulation of miR-203 Induces the Differentiation of Human Keratinocytes. *Journal of Investigative Dermatology*, 130 (1), 124-134.
- Springate, D.A., Parisi, R., Kontopantelis, E., Reeves, D., Griffiths, C.E. and Ashcroft, D.M. (2017) Incidence, prevalence and mortality of patients with psoriasis: a U.K. population-based cohort study. *Br J Dermatol*, 176 (3), 650-658.
- Srivastava, A., Nikamo, P., Lohcharoenkal, W., Li, D., Meisgen, F., Xu Landén, N., Stähle, M., Pivarcsi, A. and Sonkoly, E. (2017) MicroRNA-146a suppresses IL-17-mediated skin inflammation and is genetically associated with psoriasis. *Journal of Allergy and Clinical Immunology*, 139 (2), 550-561.
- Sun, T.T. and Green, H. (1976) Differentiation of the epidermal keratinocyte in cell culture: formation of the cornified envelope. *Cell*, 9 (4 Pt 1), 511-521.
- Sundaram, G.M., Common, J.E.A., Gopal, F.E., Srikanta, S., Lakshman, K., Lunny, D.P., Lim, T.C., Tanavde, V., Lane, E.B. and Sampath, P. (2013) 'See-saw' expression of microRNA-198 and FSTL1 from a single transcript in wound healing. *Nature*, 495, 103.

Taganov, K.D., Boldin, M.P., Chang, K.-J. and Baltimore, D. (2006) NF- $\kappa$ B-dependent induction of microRNA miR-146, an inhibitor targeted to signaling proteins of innate immune responses. *Proceedings of the National Academy of Sciences*, 103 (33), 12481.

Taliaferro, J.M., Aspden, J.L., Bradley, T., Marwha, D., Blanchette, M. and Rio, D.C. (2013) Two new and distinct roles for *Drosophila* Argonaute-2 in the nucleus: alternative pre-mRNA splicing and transcriptional repression. *Genes & development*, 27 (4), 378-389.

Tattikota, S.G., Rathjen, T., McAnulty, S.J., Wessels, H.H., Akerman, I., van de Bunt, M., Hausser, J., Esguerra, J.L., Musahl, A., Pandey, A.K., You, X., Chen, W., Herrera, P.L., Johnson, P.R., O'Carroll, D., Eliasson, L., Zavolan, M., Gloyn, A.L., Ferrer, J., Shalom-Feuerstein, R., Aberdam, D. and Poy, M.N. (2014) Argonaute2 mediates compensatory expansion of the pancreatic beta cell. *Cell Metab*, 19 (1), 122-134.

Tay, Y., Zhang, J., Thomson, A.M., Lim, B. and Rigoutsos, I. (2008) MicroRNAs to Nanog, Oct4 and Sox2 coding regions modulate embryonic stem cell differentiation. *Nature*, 455 (7216), 1124-1128.

Teixeira, L.K., Carrossini, N., Secca, C., Kroll, J.E., DaCunha, D.C., Faget, D.V., Carvalho, L.D., de Souza, S.J. and Viola, J.P. (2016) NFAT1 transcription factor regulates cell cycle progression and cyclin E expression in B lymphocytes. *Cell Cycle*, 15 (17), 2346-2359.

Teng, M.W., Bowman, E.P., McElwee, J.J., Smyth, M.J., Casanova, J.L., Cooper, A.M. and Cua, D.J. (2015) IL-12 and IL-23 cytokines: from discovery to targeted therapies for immune-mediated inflammatory diseases. *Nat Med*, 21 (7), 719-729.

Tili, E., Michaille, J.-J., Cimino, A., Costinean, S., Dumitru, C.D., Adair, B., Fabbri, M., Alder, H., Liu, C.G., Calin, G.A. and Croce, C.M. (2007) Modulation of miR-155 and miR-125b Levels following Lipopolysaccharide/TNF- $\alpha$  Stimulation and Their Possible Roles in Regulating the Response to Endotoxin Shock. *The Journal of Immunology*, 179 (8), 5082.

Tobin, D.J. (2006) Biochemistry of human skin--our brain on the outside. *Chem Soc Rev*, 35 (1), 52-67.

Topley, G.I., Okuyama, R., Gonzales, J.G., Conti, C. and Dotto, G.P. (1999) p21(WAF1/Cip1) functions as a suppressor of malignant skin tumor formation and a determinant of keratinocyte stem-cell potential. *Proc Natl Acad Sci U S A*, 96 (16), 9089-9094.

Tsoi, L.C., Spain, S.L., Knight, J., Ellinghaus, E., Stuart, P.E., Capon, F., Ding, J., Li, Y., Tejasvi, T., Gudjonsson, J.E., Kang, H.M., Allen, M.H., McManus, R., Novelli, G., Samuelsson, L., Schalkwijk, J., Stahle, M., Burden, A.D., Smith, C.H., Cork, M.J., Estivill, X., Bowcock, A.M., Krueger, G.G., Weger, W., Worthington, J., Tazi-Ahnini, R., Nestle, F.O., Hayday, A., Hoffmann, P., Winkelmann, J., Wijmenga, C., Langford, C., Edkins, S., Andrews, R., Blackburn, H., Strange, A., Band, G., Pearson, R.D., Vukcevic, D., Spencer, C.C., Deloukas, P., Mrowietz, U., Schreiber, S., Weidinger, S., Koks, S., Kingo, K., Esko, T., Metspalu, A., Lim, H.W., Voorhees, J.J., Weichenthal, M., Wichmann, H.E., Chandran, V., Rosen, C.F., Rahman, P., Gladman, D.D., Griffiths, C.E., Reis, A., Kere, J., Collaborative Association Study of, P.,

Genetic Analysis of Psoriasis, C., Psoriasis Association Genetics, E., Wellcome Trust Case Control, C., Nair, R.P., Franke, A., Barker, J.N., Abecasis, G.R., Elder, J.T. and Trembath, R.C. (2012) Identification of 15 new psoriasis susceptibility loci highlights the role of innate immunity. *Nat Genet*, 44 (12), 1341-1348.

Tung, M.C., Lin, P.L., Cheng, Y.W., Wu, D.W., Yeh, S.D., Chen, C.Y. and Lee, H. (2016) Reduction of microRNA-184 by E6 oncoprotein confers cisplatin resistance in lung cancer via increasing Bcl-2. *Oncotarget*, 7 (22), 32362-32374.

Vandenberghe, M., Raphaël, M., Lehen'kyi, V.y., Gordienko, D., Hastie, R., Oddos, T., Rao, A., Hogan, P.G., Skryma, R. and Prevarskaya, N. (2013) ORA1 calcium channel orchestrates skin homeostasis. *Proceedings of the National Academy of Sciences of the United States of America*, 110 (50), E4839-E4848.

Völler, D., Linck, L., Bruckmann, A., Hauptmann, J., Deutzmann, R., Meister, G. and Bosserhoff, A.K. (2016) Argonaute Family Protein Expression in Normal Tissue and Cancer Entities. *PLoS One*, 11 (8), e0161165-e0161165.

Volpe, T.A., Kidner, C., Hall, I.M., Teng, G., Grewal, S.I. and Martienssen, R.A. (2002) Regulation of heterochromatic silencing and histone H3 lysine-9 methylation by RNAi. *Science*, 297 (5588), 1833-1837.

Wang, D., Zhang, Z., O'Loughlin, E., Lee, T., Houel, S., O'Carroll, D., Tarakhovsky, A., Ahn, N.G. and Yi, R. (2012) Quantitative functions of Argonaute proteins in mammalian development. *Genes Dev*, 26 (7), 693-704.

Wang, D., Zhang, Z., O'Loughlin, E., Wang, L., Fan, X., Lai, E.C. and Yi, R. (2013) MicroRNA-205 controls neonatal expansion of skin stem cells by modulating the PI(3)K pathway. *Nat Cell Biol*, 15 (10), 1153-1163.

Wang, F., Li, X., Xie, X., Zhao, L. and Chen, W. (2008) UCA1, a non-protein-coding RNA up-regulated in bladder carcinoma and embryo, influencing cell growth and promoting invasion. *FEBS Lett*, 582 (13), 1919-1927.

Wang, X., Xu, X., Ma, Z., Huo, Y., Xiao, Z., Li, Y. and Wang, Y. (2011) Dynamic mechanisms for pre-miRNA binding and export by Exportin-5. *RNA*, 17 (8), 1511-1528.

Wang, Y.-B., Zhao, X.-H., Li, G., Zheng, J.-H. and Qiu, W. (2017) MicroRNA-184 inhibits proliferation and promotes apoptosis of human colon cancer SW480 and HCT116 cells by downregulating C-MYC and BCL-2. *Journal of Cellular Biochemistry*, 119 (2), 1702-1715.

Wassenegger, M., Heimes, S., Riedel, L. and Sanger, H.L. (1994) RNA-directed de novo methylation of genomic sequences in plants. *Cell*, 76 (3), 567-576.

Wei, T., Folkersen, L., Biskup, E., Xu, N., Manfe, V., Niazi, O. and Gniadecki, R. (2017) Ubiquitin-specific peptidase 2 as a potential link between microRNA-125b and psoriasis. *176 (3)*, 723-731.

Weitzel, R.P., Lesniewski, M.L., Greco, N.J. and Laughlin, M.J. (2011) Reduced methyl-CpG protein binding contributing to miR-184 expression in umbilical cord blood CD4+ T-cells. *Leukemia*, 25 (1), 169-172.

Weitzel, R.P., Lesniewski, M.L., Haviernik, P., Kadereit, S., Leahy, P., Greco, N.J. and Laughlin, M.J. (2009) microRNA 184 regulates expression of NFAT1 in umbilical cord blood CD4+ T cells. *Blood*, 113 (26), 6648-6657.

Wightman, B., Ha, I. and Ruvkun, G. (1993) Posttranscriptional regulation of the heterochronic gene *lin-14* by *lin-4* mediates temporal pattern formation in *C. elegans*. *Cell*, 75 (5), 855-862.

Wilson, N.J., Boniface, K., Chan, J.R., McKenzie, B.S., Blumenschein, W.M., Mattson, J.D., Basham, B., Smith, K., Chen, T., Morel, F., Lecron, J.C., Kastelein, R.A., Cua, D.J., McClanahan, T.K., Bowman, E.P. and de Waal Malefyt, R. (2007) Development, cytokine profile and function of human interleukin 17-producing helper T cells. *Nat Immunol*, 8 (9), 950-957.

Wolf, H., Rols, M.P., Boldt, E., Neumann, E. and Teissie, J. (1994) Control by pulse parameters of electric field-mediated gene transfer in mammalian cells. *Biophys J*, 66 (2 Pt 1), 524-531.

Wolk, K., Haugen, H.S., Xu, W., Witte, E., Waggle, K., Anderson, M., Vom Baur, E., Witte, K., Warszawska, K., Philipp, S., Johnson-Leger, C., Volk, H.D., Sterry, W. and Sabat, R. (2009) IL-22 and IL-20 are key mediators of the epidermal alterations in psoriasis while IL-17 and IFN-gamma are not. *J Mol Med (Berl)*, 87 (5), 523-536.

Wu, C., So, J., Davis-Dusenbery, B.N., Qi, H.H., Bloch, D.B., Shi, Y., Lagna, G. and Hata, A. (2011) Hypoxia potentiates microRNA-mediated gene silencing through posttranslational modification of Argonaute2. *Mol Cell Biol*, 31 (23), 4760-4774.

Wu, G.G., Li, W.H., He, W.G., Jiang, N., Zhang, G.X., Chen, W., Yang, H.F., Liu, Q.L., Huang, Y.N., Zhang, L., Zhang, T. and Zeng, X.C. (2014) Mir-184 post-transcriptionally regulates SOX7 expression and promotes cell proliferation in human hepatocellular carcinoma. *PLoS One*, 9 (2), e88796.

Wu, R., Zeng, J., Yuan, J., Deng, X., Huang, Y., Chen, L., Zhang, P., Feng, H., Liu, Z., Wang, Z., Gao, X., Wu, H., Wang, H., Su, Y., Zhao, M. and Lu, Q. (2018) MicroRNA-210 overexpression promotes psoriasis-like inflammation by inducing Th1 and Th17 cell differentiation. *The Journal of Clinical Investigation*, 128 (6), 2551-2568.

Wu, Y., Zhong, J.L., Hou, N., Sun, Y., Ma, B., Nisar, M.F., Teng, Y., Tan, Z., Chen, K., Wang, Y. and Yang, X. (2017) MicroRNA Let-7b inhibits keratinocyte migration in cutaneous wound healing by targeting IGF2BP2. *Exp Dermatol*, 26 (2), 116-123.

- Xia, P., Fang, X., Zhang, Z.-h., Huang, Q., Yan, K.-x., Kang, K.-f., Han, L. and Zheng, Z.-z. (2012) Dysregulation of miRNA146a versus IRAK1 induces IL-17 persistence in the psoriatic skin lesions. *Immunology Letters*, 148 (2), 151-162.
- Xie, M., Li, M., Vilborg, A., Lee, N., Shu, M.D., Yartseva, V., Sestan, N. and Steitz, J.A. (2013) Mammalian 5'-capped microRNA precursors that generate a single microRNA. *Cell*, 155 (7), 1568-1580.
- Xu, N., Brodin, P., Wei, T., Meisgen, F., Eidsmo, L., Nagy, N., Kemeny, L., Stähle, M., Sonkoly, E. and Pivarcsi, A. (2011) MiR-125b, a MicroRNA Downregulated in Psoriasis, Modulates Keratinocyte Proliferation by Targeting FGFR2. *Journal of Investigative Dermatology*, 131 (7), 1521-1529.
- Xu, N., Meisgen, F., Butler, L.M., Han, G., Wang, X.-J., Söderberg-Nauclér, C., Stähle, M., Pivarcsi, A. and Sonkoly, E. (2013) MicroRNA-31 Is Overexpressed in Psoriasis and Modulates Inflammatory Cytokine and Chemokine Production in Keratinocytes via Targeting Serine/Threonine Kinase 40. *The Journal of Immunology*, 190 (2), 678.
- Yan, S., Xu, Z., Lou, F., Zhang, L., Ke, F., Bai, J., Liu, Z., Liu, J., Wang, H., Zhu, H., Sun, Y., Cai, W., Gao, Y., Su, B., Li, Q., Yang, X., Yu, J., Lai, Y., Yu, X.-Z., Zheng, Y., Shen, N., Chin, Y.E. and Wang, H. (2015) NF- $\kappa$ B-induced microRNA-31 promotes epidermal hyperplasia by repressing protein phosphatase 6 in psoriasis. *Nature Communications*, 6, 7652.
- Yang, X., Wang, J., Guo, S.L., Fan, K.J., Li, J., Wang, Y.L., Teng, Y. and Yang, X. (2011) miR-21 promotes keratinocyte migration and re-epithelialization during wound healing. *Int J Biol Sci*, 7 (5), 685-690.
- Yi, R., Poy, M.N., Stoffel, M. and Fuchs, E. (2008a) A skin microRNA promotes differentiation by repressing 'stemness'. *Nature*, 452 (7184), 225-229.
- Yi, R., Poy, M.N., Stoffel, M. and Fuchs, E. (2008b) A skin microRNA promotes differentiation by repressing 'stemness'. *Nature*, 452 (7184), 225-229.
- Yi, R., Qin, Y., Macara, I.G. and Cullen, B.R. (2003) Exportin-5 mediates the nuclear export of pre-microRNAs and short hairpin RNAs. *Genes Dev*, 17 (24), 3011-3016.
- Yim, K.M. and Armstrong, A.W. (2017) Updates on cardiovascular comorbidities associated with psoriatic diseases: epidemiology and mechanisms. *Rheumatol Int*, 37 (1), 97-105.
- Yu, J., Peng, H., Ruan, Q., Fatima, A., Getsios, S. and Lavker, R.M. (2010) MicroRNA-205 promotes keratinocyte migration via the lipid phosphatase SHIP2. *FASEB J*, 24 (10), 3950-3959.
- Yu, J., Ryan, D.G., Getsios, S., Oliveira-Fernandes, M., Fatima, A. and Lavker, R.M. (2008) MicroRNA-184 antagonizes microRNA-205 to maintain SHIP2 levels in epithelia. *Proc Natl Acad Sci U S A*, 105 (49), 19300-19305.

Yuan, Q., Gao, W., Liu, B. and Ye, W. (2014) Upregulation of miR-184 enhances the malignant biological behavior of human glioma cell line A172 by targeting FIH-1. *Cell Physiol Biochem*, 34 (4), 1125-1136.

Yuan, Y.R., Pei, Y., Ma, J.B., Kuryavyi, V., Zhadina, M., Meister, G., Chen, H.Y., Dauter, Z., Tuschl, T. and Patel, D.J. (2005) Crystal structure of *A. aeolicus* argonaute, a site-specific DNA-guided endoribonuclease, provides insights into RISC-mediated mRNA cleavage. *Mol Cell*, 19 (3), 405-419.

Zanet, J., Freije, A., Ruiz, M., Coulon, V., Sanz, J.R., Chiesa, J. and Gandarillas, A. (2010) A mitosis block links active cell cycle with human epidermal differentiation and results in endoreplication. *PLoS One*, 5 (12), e15701.

Zardo, G., Ciolfi, A., Vian, L., Starnes, L.M., Billi, M., Racanicchi, S., Maresca, C., Fazi, F., Travaglini, L., Noguera, N., Mancini, M., Nanni, M., Cimino, G., Lo-Coco, F., Grignani, F. and Nervi, C. (2012) Polycombs and microRNA-223 regulate human granulopoiesis by transcriptional control of target gene expression. *Blood*, 119 (17), 4034-4046.

Zeng, Y. and Cullen, B.R. (2004) Structural requirements for pre-microRNA binding and nuclear export by Exportin 5. *Nucleic Acids Res*, 32 (16), 4776-4785.

Zeng, Y., Sankala, H., Zhang, X. and Graves, P.R. (2008) Phosphorylation of Argonaute 2 at serine-387 facilitates its localization to processing bodies. *Biochem J*, 413 (3), 429-436.

Zhang, L., Stokes, N., Polak, L. and Fuchs, E. (2011) Specific microRNAs are preferentially expressed by skin stem cells to balance self-renewal and early lineage commitment. *Cell Stem Cell*, 8 (3), 294-308.

Zhang, S., Al-Maghout, T., Zhou, Y., Bissinger, R., Abousaab, A., Salker, M.S., Pelzl, L., Cobb, B.S., Cheng, A., Singh, Y. and Lang, F. (2016) Role of Dicer Enzyme in the Regulation of Store Operated Calcium Entry (SOCE) in CD4+ T Cells. *Cell Physiol Biochem*, 39 (4), 1360-1368.

Zhao, M., Wang, L.-t., Liang, G.-p., Zhang, P., Deng, X.-j., Tang, Q., Zhai, H.-y., Chang, C.C., Su, Y.-w. and Lu, Q.-j. (2014) Up-regulation of microRNA-210 induces immune dysfunction via targeting FOXP3 in CD4+ T cells of psoriasis vulgaris. *Clinical Immunology*, 150 (1), 22-30.

Zheng, Y., Danilenko, D.M., Valdez, P., Kasman, I., Eastham-Anderson, J., Wu, J. and Ouyang, W. (2007) Interleukin-22, a T(H)17 cytokine, mediates IL-23-induced dermal inflammation and acanthosis. *Nature*, 445 (7128), 648-651.

Zhou, F., Wang, W., Shen, C., Li, H., Zuo, X., Zheng, X., Yue, M., Zhang, C., Yu, L., Chen, M., Zhu, C., Yin, X., Tang, M., Li, Y., Chen, G., Wang, Z., Liu, S., Zhou, Y., Zhang, F., Zhang, W., Li, C., Yang, S., Sun, L. and Zhang, X. (2016) Epigenome-Wide Association Analysis Identified Nine Skin DNA Methylation Loci for Psoriasis. *J Invest Dermatol*, 136 (4), 779-787.

Zhou, Y., Wang, X., Zhang, J., He, A., Wang, Y.L., Han, K., Su, Y., Yin, J., Lv, X. and Hu, H. (2017) Artesunate suppresses the viability and mobility of prostate cancer cells through UCA1, the sponge of miR-184. *Oncotarget*, 8 (11), 18260-18270.

Zhu, H.M., Jiang, X.S., Li, H.Z., Qian, L.X., Du, M.Y., Lu, Z.W., Wu, J., Tian, X.K., Fei, Q., He, X. and Yin, L. (2018) miR-184 Inhibits Tumor Invasion, Migration and Metastasis in Nasopharyngeal Carcinoma by Targeting Notch2. *Cell Physiol Biochem*, 49 (4), 1564-1576.

Zibert, J.R., Løvendorf, M.B., Litman, T., Olsen, J., Kaczkowski, B. and Skov, L. (2010) MicroRNAs and potential target interactions in psoriasis. *Journal of Dermatological Science*, 58 (3), 177-185.

Zilberman, D., Cao, X. and Jacobsen, S.E. (2003) ARGONAUTE4 control of locus-specific siRNA accumulation and DNA and histone methylation. *Science*, 299 (5607), 716-719.

Zong, R., Zhou, T., Lin, Z., Bao, X., Xiu, Y., Chen, Y., Chen, L., Ma, J.X., Liu, Z. and Zhou, Y. (2016) Down-Regulation of MicroRNA-184 Is Associated With Corneal Neovascularization. *Invest Ophthalmol Vis Sci*, 57 (3), 1398-1407.

Zuo, Z.K., Gong, Y., Chen, X.H., Ye, F., Yin, Z.M., Gong, Q.N. and Huang, J.S. (2017) TGFbeta1-Induced LncRNA UCA1 Upregulation Promotes Gastric Cancer Invasion and Migration. *DNA Cell Biol*, 36 (2), 159-167.